Dissertation
submitted to the
Combined Faculties for the Natural Sciences and for Mathematics
of the Ruperto-Carola University of Heidelberg, Germany
for the degree of
Doctor of Natural Sciences

presented by

Master of Science Suchanek, Verena Maria
born in: Saulgau, now Bad Saulgau
Oral-examination: 21.09.2016

Role of Motility and its Regulation in *Escherichia coli* Biofilm formation

Referees: Prof. Dr. Victor Sourjik
Dr. Axel Mogk

Für Jakob und Noah

ZUSAMMENFASSUNG

Biofilme sind mehrzellige Zusammenschlüsse von Bakterien, die häufig auf Oberflächen wachsen. Bakterien in Biofilmen sind nicht motil und sind von einem komplexen Geflecht umgeben, der sogenannten Biofilmmatrix, welche Proteine, Polysaccharide und DNA enthält. Die Matrix verleiht dem Biofilm Stabilität und Festigkeit und ist für das gegenseitige Ankleben der Zellen sowie das Anheften an die Oberfläche wichtig. Der Übergang von der motilen planktonischen Wachstumsphase in den sesshaften Biofilmzustand erfordert eine strenge Regulierung von Motilität und Matrixproduktion.
In meiner Arbeit habe ich die verschiedenen Beiträge sowie die Regulierung der Motilität während der Biofilmbildung des Bakteriums *Escherichia coli* untersucht. Ich konnte dabei zeigen, dass Flagellen in verschiedenen Stadien der Biofilmbildung eine Rolle spielen, da sie eine Fortbewegung durch Schwimmen zu Beginn der Biofilmbildung erlauben und zur strukturellen Integrität der reifen Biofilme beitragen. Fortbewegung durch Schwimmen ist zum einen wichtig für das anfängliche Ankleben der Bakterien an die Oberfläche und hilft zum anderen, die reifen Biofilmstrukturen zu formen. Meine Ergebnisse zeigen, dass zu Beginn der Biofilmbildung gleichmäßiges Schwimmen an der Oberfläche zu einem hydrodynamischen Einfangen der Zellen führt, was das Ankleben der Zellen begünstigt.
Des weiteren beeinflusst die Schwimmgeschwindigkeit das Ankleben, wobei schnelleres Schwimmen das Ankleben verbessert. Schwimmgeschwindigkeit wird durch den sekundären Botenstoff bis-(3'-5')-zyklischem di-Guanosinmonophosphat (c-di-GMP) reguliert, der eine Schlüsselrolle im Übergang von der motilen zur sessilen Phase spielt. C-di-GMP hemmt auf der einen Seite Motilität, was durch das Motor-Bindeprotein YcgR vermittelt wird, und fördert auf der anderen Seite die Synthese von Biofilmmatrixkomponenten. Dadurch, dass in meinen Experimenten Schwimmen für das Ankleben der Zellen benötigt wurde, konnte ich zeigen, dass c-di-GMP eine duale Rolle während der Biofilmbildung spielt, und zwar inhibiert es den Anfang der Biofilmbildung durch Hemmung der Motilität und fördert die Reifung des Biofilms durch Hochregulierung von Adhäsionsfaktoren. Zellen, die einen dauerhaft erniedrigten c-di-GMP-Spiegel haben, zeigen besseres Ankleben, haben jedoch Störungen in der Biofilmreifung und -architektur. Im Gegensatz dazu zeigen Zellen mit dauerhaft erhöhtem c-di-GMP-Spiegel schlechteres Ankleben, können aber strukturierte dreidimensionale Anordnungen in reifen Biofilmen bilden. Die Auswirkung auf das Ankleben wird durch das Motorbindeprotein YcgR vermittelt, was die Schwimmgeschwindigkeit reguliert.
Mit Hilfe der oben beschriebenen Ergebnisse konnte ich des Weiteren einen neuen Regler des c-di-GMP-Signalsystems in *Escherichia coli* beschreiben. Meine Ergebnisse deuten darauf hin, dass das bakterielle Dynamin YjdA zusammen mit dem kleinen Protein YjcZ die c-di-GMP-Produktion durch die di-Guanylat-Zyklase YegE reguliert. Das konnte ich phänotypisch durch verändertes Schwimmverhalten, Ankleben der Zellen und Biofilmreifung einer *yjdA*-Deletion zeigen. Damit kopiert diese Deletion das phänotypische Verhalten einer Deletion der Zyklase YegE. Außerdem ist die c-di-GMP-abhängige Wechselwirkung zwischen YcgR und dem Flagellenmotor in beiden Deletionsstämmen gleichermaßen beeinträchtigt. Zudem habe ich mit Hilfe des Bakterien-Zwei-Hybrid-Systems eine Interaktion zwischen YjdA und YegE gezeigt. Meine Ergebnisse deuten außerdem darauf

hin, dass die bakteriellen Flotilline HflK/C auch eine Rolle in der Regulierung von YegE durch YjdA spielen.
Zusammenfassend ergeben die Ergebnisse dieser Arbeit einen Überblick über die Rollen der Flagellen und der Motilität während der Biofilmbildung in *Escherichia coli*, zum einen gezeigt durch die Notwendigkeit des Schwimmens zu Beginn der Biofilmbildung, wodurch auch eine genaue Regulierung des c-di-GMP-Signalwegs während der Biofilmbildung wichtig ist, und zum anderen durch eine strukturelle Rolle der Flagellen in späteren Biofilmstadien.

SUMMARY

Biofilms are multicellular communities of bacterial cells that usually grow on surfaces. Bacteria in biofilms are non-motile and are surrounded by a complex meshwork containing proteins, polysaccharides and DNA, the so-called biofilm matrix. The matrix provides stability and rigidity to the biofilm and is important for sticking cells to the surface and towards each other. The transition from the motile planktonic growth state to the sessile biofilm state requires therefore tight regulation of motility and matrix synthesis. In this work, I have investigated the roles and regulation of motility during biofilm formation of *Escherichia coli*. I could show that flagella play roles at different stages of biofilm formation, providing swimming motility at biofilm initiation and structural integrity in mature biofilms. Swimming motility is required for initial cell attachment to the surface and helps to shape mature biofilm structures. My results show that during biofilm initiation, smooth swimming at the surface leads to hydrodynamic entrapment, thereby promoting cell attachment.

Additionally, swimming speed seems to influence surface attachment with enhanced swimming speed increasing attachment. Swimming speed is regulated by the second messenger bis-(3'-5')-cyclic dimeric guanosine monophosphate (c-di-GMP), which is a key factor in the transition from motility to sessility. C-di-GMP on the one hand inhibits motility via the motor binding protein YcgR and on the other hand promotes the synthesis of biofilm matrix factors. With the requirement of swimming for cell attachment, I could show that c-di-GMP plays a dual role during the course of biofilm formation, inhibiting biofilm initiation through motility inhibition and promoting biofilm maturation through upregulation of adhesion factors. Cells with permanently decreased c-di-GMP levels show increased cell attachment, however, have defects in biofilm maturation and architecture. In contrast, cells with permanently increased c-di-GMP levels show decreased cell attachment, but are able to form elaborate three-dimensional structures in mature biofilms. The effect on attachment is mediated by the motor binding protein YcgR, which regulates swimming speed.

Based on the above described results, I could characterize a new regulator of c-di-GMP signaling in *Escherichia coli*. My results suggest that the bacterial dynamin YjdA, together with the small protein YjcZ, regulates c-di-GMP production by the diguanylate cyclase YegE. This is represented on the phenotypic level by changes in swimming motility, cell attachment and biofilm maturation in the *yjdA* deletion. It thereby phenotypically copies the deletion of the cyclase YegE. Additionally, the c-di-GMP dependent interaction of YcgR with the flagellar motor is decreased similarly in both *yjdA* and *yegE* deletion strains. Last but not least, bacterial two-hybrid experiments show an interaction between YjdA and YegE. My results further suggest the aid of the bacterial flotillins HflK/C in the regulation of YegE by the dynamin YjdA.

Altogether, the results in this thesis provide an overview of the roles of flagella and motility during biofilm formation of *Escherichia coli*, which includes a requirement of swimming during biofilm initiation, thereby tight regulation of c-di-GMP during the course of biofilm formation, and a structural role of flagella at the later biofilm stage.

ACKNOWLEDGMENT

First and foremost, I would like to thank Prof. Dr. Victor Sourjik for the opportunity to do my PhD in his laboratory and for the chance to work on such an intriguing topic.
Secondly, I want to thank Dr. Axel Mogk for being my second supervisor and helpful discussions during my TAC meetings.
Furthermore, I want to thank Prof. Dr. Rüdiger Hell, who was also member of my TAC for his ideas and comments on my project.
I am also very thankful to Prof. Dr. Elmar Schiebel for letting me finish my experiments in his laboratory and for his efforts to support the last phase of my PhD.

Additionally, I want to thank all the former and present lab members of the Sourjik lab, who helped me on my way to finish this thesis with their advise, discussions, encouragement and enjoyable conversations. I thank Olga Besharova and Dr. Anja Paulick for proofreading my thesis and for their helpful comments.
I also want to thank all the people who supported my work with sharing strains, constructs and protocols.
I am also very grateful to the lab members of the Schiebel lab, who welcomed me in such a warm way that I never felt strange but as being part of their lab!

Ich möchte mich auch bei meiner Familie und vor allem bei meinen Eltern bedanken, da sie mich immer unterstützt haben und für mich da waren, wenn ich sie gebraucht habe.

Michael danke ich für seine aufmunternden Worte, Unterstützung und Liebe.

Schriesheim, Juli 2016

Verena Suchanek

CONTENTS

Part I

INTRODUCTION

1. BIOFILMS

The discovery of biofilms dates back to the late 1600s when the Dutch scientist Antonie van Leeuwenhoek described 'animalcules', aggregated microorganisms, that he observed in his dental plaque [1, 2]. Since then, hundreds of groups have studied biofilm formation in many different bacterial species. It has become clear that the planktonic mode of growth as studied in agitated cultures in the laboratory does not provide a sufficient picture about bacteria in natural settings but rather an incomplete one. In natural settings, especially in aquatic settings, most microorganisms exist in multicellular communities, often as submerged biofilms on surfaces [3, 4].

Biofilms are defined as multicellular communities of microorganisms that are embedded in a self-produced matrix and often grow on surfaces. Through the matrix, biofilm cells stick to each other and, in the case of surface-attached biofilms, to the surface. In addition, the matrix provides protection against environmental cues, such as predation by protozoans or bacteriophages in nature and the host immune defence in medical settings. Especially the occurrence of biofilms in medical settings makes it important to analyze and study biofilm formation. The probably most studied organism in biofilm research is the opportunistic pathogen *Pseudomonas aeruginosa* (*P. aeruginosa*), which for example forms biofilms in the lungs of cystic fibrosis (CF) patients. These biofilm infections are difficult to treat with antibiotics and many CF patients die of lung failure as a consequence of multiresistant *P. aeruginosa* infections.[5].

Despite the pivotal role of *P. aeruginosa* in biofilms, many genetic analyses in biofilms have been performed with *Escherichia coli* (*E. coli*) because it can be handled in the laboratory with relative ease and its genetic background has been extensively studied in the past decades. Besides the harmless gut commensal *E. coli* serotypes, there are many pathogenic *E. coli* strains that can cause severe infections in humans that include biofilm formation. Pathogenic *E. coli* can cause intestinal infections, such as enteropathogenic *E. coli* (EPEC) and enterohaemorrhagic *E. coli* (EHEC), or extra-intestinal infections. Extra-intestinal *E. coli* are a common cause of urinary tract infections (uropathogenic *E. coli* (UPEC)), sepsis or meningitis (meningitis-associated *E. coli* (MNEC)) [6]. Furthermore, *E. coli* has also been found in medical device related infections, such as urinary cathether cystitis [2].

Altogether, understanding *E. coli* biofilms might help to find new strategies to combat many biofilm-related infections.

1.1 Phases of biofilm formation

Many naturally occurring biofilms exist as submerged biofilms, i. e. growing on liquid-surrounded surfaces [7]. Biofilm formation of *E. coli* and other motile bacteria on a surface has been described to involve several stages [8, 9] (see figure 1.1). The main developmental step in biofilm formation is the transition from a planktonic, often motile stage, to a sessile stage. Bacteria from the motile planktonic phase attach to the surface, where the production of biofilm matrix factors is increased. Attached cells aggregate into microcolonies, which are held together by the matrix. In *E. coli*, the matrix includes proteinaceous curli fibers on the cell surface and exopolysaccharides (Poly-N-acetylglucosamine (PGA) and colanic acid). The microcolonies mature into macrocolonies and finally develop into a biofilm. The mature biofilm can subsequently dissolve in a phase called dispersion.
One of the most important regulatory steps in biofilm formation is the transition from motility to sessility. This involves downregulation of motility when cells attach and upregulation of matrix factors during biofilm maturation. A central player in this transition is the second messenger bis-(3'-5')-cyclic dimeric guanosine monophosphate (c-di-GMP), which negatively regulates motility and positively regulates the production of matrix factor in many bacterial species [10, 11, 12]. In the following, I will discuss the aspects of biofilm formation in *E. coli*, especially with regards to the role of motility, c-di-GMP signaling and the biofilm matrix.

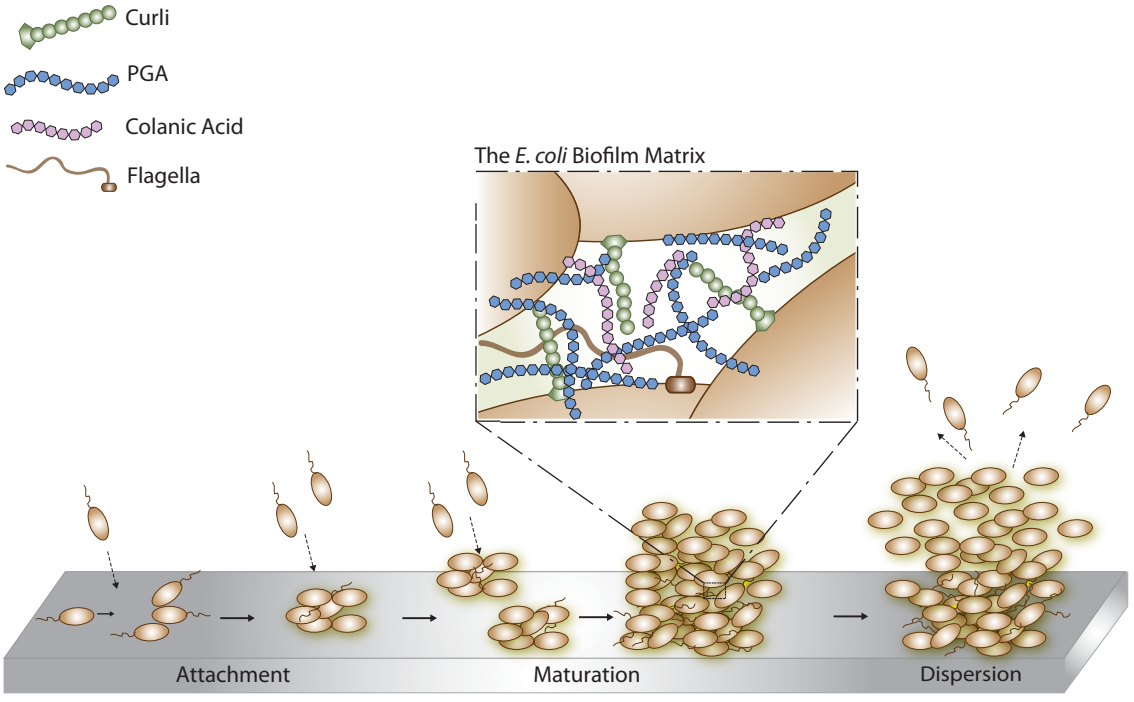

Fig. 1.1. Phases of biofilm formation in *E. coli*.
Submerged biofilm formation on a surface involves the attachment of planktonic cells at the surface (attachment phase), where the cells aggregate into microcolonies. These microcolonies mature into a biofilm, which contains characteristic biofilm matrix (maturation phase). The biofilm can dissolve again (dispersion), where cells are released from the biofilm.

2. MOTILITY AND ITS REGULATION IN BIOFILM FORMATION

2.1 Bacterial motility and surface attachment

Bacterial cells exhibit several ways of motility ranging from swimming in liquid to swarming and gliding on surfaces. Many bacteria, including *E. coli*, move by means of flagella that propel the cells forward in aqueous environments (swimming) or on surfaces (swarming). In a different mechanism, *P. aeruginosa* use Type IV pili for twitching motility whereas others, such as *Myxococcus xanthus*, glide on surfaces with a focal adhesion-based mechanism [13, 14, 15, 16].

Flagella-mediated motility is the most studied form of motility in bacteria and many biofilm-forming cells swim in their planctonic state. Nevertheless, in their biofilm state, bacteria are usually non-motile [9]. Hence, one of the main cellular processes during biofilm formation is the regulation of motility to allow a transition from the motile to the sessile state. A key player in this regulation is the second-messenger c-di-GMP. In *E. coli* and *Salmonella*, c-di-GMP negatively controls flagellar motility via motor curbing ([10, 11, 12]; see section 2.3 and chapter 3). Additionally, c-di-GMP is a positive regulator of biofilm matrix production, which is required for biofilm maturation (see section 3.4). Another pathway regulating flagella-mediated motility is the bacterial chemotaxis pathway, which is probably the most studied two-component signaling system in bacteria ([17], see section 2.2). Bacterial chemotaxis allows cells to reorient in gradients of attractants and repellents by changing the rotation direction of the flagellum in response to stimuli. In contrast to the generally accepted view of c-di-GMP as a biofilm promoting factor, the contribution of the chemotaxis pathway to biofilm formation has not been clarified yet. There are studies supporting the idea that chemotaxis might be important in biofilms, whereas others neglect that hypothesis (see section 2.2.1). Irrespective of the exact contribution of chemotaxis, the transition from the motile to the sessile state requires tight regulation of motility, especially regarding the possible roles motility might play at several biofilm stages, which excludes a simple shut-off of motility. First of all, motility may be important during attachment for bacteria to reach surfaces and secondly to overcome repulsive forces at the surface. Additionally, moving along the surface may be an important step before attachment and later during biofilm expansion [18]. Indeed, interfering with motility and its regulation has been reported to result in changes in biofilm formation in several bacterial species, such as *E. coli* or *P. aeruginosa* (e. g. [19, 18, 20, 21, 22, 23, 24, 25, 26]). *E. coli* strains with impaired motility show reduced surface attachment and fail to develop biofilms [19, 18, 25]. Furthermore, biofilm initiation is defective in *P. aeruginosa* strains

that carry mutations interfering with flagellar and twitching motility [20]. Later studies, however, suggest that initial microcolonies of *P. aeruginosa* develop by clonal growth rather by motility-driven cell aggregation. Nevertheless, twitching motility has been shown to be required for the formation of the mushroom-like structures in mature biofilms of *P. aeruginosa* [22, 23]. Similarly, studies in *E. coli* suggest a contribution of motility and / or flagella to mature biofilm architecture [24, 27]. Altogether, these studies indicate that motility might affect biofilm formation in multiple ways and requires differentiated regulation at the respective biofilm stages. However, the timing of the motility regulation and the exact contribution of motility during the different biofilm stages remain to be elucidated.

2.2 Chemotaxis

Bacteria can sense and respond to environmental signals, such as nutrient availability, pH, or temperature (for reviews see [28, 17, 29]). The chemotaxis signaling pathway is the two-component-like system that is responsible for coupling sensing of environmental cues to bacterial motility (see figure 2.1) [30, 31, 32]. In *E. coli*, chemotaxis governs the rotation direction of the flagellum, thereby controlling whether the cell swims forward (counter-clockwise rotation) or reorients in a tumble (clockwise rotation) [33]. *E. coli* possesses six to eight flagella that are randomly distributed over the cell. Flagella rotation is driven by ion motive force that is generated by the flagellar motor. The motor consists of the rotor and stator complexes that interact for flagella rotation [34]. Rotational direction of the flagellum is regulated by the interaction of the response regulator CheY and the switch protein FliM at the motor [35, 36]. CheY activity in turn is regulated by the histidine kinase CheA [37, 38].

Gradients of nutrients or repellents are sensed by periplasmic domains of chemotaxis receptors, the methyl-accepting chemotaxis proteins (MCPs). *E. coli* possesses five different receptors, Tar, Tsr, Trg, Tap and Aer, which are responsible for sensing different signals. The receptors together with the kinase CheA and the small adaptor protein CheW cluster in chemoreceptor signaling complexes at the cell poles [39]. CheA activity depends on the activation state of the receptors, which is modulated by ligand binding and receptor methylation. In the absence of attractant, CheA is autophosphorylated and in turn phosphorylates the response regulator CheY. Phospho-CheY interacts with FliM at the motor and induces clockwise rotation. The signal is terminated by dephosphorylation of CheY by the phosphatase CheZ [40, 41].

Apart from CheY, there is a second response regulator of the kinase CheA, which is the methylesterase CheB [42]. CheB, together with the S-adenosyl methionine-dependent methyltransferase CheR constitute the adaptation system of chemotaxis providing a short-term memory of gradient sensing. CheR and CheB methylate and demethylate the receptors at specific glutamate residues thereby modulating their activation state. Methylation of the receptors increases receptor activity, which in turn increases CheA activity. This

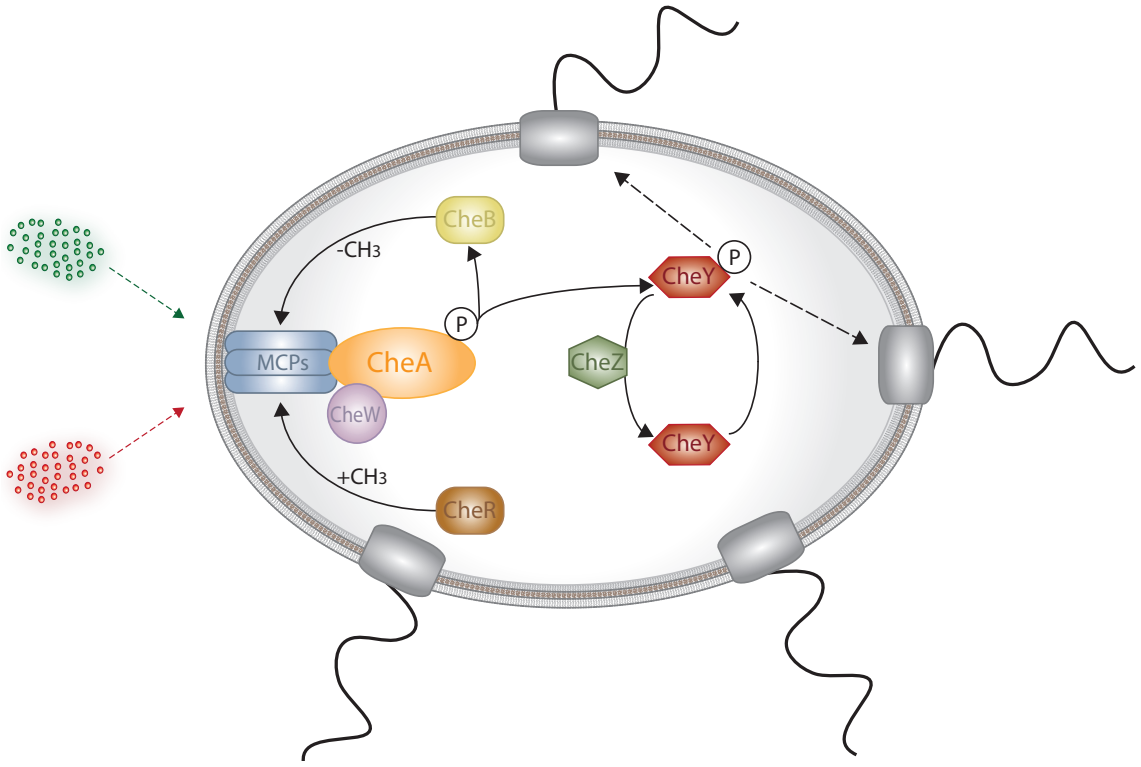

Fig. 2.1. Schematic representation of the chemotaxis signaling pathway.
Using chemotaxis, *E. coli* and other bacteria respond to environmental gradients of attractants (green) and repellents (red). Binding of ligands to the receptors (MCPs; methyl-accepting chemotaxis proteins) regulates autophosphorylation of the kinase CheA, which in turn regulates phosphorylation of the response regulator CheY. CheY binds to the flagellar motor where it changes flagella rotation from counter-clockwise to clockwise rotation, inducing tumbling and thereby reorientation of the cell. The sensing of attractants leads to dephosphorylation of CheY by the phosphatase CheZ and thereby counter-clockwise rotation of flagella and smooth swimming. Methylation and demethylation of MCPs by CheR and CheB influences their activation state and in turn CheA activity thereby balancing the chemotactic response.

allows to adapt to present concentrations of attractants since activity of CheA is shifted back to a pre-stimulus level, allowing sensing of new changes in attractant concentrations [43, 29].

2.2.1 Chemotaxis in biofilms

Biofilm growth is a common way of bacterial growth in nature and constitutes an important part of bacterial survival strategies. Therefore, it seems logical that the decision where to form biofilms in an ever changing environment takes an important role. Chemotaxis could help to coordinate behavior of bacterial communities in a way that biofilms form in response to environmental changes. One possibility is that bacteria could sense attractants, which are in proximity to a surface, and as a response colonize this surface. Another possible role of chemotaxis could be the sensing of attractants present in an already forming biofilm to sample more bacteria into that biofilm. Unpublished results from

our laboratory (Lagonenko *et al.*) show that *E. coli* can aggregate via chemotaxis to the quorum sensing molecule autoinducer 2 (AI-2) and the aggregates can continue to form a biofilm when settling on a surface. Last but not least, during dispersal, repellents in the biofilm or attractants in the surrounding environment could elicit a chemotactic response and directed movement out of the biofilm.
The role of chemotaxis in biofilms has been studied in different organisms. For *E. coli*, it was shown by Pratt and Kolter that chemotaxis per se is not essential for *E. coli* biofilm formation [18, 21]. They demonstrated normal biofilm formation of the chemotaxis knockout strain Δ*cheA-Z* in microtiter dishes. However, other studies showed later that mutations in the chemotaxis system affect biofilm formation in *E. coli* and several other species [25, 44, 45, 26, 46]. Niba and colleagues for instance showed a defect in *E. coli* biofilm formation if the chemotaxis phosphatase CheZ was deleted [25]. Two other studies in *P. aeruginosa* suggested that chemotaxis was required for surface sampling in microtiter dish biofilms [26] and for cap formation in the typical mushroom-like flow-chamber biofilms [45]. Yet another study claims a role of aerotaxis in pellicle bioiflm formation of *Shewanella oneidensis* [46]. Hence, it remains to be elucidated if and to what extent chemotaxis is needed for biofilm formation in *E. coli*.

2.3 YcgR: A breaking mechanism to reduce flagellar motility

The first connection between c-di-GMP and motility has been discovered by Ko and Park in 2000, where they used an *hns* deletion strain [47]. H-NS (Histone-like nucleoid structuring protein) is a DNA-binding protein that amongst other genes regulates the expression of the flagella master regulator genes *flhDC*. A *hns* deletion strain is therefore unflagellated and non-motile. Ko and Park found that expression of FlhDC in Δ*hns* restores flagellation, however motility is still reduced. If they in addition introduced a mutation in *ycgR* or overexpressed the phosphodiesterase YhjH, an enzyme that degrades c-di-GMP (see chapter 3), the motility defect of Δ*hns* was suppressed. Later, it was found that deletion of *yhjH* reduces motility in Salmonella [48, 49]. In a motility screen [50], Girgis and colleagues observed in agreement with the previous studies in *Salmonella* that deletion of the phosphodiesterase YhjH in *E. coli* leads to inhibition of swimming motility on soft agar plates. They could suppress this motility defect by additionally deleting the diguanylate cyclase YegE, an enzyme that generates c-di-GMP (see chapter 3). Furthermore, deletion of the *ycgR* gene restored motility in Δ*yhjH*. YcgR contains a PilZ domain, a domain that at that time was already known to bind c-di-GMP [51]. Binding of c-di-GMP to the PilZ domain in YcgR introduces a significant conformational change of the protein that stabilizes c-di-GMP binding [52]. The idea that c-di-GMP regulates flagellar motility via YcgR has been suggested in reviews [53, 54] and led to a series of new studies, where the functional mechanism was investigated.
The c-di-GMP pool that locally acts on the flagella via YcgR is supposedly controlled by a subset of four diguanylate cyclases - YegE, YedQ, YfiN and DosC - and the phosphodi-

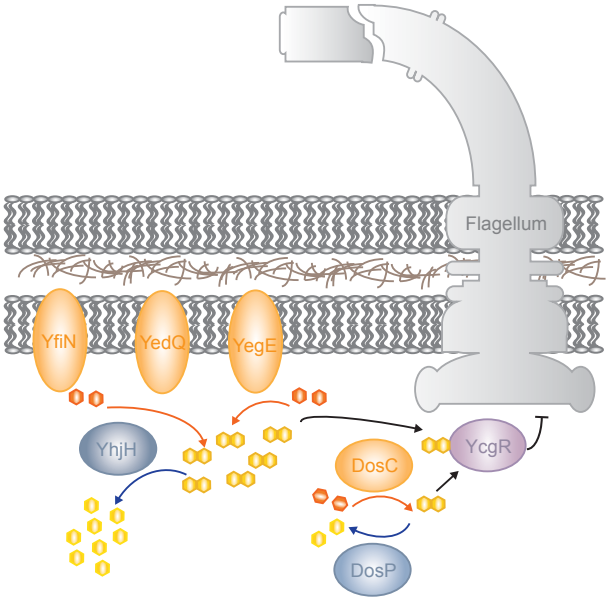

Fig. 2.2. Model of regulation of flagellar motility by c-di-GMP in *E. coli*.
The local pool of c-di-GMP, which controls flagellar motility in *E. coli* is balanced by the actions of the diguanylate cyclases YegE, YedQ, YfiN and DosC and the phosphodiesterase YhjH. C-di-GMP binds to YcgR, which in turn interacts with the motor.

esterase YhjH [55, 56] (see also figure 2.2). Two models about YcgR action at the flagellar motor have been proposed. In the first, which is based on studies in *Salmonella* and *E. coli*, YcgR supposedly interacts with the switch complex proteins FliG and FliM [57, 58], which are responsible for setting the rotation direction of the flagellum. In the presence of c-di-GMP, this interaction is strengthened and induces a counter-clockwise bias of flagellar rotation. Consistently, c-di-GMP was shown to induce a counter-clockwise bias in the above described screen from Girgis et al [50]. Additionally, Paul and colleagues [58] showed that c-di-GMP binding to YcgR leads to a reduction of flagella rotation speed. The second model, which is based on experimental work in *E. coli*, has been suggested by Boehm and colleagues [56]. They showed that YcgR interacts with the flagellar motor protein MotA thereby inactivating individual stator units. This leads to curbing of the motor and reduction in swimming speed.

2.4 Regulation of motility gene expression in biofilms

Apart from post-translational mechanisms, such as c-di-GMP mediated adjustment of swimming, there are multiple transcriptional events that control motility during biofilm formation [59]. Many of the transcriptional regulators of motility inversely regulate the synthesis of adhesion factors. In this way, the cascades controlling motility and adhesion are strongly interconnected allowing the establishment of a delicate balance between the two lifestyles.

Motility gene expression in biofilms is mainly regulated on the level of the flagella master regulator FlhDC. The Rcs (Regulator of capsule synthesis) phosphorelay system is a potential candidate for this transcriptional regulation [60]. In the Rcs system, a sensor kinase RcsC autophosphorylates and the phosphate is transferred via RcsC to the response regulator RcsB. Phospho-RcsB together with the protein RcsA regulates the expression of diverse genes, amongst which are the flagella master regulator genes *flhDC*. FlhDC and thereby motility are downregulated by the Rcs system and disruptions in Rcs signaling on the one hand enhance motility and on the other hand impair biofilm formation. This inhibition of biofilm formation in Rcs mutants is explained by the fact that Rcs positively regulates the synthesis of colanic acid, which constitutes part of the *E. coli* biofilm matrix. Thus, Rcs inversely coordinates motility and biofilm formation.

FlhDC expression is further negatively controlled through the regulatory protein FliZ, a repressor of σ^S regulated genes, which is part of the inverse regulatory control of motility and curli-mediated adhesion in *E. coli* [55, 61]. Curli are amyloid fibers on the cell surface and require the transcription factor CsgD for expression, which in turn is controlled by a cascade of σ^S regulated genes. FliZ itself is expressed under the control of FlhDC and thereby constitutes a negative feedback loop on FlhDC. This inhibition of motility in the context of the inhibitory role of FliZ on the curli (sessility) cascade might help to balance the switch from motility to sessility [61]. CsgD, the transcription factor for curli expression, is a major player in this switch. Its expression is c-di-GMP dependent and raises with cells entering the stationary phase and with the onset of biofilm formation (see also chapter 3). Consistently, CsgD inhibits the expression of flagella genes thereby balancing the motility versus adhesion decision towards sessility [62].

Another important regulator during biofilm formation is the RNA-binding protein CsrA [63, 64]. CsrA is a master regulator that in addition to regulating motility and biofilm formation regulates several other pathways, such as glycolysis or gluconeogenesis. Motility is positively regulated by CsrA on the level of FlhDC [65]. Additionally, CsrA decreases expression of the diguanlate cyclases YdeH and YcdT [66] and the *pgaABCD* genes [67] that encode enzymes for the synthesis of PGA (Poly-N-acetylglucosamine), another component of the *E. coli* biofilm matrix. Thereby, CsrA positively regulates motility and negatively regulates biofilm formation by inhibiting PGA synthesis.

In summary, the transcriptional events regulated by the Rcs system, FliZ, CsgD and CsrA inversely coordinate the expression of motility genes and the biofilm matrix factors colanic acid, curli and PGA synthesis, constituting an important role in the transition from the motile to sessile lifestyle.

In addition to the transcriptional control of motility, there is also a network of small regulatory RNAs (sRNAs), regulating motility and biofilm formation on the mRNA level (for a review see [68]). Most of the sRNAs that affect motility control FlhDC expression by directly binding to *flhDC* mRNA. Some of these sRNAs have additional impact on the expression on biofilm genes and thereby motility and biofilm formation are linked on yet another level.

3. C-DI-GMP SIGNALING

The second messenger bis-(3'-5')-cyclic dimeric guanosine monophosphate (c-di-GMP) has been discovered in 1987 by Ross and colleagues as cellulose synthase activator (CSA) in *Acetobacter xylinum*, now *Gluconacetobacter xylinus* [69]. Since then, hundreds of studies about this bacterial second messenger have been published and numerous reviews have summarized the actions of c-di-GMP (for references see e. g. [70, 10, 71, 11, 72, 73, 74, 12]). Today, c-di-GMP is recognized as a universal bacterial second messenger and has established a huge new field of research. C-di-GMP controls a vast variety of cellular functions including cell cycle, virulence, cell morphogenesis and most importantly for this work, motility and biofilm formation. It is a key factor in the transition from the motile to the sessile lifestyle inversely regulating motility and the synthesis of biofilm matrix factors.

3.1 Synthesis and degradation of c-di-GMP

C-di-GMP is synthesized by GGDEF (Gly-Gly-Asp-Glu-Phe) domain containing diguanylate cyclases (DGCs) from two guanosine triphosphates (GTPs) [69, 75]. Degradation of c-di-GMP into phosphoguanylyl-guanosine (pGpG) and guanosine monophosphate (GMP) is performed by EAL (Glu-Ala-Leu) or HD-GYP (His-Asp, Gly-Tyr-Pro) domain containing phosphodiesterases (PDEs) [76, 77, 78]. In many cases, these enzymes contain both GGDEF and EAL domains, however, possess only one of the enzymatic functions. Therefore, in addition to the active GGDEF and EAL domains that confer DGC or PDE activity, there are also degenerate, inactive GGDEF and EAL domains. These degenerate domains can have structural or regulatory roles, such as constituting c-di-GMP receptors that orchestrate downstream processes [79]. For example, the LapD protein of *Pseudomonas fluorescens* (*P. fluorescens*) contains a functionally inactive GGDEF and EAL domain. C-di-GMP binds to the EAL domain of LapD. LapD regulates secretion and surface retention of the adhesin LapA, which is required for *P. fluorescens* surface attachment. Thereby, c-di-GMP binding to LapD controls adhesin secretion and biofilm formation of *P. fluorescens* [80, 81, 74].

Most of the DGCs and PDEs contain one or more sensory domains that allow control of enzymatic activity through environmental and cellular signals, such as PAS (Per-ARNT-Sim), MASE (membrane-associated sensor), REC (Receiver domain) or BLUF (blue light sensing; sensors of blue-light using FAD) domains. In many cases, DGCs and PDEs are membrane-standing and have periplasmic loops that can have roles in ligand binding (see

e. g. [11, 71, 12]).

3.2 Sensing of c-di-GMP

The integration of c-di-GMP into the cellular signaling network needs sensing of distinct c-di-GMP concentrations. In the cell, there are different types of c-di-GMP receptors, such as diverse protein receptors and riboswitches [79]. The first type of c-di-GMP sensors has been named after the PilZ protein in *P. aeruginosa* [82]. The discovery that the PilZ domain (Pfam: PF07238) is a c-di-GMP receptor is based on a bioinformatical study that predicted this function for the PilZ domain in the cellulose synthase BcsA from *G. xylinus* [51] and was confirmed experimentally for the PilZ of BcsA and YcgR [83]. YcgR, as described previously (see section 2.3), is the c-di-GMP receptor in *E. coli* that controls swimming motility through interacting with the flagellum.
As mentioned above in section 3.1, there are GGDEF and EAL domain containing proteins that have lost there enzymatic activities. However, degenerate GGDEF domain proteins often retain there so-called I-site, which is the site where c-di-GMP can allosterically bind. In many cases, the I-sites of degenerate GGDEF proteins can serve as c-di-GMP receptors, as e. g. in PopA, a cell cycle regulator in *Caulobacter crescentus* [84]. Degenerate EAL domains can also serve as c-di-GMP receptor domains, such as in LapD in *P. fluorescens* [80, 81, 74].
Last but not least, c-di-GMP responsive riboswitches have been discovered [85, 79]. Riboswitches are domains in mRNAs that respond to binding of ligands by changing gene expression on the level of transcription, mRNA stability or translation.

3.3 Physiological relevance of c-di-GMP in biofilms

Biofilm formation in many bacterial species coincides with c-di-GMP production. In general, c-di-GMP is viewed as a biofilm-promoting factor that drives the transition from a motile to a sessile lifestyle. C-di-GMP has been recognized as an inhibitor of swimming, swarming, twitching and gliding motility and can therefore be considered a global motility suppressor. The transition from motility to sessility not only requires shut down of motility, but also the production of biofilm matrix. This is the second role c-di-GMP plays during biofilm formation: it is a positive regulator of biofilm matrix synthesis.

3.3.1 The motility-to-sessility transition in *E. coli*

In *E. coli*, the motility-to-sessility transition involves inhibition of motility by c-di-GMP through the effector protein YcgR (see chapter 2.3). As c-di-GMP levels rise, c-di-GMP loaded YcgR interacts with the flagellar motor and induces motor curbing resulting in a decrease of swimming speed, driving the bacteria from motility into sessility. With the increase in intracellular c-di-GMP levels, the synthesis of the *E. coli* matrix components is induced (see figure 3.1). In general, the biofilm matrix provides stability to the biofilm,

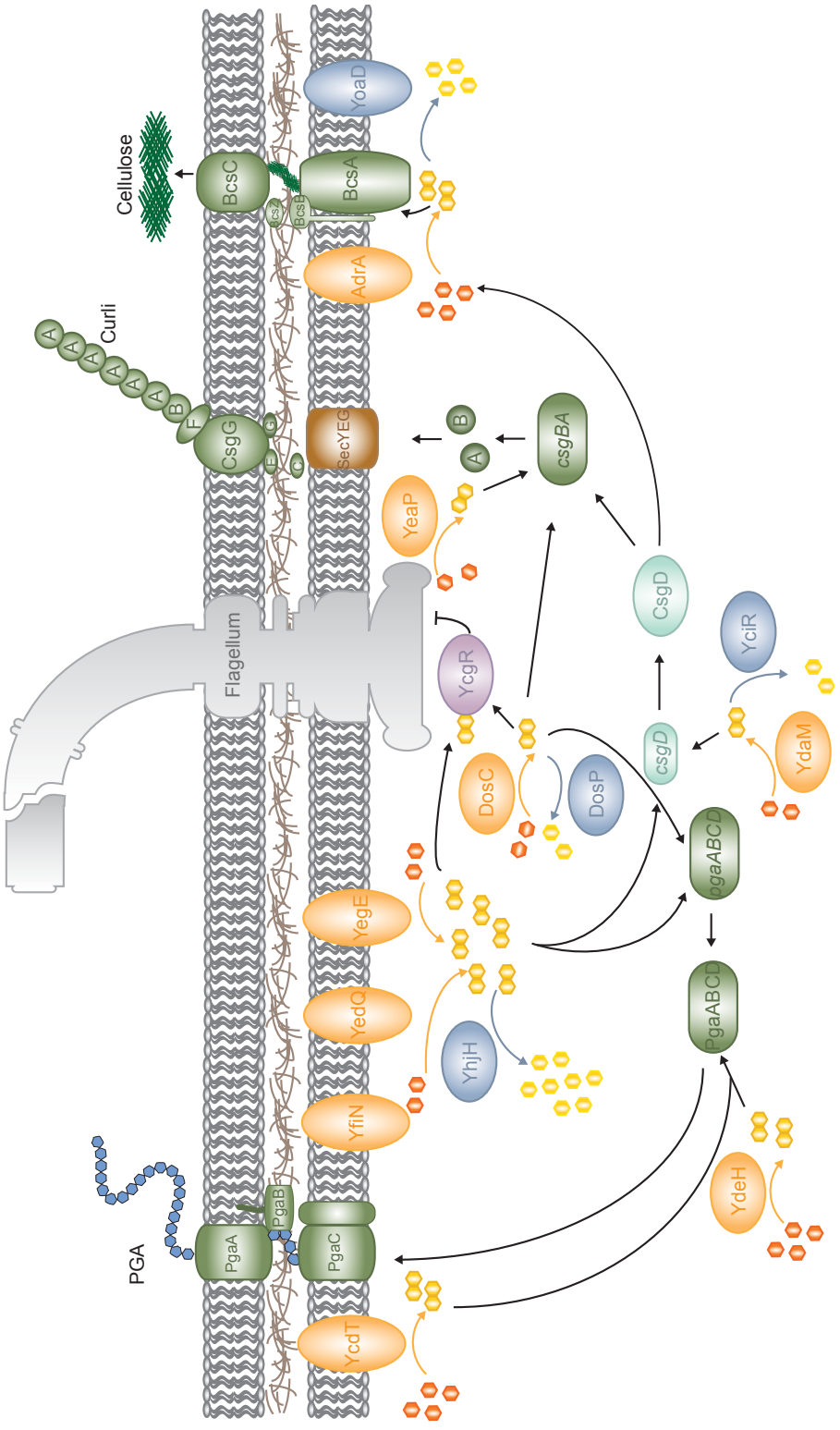

Fig. 3.1. Overview of c-di-GMP signaling in *E. coli*.
C-di-GMP is synthesized by diguanylate cyclases (DGCs; shown in orange) and turned over by phosphodiesterases (PDEs; shown in blue). A local c-di-GMP pool, controlled mainly by the DGCs YegE, YedQ, YfiN and DosC and the PDE YhjH, negatively regulates motility via the PilZ-domain protein YcgR (violet). Positive regulation of matrix production by c-di-GMP is shown for Poly-N-acetylglucosamine (PGA), Curli fibers and Cellulose.

helping cells to adhere to each other and the surface, on which the biofilm forms. The c-di-GMP dependent matrix of *E. coli* includes the polysaccharides Poly-N-acetylglucosamine (PGA) and Cellulose and the amyloid curli fibers. In contrast to curli and PGA, cellulose is not produced by the commonly used *E. coli* K-12 lab strains due to a premature STOP codon in one of the *bcs* (bacteral cellulose synthesis) genes [86]. Thus, caution has to be taken if experimental results from the laboratory are transposed to the environmental setting.

3.4 Regulation of matrix components

PGA

The polysaccharide Poly-N-acetylglucosamine is produced by several bacterial species including *Staphylococcus epidermidis* (PIA; polysaccharide intercellular adhesin), *Staphylococcus aureus* (PNAG; *Poly-N-acetyl-glucosamine*) and *E. coli* (PGA; Poly-N-acetylglucosamine). The differences between PNAG, PIA and PGA lie in the chain length and modifications of linked glucosamine (for a review see [87]).
In *E. coli*, the genes for the PGA synthesis apparatus lie on the *pgaABCD* operon [88]. C-di-GMP regulates PGA production both on a transcriptional and posttranscriptional level (see figure 3.1). C-di-GMP produced by the DGC DosC controls the expression from the *pgaABCD* locus [89]. Posttrancriptional control is driven by the activity of the DGCs YdeH and YcdT [90, 91]. C-di-GMP binds to PgaC and PgaD increasing PgaD stability and promoting the PgaC-D interaction. The net result of increased c-di-GMP production by DosC, YdeH and YcdT is thereby stimulating PGA synthesis.

Curli

Curli are amyloid protein fibers on the cell surface that are part of the biofilm matrix in enterobacteria (for curli reviews see [92, 93, 94]). The genes for curli synthesis lie on the curli structural operon *csgBAC* and the *csgDEFG* operon (csg for curli-specific genes) [95]. While CsgD is the master regulator for curli production, CsgB and CsgA make up the structural components. Soluble curlin subunits of CsgA are produced in the cytoplasm and secreted through SecYEG into the periplasm (see figure 3.1). Further transport to the cell surface is facilitated via the CsgG channel. Nucleation into curli fibers occurs at the cell surface and requires the nucleator protein CsgB [92, 96, 93, 94].
C-di-GMP regulates curli biogenesis both on the transcriptional and posttranscriptional levels (see figure 3.1). CsgD transcription is controlled by the DGC-PDE modules made up by YegE and YhjH and YdaM and YciR [97, 55, 11, 98]. YdaM and YciR form a complex with the transcription factor MlrA with YciR both inhibiting YdaM and MlrA. When c-di-GMP produced by the YegE/YhjH module increases, YciR binds c-di-GMP, which results in a relieve of its inhibitory role on YdaM. As a consequence, c-di-GMP levels made by YdaM raise. MlrA activity is stimulated by YdaM and activates CsgD transcription [98].

CsgD in turn regulates transcription from the curli operons *csgDEFG-csgBAC*. Apart from this indirect control via CsgD, there is also direct control of *csgBAC* expression, which is exerted through the activity of the DGC/PDE pair DosC/DosP, [99, 100]. A third DGC, YeaP has also been shown to be involved in *csgBAC* expression, however whether it controls CsgBA synthesis on a transcriptional or post-transcriptional level has to be unravelled [99].

Cellulose

Regulation of bacterial cellulose production by c-di-GMP has been originally described by Ross and colleagues in the 1980s in *G. xylinus* [69]. Cellulose is comprised of β-1,4-linked D-Glucose that arranges in microfibrils, which in turn form a mesh-like structure in the matrix of several bacterial species, including *E. coli* strains, *Salmonella* and *P. fluorescence* [101, 102, 103, 104, 87]. As mentioned above, *E. coli* K-12 laboratory strains do not produce cellulose, however, a W3110 derivative, in which cellulose synthesis was restored by Serra and colleagues [86] was used in this thesis. This strain forms highly structured biofilm macrocolonies on agar plates with cellulose making the colonies more elastic and stable [86]. In *E. coli*, genes for cellulose synthesis lie on the *bcs* locus (*yhjR-bcsQABZC* and *bcsEFG*; *bcs* for bacterial cellulose synthesis) [103, 105, 106]. BcsA is the cellulose synthase, which together with BcsB foms a complex in the inner membrane (see figure 3.1). BcsA contains the PilZ domain required for c-di-GMP regulation [51, 83]. BcsC is thought to form a channel in the outer membrane through which the nascent chains of linked D-Glucose are transported into the extracellular space [106]. Cellulose synthesis in *E. coli* is regulated by c-di-GMP on several levels. First of all, similar to curli synthesis, the expression of the master regulator CsgD is a prerequisite for the synthesis of cellulose. As described previously (section 3.4), CsgD transcription is controlled by two DGC-PDE modules (YegE-YhjH and YdaM-YciR) [97, 55, 11, 98]. CsgD drives the expression of the *adrA* gene encoding a DGC required for cellulose synthase activity and of the PDE YoaD, which has the opposing activity to AdrA, namely degrading c-di-GMP [107]. C-di-GMP in turn binds to the PilZ domain of BcsA [51, 83].

4. A NEW REGULATOR OF C-DI-GMP SIGNALING IN *E. COLI*

The second messenger c-di-GMP regulates a variety of cellular processes including biofilm formation. Even within its role as a biofilm promoting factor, c-di-GMP regulates several aspects of biofilm formation, such as synthesis of curli fibers, synthesis of PGA or inhibition of motility in *E. coli*. This raises the question how specificity is achieved with one molecule regulating such diverse signaling processes? How are environmental signals or signals from the inside of the cell integrated into the c-di-GMP network resulting in specific outputs? Especially the question of how specificity of c-di-GMP signaling is achieved is a pending question in the field. Possible solutions would be different specificities of c-di-GMP receptors or regulation of the expression or activity of specific DGC/PDE modules [73]. *E. coli* expresses more than twenty GGDEF and EAL domain proteins that are specifically expressed depending on growth phase and temperature [99]. Apart from the establishment of different expression patterns of DGCs and PDEs to time c-d-GMP production, another intriguing idea would be the generation of local c-di-GMP peaks. This could be achieved by restricting individual DGC/PDE modules to specific locations in the cell. This scenario is however difficult to imagine due to the lack of compartmentalization in bacteria. With the ubiquitous nature of c-di-GMP in bacteria and its importance in biofilm-related processes, it is important to understand the regulation of c-di-GMP signaling and identify new regulators of c-di-GMP signaling.

In their screen for motility mutants, Girgis and colleagues observed that the deletion of a so far uncharacterized ORF, *yjdA*, complemented the motility defect of a strain, which lacks the PDE YhjH [50]. The gene product of *yjdA* is a homologue to eukaryotic dynamin containing a dynamin-like GTPase sequence, which might have similar functions as eukaryotic dynamins [108]. How the dynamin YjdA is related to regulation of c-di-GMP signaling has not been investigated so far. Nevertheless, the involvement of a dynamin in c-di-GMP signaling might provide a new interesting mechanism of how this second messenger is regulated. The dynamin could impose local membrane curvature affecting the activity of membrane-bound DGCs or EALs. However, this idea is mere speculation at this point and needs thorough investigation.

Apart from its obvious involvement in c-di-GMP dependent regulation of motility [50], a role of YjdA in chromosome segregation has been suggested [109]. The authors describe that YjdA, which they renamed to CrfC (colocalization of the replication fork DNA by the clamp), forms homomultimers as has been described for dynamins. However, they do not refer to the involvement of YjdA in c-di-GMP signaling.

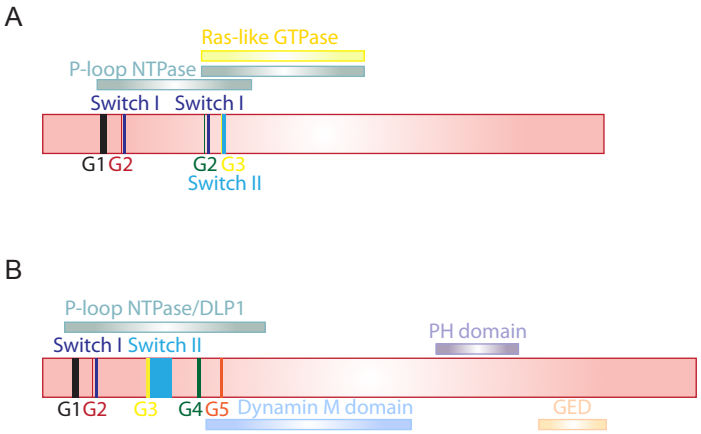

Fig. 4.1. Schematic drawing of YjdA and human Dynamin 1 structures.
(A) The bacterial DLP YjdA contains a G1 domain, two G2 domains, a G3 domain, Switch I and Switch II regions, and two P-loop NTPase domains.
(B) The human dynamin 1 contains G1-G5 domains, Switch I and Switch II domains, a P-loop NTPase domain, the dynamin M (central region) domain, a PH (Pleckstrin homology) domain, and a GED (GTPase effector domain).
Drawings of YjdA and dynamin 1 domain architecture were created after similarity search using the Conserved Domain Architecture Retrieval Tool (CDART) [110], which is available on http://www.ncbi.nlm.nih.gov/Structure/lexington/lexington.cgi

4.1 Dynamins and dynamin-like proteins

The discovery of dynamins dates back to the early 1970s when the *Drosophila* temperature-sensitive *shibire* mutant was described, which resulted in a paralytic phenotype [111]. Some years later, dynamin was discovered in a preparation of microtubules from calf brain as a nucleotide triphosphatase and its similarity to Mx proteins and yeast vacuolar protein sorting gene VPS1 suggested that they were a new family of GTPases [112, 113]. Finally, the *shibire* mutant phenotype was described to result from a defect in endocytosis and the *shibire* gene was mapped to dynamin [114, 115].
Today, we know that dynamin is a member of a large family of proteins - the dynamin superfamily. Dynamins are generally implicated in membrane scission events, which are e. g. required for vesicular trafficking. In eukaryotes, the dynamin superfamily includes the classical dynamins, the interferon-induced Mx-proteins, dynamin-like proteins (DLPs), optic atrophy 1 (OPA1), mitofusins and guanylate binding proteins / atlastins. The members of this superfamily are e. g. involved in the budding of vesicles (classical dynamins), RNA virus defense (Mx proteins), division of organelles (DLPs) and mitochondrial fusion (mitofusins and OPA1) (for reviews see [108, 116, 117]). The typical domain structure of dynamins comprises a large GTPase domain (around 300 amino acids), a middle domain (M domain), and a GTPase effector domain (GED) (see figure 4.1 B). The M domain and GED are responsible for oligomerization and thereby regulation of GTPase activity, which is dependent on and increases with the level of oligomerization [118, 119, 120, 116]. The GTPase domain comprises the G1-G4 regions (see figure 4.1), which contain the

GTP binding motif. Mutations in these regions have been described to e. g. block GTPase activity or leave the dynamin in a nucleotide-free state (GTPase domain website: http://www2.mrc-lmb.cam.ac.uk/Dynamin/GTPase.html, [121, 122]). In addition to the GTPase, the M domain and the GED, many dynamins contain targeting domains, such as a Pleckstrin homology (PH) domain or a proline-rich domain (PRD). The PH domain in the classical dynamin for example is responsible for interaction with lipid membranes [123].
In addition to eukaryotic dynamins, there is also a family of bacterial dynamin-like proteins (BDLPs), which comprises GTPases with a domain architecture that is similar to eukaryotic dynamins [108]. These BDLPs include BDLP of the cyanobacterium *Nostoc punctiforme* (*N. punctiforme*) and YjdA in *E. coli* [108, 124, 125, 126].

4.2 Bacterial dynamin-like proteins

In 2006, the structure of the bacterial dynamin-like protein BDLP from *N. punctiforme* has been dissolved by Low and colleagues [124]. The domain architecture of BDLP comprises a GTPase domain, a GED and M domain. The GED and M domain, however, are not separate domain entities as in classical dynamins but run in parallel. In the presence of a non-hydrolysable GTP analogue, BDLP shows self-assembling properties and binds to lipid bilayers. Lipid binding is mediated by a mobile paddle domain and induces membrane curvature [124, 125]. Low and Löwe have provided a model how BDLP and other DLPs might affect membrane topology [125]. They predict that upon GTP binding BDLP undergoes conformational changes that allow binding to the lipid bilayer. There, cooperative polymerization occurs, which leads to coating of the membrane with BDLP molecules inducing membrane curvature. When GTP is hydrolyzed, the BDLP-GDP coat on the membrane becomes unstable and disassembles. Disassembly is supposed to either cause relaxation of the membrane curvature back to the previous state or to induce membrane fission or fusion events (see reference [125] for details). The *E. coli* DLP YjdA (see figure 4.1 A) is a structural homologue to BDLP and has a GTPase sequence that is characteristic for dynamin family members [108]. YjdA, however, lacks the membrane-binding paddle domain that is present in BDLP [109]. It therefore remains to be elucidated how and whether YjdA might be involved in rearrangements of membrane topology and if this potential function is reated to its role in c-di-GMP signaling [50].

5. AIMS OF THIS THESIS

The formation of sessile biofilm communities from motile planktonic bacteria requires a balanced regulation of motility throughout several phases of biofilm formation. Although *E. coli* biofilm cells are immotile, previous research suggested multiple roles of flagella and flagella-regulated motility in *E. coli* biofilm formation. *E. coli* strains that either lack flagella or are flagellated but non-motile have a severely reduced ability to form biofilms [19, 18, 21, 25]. Flagella and motility could influence biofilm formation at different stages. During the early phase, swimming motility might enhance attachment, either by bringing bacteria to the surface [18, 21] or by flagella functioning as adhesins [127, 128, 129]. Flagella may further mediate surface sensing to trigger expression of biofilm-specific genes, such as those involved in matrix production [130, 131, 132, 133]. At the later biofilm stages, flagella may fulfil a structural role within the matrix, thereby contributing to the overall biofilm architecture [24, 27].

Regulation of flagella-mediated motility is mediated by the chemotaxis signaling pathway as well as by the second messenger c-di-GMP. Although chemotaxis per se is not essential for *E. coli* biofilm formation [18, 21], mutations in the chemotaxis system affect biofilm formation in *E. coli* and in several other species [25, 44, 45, 26, 46].

The goal of our study was to comprehensively analyse the functions of motility and flagella, both during early stages of *E. coli* submerged biofilm formation and in three-dimensional structures of mature biofilms.

Therefore, motility and chemotaxis genes were systematically deleted in the *E. coli* K-12 strain W3110. The mutants were screened for biofilm defects in a microtiter dish biofilm assay using crystal violet staining to quantify biomass. In our assay, flagella and motility were absolutely required for biofilm formation. Deletions that render *E. coli* immotile or severely impaired its motility were unable to form biofilms. Considering that biofilm formation is a dynamic process, we wanted to find out whether motility might affect biofilm formation differently depending on the biofilm stage. The effect of the respective gene deletions was therefore characterized in time-resolved biofilm formation assays using both crystal violet and microscopy as a readout.

In addition to chemotaxis deletion mutants, we further analyzed the effect of c-di-GMP signaling mutant strains that are supposed to have deregulated flagellar motility. For this purpose, we additionally used a second W3110 strain, which in contrast to our laboratory strain expresses a functional RpoS, the stationary phase σ factor. σ^S regulates many biofilm-related genes, among which are genes required for c-di-GMP signaling.

Besides their role in attachment, we investigated the involvement of flagella and motility

on three-dimensional structure formation in submerged biofilms. For this purpose, mature biofilms were grown and analyzed by confocal microscopy. We aimed to characterize the role of motility in biofilm architecture in two W3110 strain backgrounds, W3110^{RH} and AR3110. Both strains are RpoS-positive, however, their difference lies in the expression of biofilm matrix. The AR3110 matrix contains both curli fibers and cellulose, whereas in W3110^{RH}, cellulose synthesis is absent due to a mutation in the cellulose biosynthesis apparatus genes. Therefore, biofilm properties and overall architecture differ between the two strains and it is unclear whether motility might have similar effects in both strains.
Considering our results about the role of motility during attachment and in biofilm architecture, we next aimed to investigate the impact of the bacterial dynamin YjdA. YjdA has been shown to be involved in c-di-GMP regulated motility in *E. coli* [50]. We aimed to find out by which means YjdA affects c-di-GMP signaling and thereby motility regulation. We hypothesized that YjdA, considering known functions of dynamins, might modulate the plasma membrane in a way that c-di-GMP metabolizing enzymes in the membrane are affected in their activity. In this way, YjdA would enable the formation of local c-di-GMP pools. For this purpose, we investigated the role of YjdA in biofilm formation during attachment when swimming motility was required. Additionally, the effects of YjdA on biofilm architecture were analyzed. The search for potential interactors of YjdA that place the dynamin within the c-di-GMP signaling pathway included swimming assays, microscopy, fluorescence resonance energy transfer (FRET), bacterial two-hybrid assays and mass spectrometry.
Altogether, in this thesis we present multiple roles of flagella and motility throughout different stages of biofilm formation. Additionally, we describe a new regulator of c-di-GMP signaling, which influences both attachment and biofilm maturation.

Part II

ATTACHMENT OF *E. COLI* W3110 AND W3110^{RH} DURING BIOFILM FORMATION

6. ROLE OF MOTILITY DURING ATTACHMENT IN *E. COLI* BIOFILM FORMATION

Biofilms are usually considered as the immotile state of bacterial growth. However, most biofilm-forming bacteria are motile in their planktonic state and their biofilm formation involves the transition from motility to sessility. Therefore, regulation of motility during the process of biofilm formation is of utmost importance and exact contributions of motility during the different phases of biofilm formation have not been fully understood yet. During the formation of submerged biofilms at a surface, motile planktonic cells have to swim to the surface, start to attach and grow at the surface. Therefore, the first step of submerged biofilm formation is attachment at the surface, which can be quantified in the laboratory by different methods (see figure 6.1). I established and used two main different ways of quantification - staining of the whole biomass and imaging of attached bofilm cells. In general, biofilm precultures are grown in 24-well plates and subcultured into 96-well plates, where biofilm formation is monitored (figure 6.1 A, B). Non-attached cells are removed by washing and attached cells are quantified. The most common method is to stain attached biomass with crystal violet (CV) [134, 135, 136, 137], which basically stains cells and matrix components at the bottom and the wall of the microtiter dish well. The drawback of this method is, that it is not sensitive enough to monitor the very early phases of attachment, where single cells adhere to the surface. To do so, I established a microscopy assay, where I mix wild type with mutant cells labeled with different fluorescent proteins at similar ratio. This allows for a direct comparison between the number of attached wild type and mutant cells at the bottom of imaging plates (figure 6.1 B). Alternative methods to quantify biomass are shown in figure 6.1 C. To correlate biomass stained with CV with the actual amount of living cells, I used the commercial BacTiter-Glo^{TM} assay from Promega, which relatively quantifies the amount of metabolically active cells by measuring the ATP content of cells with a luciferase assay. The carbohydrate part of biomass can be stained with fluorescently labeled wheat-germ agglutinin. The difference in quantified biomass for Δ*fliC* in figure 6.1 C arise most probably through differences in the sensitivity of the staining methods. However, due to its fast and easy application, I chose to use the crystal violet assay for quantification of biomass in the results shown in this thesis.

The role of motility during attachment of *E. coli* cells was studied with two different wild type strains. From our laboratory strain collection, I chose the *E. coli* K-12 strain W3110, which showed highest biofilm forming capacity among our wild type strains. The major drawback of this strain however is, that it carries the *rpoS396(Amber)* (*Am*) allele

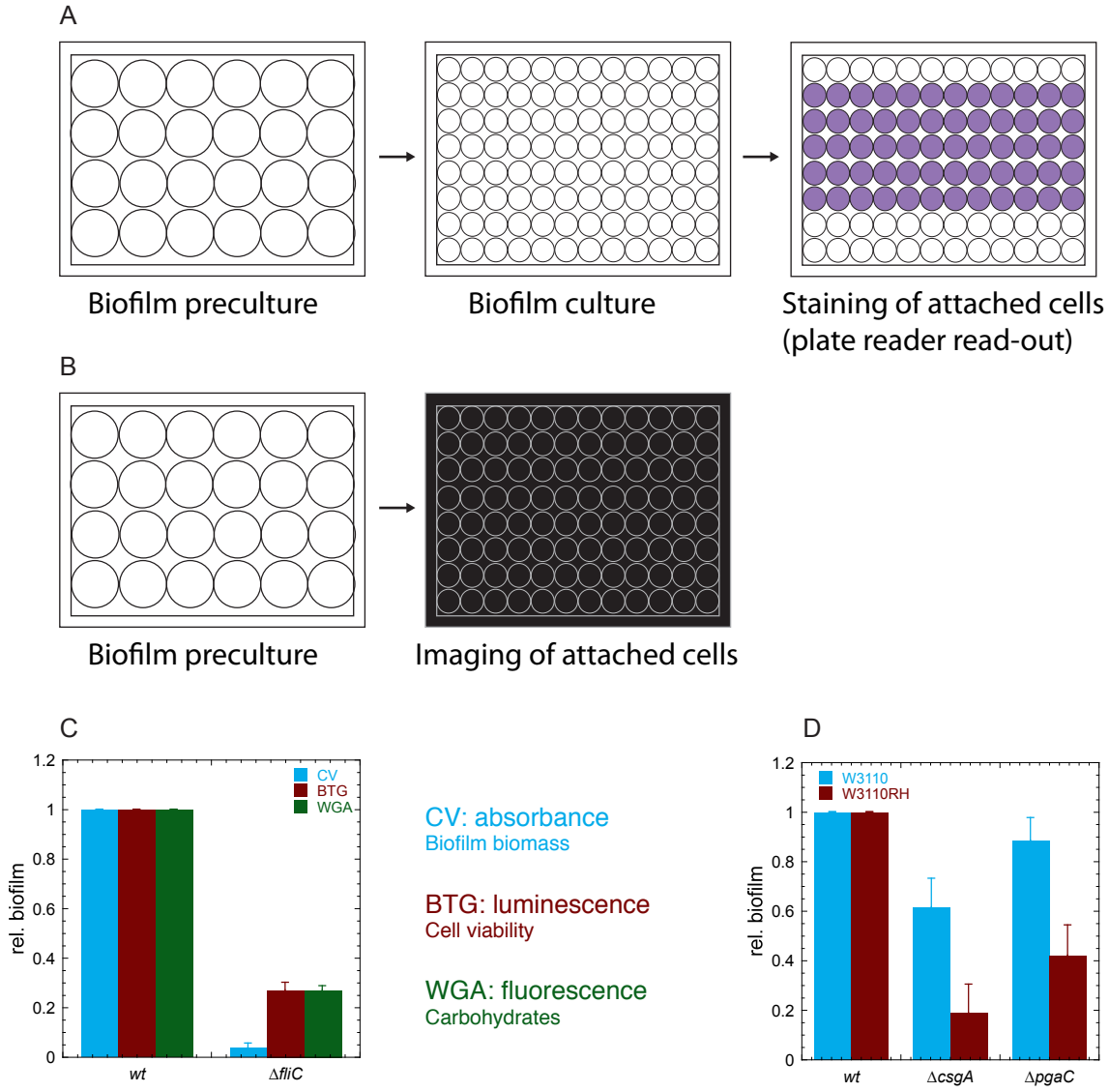

Fig. 6.1. Overview of assays to assess attachment in biofilms:
(A) Biofilm precultures are grown in 24-well plates for 48 h and diluted into fresh medium in 96-well plates. Attached cells can be stained, which is most commonly done with crystal violet (CV). Absorbance of CV staining can be measured in a plate reader.
(B) Attached cells of biofilm cultures can also be visualized by fluorescence microscopy in imaging plates.
(C) Three different methods can be used to quantify biofilm formation. The graph shows relative biofilm formation of W3110 wild type and Δ*fliC*. Attached cells were stained with crystal violet (CV), assessed for their viability with the BacTiter-Glo^{TM} assay (Promega), which measures the relative ATP content of cells corresponding to cell viability, or stained with fluorescently labeled wheat-germ agglutinin (WGA), which stains carbohydrates.
(D) Relative biofilm formation of W3110 and W3110^{RH} wild type and biofilm matrix mutants showing the relative importance of Curli and PGA in the respective strain background. Mean and standard error of three replicates are shown.

[138, 139]. This means that a functional RpoS is not expressed, which renders this strain unable to turn on many biofilm-related signals. The absence of a functional RpoS makes the strain a suitable model for early biofilm stages before activation of RpoS. To correlate results obtained with our W3110 with a RpoS-positive strain, I received another W3110 strain, which I label W3110^{RH} throughout this thesis, from Prof. Dr. Regine Hengge from the Humboldt University, Berlin. This W3110^{RH} strain contains a functional *rpoS* gene. Figure 6.1 D shows the impact of the biofilm matrix mutants Δ*csgA* (negative for curli) and Δ*pgaC* (negative for PGA) on attachment of both strains. For both, W3110 and W3110^{RH}, curli are the major component of the matrix that is required for attachment. In the following chapter, I will discuss the impact of flagella-driven motility on attachment, which in addition to biofilm matrix, influences surface attachment massively.

6.1 Attachment of *E. coli* W3110

Flagella-driven motility is required for static biofilm formation

I systematically tested the effect of motility on attachment in W3110. Therefore, knock-outs of motility and chemotaxis genes were created. Figure 6.2 shows the effect of motility on swimming in soft agar (A) and attachment, as quantified by CV staining after 24 h (B). As published previously [140], the chemotaxis mutants Δ*cheZ*, Δ*cheA* and Δ*cheY* and the non-motile flagella-less Δ*fliC* and stator mutant Δ*motA* are unable to perform in a gra-

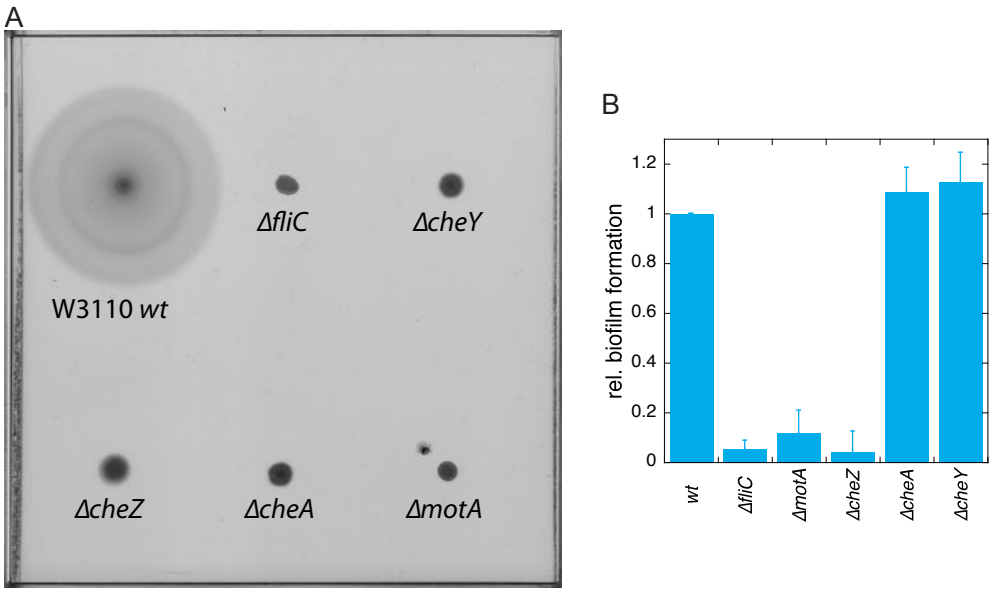

Fig. 6.2. Effect of motility KOs on W3110 biofilm formation:
(A) Swimming of W3110 wild type and motility mutant strains on soft agar plates.
(B) Biofilm formation of W3110 wild type, Δ*fliC*, Δ*motA*, Δ*cheZ*, Δ*cheA* and Δ*cheY* after 24 h in M9 medium at 30°C. Biofilms were formed on 96-well Corning® Costar®plates and stained with crystal violet (CV). Shown are mean and standard error of three to eight replicates.

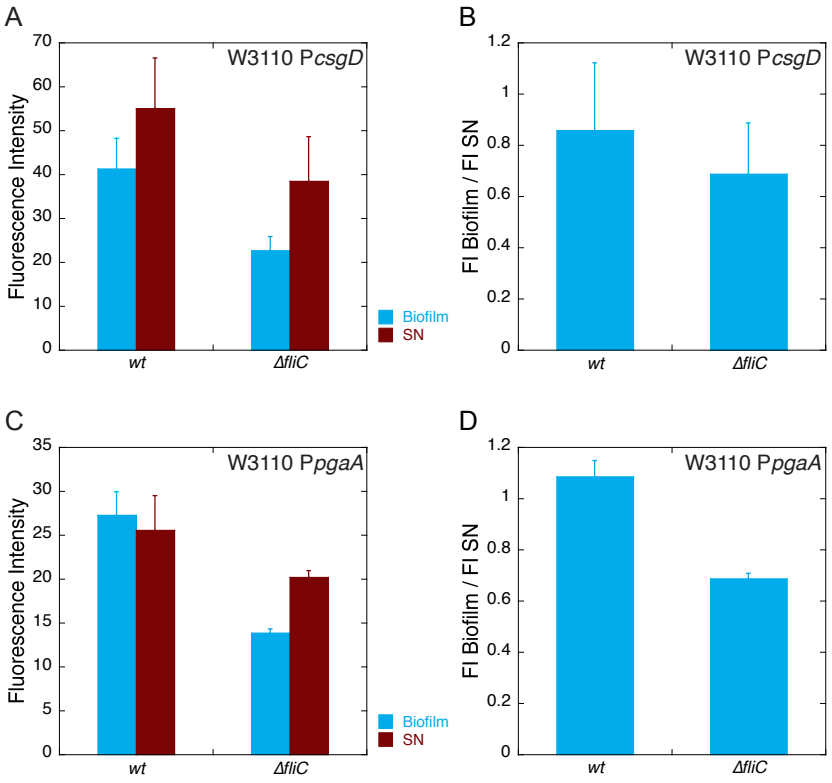

Fig. 6.3. In W3110 early biofilm formation, surface sensing by flagella does not seem to play a role:
GFP-Reporter activity was quantified in 7 h old biofilms of W3110 wild type and Δ*fliC* grown in M9 medium at 30°C on ibidi® imaging plates. Fluorescence intensity (FI) was quantified in attached (biofilm) and supernatant (SN) cells.
(A) Activity of the *csgD* promoter expressed from plasmid pVM49. Shown are mean and standard error of three replicates.
(C) Activity of the *pgaA* promoter expressed from plasmid pVM53. Shown are mean and standard error of three replicates.
(B, D) Ratios of GFP expression in biofilm and SN cells were determined for the *csgD* (B) and the *pgaA* promoter.

dient of a soft agar plate. Additionally, the non-motile mutants are also not able to form static biofilms (figure 6.2 B). Similarly, the chemotaxis phosphatase mutant Δ*cheZ*, which has a strong bias towards tumbling and thereby can be considered as less motile, cannot form biofilms. In contrast, the biomass of the smooth swimming mutants Δ*cheA* and Δ*cheY* is indistinguishable from the wild type biomass. These results show in consistence with previous publications [18, 25] that flagella are clearly required for static biofilm formation. In contrast to the requirement of flagella-driven motility for attachment, chemotaxis per se does not seem to be a prerequisite, as shown by the biofilm formation of Δ*cheA* and Δ*cheY*.

Flagella are no major adhesins or surface sensors

In addition to the prerequisite of flagella-driven motility for surface attachment, flagella

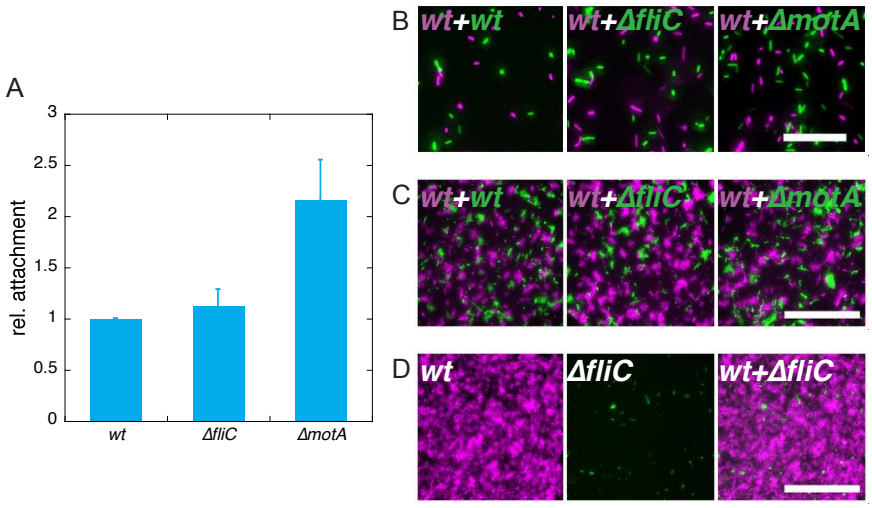

Fig. 6.4. Flagella in W3110 are no major adhesins:
(A-C) W3110 wild type and mutant cells labeled with different fluorescent proteins were mixed 1:1 in M9 medium and centrifuged on BD Falcon^{TM} imaging plates. Wild type cells labeled with two different fluorescent proteins served as a control. Non-attached cells were removed by washing.
(A) Attached cells were identified and segmented in brightfield images and the number of attached cells in each fluorescent channel was determined. The number of mutant cells was normalized to the number of wild type cells in the same image series and the mutant/wild type ratio was further normalized to the wild type/wild type control. Shown are mean and standard error of four to five replicates.
(B) Exemplary images showing attached cells after washing. Wild type (magenta) cells were mixed 1:1 with wild type, Δ*fliC* and Δ*motA* cells (green). Scalebar: 25 μm.
(C) Exemplary images showing surface growth of attached cells after centrifugation. Cells were washed as in (B) and grown for 24 h at 30°C in M9 medium. Unattached cells were removed again. Colors are as in (B). Scalebar: 100 μm.
(D) Mixed biofilm of wild type (magenta) and Δ*fliC* (green). Cells were prepared as for (A-C), however, incubated at 30°C for 24 h in M9 medium without centrifugation. Scalebar: 100 μm.

could have additional roles during biofilm formation, such as a role as adhesins [127, 128, 129] when the initial surface contact is established or as surface sensors [130, 131, 132, 133]. I tested both possibilities as shown in figures 6.3 and 6.4. To check for surface sensing by flagella, GFP-reporters to monitor expression of the major curli regulator CsgD and of the outer membrane protein PgaA were cloned and used as reporters for curli (figure 6.3 A, B) and PGA (figure 6.3 C, D) , respectively. Expression was monitored at early biofilm formation (7 h) in unattached (supernatant, SN) and attached (biofilm) cells. Overall, expression of matrix reporters was slightly reduced in flagella-less cells. However, with wild-type biofilm/SN ratios of roughly 0.8-1.1, even in wild-type there was no sign of apparent surface sensing, which would lead to increased matrix gene expression in biofilm cells. I therefore conclude that for the genes monitored, surface sensing by flagella does not seem to play a role. The observed reduced expression of matrix genes in the Δ*fliC* strain, however, has no effect on the stickiness of the mutant (see figure 6.4). Here, I tested the possible role of flagella as adhesins during attachment. This was done by artificially forc-

ing the bacteria to the surface of microtiter dishes by centrifugation to avoid the necessity of swimming for attachment. Wild type and mutant cells were labeled with two different fluorescent proteins and mixed at 1:1 ratios. Wild type mixed with wild type served as a control. Figures 6.4 A and B show that similar numbers of wild type and Δ*fliC* cells attached to the surface after centrifugation, meaning that stickiness of the strains is similar. The stability of attachment was also similar, as shown in figure 6.4 C, where cell attachment 24 h after centrifugation is shown. Once at the surface, flagella-less cells formed microcolonies that resembled wild type colonies. In contrast, without centrifugation no microcolonies were observed (figure 6.4 D). Attachment of Δ*motA* cells after centrifugation was slightly increased in comparison to the wild type attachment (figures 6.4 A and B). This might indicate that flagella can increase surface adhesion. However, since the effect was modest, a specific function of flagella as surface adhesins seems unlikely. Together, the results in figures 6.3 and 6.4 show that the primary role of flagella during attachment lies in their motility function and that flagella function neither as major adhesins nor surface sensors during W3110 attachment.

Chemotaxis is not required for static biofilm formation

Based on the first observation that motility but not chemotaxis is required for attachment (figure 6.2), I suspected that deletion of other chemotaxis genes would also not affect biofilm formation of W3110. To investigate this, I constructed chemotaxis gene knockouts in W3110 and tested their behavior on soft agar plates and during biofilm formation (figure 6.5). Swimming on soft agar plates was as expected for all strains except for Δ*tar*. A Δ*tar* strain is unable to perform chemotaxis towards aspartate, which is shown by the inner ring of the wild type strain [141, 140]. However, chemotaxis to serine should be unaffected, which is why a swarm ring with the size of the wild type outer ring would be expected. This means that in the W3110 Δ*tar* strain, motility is reduced, which might be due to a secondary mutation transferred by P1 transduction from the Keio collection [142] during the strain construction. This might also explain the effect of the *tar* knockout on biofilm formation (figure 6.5 B), which I could not complement with expression of wild type Tar from a plasmid (not shown). In contrast, knockouts of the other chemotaxis receptors did not reduce biofilm formation. Deletion of *tsr* showed even a slight increase in biomass. Knockout of the chemotaxis adaptation system containing of the methyltransferase CheR and the methylesterase CheB resulted in no effect for Δ*cheR* and slightly decreased biofilm formation of Δ*cheB*. Δ*cheB* has a bias towards tumbling, which might explain the effect on biofilm formation. Knockout of the adaptor protein CheW abolished biofilm formation, which was not expected, since knockout of *cheA* had no effect. However, it is important to mention that the Δ*cheA* strain used in figures 6.2 and 6.5 A, B is a self-made strain, i. e. was made by replacing the *cheA* gene with a PCR-amplified PCR cassette, whereas the Δ*cheW* strain was constructed by P1 transduction from the Keio collection [142]. If *cheA* is deleted in W3110 by transfer from the Keio collection, biofilm formation is also strongly decreased (figure 6.5 C). This was tested with a subset of more than ten clones received by

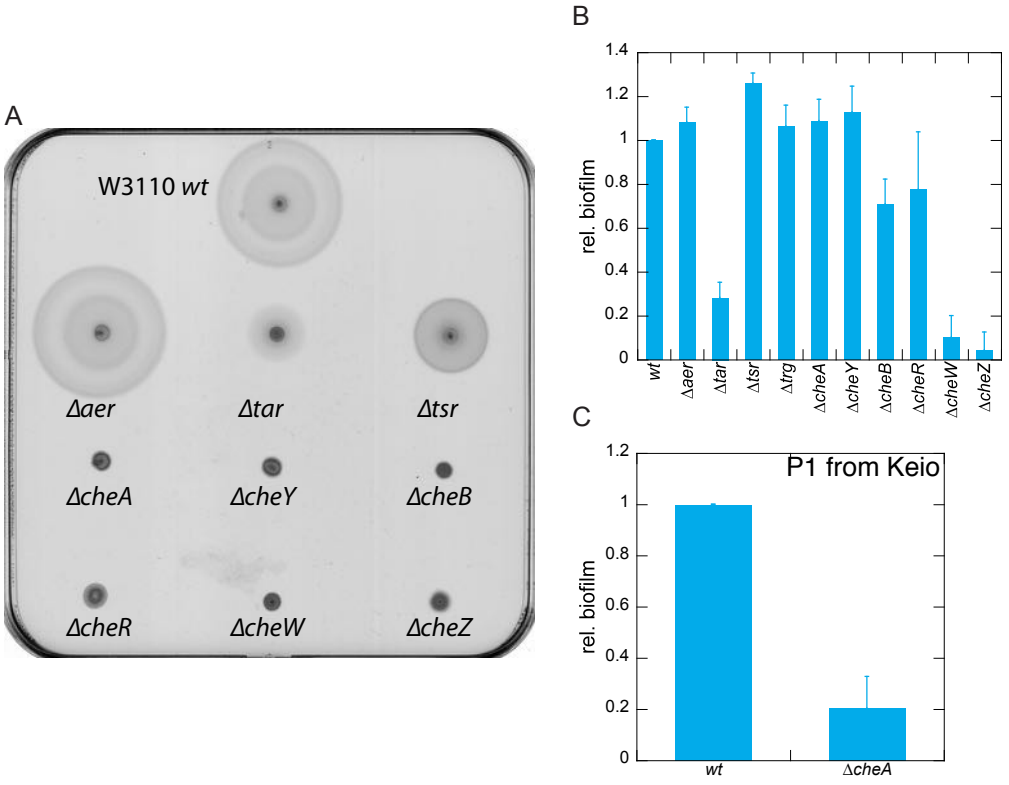

Fig. 6.5. Effect of chemotaxis KOs on W3110 biofilm formation:
(A) Swimming of W3110 wild type and chemotaxis mutant strains on soft agar plates.
(B) Biofilm formation of W3110 wild type, Δ*aer*, Δ*tar*, Δ*tsr*, Δ*trg*, Δ*cheA*, Δ*cheY*, Δ*cheB*, Δ*cheR*, Δ*cheW* and Δ*cheZ* after 24 h in M9 medium at 30°C. The Δ*cheA* strain in (B) was constructed by genomic integration of a PCR cassette. Biofilms were formed on 96-well Corning® Costar®plates and stained with crystal violet (CV). Shown are mean and standard error of three to eight replicates.
(C) Biofilm formation of W3110 wild type and Δ*cheA* after 24 h in M9 medium at 30°C. The Δ*cheA* strain in (C) was constructed by P1 transduction from the Keio collection. Biofilms were and stained as in (B). Shown are mean and standard error of six replicates.

P1 transduction (not shown). Similarly to the Δ*tar* strain, this defect of the P1-Δ*cheA* strain in biofilm formation could not be rescued by expression of CheA from a plasmid (not shown). In contrast, the defect in swimming in soft agar plate of the P1-Δ*cheA* strain could be rescued (not shown). The results of the Δ*tar*, Δ*cheW* and Δ*cheA* strains that were constructed by P1 transduction indicate that there might be a secondary mutation in the Keio strains that can be co-transferred by P1 transduction and impairs biofilm formation. However, altogether, results of figure 6.5 confirm the results from figure 6.2 that in *E. coli*, motility but not chemotaxis is required for attachment, which is consistent with previously published results [18].

Smooth swimming promotes attachment to surfaces

So far, I only monitored attachment after 24 h of biofilm formation (figures 6.2 and 6.5). To gain insight into the timing of the requirement of motility for attachment, I performed

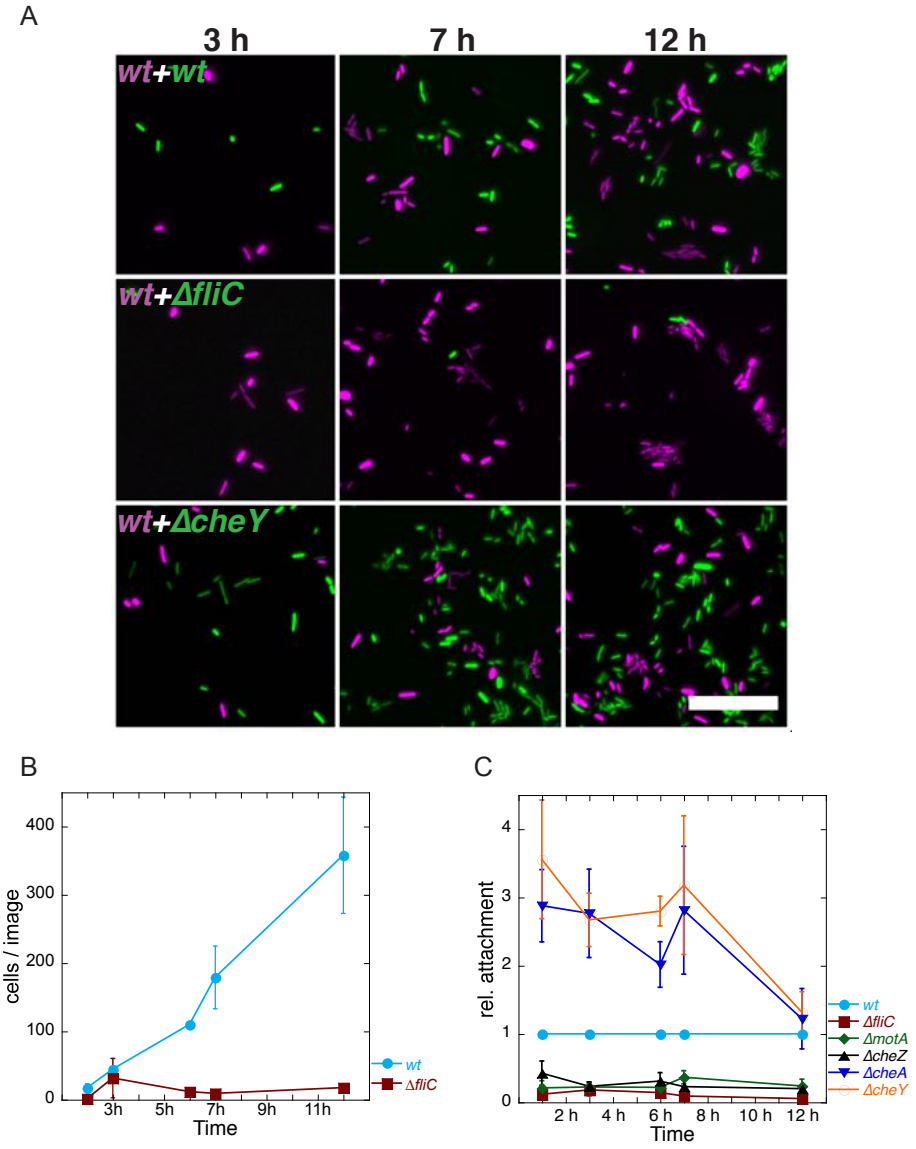

Fig. 6.6. Smooth swimming promotes attachment during early biofilm formation: Early biofilm formation of mixed cultures of W3110 wild type, Δ*fliC*, Δ*motA*, Δ*cheZ*, Δ*cheA* and Δ*cheY* on BD Falcon^{TM} imaging plates. Wild type cells were mixed with wild type or mutant cells 1:1 and mixed biofilm cultures were grown in M9 at 30°C for the indicated time. Non-attached cells were removed and attached cells were imaged. Attached cells were quantified as in 6.4.

(A) Exemplary images of mixed cultures of wild type (magenta) and mutant (green) cells. Control: wild type mixed with wild-type. Scalebar 25 μm.

(B) Cell numbers per image of W3110 wild type and Δ*fliC*. Shown are mean and standard error of three replicates.

(C) Quantified relative attachment of W3110 wild type, Δ*fliC*, Δ*motA*, Δ*cheZ*, Δ*cheA* and Δ*cheY*. Shown are mean and standard error of three replicates.

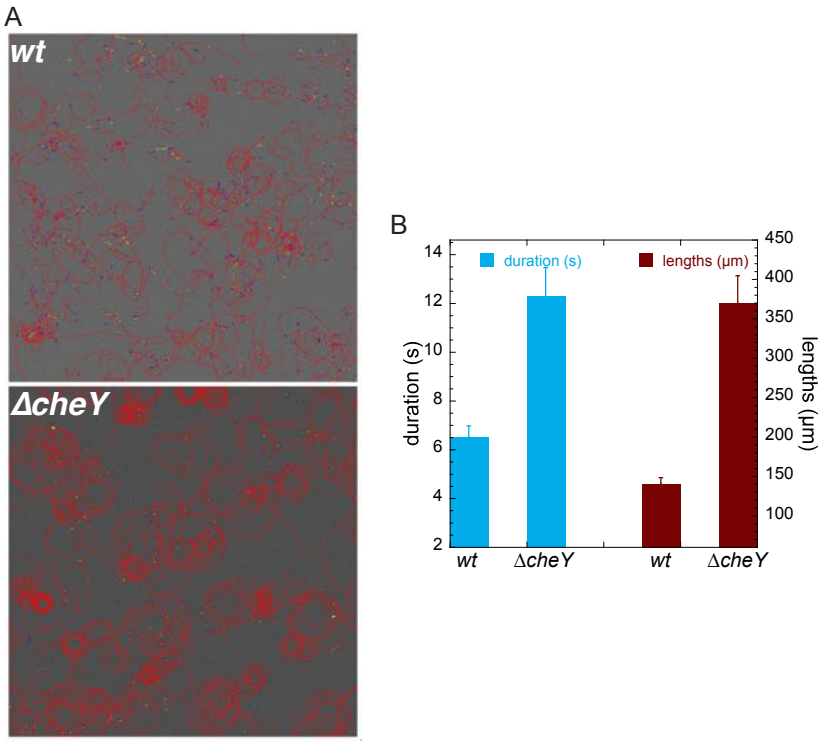

Fig. 6.7. Smooth swimming leads to surface trapping:
Surface swimming of W3110 cells grown in planktonic cultures.
(A) Exemplary images showing tracks of W3110 wild type and Δ*cheY* cells swimming at the surface. Experiment was performed by Dr. Remy Colin.
(B) Trajectory duration and lengths of W3110 wild type and Δ*cheY* swimming at the surface. Cells were grown in planktonic cultures to postexponential phase. Shown are mean and standard error of three replicates. Experiment was performed by Dr. Remy Colin.

a time-resolved analysis of attachment using the motility mutants Δ*fliC*, Δ*motA*, Δ*cheZ*, Δ*cheA* and Δ*cheY* (figure 6.6). For this, wild type and mutant cells labeled with different fluorescent proteins were mixed at 1:1 ratio and biofilms were grown on BD falcon^{TM} imaging plates. Attached cells were imaged (figure 6.6 A), the number of cells per image was quantified (figure 6.6 B) and ratios of mutant to wild type cells were determined and normalized to the wild type/wild type control (figure 6.6 C). The number of wild type cells that are attached to the surface steadily increased during the first 12 h of biofilm formation whereas flagella-less cells clearly could not attach from the beginning (figure 6.6 A-C and figure A.1). Similarly, I could observe almost no attached Δ*motA* and Δ*cheZ* cells. In contrast to previous results based on CV staining [18], I observed increased attachment of the smooth swimming mutants Δ*cheA* and Δ*cheY* during the first 7 h of biofilm formation (figure 6.6 A, C and A.1). In consistence with results after 24 h in figures 6.2 and 6.5, the effect was gone after 12 h, suggesting that smooth swimming promotes attachment during the very initial phases of attachment.

To understand the advantage of smooth swimming during the initial attachment phase, swimming behavior of wild type and Δ*cheY* was analyzed. These tracking experiments

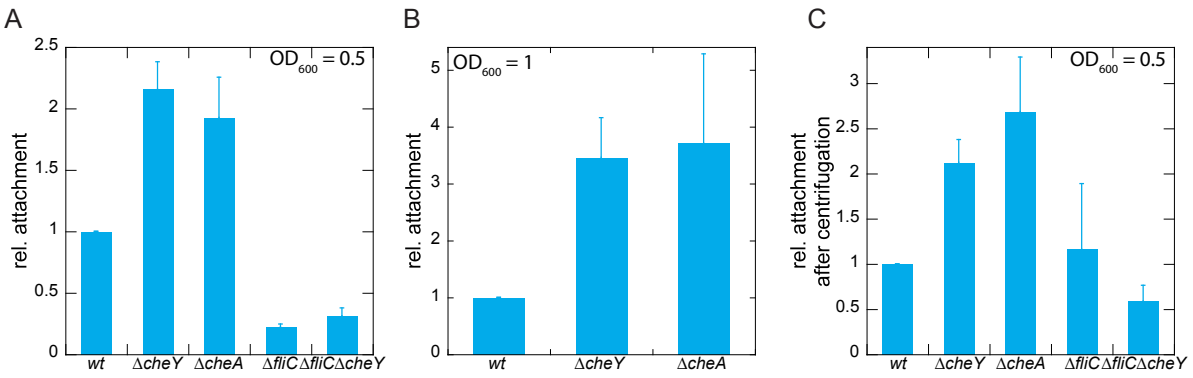

Fig. 6.8. Smooth swimming promotes attachment through surface trapping:
Surface attachment of W3110 cells grown in planktonic cultures.
(A) Surface attachment of W3110 wild type, Δ*cheY*, Δ*cheA*, Δ*fliC* and Δ*fliC*Δ*cheY*. Cells were grown to OD_{600} 0.5, prepared for surface attachment in motility buffer and allowed to attach for 1 h. Unattached cells were removed. Shown are mean and standard error of two to seven replicates.
(B) Surface attachment of W3110 wild type, Δ*cheY* and Δ*cheA*. Cells were grown to OD_{600} 1, prepared for surface attachment in motility buffer and allowed to attach for 1 h. Unattached cells were removed. Shown are mean and standard error of two to five replicates.
(C) Surface attachment after centrifugation of W3110 wild type, Δ*cheY*, Δ*cheA*, Δ*fliC* and Δ*fliC*Δ*cheY*. Cells were grown to OD_{600} 0.5 and forced onto the surface by mild centrifugation in motility buffer. Shown are mean and standard error of two to four replicates.

were performed by Dr. Remy Colin from our group. Figure 6.7 shows trajectories of planktonic wild type and Δ*cheY* cells swimming at a glass surface (A) and quantification of trajectory duration (B, blue bars) and length (B, red bars). In consistence with previous results [143], wild type cells that reach the surface can swim at the surface but can also efficiently escape by tumbling (see figure 6.7 A, upper panel). In contrast, Δ*cheY* cells get entrapped at the surface, where they swim in a circular path (see figure 6.7 A, lower panel). Quantification in B reflects this behavior with Δ*cheY* cells showing both longer trajectory duration (blue bars) and longer tracks (red bars).

To correlate the results obtained with planktonic cultures (figure 6.7) to the attachment results in biofilms (figure 6.6), I tested attachment of planktonic cells to the surface of imaging plates, preparing the cultures in the same way as it was done for the tracking experiments (see figure 6.8). Attachment was performed at two optical densities, OD_{600} 0.5 (A) and OD_{600} 1 (B). Consistent with the biofilm results, attachment of the smooth swimming mutants Δ*cheY* and Δ*cheA* was approx. 2-3 higher than attachment of wild type cells. Δ*fliC* and Δ*fliC*Δ*cheY* served as negative controls. To rule out the possibility that deletion of *cheA* or *cheY* increases stickiness of bacteria, I performed the centrifugation experiment described in figure 6.4. Again, Δ*fliC* and Δ*fliC*Δ*cheY* served as negative controls. Indeed, more Δ*cheY* and Δ*cheA* cells attached to the surface after centrifugation, suggesting a higher stickiness of those cells in comparison to wild type. However, calculations including centrifugation force, swimming speed and tumbling rate performed by Dr. Remy Colin (data not shown), argue against such an interpretation since at the

mild centrifugation used in the experiment, a larger number of smooth swimming than wild type cells would get entrapped at the surface. Altogether, results in figures 6.6-6.8 show that smooth swimming promotes surface attachment through hydrodynamic entrapment.

C-di-GMP inhibits motility and thereby attachment during early biofilm formation

Apart from the chemotaxis system, signaling by c-di-GMP regulates motility in *E. coli* in a way that high c-di-GMP levels inhibit motility. The observed strong dependence of attachment during biofilm formation on motility suggests that modulation of c-di-GMP would also influence cell attachment. I therefore tested the effect of different deletion strains affected in c-di-GMP signaling on attachment (see figure 6.9). YhjH is the main phosphodiesterase regulating the c-di-GMP pool for the motility control and its deletion impairs motility (see figure 6.9 A), as was described previously [144, 145]. Deletion of *ycgR* or *yegE* in the Δ*yhjH* background suppress the motility phenotype (see figure 6.9 A, [145]), whereas deletion of *ycgR* or *yegE* in the wild type background leads to swarm rings comparable to the wild type. In contrast to its generally assumed role as a biofilm-promoting factor, c-di-GMP seems to inhibit attachment during biofilm formation (see figure 6.9 B-E). CV staining after 24 h gave us the first hint that high levels of c-di-GMP, as assumed for Δ*yhjH*, inhibit attachment whereas deletion of the diguanylate cyclase YegE increased attachment to a similar level as deletion of the motor-binding protein YcgR. Double knockouts of *yegE* and *yhjH* with *ycgR* show that the effects of the single knockouts are mediated by the motility control, since Δ*yegE*Δ*ycgR* showed similar increased biofilm formation in comparison to the single knockout and the inhibitory effect of the *yhjH* deletion was abolished in Δ*yhjH*Δ*ycgR*. Time-resolved analysis of biofilm formation of the c-di-GMP mutants, as performed with CV staining (figures 6.9 C and A.2) and microscopy (figure 6.9 D-E) shows that these difference in the amount of biofilm stem from initial differences in attachment developing between 3-6 h of attachment (figure 6.9 E).

The difference in the motility control between strains Δ*ycgR*, Δ*yegE* and Δ*yhjH* is the swimming speed (see figure 6.10 A), which is regulated by c-di-GMP-loaded YcgR binding to the motor [146, 58, 147]. Δ*ycgR* and Δ*yegE* show higher swimming speeds whereas speed is reduced in Δ*yhjH*. The differences, however, are rather small. Nevertheless, we speculated that an increased swimming speed could influence surface trapping and thereby trajectory length (figure 6.10 B) and duration (figure A.3). However, no significant differences in trajectory length were observed (figure 6.10 B). Due to its lower swimming speed (figure 6.10 A) but unaffected trajectory length (figure 6.10 B), Δ*yhjH* cells stay longer at the surface than wild type cells (figure A.3). However, these results cannot explain the effect on biofilm formation in figure 6.9. Analysis of tumbling rates (figure 6.10 C) also did not clarify the observations, since no significant differences between strains were observed. To correlate the tracking data from planktonic cultures with the biofilm results

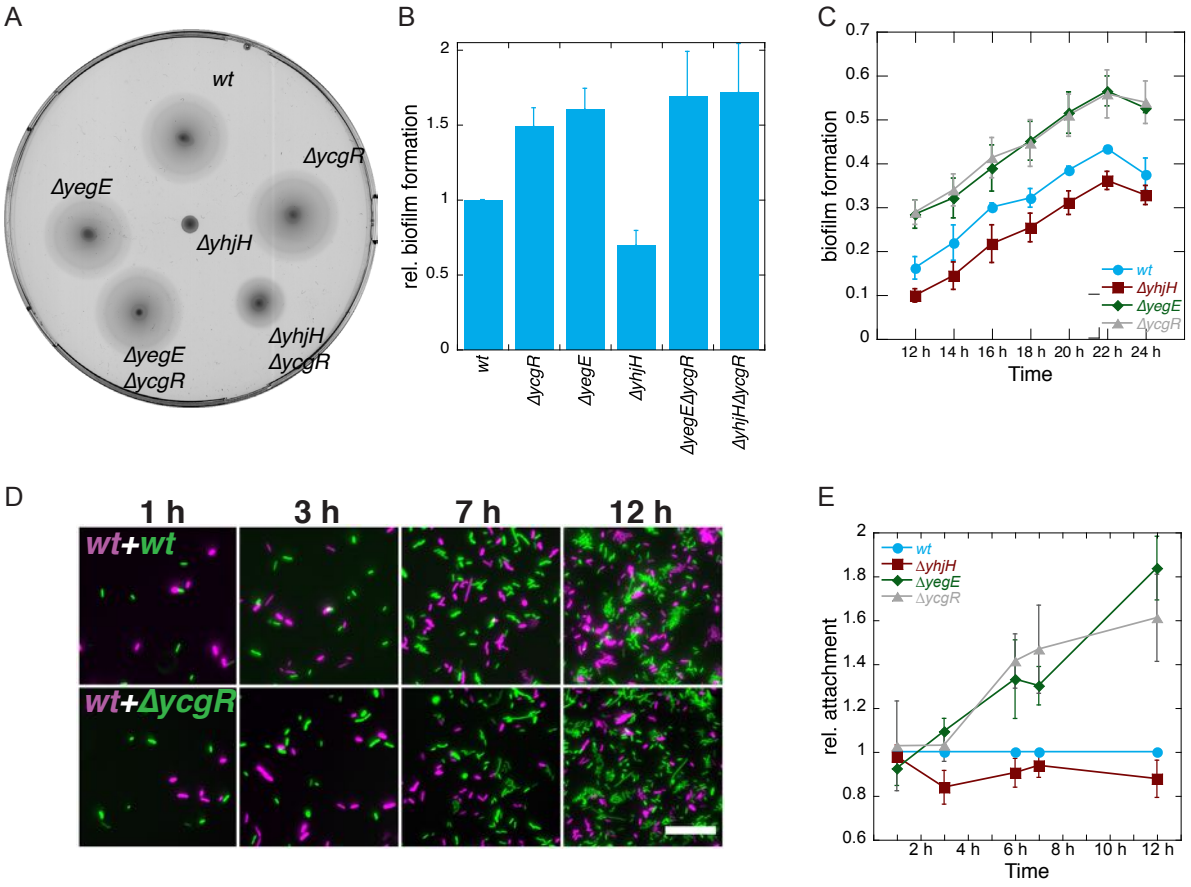

Fig. 6.9. Motility regulation by c-di-GMP alters biofilm formation in W3110:
(A) Swimming on soft agar plates of W3110 wild type, Δ*yegE*, Δ*yhjH*, Δ*ycgR*, Δ*yegE*Δ*ycgR* and Δ*yhjH*Δ*ycgR*.
(B) Biofilm formation of W3110 wild type, Δ*ycgR*, Δ*yegE*, Δ*yhjH*, Δ*yegE*Δ*ycgR* and Δ*yhjH*Δ*ycgR* after 24 h in M9 medium at 30°C. Biofilms were formed on 96-well Corning® Costar®plates and stained with crystal violet (CV). Shown are mean and standard error of eight to twenty-one replicates.
(C) Early biofilm formation of W3110 wild type, Δ*yhjH*, Δ*yegE* and Δ*ycgR* in M9 medium at 30°C. Biofilms were formed on 96-well Corning® Costar®plates and stained with crystal violet (CV). Shown are mean and standard error of three replicates.
(D) Exemplary images of early biofilm formation of mixed cultures of W3110 wild type and Δ*ycgR* cells. Wild type and mutant cells were labeled with different fluorescent proteins and mixed 1:1 for biofilm growth on BD Falcon^{TM} imaging plates in M9 medium at 30°C. Scalebar: 25 μm.
(E) Quantification of surface attachment during early biofilm formation of mixed cultures of W3110. Cells and cell clumps were identified in the fluorescence images and area covered by the cells was quantified. Area of mutant cells was normalized to the area of wild type cells in the same image series and the mutant/wild type ratio was normalized to the wild type/wild type control. Shown are mean and standard error of five to eight replicates.

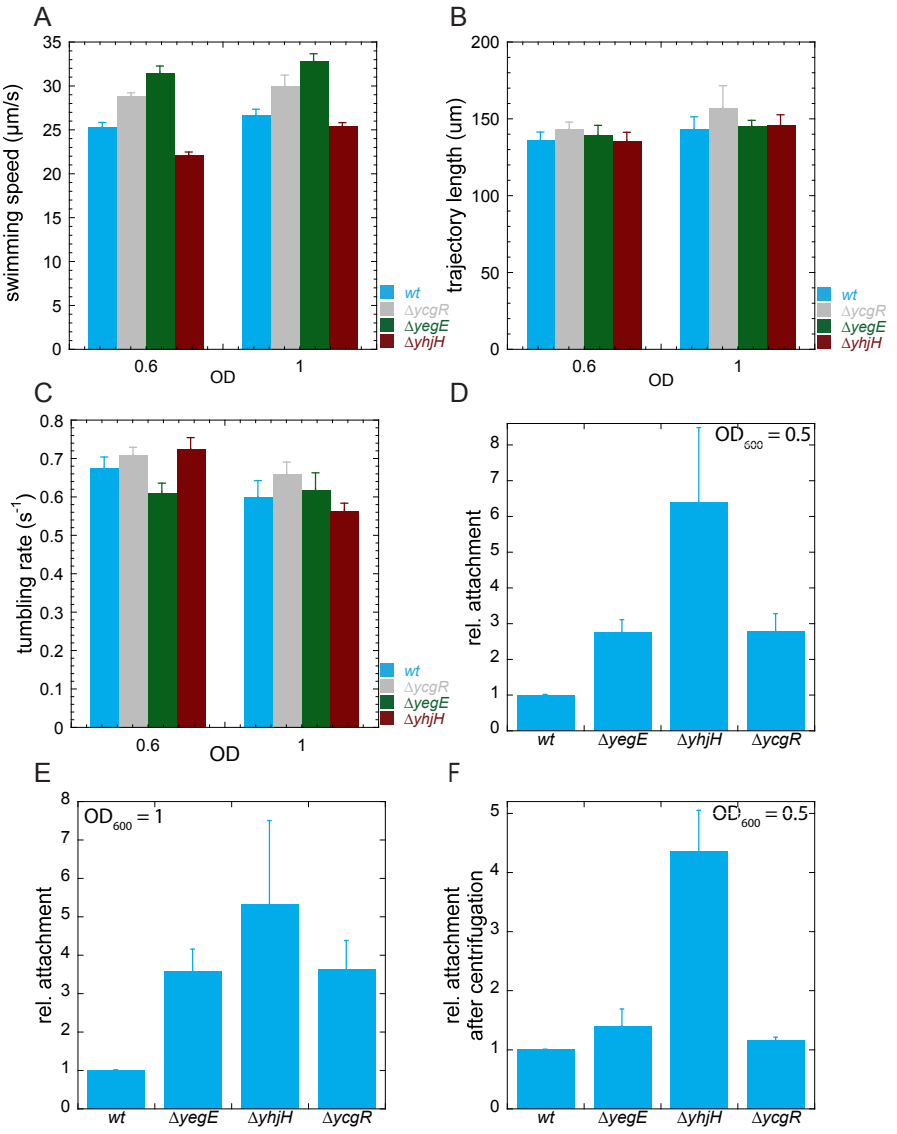

Fig. 6.10. Swimming behavior and attachment of planktonic W3110 cells with defects in c-di-GMP signaling:
(A) Swimming speed (μm/s) of W3110 wild-type, Δ*ycgR*, Δ*yegE* and Δ*yhjH* grown in planktonic culture until OD_{600} 0.6 and 1. Shown are mean and standard error of three replicates. Experiment was performed by Dr. Remy Colin.
(B) Trajectory lengths of W3110 wild-type, Δ*ycgR*, Δ*yegE* and Δ*yhjH* grown in planktonic culture until OD_{600} 0.6 and 1. Shown are mean and standard error of three replicates. Experiment was performed by Dr. Remy Colin.
(C) Tumbling rates of of W3110 wild-type, Δ*ycgR*, Δ*yegE* and Δ*yhjH* grown in planktonic culture until OD_{600} 0.6 and 1. Shown are mean and standard error of three replicates. Experiment was performed by Dr. Remy Colin.
(D-F): Surface attachment of W3110 wild-type, Δ*yegE*, Δ*yhjH* and Δ*ycgR* on ibidi® imaging plates. Mixed cultures of wild type and mutant cells at 1:1 ratio and labeled with different fluorescent proteins were prepared for attachment. Cells were identified and segmented in brightfield images and the ratio of mutant to wild type cells was determined and further normalized to the wild type/wild type control in each experimental series.
(D) Cells were grown to OD_{600} 0.5, prepared for surface attachment in motility buffer and allowed to attach for 1 h. Unattached cells were removed. Shown are mean and standard error of six replicates.
(E) Cells were grown to OD_{600} 1, prepared for surface attachment in motility buffer and allowed to attach for 1 h. Unattached cells were removed. Shown are mean and standard error of five replicates.
(F) Surface attachment after centrifugation. Cells were grown to OD_{600} 0.5 and forced onto the surface by mild centrifugation in motility buffer. Shown are mean and standard error of four replicates.

in figure 6.9, attachment experiments with planktonic c-di-GMP mutants were performed at OD_{600} 0.6 and 1 (figure 6.10 D, E). I could confirm the results obtained for the faster swimming mutants Δ*ycgR* and Δ*yegE*, which showed around 3-fold increased attachment in comparison to wild type cells. Attachment after centrifugation (figure 6.10 F) confirmed that the increased attachment stems from the difference in swimming speed rather than from a difference in stickiness. The opposite was observed for Δ*yhjH*. Despite its decreased attachment in biofilms (figure 6.9), several fold more Δ*yhjH* cells attached to the surface in comparison to wild type. However, centrifugation experiments showed that these effects are a result of increased stickiness of the Δ*yhjH* strain (figure 6.10 F).
With no effect on trajectory length and duration, another possibility is that swimming speed could influence the strength of attachment. For the attachment experiments so far, loosely attached cells were washed away and only cells that stayed attached to the surface after washing were considered for quantification of attachment. I therefore compared attachment of wild type and Δ*ycgR* cells before and after washing (see figure 6.11). I could observe a tendency that indeed the ratio of Δ*ycgR* to wild type cells was higher in washed samples than in unwashed samples, however, these results need more replicates for confirmation.

6.2 Attachment of *E. coli* W3110^{RH}

Smooth swimming promotes attachment in the RpoS-positive W3110^{RH}

Since the expression of many genes relevant for biofilm formation depends on the stationary phase sigma factor RpoS ([148, 97, 99], we performed attachment experiments additionally with the RpoS-positive W3110^{RH} strain. We could confirm the results obtained with W3110 from figure 6.2 showing that flagella-driven motility is absolutely required for attachment (see figure 6.12 A-C). As in W3110, I could not observe a major surface-sensing function of flagella (see figure A.4). As in W3110, overall expression of *csgD* and *pgaA* was slightly reduced in Δ*fliC* and also in Δ*motA*. However, surface-induced expression of *csgD* and *pgaA* was neither observed in wild type nor mutant strains. In fact *csgD* and *pgaA* expression seems to be higher in supernatant cells (figure A.4). We further checked expression from a third promoter, P*wzxC*, as a reporter for colanic acid. However, this reporter was inactive for W3110 (not shown) and W3110^{RH} (figure A.4 E, F). Together, the results in figures 6.12 and A.4 confirm that the main function of flagella during attachment at the early stages of biofilm growth is driving motility and not surface sensing. Similar to effects in W3110, chemotaxis was not required for attachment in W3110^{RH}, although a mild reduction in biomass was measured for the W3110^{RH} Δ*cheY* strain (figure 6.12 B). However, analysis of planktonic cultures could still confirm the theory that smooth swimming promotes surface attachment through hydrodynamic entrapment since planktonic W3110^{RH} Δ*cheY* cells showed approx. 2.5-fold more attachment than wild type cells (figure 6.12 D). Supporting those data, tracking of cells confirmed longer tracks

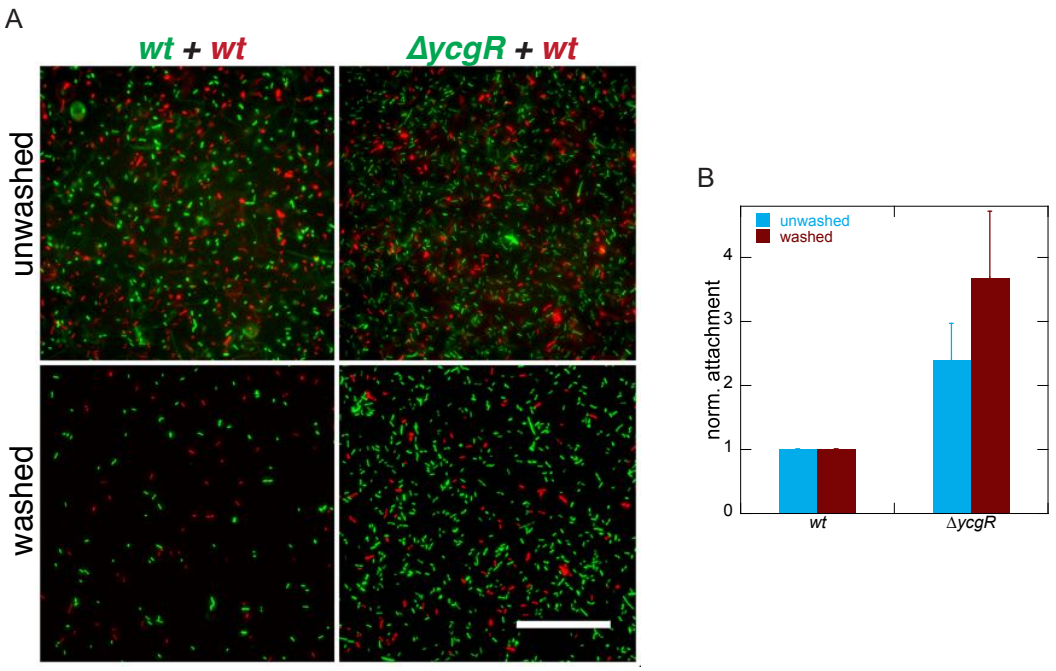

Fig. 6.11. YcgR might influence the strength of surface attachment:
(A) Surface attachment of planktonic W3110 wild type and Δ*ycgR* on ibidi® imaging plates. Exemplary images of mixed cultures of W3110 wild type and Δ*ycgR* are shown. Cells were grown to OD_{600} 0.5, prepared for surface attachment in motility buffer and allowed to attach for 1 h. Cells at the surface were imaged before and after washing. Scalebar: 25 μm.
(B) Quantification of the number of cells at the surface in unwashed and washed samples. Cells were identified and segmented in the fluorescence images and ratios of Δ*ycgR* to wild type cell numbers were calculated for each image series and further normalized to the wild type/wild type control. Shown are mean and standard error of three replicates.

and longer trajectory duration for W3110^{RH} Δ*cheY* (figure 6.12 E).

A dual role of c-di-GMP?

With W3110, I could show that low c-di-GMP promotes attachment during biofilm formation, supposedly through higher motility (figure 6.9). Since c-di-GMP is crucial for the upregulation of biofilm matrix factors, such as curli fibers in *E. coli* [55, 99, 149], which are required both for attachment (see figure 6.1 D) and for three-dimensional structure formation (see references [150], [27] and figure 7.2), we analyzed the effect of c-di-GMP on attachment in W3110^{RH} (see figure 6.13). Indeed, time-resolved analysis of biofilm formation of W3110^{RH} showed a dual role of c-di-GMP (see figure 6.13 A, B). During the first 14 h, c-di-GMP clearly inhibits attachment with deletion strains of *ycgR* and *yegE* showing increased and Δ*yhjH* showing decreased attachment. The differences between the strains reduce with time and at 48 h, attachment of *yegE* is significantly reduced in comparison to the other strains. The effect of Δ*ycgR* vanishes at later timepoints, suggesting that the reduction in biofilm levels of the Δ*yegE* strain at the late timepoints is not me-

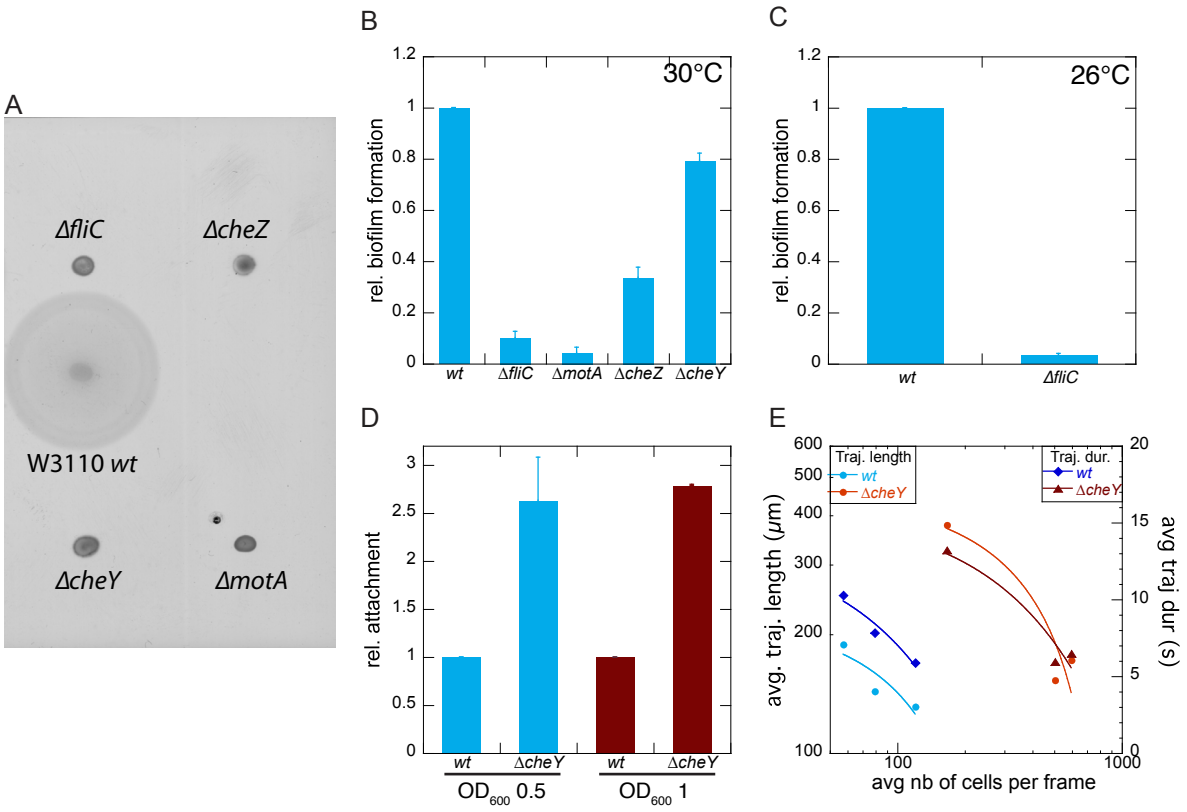

Fig. 6.12. Effect of motility KOs on W3110^{RH} biofilm formation:
(A) Swimming of W3110^{RH} wild type and motility mutant strains on soft agar plates.
(B) Biofilm formation of W3110^{RH} wild type, Δ*fliC*, Δ*motA*, Δ*cheZ* and Δ*cheY* after 24 h in TB medium at 30°C. Biofilms were formed on 96-well Corning® Costar®plates and stained with crystal violet (CV). Shown are mean and standard error of two to six replicates.
(C) Biofilm formation of W3110^{RH} wild type and Δ*fliC* after 24 h in TB medium at 26°C. Biofilms were formed on 96-well Corning® Costar®plates and stained with crystal violet (CV). Shown are mean and standard error of three replicates.
(D) Surface attachment of W3110^{RH} wild type and Δ*cheY* on ibidi® imaging plates. Cells were grown to OD_{600} 0.5 and 1, prepared for surface attachment in motility buffer and allowed to attach for 1 h. Unattached cells were removed. For quantification, cells were identified and segmented in brightfield images and the ratio of mutant to wild type cells was determined and further normalized to the wild type/wild type control in each experimental series. Shown are mean and standard error of two to three replicates.
(E) Trajectory lengths and duration of W3110^{RH} wild type and Δ*cheY* swimming at the surface. Cells were grown in planktonic cultures to OD_{600} 0.5. Trajectory length and duration were plotted against the average cell number per image. Shown are three independent replicates per strain. Experiment was performed by Dr. Remy Colin.

diated by the motility control but rather through c-di-GMP-dependent effects on matrix production. Similarly, the attachment defect of Δ*yhjH* diminishes with time and at 48 h, Δ*yhjH* attachment reaches almost wild type levels. During the time course, Δ*fliC* served as a negative control and showed almost no surface attachment until the 48 h timepoint, where levels of Δ*fliC* attachment are almost similar to wild type levels. Time-resolved microscopy was performed to gain more insight into the early events of surface attachment (figure 6.13 C). However, only faint differences between strains could be observed, which

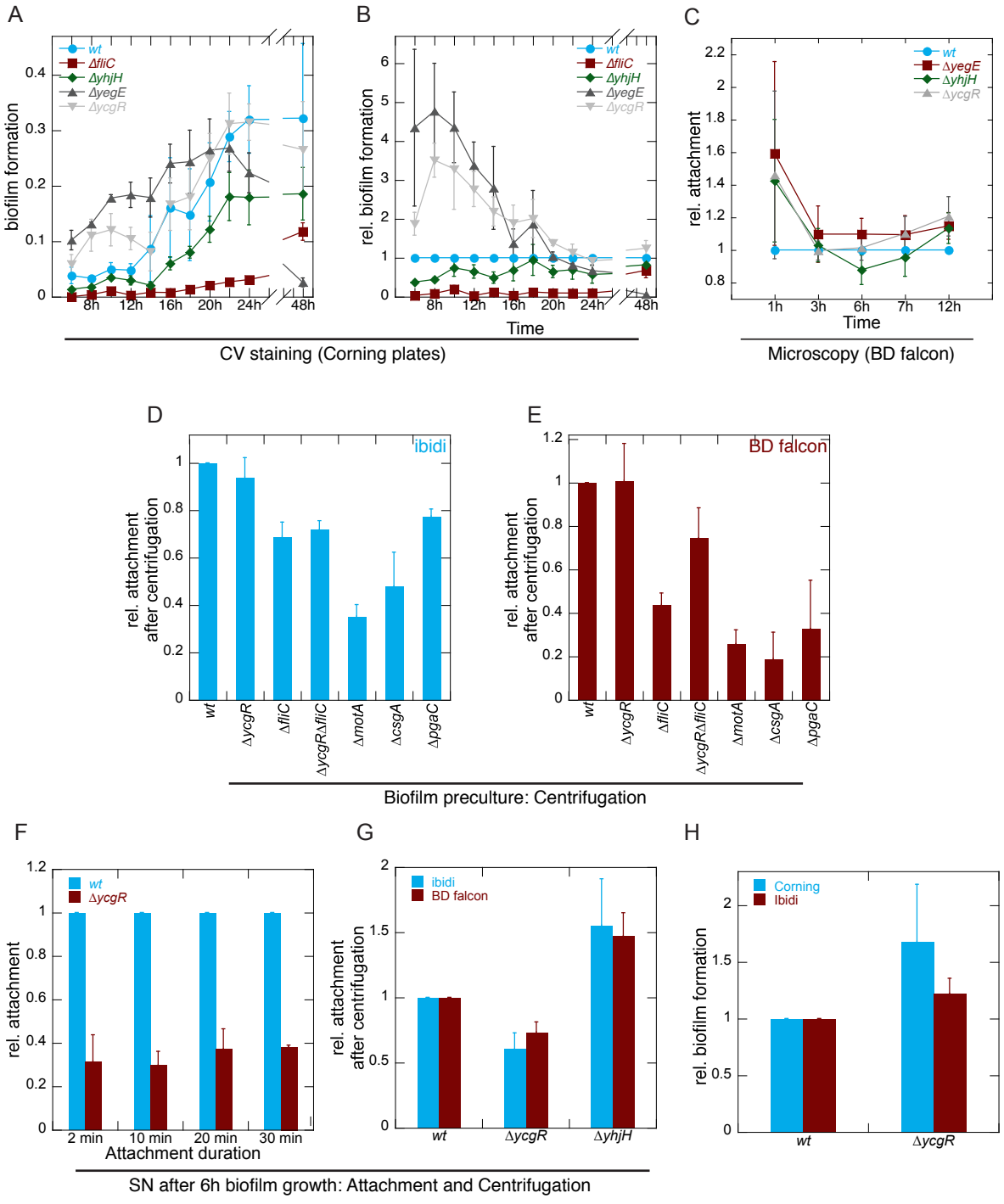

Fig. 6.13. Motility regulation by c-di-GMP alters biofilm formation in W3110^{RH}: (A) Early biofilm formation of W3110^{RH} wild type, Δ*fliC*, Δ*yhjH*, Δ*yegE* and Δ*ycgR* in TB medium at 30°C. Biofilms were formed on 96-well Corning® Costar®plates and stained with crystal violet (CV). Shown are mean and standard error of three to six replicates.
(B) Same experiment as in (A). Values from CV staining were first normalized to the OD_{600} of the culture and further to the wild type CV/OD values.
(C) Surface attachment during early biofilm formation of mixed cultures of W3110^{RH} wild type, Δ*yegE*, Δ*yhjH* and Δ*ycgR*. Cultures of wild type and mutant strains with different fluorescent labels were mixed 1:1 and biofilms were grown at in TB medium at 30°C on BD falcon^{TM} imaging plates. Unattached cells were removed an attached cells were quantified as in figure 6.9 (E). Mean and standard error of four to five replicates are shown.
(D-E) Surface attachment of biofilm precultures of W3110^{RH} wild type, Δ*ycgR*, Δ*fliC*, Δ*ycgR*Δ*fliC*, Δ*motA*, Δ*csgA* and Δ*pgaC* after centrifugation. W3110^{RH} wild type and mutant cells labeled with different fluorescent proteins were mixed 1:1 in TB medium and centrifuged on imaging plates. (*Continued on the following page.*)

Fig. 6.13. (*Continued from previous page.*)
Wild type cells labeled with two different fluorescent proteins served as a control. Non-attached cells were removed by washing. Attachment was quantified as in figure 6.4. Mean and standard error of two to five replicates are shown.
(D) Cells were centrifuged on ibidi® imaging plates.
(E) Cells were centrifuged on BD falcon^{TM} imaging plates.
(F) Surface attachment of W3110^{RH} wild type and Δ*ycgR* on ibidi® imaging plates. W3110^{RH} wild type and mutant cells labeled with different fluorescent proteins were grown in biofilm cultures on Corning® Costar®plates for 6 h at 30°C. Biofilm supernatant cells (i. e. unattached cells) were removed, washed in motility buffer, mixed 1:1, and incubated on ibidi® imaging plates for 2-30 min. Unattached cells were removed and attachment was quantified as in (D-E). Shown are mean and standard deviation of two replicates.
(G) Surface attachment of W3110^{RH} wild type and Δ*ycgR* on imaging plates. W3110^{RH} wild type and mutant cells labeled with different fluorescent proteins were grown in biofilm cultures on Corning® Costar®plates for 6 h at 30°C. Biofilm supernatant cells (i. e. unattached cells) were removed, mixed 1:1, and centrifuged on ibidi® and BD falcon^{TM} imaging plates. Unattached cells were removed and attachment was quantified as in (D-E). Shown are mean and standard error of two to six replicates.
(H) Biofilm formation of W3110^{RH} wild type and Δ*ycgR* on Corning® Costar®and ibidi® plates stained with CV. Biofilms were grown in TB medium at 30°C for 6 h. Unattached cells were removed and attached cells were stained with CV. Shown are mean and standard deviation of two replicates.

are hardly significant. These discrepancies to results observed in figures 6.13 A, B could stem from the fact that with CV staining, cells at the surface of the bottom and of the wall of the well are taken into account, whereas for the microscopy experiments, only cells at the bottom of the well are counted. To gain deeper insights into what happens on the imaging plates, I performed a more thorough analysis of attachment using a combination of centrifugation and attachment experiments in different imaging plates (see figure 6.13 D-H and 6.14 D). First of all, stickiness of biofilm precultures was investigated (figure 6.13 D, E). Cultures were prepared as for biofilm growth and centrifuged onto two different imaging plates (from ibidi® and BD falcon^{TM}). Attachment was quantified after washing off non-attached cells. Knockouts of *csgA* and *pgaC* show the requirement of curli and PGA on both plate types. Therefore, I speculate that if stickiness of a strain is affected, this might result from decreased expression of these matrix components. Deletion of *ycgR* did not change attachment on both surfaces, suggesting that sufficient biofilm matrix is produced. In contrast to the W3110 background (figure 6.4), deletion of *fliC* and *motA* seems to affect adhesion of W3110^{RH}. Similarly, deletion of *fliC* in the W3110^{RH} Δ*ycgR* mutant reduces attachment after centrifugation. These defects might indeed be mediated by decreased matrix production, as decreased *csgBA* expression was observed in W3110^{RH} Δ*fliC* and Δ*motA* (see figure A.12). However, to solve the fact that deletion of *ycgR* resulted in increased CV staining but not increased attachment in biofilm microscopy experiments, further analyses of attachment and stickiness of biofilm cultures were performed (see figure 6.13 F-H). For the attachment experiment in figure 6.13 F, I chose to take samples at 6 h of biofilm growth, which is the earliest time point in the

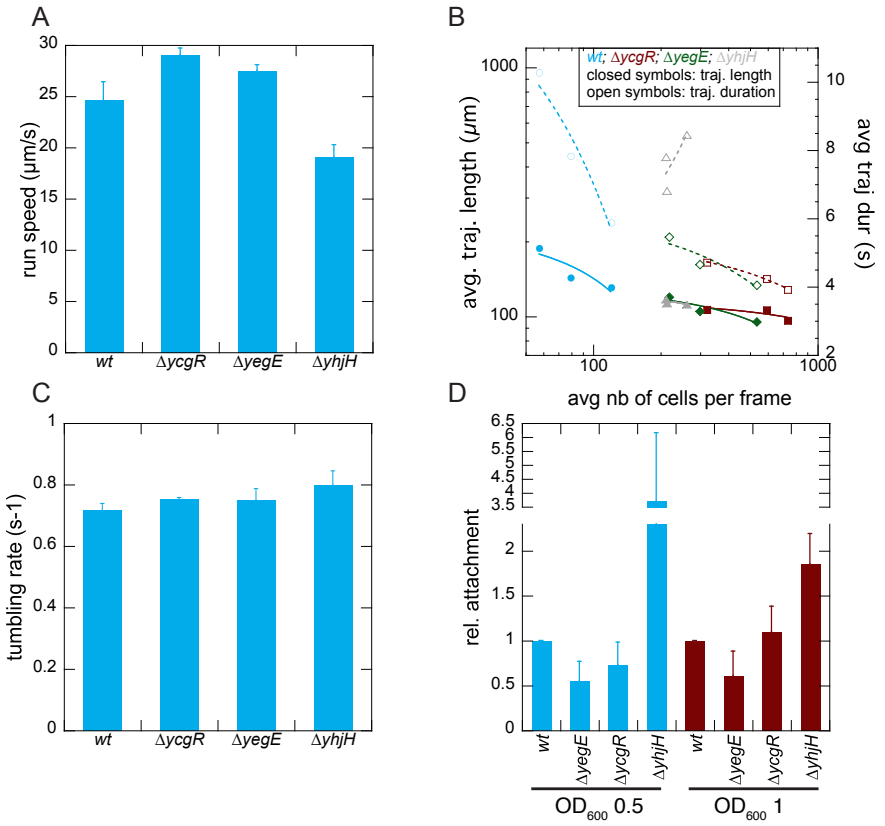

Fig. 6.14. Swimming behavior and attachment of W3110^{RH} strains with altered c-di-GMP signaling:
(A) Swimming speed of W3110^{RH} wild type, Δ*ycgR*, Δ*yegE* and Δ*yhjH* swimming grown in planktonic culture until OD_{600} 0.5. Shown are mean and standard error of three replicates. Experiment was performed by Dr. Remy Colin.
B) Trajectory lengths of W3110^{RH} wild-type, Δ*ycgR*, Δ*yegE* and Δ*yhjH* grown in planktonic culture until OD_{600} 0.5. Trajectory length and duration were plotted against the average cell number per image. Shown are three independent replicates per strain. Experiment was performed by Dr. Remy Colin.
(C) Tumbling rates of of W3110^{RH} wild-type, Δ*ycgR*, Δ*yegE* and Δ*yhjH* grown in planktonic culture until OD_{600} 0.5. Shown are mean and standard error of three replicates. Experiment was performed by Dr. Remy Colin.
(D) Surface attachment of W3110^{RH} wild-type, Δ*yegE*, Δ*ycgR* and Δ*yhjH* grown in planktonic culture until OD_{600} 0.5 and 1. Cells were prepared for surface attachment in motility buffer on ibidi® imaging plates and allowed to attach for 1 h. Unattached cells were removed. Surface attachment was quantified as in figure 6.4. Shown are mean and standard deviation of two replicates.

CV staining experiment (figure 6.13 A). Therefore, biofilms with fluorescently labeled cells were grown for 6 h in Corning® Costar® plates (same plates as used in figures 6.13 A, B), unattached cells were removed and wild type and Δ*ycgR* cells were mixed at 1:1 ratio for attachment on ibidi® plates. At 6 h, Δ*ycgR* shows increased attachment with CV staining and therefore, increased attachment on microscopy plates was expected. In contrast, attachment of Δ*ycgR* was reduced in comparison to wild type (figure 6.13 F). This reduced attachment seems to stem from reduced stickiness of Δ*ycgR* (figure 6.13 G). In contrast,

Δ*yhjH* seems to be stickier than the wild type, as was observed for planktonic W3110 Δ*yhjH* (figure 6.10). One possibility to explain the discrepancies between attachment on imaging plates in figures 6.13 C, F to the attachment on Corning® Costar® plates in figures 6.13 A, B would be that the surface of the plates influences the attachment behavior. Therefore, a comparison of CV staining of wild type and Δ*ycgR* biofilms at 6 h on Corning® Costar® and ibidi® plates was performed. Indeed, the difference in attachment between wild type and Δ*ycgR* is less pronounced on the imaging plates, however, this does not explain why attachment of Δ*ycgR* was reduced in figure 6.13 F.
Regardless of the ambiguity of the Δ*ycgR* attachment results, tracking experiments with planktonic cells showed that effects of c-di-GMP on swimming speed are similar between W3110 and W3110^{RH} (figures 6.10 A and 6.14 A). Similarly, analysis of W3110^{RH} trajectories at the surface gave no difference in trajectory lengths between the strains but longer trajectory duration for Δ*yhjH*, which again can be explained by its lower swimming speed (figure 6.14 B). Importantly, tumbling rates were also similar between wild type and c-di-GMP mutant strains (figure 6.14 C). To correlate the tracking data (figure 6.14 A-C) to the biofilm attachment data (figure 6.13 A, B), attachment with planktonic cultures were performed at OD_{600} 0.5 and 1 (figure 6.14 D). In contrast to the increased attachment of Δ*ycgR* and Δ*yegE* in the CV-stained biofilms, these strains showed similar (Δ*ycgR*) or even reduced (Δ*yegE*) attachment in comparison to the wild type. Δ*yhjH* on the contrary showed increased attachment, as was also observed for planktonic W3110 cultures (figure 6.10 D, E). Altogether, I was not able to explain the attachment data for Δ*ycgR* in the W3110^{RH} background, although CV staining data (figure 6.13 A, B) suggest a dual role of c-di-GMP, inhibiting early attachment and promoting biofilm maturation. Further experiments regarding c-di-GMP-dependence of mature biofilms will be discussed in the following chapter.

Part III

THREE-DIMENSIONAL STRUCTURE FORMATION IN STATIC SUBMERGED BIOFILMS

7. DETERMINANTS OF 3-D STRUCTURE IN *E. COLI* W3110^{RH} BIOFILM FORMATION

Three-dimensional (3-D) structure formation in biofilms can be analyzed with different methods, such as in dynamic flow systems [151, 152, 153], on agar surfaces (e. g. [150, 27]) or in static cultures [136]. In this thesis, static biofilms were grown on 8-well slides from ibidi® (see figure 7.1 A). The RpoS-deficient W3110 strain is not able to form elaborate three-dimensional structures as the RpoS-positive W3110^{RH} (figure 7.1 B). In W3110^{RH} wild type, the 3-D structures consist of large clumps of cells that are loosely attached to each other and to the surface of the wells (figure 7.1 C). A third strain used in this work is the cellulose-producing *E. coli* K-12 strain AR3110. AR3110 is a cured W3110^{RH} derivative, in which an SNP in the *bcsQ* gene that creates a *STOP* codon was repaired [86]. The cellulose-positive AR3110 is able to form 3-D structures that are flatter and more compact than the structures observed for W3110^{RH} (see figure 7.1 D).

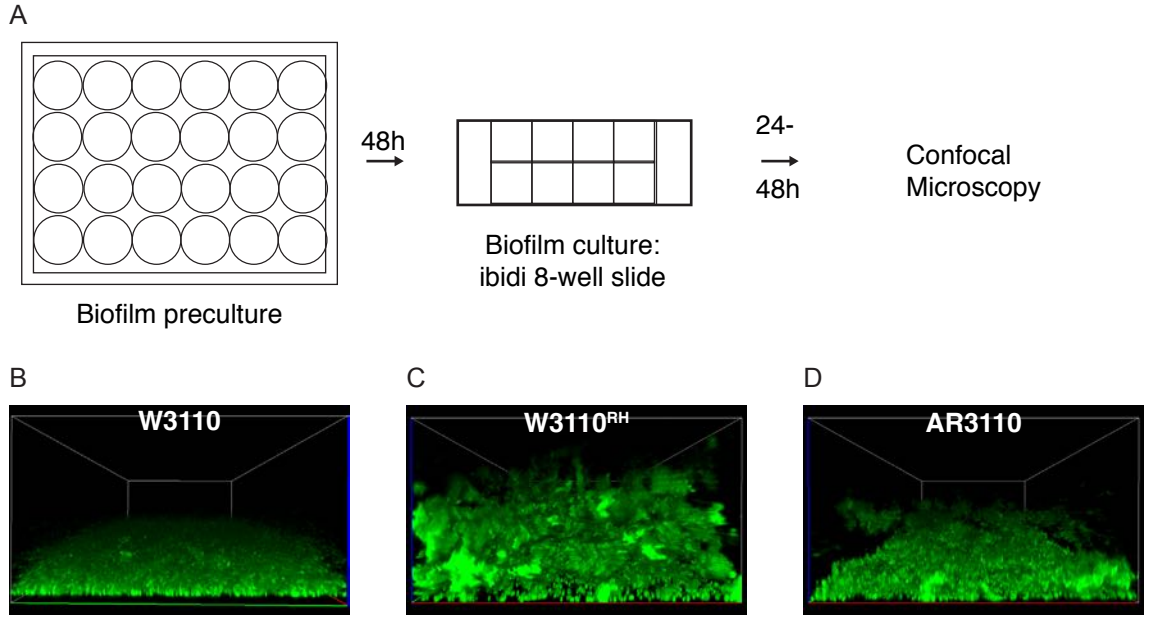

Fig. 7.1. Overview of static submerged biofilm formation:
(A) Biofilm precultures were grown at 30°C for 48 h in TB. Biofilm cultures were prepared in ibidi® 8-well slides and grown for additional 24-48 h in TB at 30°C. Three-dimensional structure formation was visualized by confocal microscopy.
(B-D) Confocal images showing the structures formed by W3110, W3110^{RH} and AR3110. Cells were labeled with GFP and biofilms were grown for 48 h. Dimensions of bounding box (x:y:z): 142:142:80 μm.

7.1 Role of cell surface structures in 3-D biofilms

I aimed to investigate the role of flagella and motility in the formation of 3-D structures in W3110^{RH}. Therefore, the first step was to understand and characterize the structures that the strain forms. For this, I grew biofilms of strains lacking the main biofilm matrix components of *E. coli*, curli ($\Delta csgA$), PGA ($\Delta pgaC$) and colanic acid ($\Delta wcaF$) ([154, 9, 1]; see figure 7.2 and figures A.5 and A.6 in the Appendix). Out of the main matrix components, only curli seems to abolish 3-D structure formation with $\Delta csgA$ cells growing as a flat biofilm (figure 7.2 B and figures A.5 B, A.6 B). In contrast, structures of $\Delta pgaC$ (figure 7.2 C and figures A.5 C, A.6 C) and $\Delta wcaF$ (figure 7.2 D and figures A.5 D, A.6 D) resemble wild type. The importance of curli as part of the matrix in our static biofilm model is in consistence with its role in shaping biofilm macrocolonies, as was published previously [27]. In addition to these matrix components, cell surface structures, such as fimbriae, autoaggregative proteins or other adhesins can alter the adhesive and aggregative properties of cells and might therefore play a role in biofilm formation [1, 155, 156, 157, 158] . We therefore aimed to understand the role of different adhesins in our static W3110^{RH} biofilm model. I chose a subset of mutants that showed defects in attachment in the CV assay (unpublished results from O. Besharova) and analyzed their potential to form 3-D structures (see figure 7.3 and figures A.7 and A.8 in the Appendix). *fimA*, *sfmA*, *ybgP*, *yraH* and *yehB* are part of putative chaperone-usher fimbriae operons [155], *yfaL* and *ycgV* are potential adhesin genes [159] and *flu* encodes the autotransporter Ag43 [160, 161]. All of the knockouts were able to form 3-D structures except *yfaL* and *ycgV* (figures 7.3, A.7 F, G), which formed flat biofilms. Strikingly, $\Delta yfaL$ and $\Delta ycgV$ both did not swim on soft agar plates, whereas swimming behavior of the other knockouts was similar to wild type (see figure A.9). The results of the matrix and cell surface structure knockouts therefore suggest that curli are the main cell surface structures that help to shape the 3-D structures. YfaL and YcgV are apparently important as well, however, it is unclear whether their contribution is to support structure formation via their potential adhesin function or because they affect swimming motility.

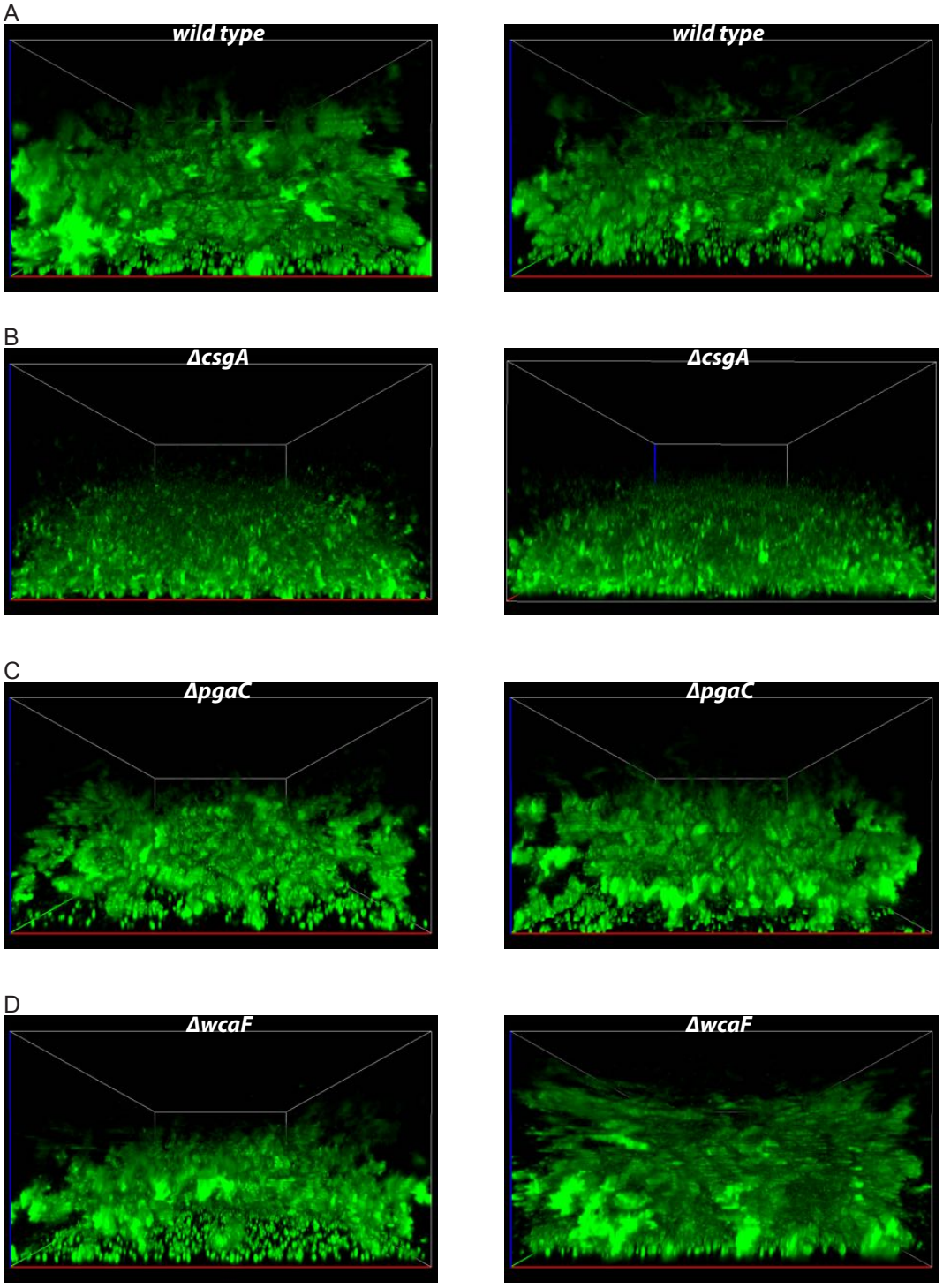

Fig. 7.2. Curli is the main structural part of the W3110^{RH} biofilm matrix: Confocal images of 48 h old biofilms of W3110^{RH} wild type (A), Δ*csgA* (B), Δ*pgaC* (C) and Δ*wcaF* (D). Images of two biological replicates are shown. Dimensions of bounding box (x:y:z): 142:142:80 μm.

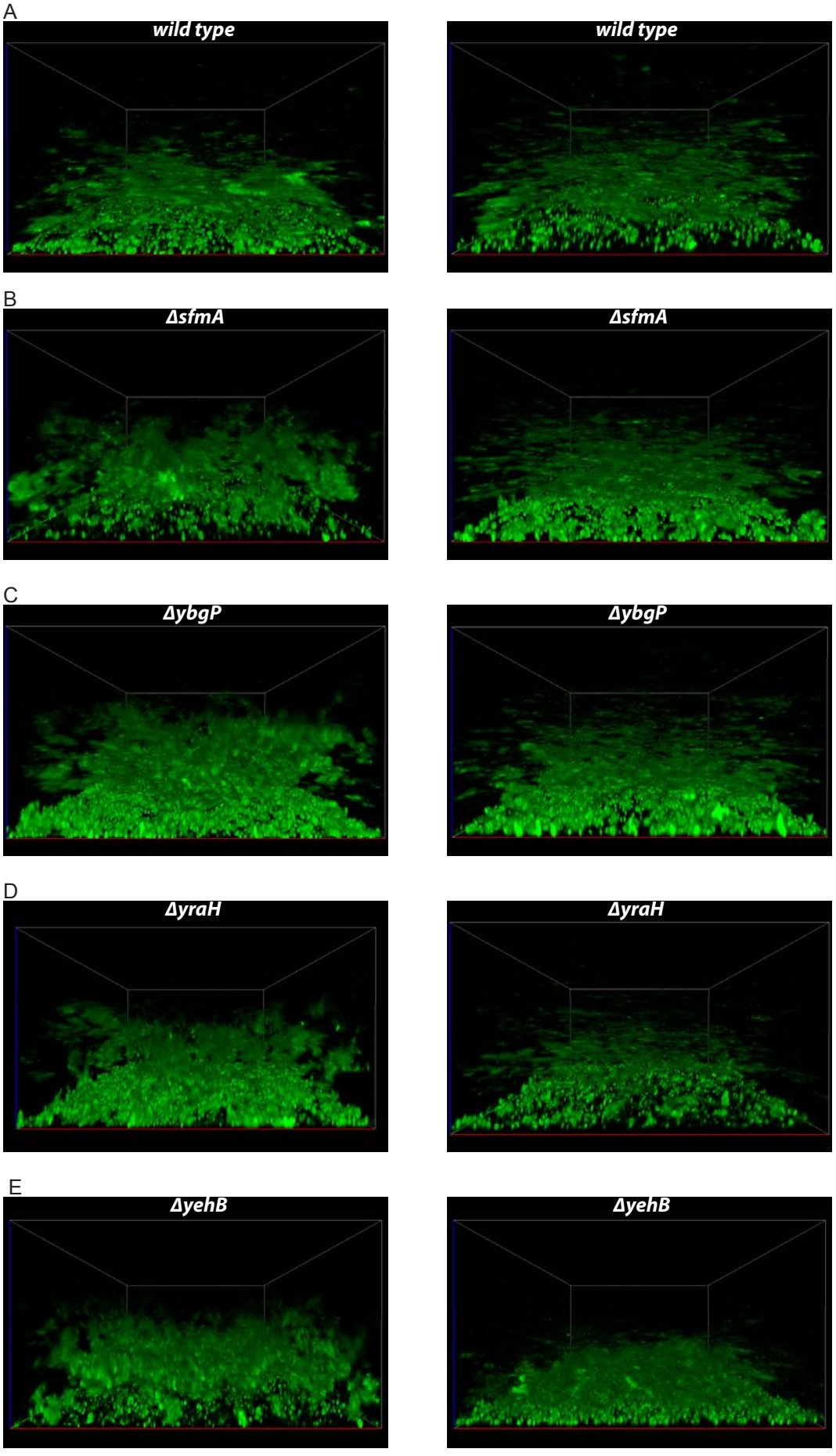
A
wild type
wild type
B
ΔsfmA
ΔsfmA
C
ΔybgP
ΔybgP
D
ΔyraH
ΔyraH
E
ΔyehB
ΔyehB

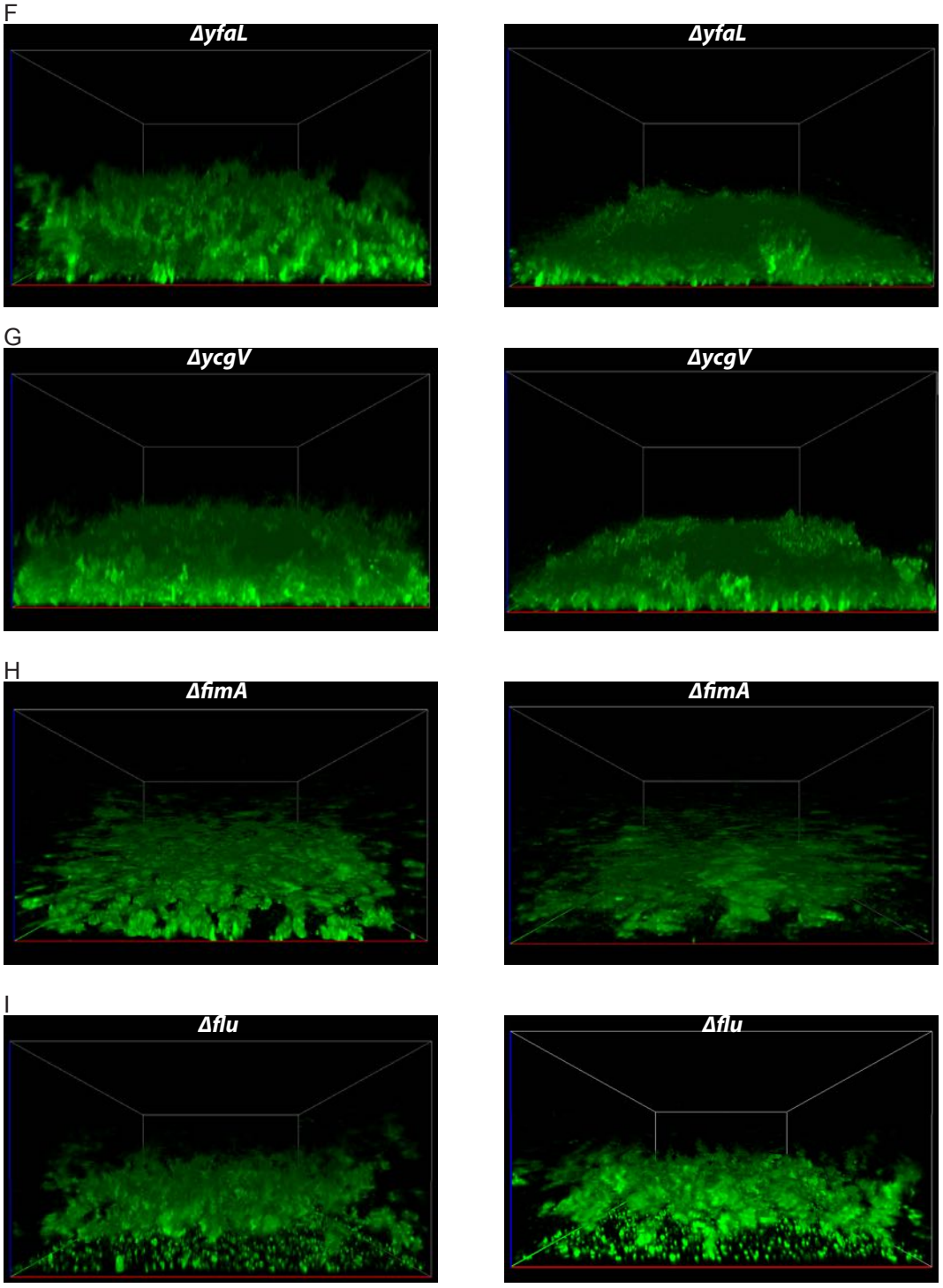

Fig. 7.3. Role of *E. coli* adhesins in three-dimensional structure formation: Confocal images of 48 h old biofilms of W3110^{RH} wild type (A), Δ*sfmA* (B), Δ*ybgP* (C), Δ*yraH* (D), Δ*yehB* (E), Δ*yfaL* (F), Δ*ycgV* (G), Δ*fimA* (H) and Δ*flu* (I). Images of two biological replicates are shown. Dimensions of bounding box (x:y:z): 142:142:80 μm.

7.2 Role of motility in 3-D biofilms

In chapter 6, I could show that flagella-driven motility is a requirement for attachment during static submerged biofilm formation. The logical question to ask was whether flagella and motility play a role in later, mature biofilm stages. We therefore checked the motility mutants from chapter 6 for their ability to form 3-D structures (see figure 7.4). As described above, W3110^{RH} wild type formed elaborate 3-D structures that consisted of large clumps of cells that are loosely associated with the surface-attached cells (see figure 7.4 A and figures A.10 A and A.11 A in the Appendix). These structures were abolished when flagella were deleted (see figure 7.4 B and figures A.10 B and A.11 B in the Appendix). This defect was not primarily due to the lack of motility since 3-D structures were observed for the non-motile Δ*motA* strain that has paralyzed flagella (see figure 7.4 C and figures A.10 C and A.11 C in the Appendix), and for the tumbly Δ*cheZ* (see figure 7.4 D and figures A.10 D and A.11 D in the Appendix). However, the overall structure was affected in these mutants, meaning that motility might contribute to the exact 3-D shape of the structures. A structural role of flagella has been suggested in a previous publication, where the authors speculate that intertwined flagella form a meshwork that stabilizes structures of bacterial macrocolony biofilms [27]. This intertwining of flagella apparently requires flagellar motor function. Since in our biofilm model, Δ*motA* is able to form 3-D structures, albeit with different shape, I speculate that flagellar rotation is dispensable for structure formation. With the flat biofilm structure of Δ*fliC* and the irregular structures of Δ*motA* with large clumps of cells being surrounded by flat layers, the mutants might be affected in matrix production. I therefore checked expression of the main biofilm matrix component curli using a genomic *csgBA::gfp*-reporter and flow cytometry (see figure A.12). Indeed, overall expression was reduced in the mutant strains. If however expression on single-cell level and not population-level is considered (not shown; and unpublished data from O. Besharova), it becomes clear that heterogeneity of gene expression is affected. Δ*motA* cells for example show high curli expression in the clump-like structure in biofilms, whereas expression is low in the surrounding flat layers (unpublished data from O. Besharova).

Mixing of wild type with Δ*fliC* cells gave some hints about a possible structural role of flagella. If wild type cells are mixed with differently labeled wild type cells at 1:1 ratio, the structures are usually dominated by one of the strains, suggesting a microcolony-like growth of the biofilm (see figure 7.5 A and figures A.13 A and A.14 A). In mixing experiments with wild type and Δ*fliC* strains, Δ*fliC* cells could integrate into 3-D structures formed by wild type whereas Δ*fliC* mixed with Δ*fliC* resulted in flat biofilms (see figure 7.5 C-E and figures A.13 C-E and A.14 C-E). Δ*fliC* cells alone seem to be able to form microcolony-like structures at the bottom of the well (see figure 7.5 C and figures A.13 C and A.14 C), however cannot arrange in 3-D structures. In mixtures with wild type, these microcolonies seem to get entrapped into wild type structures, and the degree of integration seems to depend on the ratio at which wild type and Δ*fliC* cells are mixed

(see figure 7.5 D, E and figures A.13 D, E and A.14 D, E). Altogether, the results in figures 7.2-7.5 suggest a requirement of curli, the adhesins YfaL and YcgV, as well as flagella for 3-D structure formation.

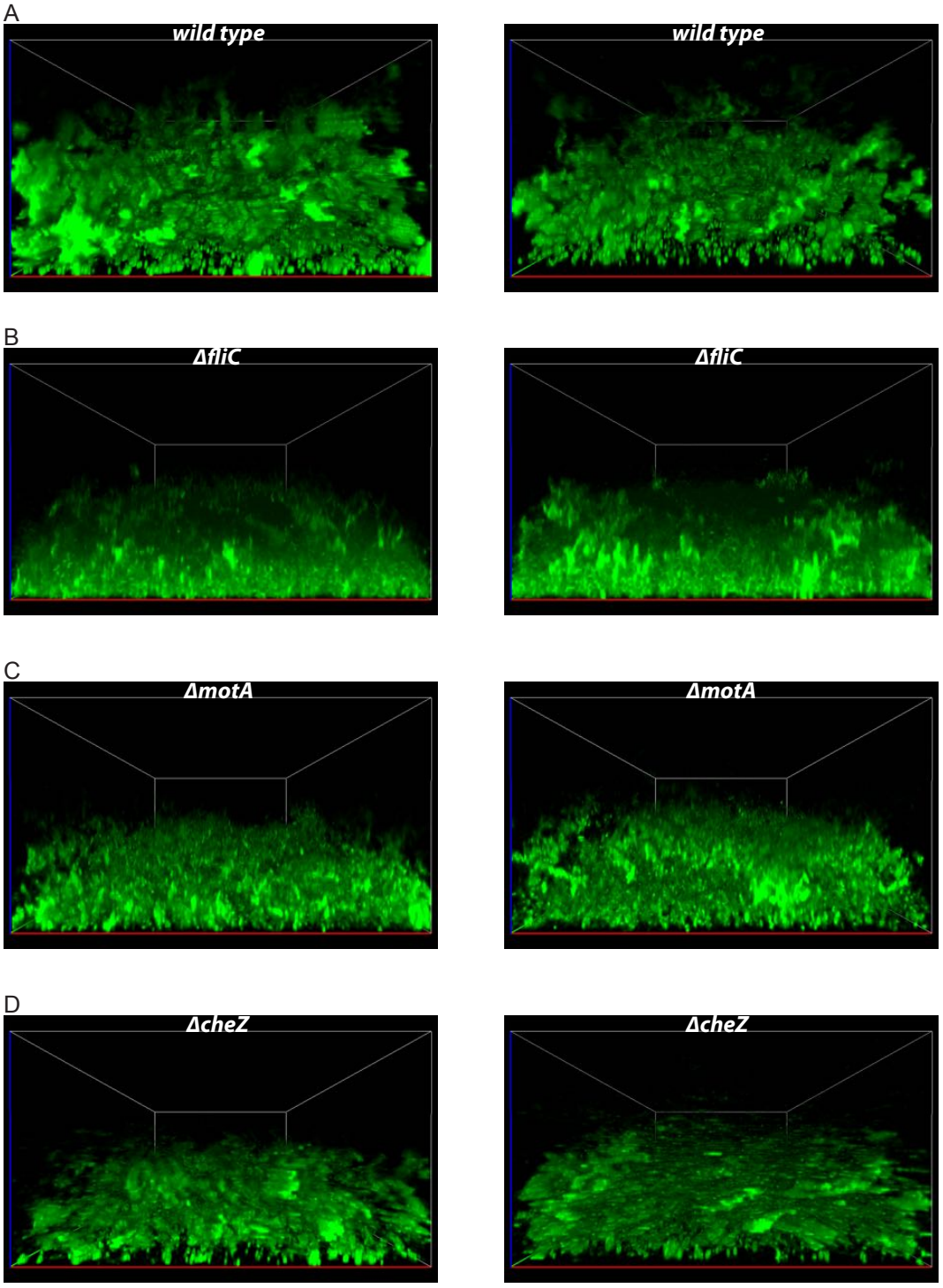

Fig. 7.4. Role of motility in three-dimensional structure formation:
Confocal images of 48 h old biofilms of W3110^{RH} wild type (A), Δ*fliC* (B), Δ*motA* (C) and Δ*cheZ* (D). Images of two biological replicates are shown. Dimensions of bounding box (x:y:z): 142:142:80 μm.

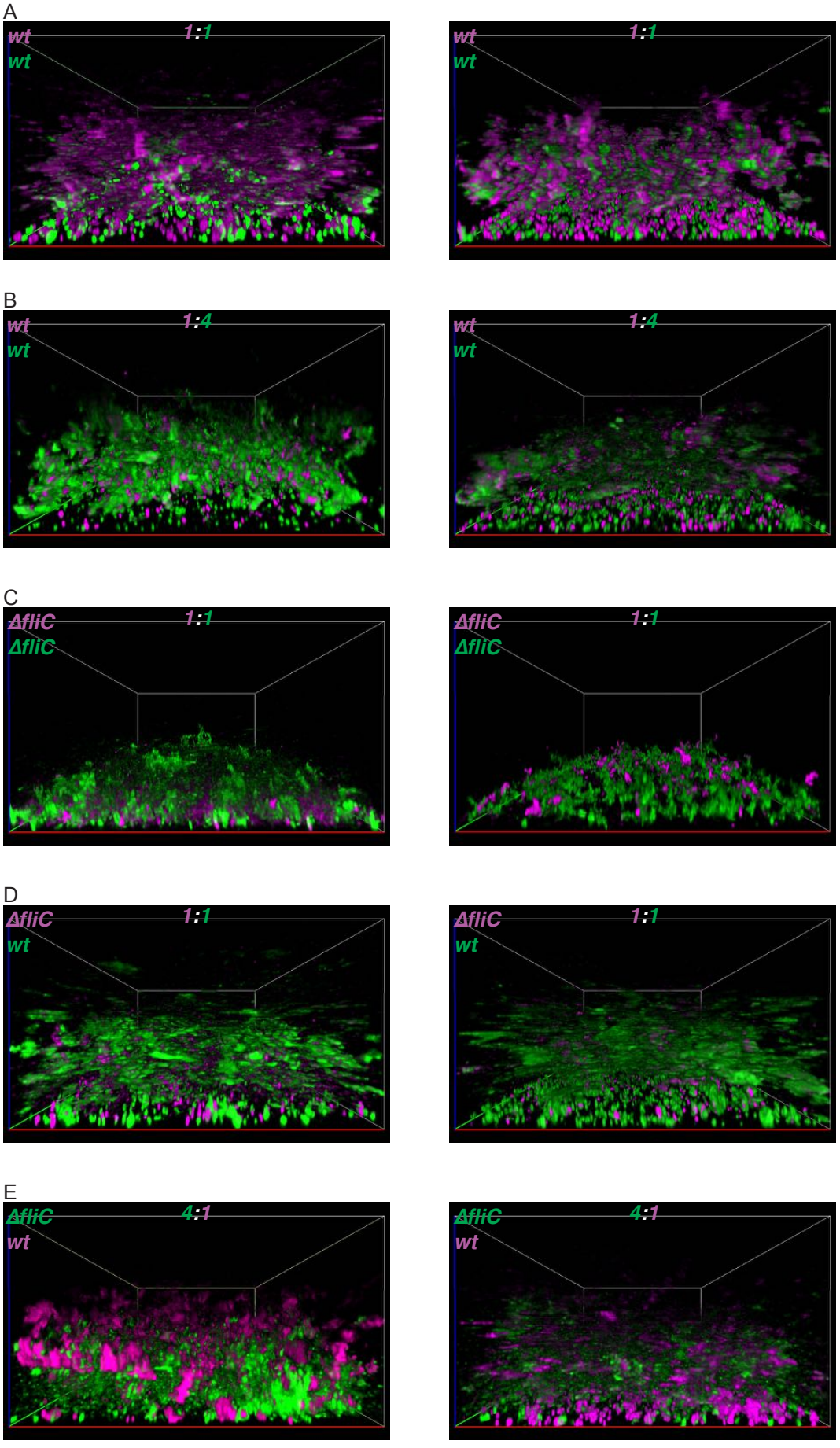

Fig. 7.5. Flagella-less cells can partially integrate into three-dimensional structures of W3110^{RH} wild type:
(*Continued on the following page.*)

Fig. 7.5. (*Continued from previous page.*)
Confocal images of 48 h old biofilms of different mixtures of W3110^{RH} wild type and Δ*fliC*. Wild type and Δ*fliC* cells labeled with different fluorescent proteins were mixed as indicated and biofilms of mixed cultures were grown.
(A) Wild type cells labeled with mCherry (magenta) and GFP (green) were mixed 1:1.
(B) Wild type cells labeled with mCherry (magenta) and GFP (green) were mixed 1:4.
(C) Δ*fliC* cells labeled with mCherry (magenta) and GFP (green) were mixed 1:1.
(D) Δ*fliC* cells labeled with mCherry (magenta) and wild type cells labeled with GFP (green) were mixed 1:1.
(E) Δ*fliC* cells labeled with GFP (green) and wild type cells labeled with mCherry (magenta) were mixed 4:1.
Images of two biological replicates are shown. Dimensions of bounding box (x:y:z): 142:142:80 μm.

7.3 Role of c-di-GMP in 3-D biofilms

In chapter 6, I suggested a dual role for c-di-GMP, inhibiting early attachment through inhibition of motility and promoting later biofilm stages through upregulation of matrix factors. This would mean that deletion of c-di-GMP modulating enzymes would lead to changes in mature biofilm formation, not only in attachment, as shown e. g. for Δ*yegE* in figure 6.13 A, B, but also in the formation of 3-D structures. Indeed, deletion of *yegE* leads to the formation of flat biofilms with little clump formation (see figure 7.6 and figures A.15 A and A.16 A in the Appendix) at 48 h, the timepoints at which also attachment of *yegE* was markedly reduced in comparison to wild type (figure 6.13 A, B). However, this defect becomes already very clear at 24 h (see figure A.17 A and A.18 A), when attachment was still almost similar to wild type (figure 6.13 A, B). The 3-D structures formed by Δ*ycgR* resemble those of wild type wild type, confirming that the effect of *yegE* in later biofilm stages is not mediated by the motility control but through effects of c-di-GMP on matrix production (see figures 7.6 C and A.15 - A.18 C). Therefore, I expected that deletion of *yhjH*, which should lead to higher c-di-GMP production, does not affect 3-D structure formation despite its defect in attachment at earlier stages (figure 6.13 A, B). Indeed, the phenotype of Δ*yhjH* is similar to wild type at both 24 h and 48 h (see figures 7.6 B and A.15 - A.18 B).

7.4 Role of motility and c-di-GMP in AR3110 3-D biofilms

Both curli and cellulose production depend on c-di-GMP (see e. g. references [150, 10, 11, 12]). Thereby, defects in c-di-GMP signaling could also affect 3-D structures in AR3110. Additionally, I aimed to investigate whether the effect of motility mutants was similar between W3110^{RH} and AR3110. As described above, biofilms formed by AR3110 are flatter than W3110^{RH} (figure 7.1 C, D), which is why I chose to show a different projection for the AR3110 strain (see figures 7.7 and figures A.19, A.20 in the Appendix). Similar to the defect in W3110^{RH} (see figures 7.4, A.10 and A.11 for comparison), deletion of flagella in AR3110 abolishes 3-D structure formation with Δ*fliC* growing in a flat layer of cells

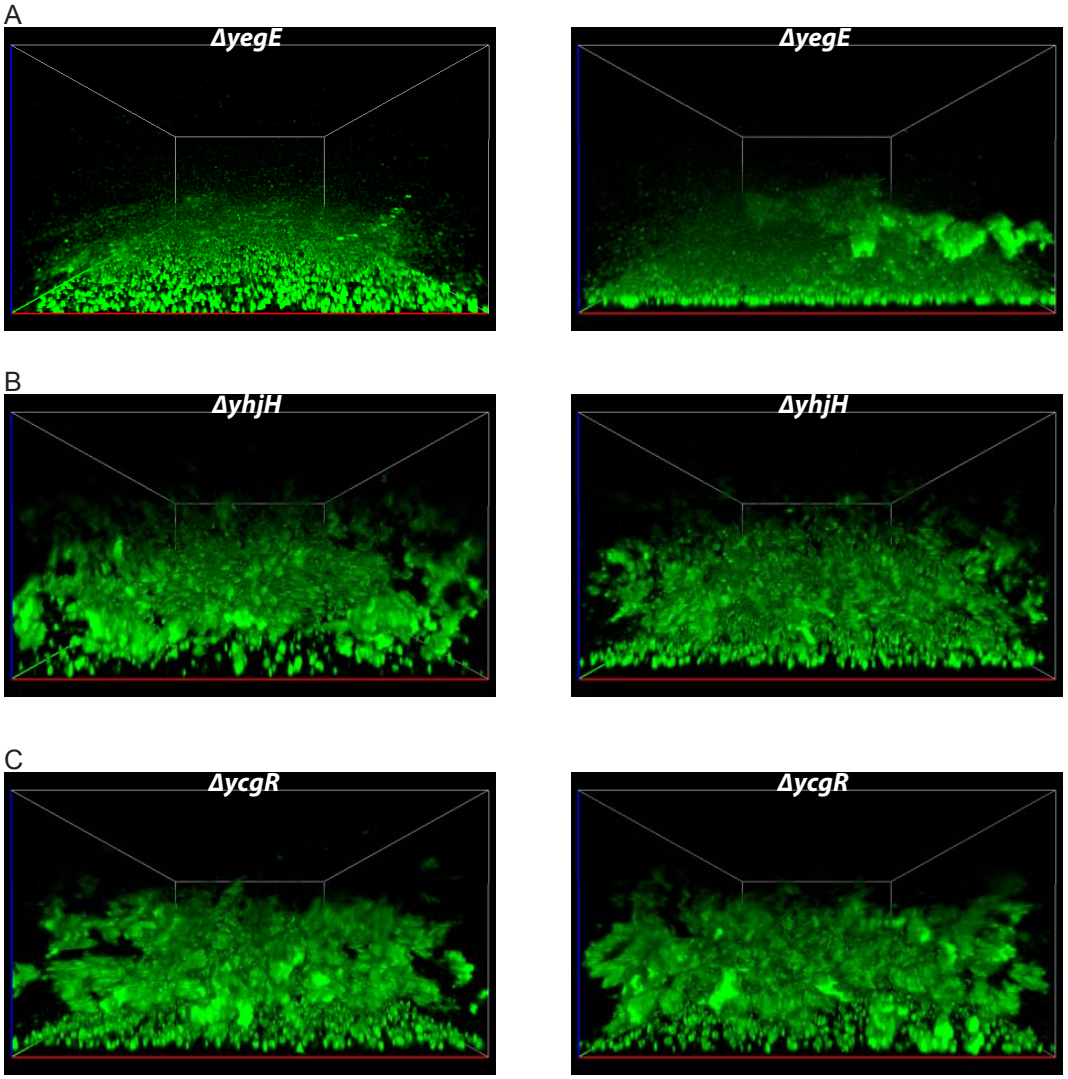

Fig. 7.6. Role of c-di-GMP in three-dimensional structure formation:
Confocal images of 48 h old biofilms of W3110^{RH} Δ*yegE* (A), Δ*yhjH* (B) and Δ*ycgR* (C). Images of two biological replicates are shown. Dimensions of bounding box (x:y:z): 142:142:80 μm.

(see figures 7.7 B and figures A.19 B, A.20 B). Also in agreement with W3110^{RH} data, flagella rotation is dispensable for structure formation (see figures 7.7 C and figures A.19 C, A.20 C). However, the shape of Δ*motA* structures differs from wild type in a way, that thick clumps of cells form within a flat and unstructured layer of cells, a phenotype that is similar in W3110^{RH} Δ*motA*. Furthermore, the effects of c-di-GMP on mature biofilm formation seem to be conserved between W3110^{RH} and AR3110 (see figures 7.6, A.15 and A.16 for comparison). Deletion of the cyclase *yegE* considerably reduces structure formation in AR3110 (see figures 7.7 D and figures A.19 D, A.20 D), whereas deletion of the PDE YhjH yields structures similar to AR3110 wild type (see figures 7.7 E and figures A.19 E, A.20 E). In summary, the effects of motility and c-di-GMP mutants on 3-D structures seem to be conserved between W3110^{RH} and AR3110.

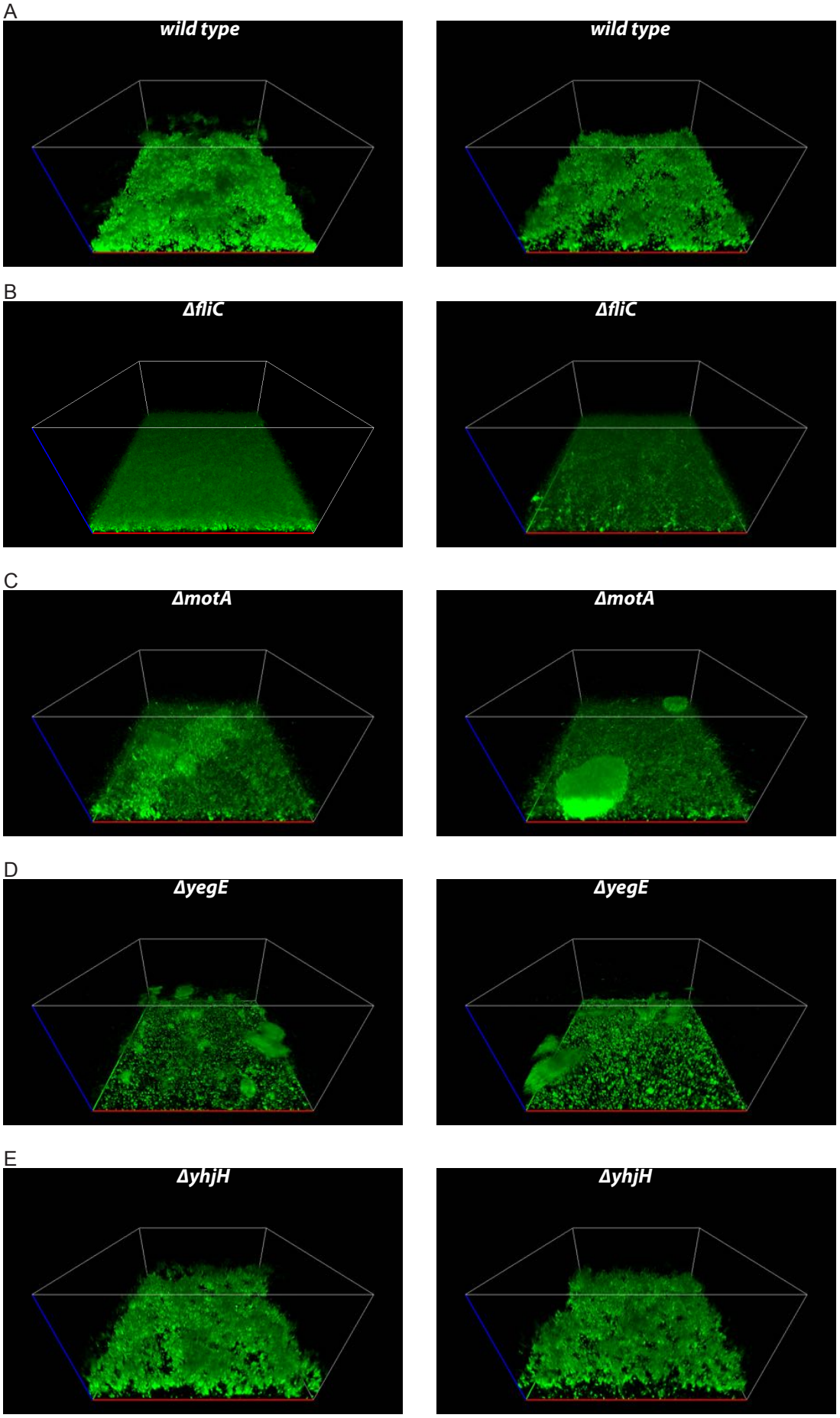

Fig. 7.7. Role of motility and c-di-GMP in AR3110 three-dimensional structure formation:
(*Continued on the following page.*)

Fig. 7.7. (*Continued from previous page.*)
Confocal images of 48 h old biofilms of AR3110 wild type (A), Δ*fliC* (B), Δ*motA* (C), Δ*yegE* (D) and Δ*yhjH* (E). Images of two biological replicates are shown. Dimensions of bounding box (x:y:z): 142:142:80 μm.

Part IV

A NEW REGULATOR OF C-DI-GMP SIGNALING

8. THE DYNAMIN-LIKE PROTEIN YJDA REGULATES MOTILITY AND BIOFILM FORMATION IN *E. COLI*

8.1 YjdA inhibits motility

In a previous screen for motility mutants, deletion of genes *yegE*, *yjdA* and *yjcZ* were identified to suppress the c-di-GMP-mediated Δ*yhjH* motility defect on soft agar plates [145]. YegE today is known to be one of the main cyclases that synthesize c-di-GMP for the pool regulating motor curbing through YcgR (see references [10, 11, 12] and [146, 58, 147]). YjdA and YjcZ are expressed from the same operon, supposedly through the flagellar sigma factor FliA (*ecocyc.org* and unpublished data from Y. Rudenko). YjcZ is a small protein of unknown function whereas YjdA is a bacterial dynamin-like protein [124, 125]. YjdA has been previously published to help in chromosomal replication and has been termed CrfC (colocalization of the replication fork DNA by the clamp) by the authors [109]. Since my data do not relate to the theory of Ozaki et al [109], I will continue to use the name YjdA in this thesis. If deletion of *yjdA* and *yjcZ* in the Δ*yhjH* background partially suppresses its motility defect, YjdA and YjcZ must regulate c-di-GMP levels in a so far unknown way. We therefore aimed to figure out, on which level YjdA or YjcZ affect c-di-GMP signaling. According to Boehm et al. [146], YhjH diminishes the c-di-GMP pool created by the activity of the four cyclases YegE, YddV, YfiN and YedQ. This c-di-GMP pool is sensed by the motor-binding protein YcgR. It is therefore plausible that YjdA and YjcZ regulate one of those main cyclases. To answer this question, an epistasis experiment on soft agar plates was performed (see figure 8.1). Deletion of all cyclases in the Δ*yhjH* background results in relieve of the motility defect (figure 8.1 A, B). Deletion of *yjdA* or *yjcZ* in the Δ*yhjH*Δ*cyclase* background however, only results in additive effects in combination with Δ*yddV*, Δ*yfiN* and Δ*yedQ*. Swimming of Δ*yhjH*Δ*yegE*Δ*yjdA* and Δ*yhjH*Δ*yegE*Δ*yjcZ* is similar to swimming of Δ*yhjH*Δ*yegE* (figure 8.1 A). Together with previous results from Dr. Hui Li in the *E. coli* K-12 strain MG1655, my data in W3110^{RH} (figure 8.1) and W3110 (not shown) show that YjdA and YjcZ regulate motility and c-di-GMP production via YegE.

8.2 YjdA reduces attachment and increases 3-D structure formation in biofilms

With my results from chapter 6 showing that c-di-GMP inhibits attachment in early biofilm formation, it was plausible to test the effects of YjdA and YjcZ on biofilm formation.

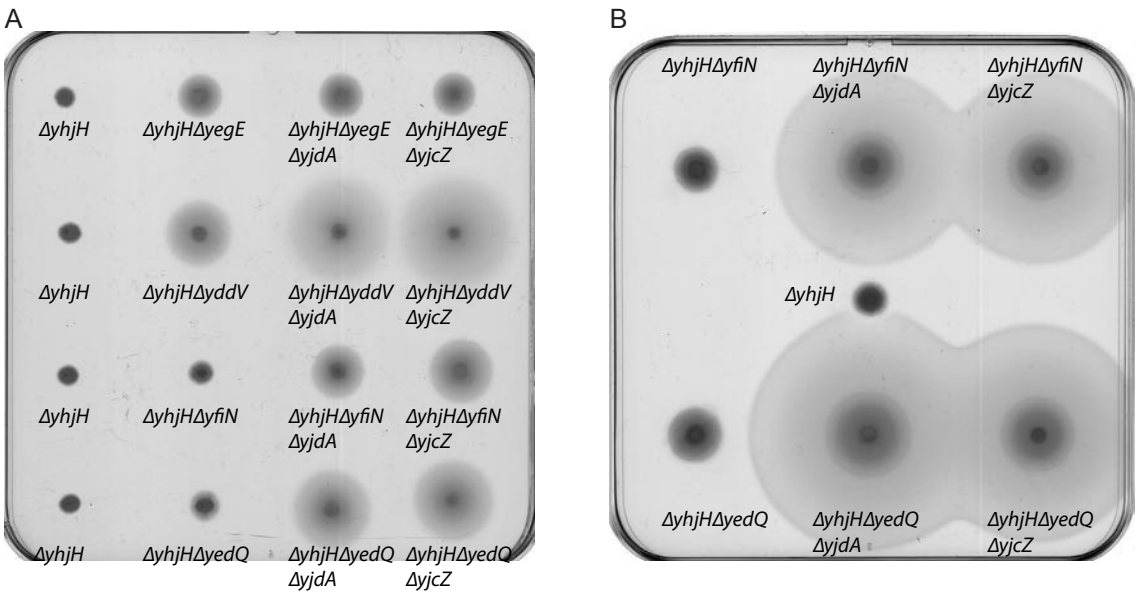

Fig. 8.1. YjdA regulates c-di-GMP production via YegE:
Swimming of W3110^{RH} mutant strains on soft agar plates. The swimming defect of W3110^{RH} Δ*yhjH* can be partially rescued by knockout of the cyclases YegE, YddV, YfiN and YedQ.
(A) Additional knockout of YjdA or YjcZ in the Δ*yhjH*Δ*yegE* strain does not lead to an additive effect, whereas knockout of YjdA or YjcZ in the Δ*yhjH*Δ*yddV*, Δ*yhjH*Δ*yfiN*, Δ*yhjH*Δ*yedQ* strains does increase the rescue of the *yhjH* knockout.
(B) Same as in the two lower panels in (A), only cells were allowed to swarm for a more prolonged time to illustrate rescue of Δ*yhjH* by Δ*yfiN* and Δ*yedQ*.

Figure 8.2 A, B shows surface attachment of W3110, figure 8.2 C, D of W3110^{RH}. After 24 h, biofilm formation of both Δ*yjdA* and Δ*yjcZ* is similarly increased as biofilm formation of Δ*yegE* (figure 8.2 A). As shown for Δ*yegE* and Δ*yhjH* in figure 6.9 B, the effect of YjdA and YjcZ was mediated by the motility control through YcgR, since Δ*yjdA*Δ*ycgR* and Δ*yjcZ*Δ*ycgR* double knockouts had similar effects as the single knockouts. Analysis of very early attachment by microscopy confirmed that YjdA and YjcZ affect biofilm formation similarly to YegE, with similar level of attachment between the strains (figure 8.2 B). Biofilm formation in W3110^{RH} supports the data from W3110 with again same effects of Δ*yegE*, Δ*yjdA* and Δ*yjcZ* (figure 8.2 C, D). To support the theory that YjdA and YjcZ regulate c-di-GMP signaling through YegE, we exploited the c-di-GMP-dependent interaction between YcgR and the stator protein MotA [146] as a tool to relatively assess c-di-GMP levels (see figure 8.2 E-G). FRET between YFP-YcgR and MotA-CFP can be measured at sufficient c-di-GMP levels and decreases if less c-di-GMP is present, as shown by decreased (W3110, see figure 8.2 F) or absent (W3110^{RH}, see figure 8.2 G) FRET in Δ*yegE*. In contrast, at high c-di-GMP as in the deletion of the PDE *yhjH*, FRET is increased (W3110^{RH}, see figure 8.2 G). In both wild type backgrounds, deletion of *yjdA* and *yjcZ* results in similar FRET as measured for Δ*yegE*, supporting the theory that YjdA and YjcZ together regulate c-di-GMP production by YegE.

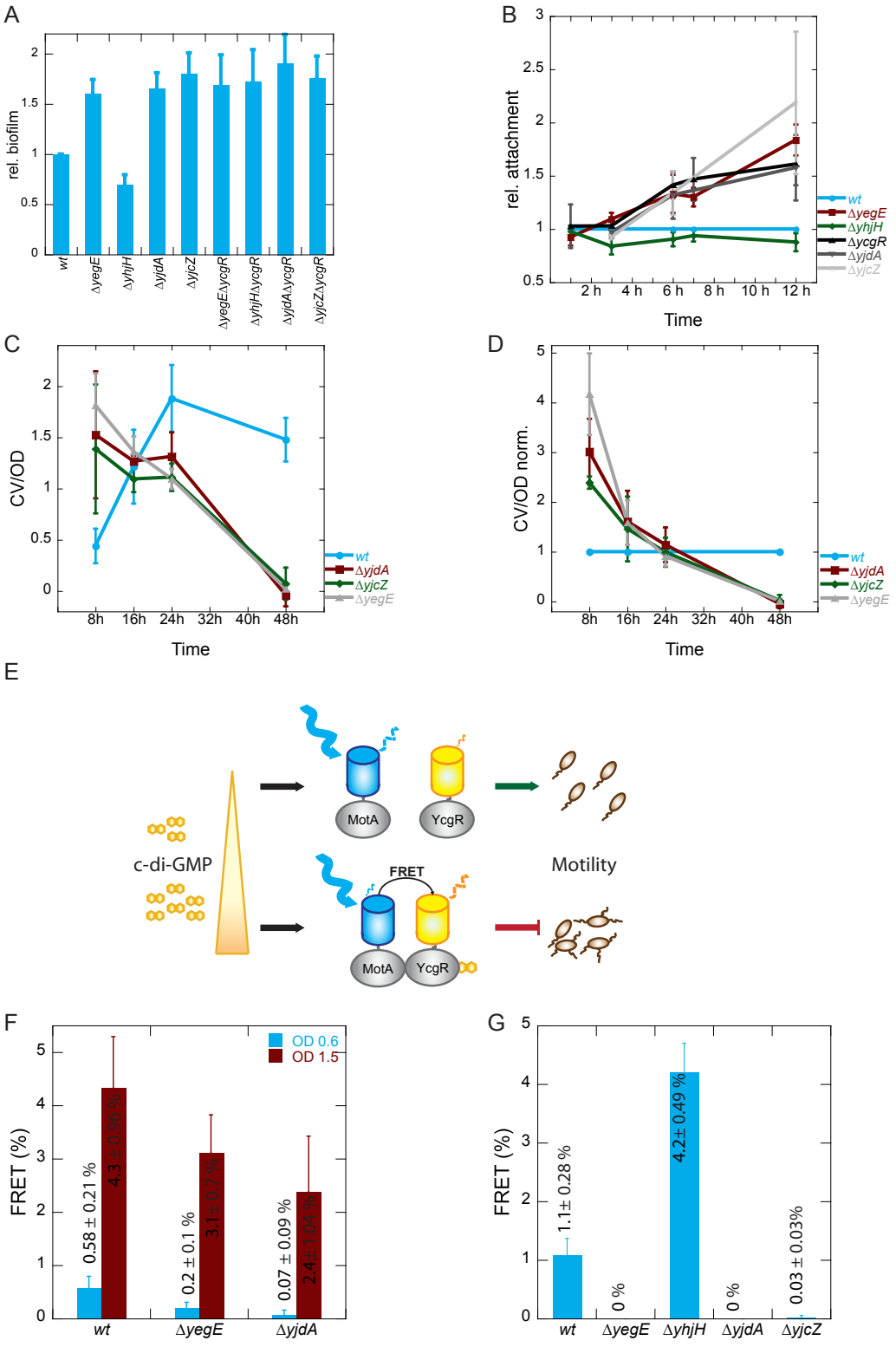

Fig. 8.2. YjdA and YjcZ affect biofilm formation and cdG levels similarly to YegE: (A) Biofilm formation of W3110 wild type, Δ*yegE*, Δ*yhjH*, Δ*yjdA*, Δ*yjcZ*, Δ*yegE*Δ*ycgR*, Δ*yhjH*Δ*ycgR*, Δ*yjdA*Δ*ycgR* and Δ*yjcZ*Δ*ycgR* on Corning® Costar® plates in M9 medium at 30°C. Biofilms were grown for 24 h and stained with crystal violet. Shown are mean and standard error of CV values of eight to twenty-one replicates.
(B) Surface attachment of W3110 wild type, Δ*yegE*, Δ*yhjH*, Δ*ycgR*, Δ*yjdA* and Δ*yjcZ* on BD Falcon^{TM} plates in M9 medium at 30°C. Relative numbers of attached cells in mixed-culture experiments were determined. Wild type cells labeled with one fluorophore (CFP or mCherry) were mixed 1:1 with wt, Δ*yegE*, Δ*yhjH*, Δ*ycgR*, Δ*yjdA* and Δ*yjcZ* cells labeled with another fluorophore (YFP or GFP). (*Continued on the following page.*)

Fig. 8.2. (*Continued from previous page.*)
The number of attached cells in each image was normalized to the number of wild type cells, and the values were normalized again to the wild type/wild type ratio in the same experimental series. Shown are mean and standard error of three to eight replicates.
(C), (D): Biofilm formation of W3110^{RH} wild type, Δ*yjdA*, Δ*yjcZ* and Δ*yegE* on Corning® Costar® plates in TB medium at 30°C.
(C) Biofilms were grown for the indicated times and stained with crystal violet. Shown are mean and standard error of CV values of three to eleven replicates.
(D) CV values of (C) were normalized first to the OD_{600} of the culture (CV/OD) and then to the wild-type CV/OD at each time point. n=2 for Δ*yjdA* and Δ*yjcZ* at 8 h timepoint.
(E) The cdG-dependent interaction between YcgR and MotA was used as a FRET-biosensor for cdG levels.
(F) FRET measurements between YcgR and MotA in planktonic cultures of W3110 wild type, Δ*yegE* and Δ*yjdA* at OD_{600} 0.6 and 1.5. Shown are mean and standard deviation of two (OD_{600} 0.6) and three (OD_{600} 01.5) replicates. Inductions were 0.001 % arabinose and 10 μM IPTG.
(G) FRET measurements between YcgR and MotA in planktonic cultures of W3110^{RH} wild type, Δ*yegE*, Δ*yhjH*, Δ*yjdA* and Δ*yjcZ* strains at OD_{600} 0.6. Shown are mean and standard error of three replicates. Inductions were 0.001 % arabinose and 20 μM IPTG.

If the dynamin YjdA together with YjcZ regulates c-di-GMP production by YegE, then they must also affect 3-D structure formation in mature submerged biofilms. I therefore grew static biofilms of *yjdA* and *yjcZ* deletion strains in W3110^{RH} (see figure 8.3 and figures A.21, A.22 in the Appendix) and AR3110 (see figure 8.4 and figures A.23, A.24 in the Appendix) backgrounds in ibidi® 8-well slides. In W3110^{RH}, YjdA and YjcZ clearly affect 3-D structure formation similarly to YegE (figures 8.3 B-D, A.21 B-D, A.22 B-D) with flat biofilms and little clump formation in the deletion strains. Effects in AR3110 are less pronounced but still visible (figures 8.4 B-D, A.23 B-D, A.24 B-D). I can therefore conclude that the dynamin YjdA together with the small protein YjcZ regulates motility, attachment and 3-D structure formation via control of the cyclase YegE.

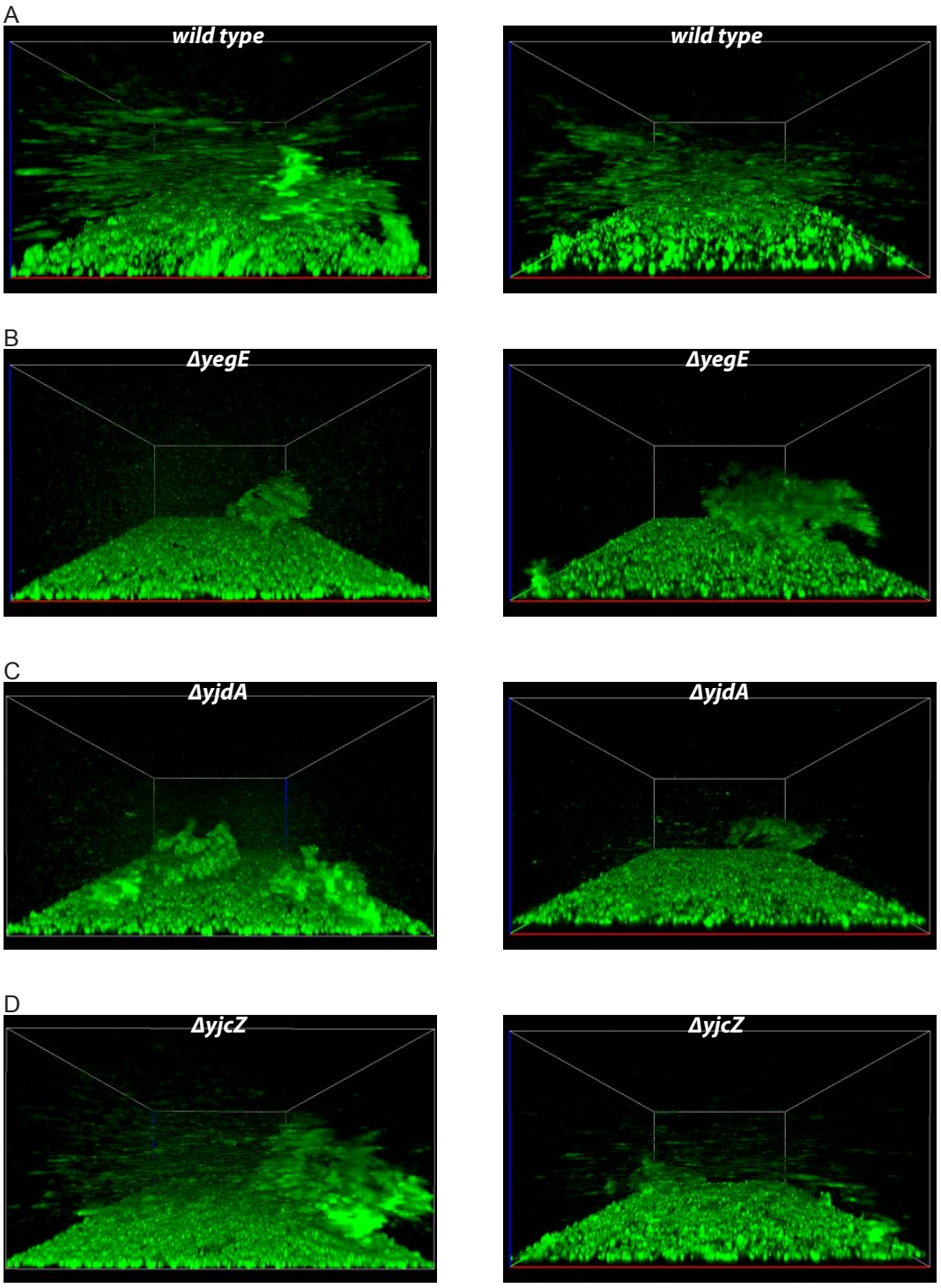

Fig. 8.3. YjdA and YjcZ affect 3D-structure formation in static W3110^{RH} biofilms similarly to YegE:
Confocal images of two biological replicates of static submerged biofilms of W3110^{RH} cells labeled with GFP and grown in TB on ibidi® 8-well slides at 30°C for 24 h, for wild type (A), Δ*yegE* (B), Δ*yjdA* (C), Δ*yjcZ* (D). Dimensions of bounding box (x:y:z) are 142:142:80 μm.

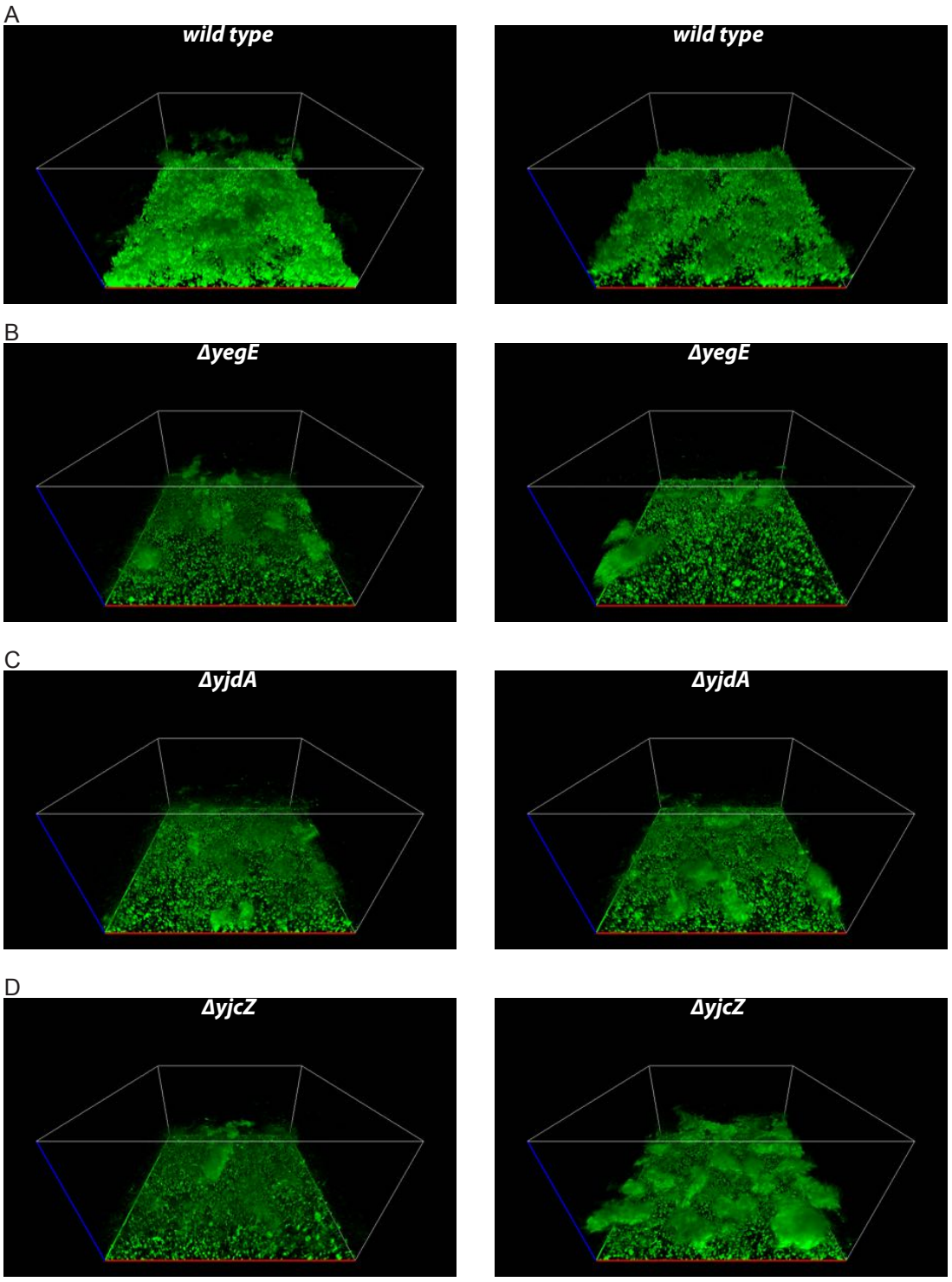

Fig. 8.4. YjdA and YjcZ affect 3D-structure formation in static AR3110 biofilms similarly to YegE:
Confocal images of two biological replicates of static submerged biofilms of AR3110 cells labeled with GFP and grown in TB on ibidi® 8-well slides at 30°C for 48 h, for wild type (A), Δ*yegE* (B), Δ*yjdA* (C), Δ*yjcZ* (D). Dimensions of bounding box (x:y:z) are 142:142:80 μm.

9. THE DYNAMIN-LIKE PROTEIN YJDA LOCALIZES TO THE PLASMA MEMBRANE AND INTERACTS WITH YJCZ

With the phenotypic evidence that the dynamin YjdA regulates YegE and thereby c-di-GMP signaling, I aimed to figure out its mechanism of action. I chose to investigate localization together with YegE and YjcZ as well as to test the interaction between the proteins by FRET. Fusions to YjdA, YjcZ and YegE were cloned on plasmids and tested for their functionality complementing deletion strains in soft agar and biofilm assays (see figures 9.1 and 9.2). In addition to the fluorescent fusions to wild type YjdA, two mutant dynamin fusions were cloned - YjdAT103D and YjdAK72A (see also figure 9.8 B). These mutants were created based on known mutations on human Dynamin 1 (see the GTPase domain website: http://www2.mrc-lmb.cam.ac.uk/Dynamin/GTPase.html and [121, 122]). YjdAT103D has a mutation in the G2 domain and is supposed to be GTPase defective, i. e. is locked in the GTP-bound state. YjdAK72A has a mutation in the G4 domain and should be nucleotide-free. As described above, deletion of *yjdA*, *yjcZ* and *yegE* in the Δ*yhjH* background complement the motility defect (see figure 9.1 A-D vector). Fluorescent fusions to YjdA (see green boxes), YjcZ (orange boxes) and YegE (rose boxes) were induced at different concentrations of IPTG (A: 0 μM, B: 5 μM, C: 20 μM, D: 50 μM). All wild type fusions were functional at all concentrations, with none or only very little complementation (YFP-YjdA at all concentrations, YjdA-YFP at 0 and 5 μM and YjdA-YFP at 0 μM) of the Δ*yhjH* phenotype. Similarly, the YjdAK72A mutant was able to suppress motility in Δ*yhjH*Δ*yjdA*, suggesting that this mutation does not affect activity of YjdA. In contrast, the YjdAT103D mutant was non-functional. I therefore conclude that GTPase activity of YjdA is required to regulate YegE.

In agreement with swimming on soft agar plates, complementation of mutants with fluorescent YjdA, YjcZ and YegE fusions in biofilm assays after 48 h (see figure 9.2) showed that all wild type fusions were fully (YegE and YjcZ, figure 9.2 B, C) or at least partially (YjdA, figure 9.2 A) functional. YjdAK72A was again functional, whereas YjdAT103D was not, supporting the idea that GTPase activity of YjdA is required to regulate YegE and thereby motility and biofilm formation.

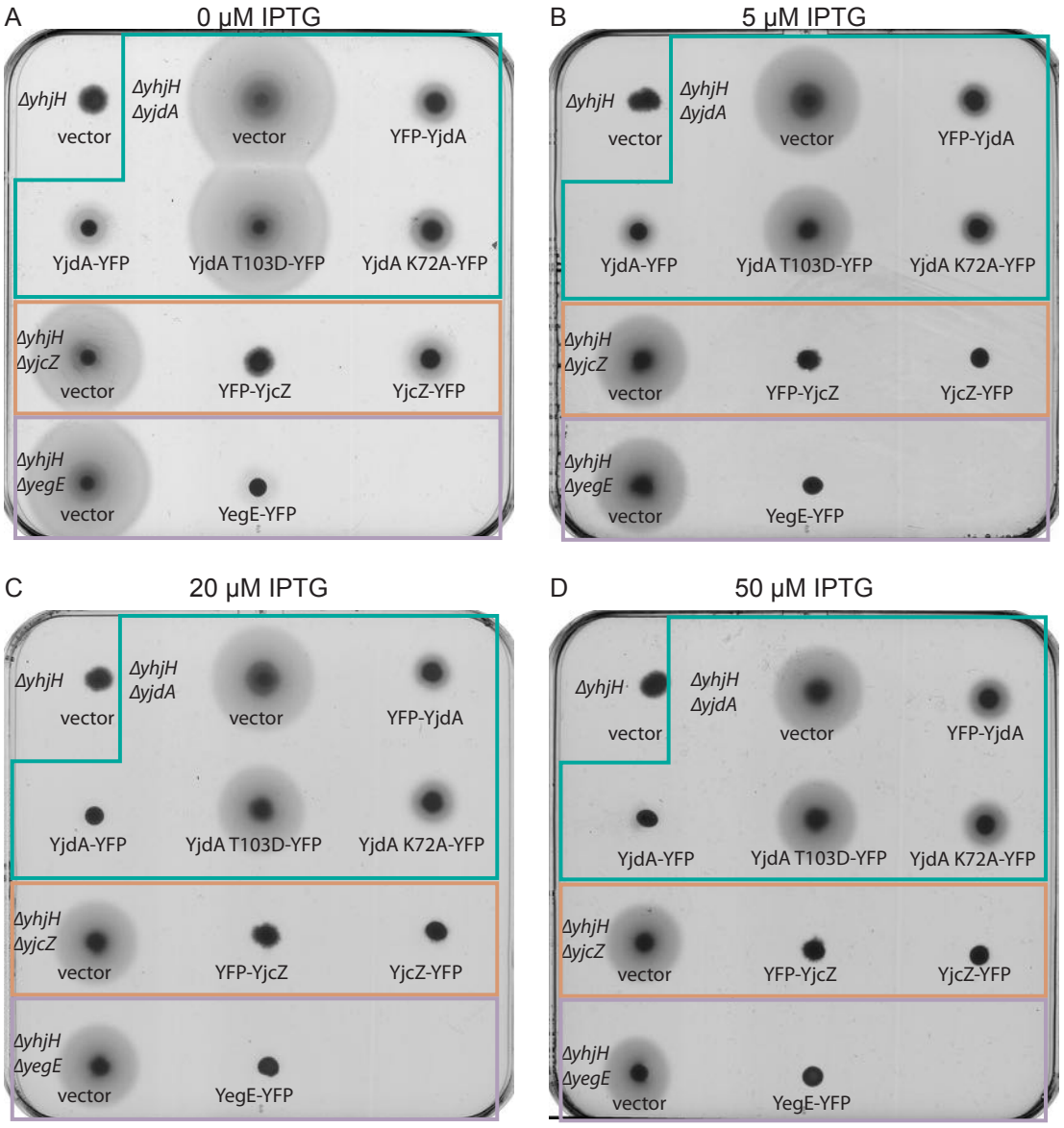

Fig. 9.1. Functionality test of YegE, YjcZ, YjdA and YjdA mutant fluorescent fusion proteins on swarm plates:
Swimming of W3110^{RH} $\Delta yhjH$, $\Delta yhjH\Delta yjdA$, $\Delta yhjH\Delta yjcZ$ and $\Delta yhjH\Delta yegE$. Cells were transformed with the empty vector control (pVS198) and with fluorescent fusions.
(A) Induction with 0 μM IPTG.
(B) Induction with 5 μM IPTG.
(C) Induction with 20 μM IPTG.
(D) Induction with 50 μM IPTG.

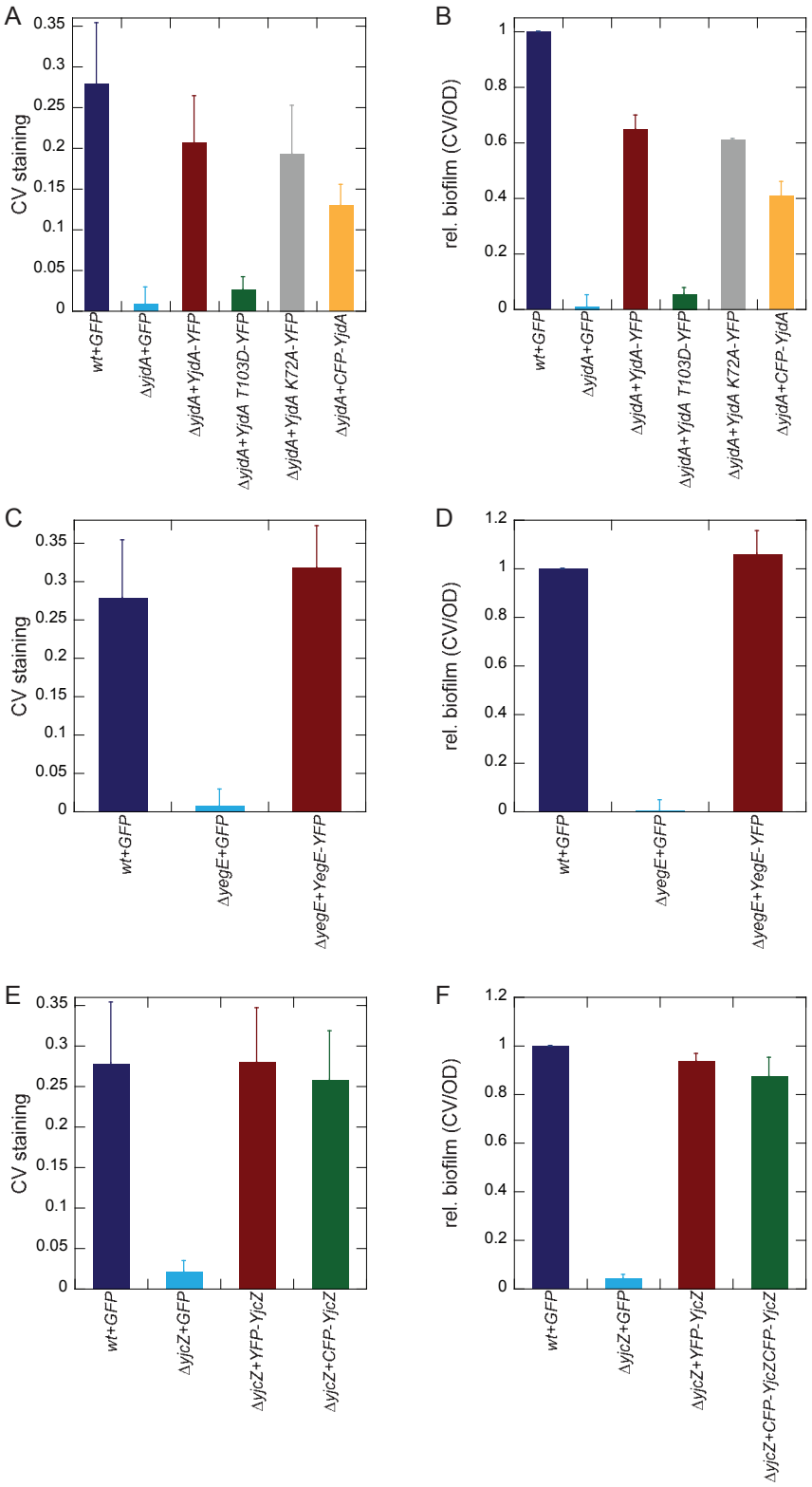

Fig. 9.2. Functionality test of YegE, YjcZ, YjdA and YjdA mutant fluorescent fusion proteins in biofilms:
Biofilm formation of W3110^{RH} Δ*yjdA*, Δ*yegE* and Δ*yjcZ* on Corning® Costar® plates in TB medium at 30°C for 48 h. Cells were transformed with the vector control (pVM42; GFP-expression vector) and with fluorescent fusions. Inductions were 0 μM IPTG and 0,001 % arabinose. Shown are mean and standard error of two replicates. Normalized CV staining before and after (B, D, F) normalization to the OD_{600} of the culture is shown.
(A, B): Expression of YjdA-YFP, YjdA K72A-YFP, and CFP-YjdA rescue Δ*yjdA*, whereas YjdA T103D-YFP is non-functional.
(C, D): Expression of YegE-YFP rescues Δ*yegE*.
(E, F): Expression of YFP-YjcZ and CFP-YjcZ rescue ΔyjcZ.

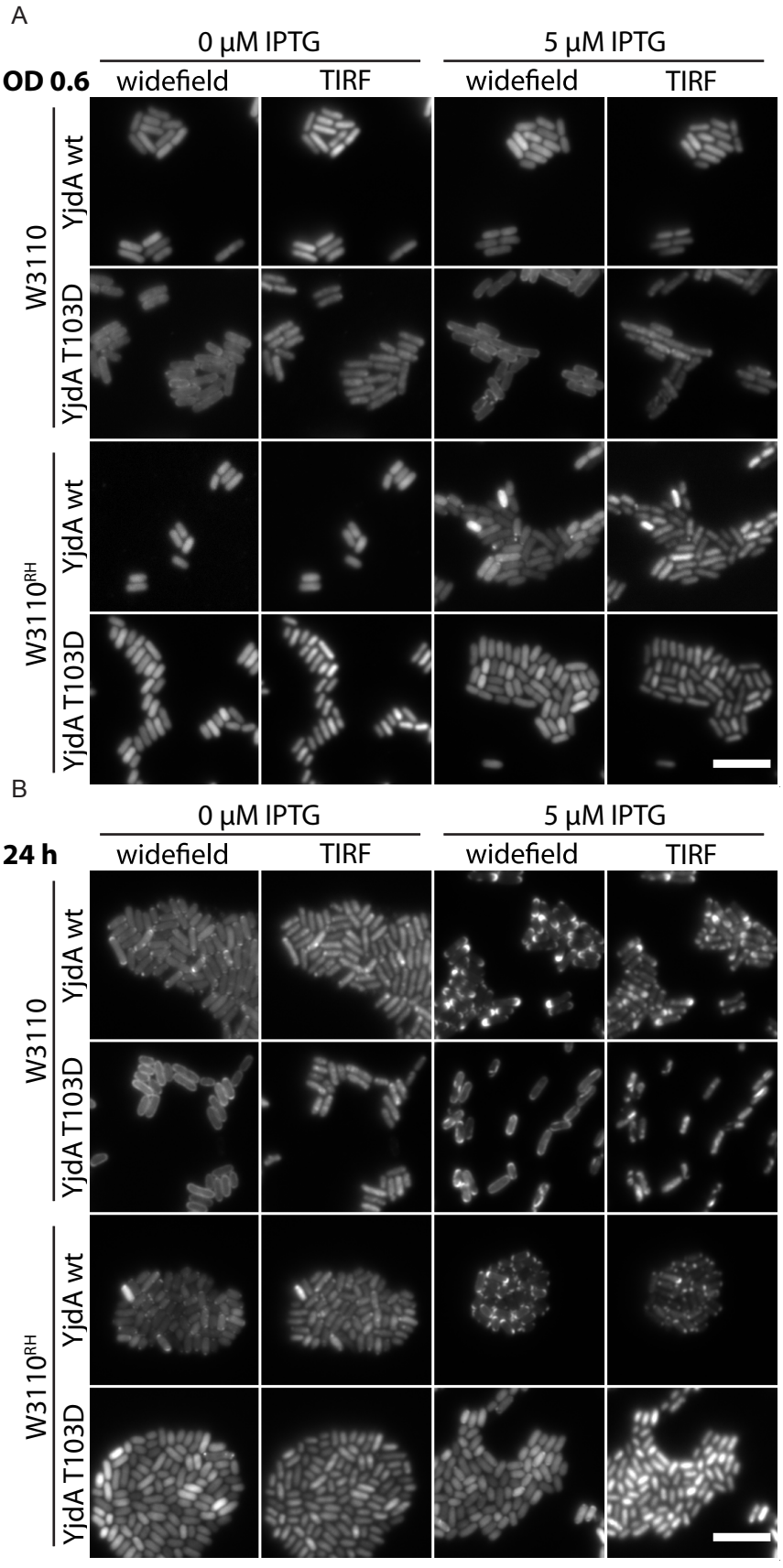

Fig. 9.3. Localization of YjdA in W3110 and W3110^{RH}:
(A, B) Localization of YjdA-YFP and YjdAT103D-YFP (GTPase mutant) in the W3110 and W3110^{RH} Δ*yjdA* background in widefield and TIRF microscopy. Cells were grown in planktonic cultures in TB medium at 30°C until OD_{600} 0.6 (A) or for 24 hours (B). Scalebar: 5 μm.

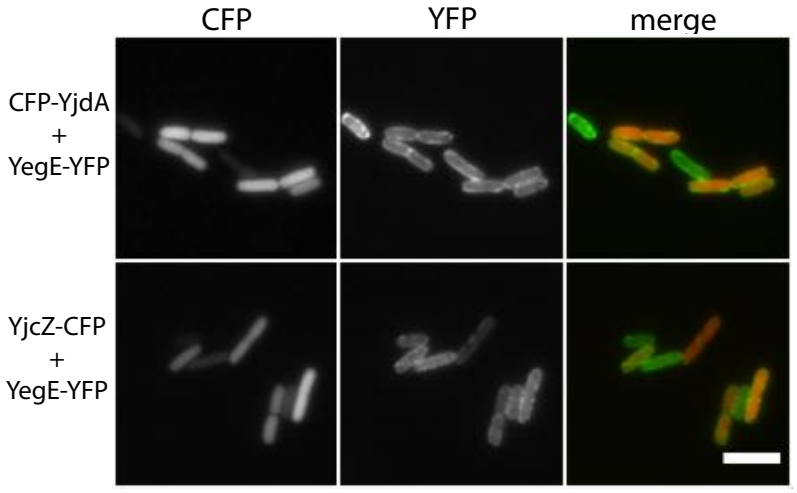

Fig. 9.4. Localization of YjdA, YegE and YjcZ in W3110:
Localization of YFP- and CFP-fusions of YjdA, YegE and YjcZ in the W3110 wild-type background. Inductions were 0.005 % arabinose for CFP-YjdA, 0.0001 % arabinose for YjcZ-CFP, and 1 μM IPTG for YegE-YFP. Scalebar: 10 μm.

If the T103D mutation renders YjdA inactive, I suspected that the mutant might as well be affected in its localization. I therefore checked localization of YjdA-YFP and YjdAT103D-YFP in W3110 and W3110^{RH} (see figure 9.3) in widefield and TIRF microscopy at two different growth stages, in the logarithmic (OD_{600} 0.6) and stationary (after 24 h) phase, and at two different induction levels (0 μM IPTG and 5 μM IPTG). At all conditions, YjdA localized to the plasma membrane. At OD_{600} 0.6 and 5 μM in W3110^{RH} and after 24 h in both strains, localization of wild type YjdA at the poles was visible. At the higher induction after 24 h, large clusters at the poles were visible, which probably reflect aggregation due to high expression levels. The GTPase mutant YjdAT103D localized as well to membrane. However, in W3110, already at OD_{600} 0.6 the membrane localization was less regular with small clusters. In W3110, after 24 h and at 5 μM, the mutant localized in elongated clusters, resembling chains of proteins that were associated with the membrane. This localization was never observed in W3110^{RH}. On the contrary, in W3110^{RH}, the GTPase mutant did not even form the small clusters that were observed for the wild type protein.
In summary, YjdA showed association to the plasma membrane, however, no consistent pattern of its specific localization could be observed in the strain backgrounds.
To test the theory that YjdA and YjcZ together regulate YegE activity (see chapter 8.1), I checked colocalization and interaction of these proteins with each other in W3110 (see figure 9.4) and W3110^{RH} (see figure 9.5). In W3110, no interaction could be measured between YjdA and YegE, and YjcZ and YegE. Similarly, no colocalization was observed (see figure 9.4). In contrast, in W3110^{RH}, colocalization of YjdA with YegE could be seen in some cells (see figure 9.5 A, upper panel), but FRET measurements showed no interaction (see figure 9.5 B). YjcZ did also neither colocalize with YegE (figure 9.5 A,

lower panel) nor interact with it (see figure 9.5 D). In contrast, YjdA clearly colocalized and interacted with YjcZ (see figures 9.5 A, middle panel and C). Together, these results suggest that YjdA and YjcZ do not directly interact with YegE, but might regulate its activity via some other mechanism.

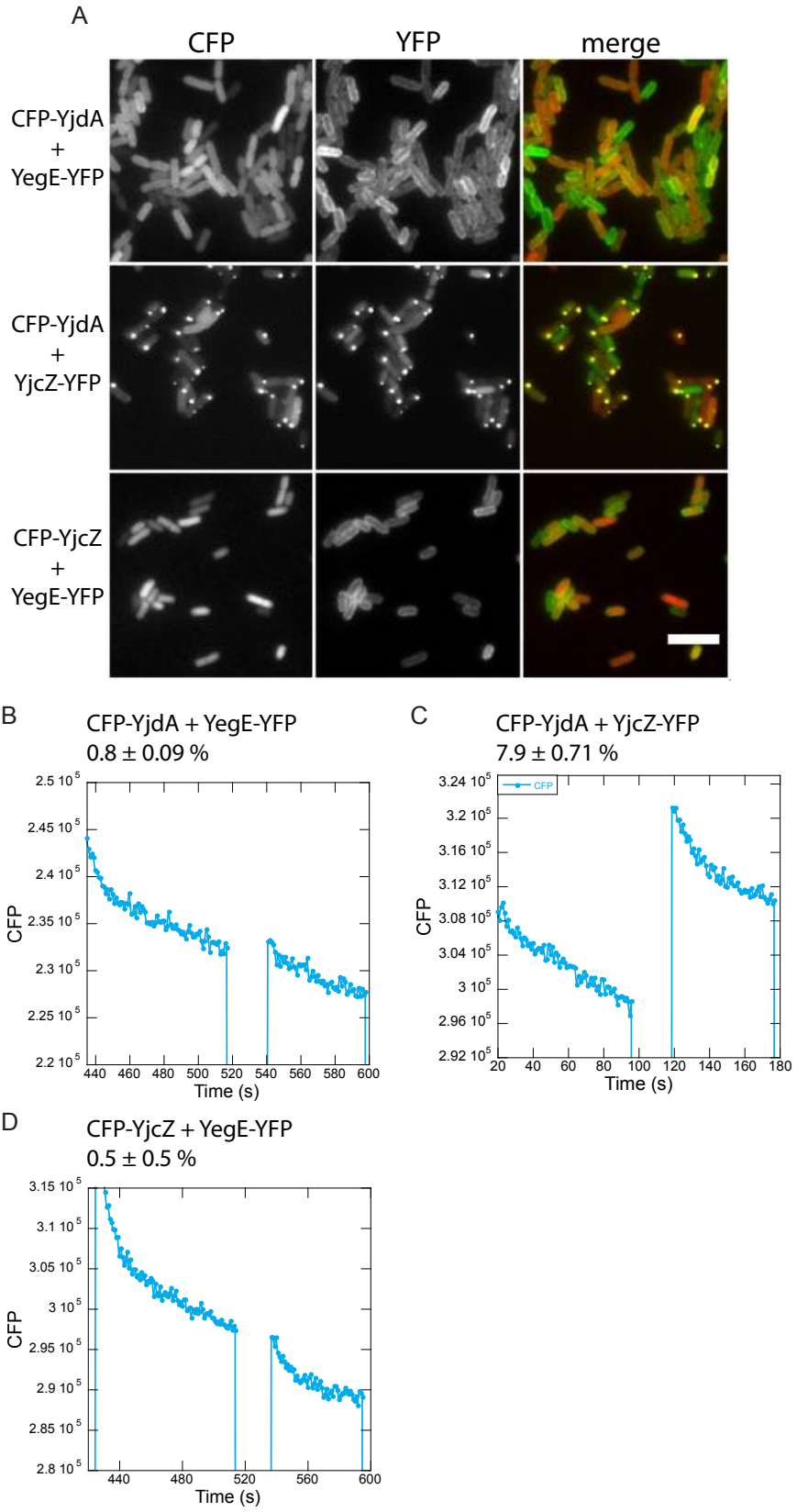

Fig. 9.5. Localization and interactions between YjdA and YjcZ, YjdA and YegE and YegE and YjcZ by FRET in W3110^{RH}:
(A) Localization of YFP- (green) and CFP- (red) fusions of YjdA, YegE and YjcZ in the W3110^{RH} wild-type background. Inductions were 0.005 % arabinose for CFP-YjdA and CFP-YjcZ, 1 μM IPTG for YegE-YFP and 15 μM IPTG for YjcZ-YFP. Scalebar: 5 μm.
(B)-(D): FRET was measured in planktonic cultures at OD_{600} 0.6.
YjdA and YjcZ interact (C) while FRET was negative for YjdA and YegE (B) and YegE and YjcZ (D). Shown are exemplary FRET measurements and FRET mean efficiency with standard error of three replicates. Inductions were as in (A).

9.1 A connection between flotillins and c-di-GMP signaling

The previous results showed that the cyclase YegE might be regulated by the dynamin YjdA together with the small protein YjcZ. Since we could not observe a direct interaction as measured by FRET (see figure 9.5), we suspected that there might be another protein that acts between YegE and YjdA/YjcZ. To solve this question, a pull-down of fluorescently labeled YjdA, YegE and YjcZ with GFP-Trap®_A beads was performed by Dr. Hui Li from our laboratory (see figure 9.6 and tables 9.1 and A.1). Samples were taken at two growth stages, at 5 h and 14 h, and analyzed by mass spectrometry at the ZMBH MS core facility. Pull-downs of YcgR and FliF served as cytoplasmic (YcgR) and a membrane protein (FliF) control. Table A.1 in the appendix shows an extended list of identified proteins for the respective fluorescent fusions in two biological replicates. All proteins, which were detected with at least two peptides in either the YjdA or the YegE pull-down are shown in the list. The color shadings reflect hits probably specific to YjdA (yellow), YegE (light blue), YjcZ (green), YjdA and YegE (blue), YjdA and YcgR (orange), and FliF (grey). Hits for YjdA and YegE are again shown in figure 9.6 A and table 9.1. YjdA and YegE both pulled down the protease FtsH and the flotillin proteins HflK and HflC as well as chemotaxis receptors (MCPs) (green shading). In contrast, proteins specific for replication or secretion were only pulled down by YjdA (blue shading). Only one YegE peptide was pulled down by YjdA, which might be due to the fact that endogenous YegE is present at only very few copies per cell. Conversely, no YjdA peptides were detected in the YegE pull-down. Figures 9.6 B-E show correlations between the two pull-down replicates with peptide counts of replicate 1 plotted against peptide counts of replicate 2. Correlations between the replicates were strong with R values between 0.7 and 0.9. The most abundant proteins from the hit list in table 9.1 are shown in green.

HflKC form a complex that interacts with the ATP-dependent protease FtsH [162]. HflKC belong to the SPFH (stomatin, prohibitin, flotillin, and HflK/C) superfamily that is found in prokaryotes and eukaryotes [163]. SPFH domain proteins are membrane-anchored and associate in lipid rafts. Previous research has shown that prokaryotes contain functional membrane microdomains (FMMs) that are related to eukaryotic lipid rafts [164]. With YjdA being a prokaryotic dynamin and dynamins being involved in membrane organization, we speculated based on the pull-down data that there might be a connection between membrane organization by the *E. coli* flotillins and the dynamin YjdA that affects activity of the cyclase YegE. To verify interactions between YjdA and YegE as well as YjdA/YegE with HflKC, I performed a bacterial two hybrid assay using the Bacterial Adenylate Cyclase-based Two-Hybrid (BACTH) system [165]. The system is based on the reconstruction of the catalytic domain of adenylate cyclase (CyaA) from *Bordetella pertussis* consisting of two adenylate cyclase fragments (T18 and T25) [165, 166] (see section 14.7). I performed the assay at 26°C (figure 9.7 A) and 30°C (figure 9.7 B) using combinations of both C- and N-terminal fusions of YjdA and YegE to the T18 or T25 fragment. With the N-terminal fusions to YjdA and YegE, I observed an interaction between the pro-

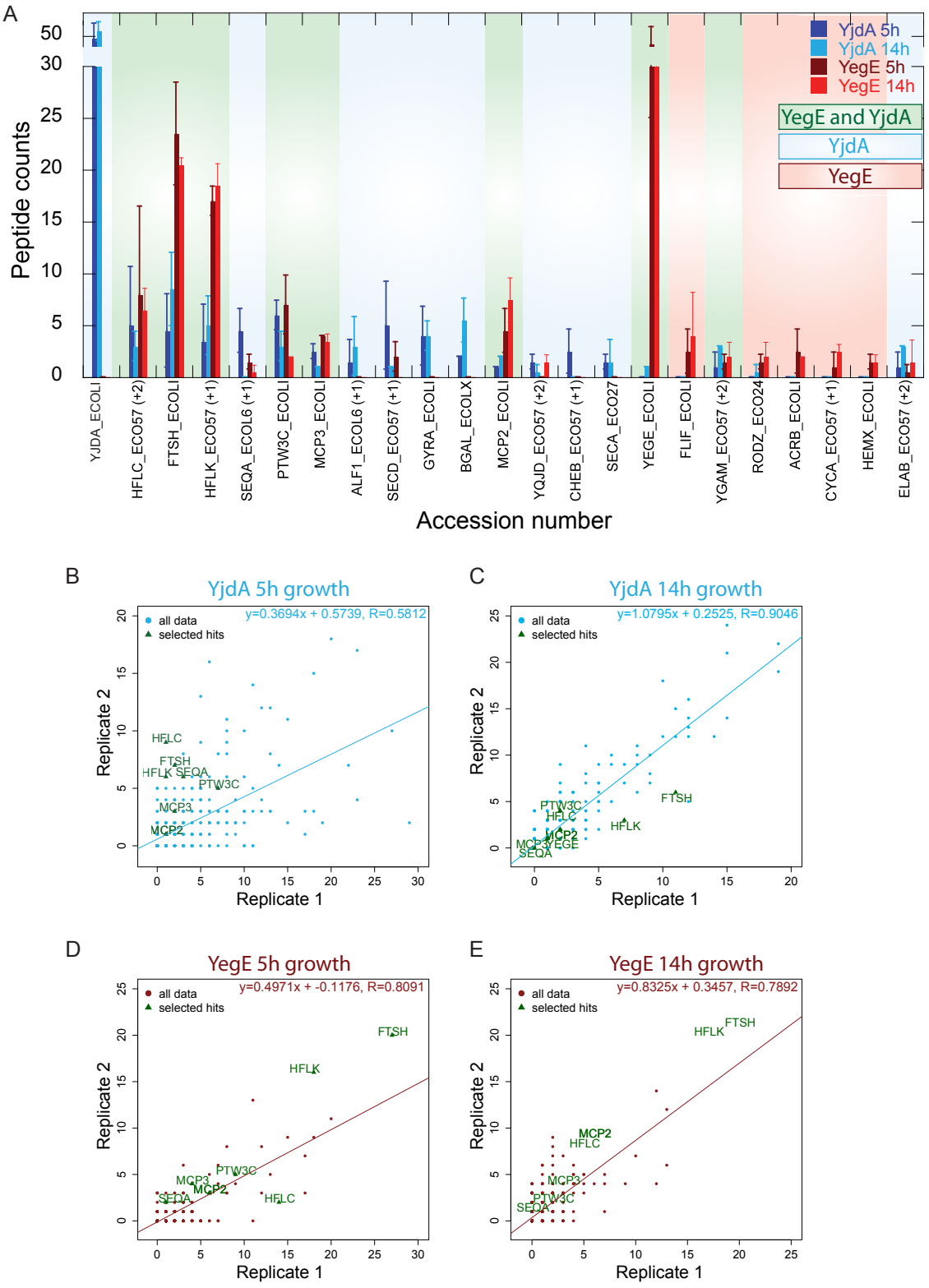

Fig. 9.6. Pull-Downs of YjdA, YegE, YjcZ, YcgR and FliF:
Fluorescent fusions to YjdA, YegE, YjcZ, YcgR and FliF were pulled down using GFP-Trap®_A beads (performed by Dr. Hui Li) and proteins were analyzed by mass spectrometry.
(A) Hits for YjdA and YegE. Shown are mean peptide counts and standard deviation of two replicates. Blue shading: Hits for YjdA; red shading: hits for YegE; green shading: hits for both YjdA and YegE.
(B, C) Correlation between the two replicates of YjdA after 5 h (B) and 14 h (C) growth.
(D, E) Correlation between the two replicates of YegE after 5 h (D) and 14 h (E) growth.

Tab. 9.1. Hit-list for Pull-Downs of YjdA, YegE, YjcZ, YcgR and FliF.
Peptide counts of two replicates are shown.

Accession number	YjdA 5 h	YjdA 14 h	YegE 5 h	YegE 14 h	YjcZ 5 h	YjcZ 1 4h	YcgR 5 h	YcgR 14 h	FliF 5 h	FliF 14 h
YJDA ECOLI	58/37	48/61	0/0	0/0	0/0	0/0	0/0	0/0	0/0	0/0
HFLC ECO57 (+2)	1/9	2/4	14/2	5/8	0/0	1/0	2/3	0/2	2/4	2/4
FTSH ECOLI	2/7	11/6	27/20	20/21	1/0	0/0	9/10	7/8	4/5	8/7
HFLK ECO57 (+1)	1/6	7/3	18/16	17/20	1/0	0/0	2/5	3/6	6/4	7/10
SEQA ECOL6 (+1)	3/6	0/0	1/2	0/1	5/3	0/0	4/5	0/0	1/2	0/0
PTW3C ECOLI	7/5	2/4	9/5	2/2	0/0	0/0	5/2	4/2	0/1	1/1
MCP3 ECOLI	2/3	1/1	4/4	3/4	0/0	0/0	2/1	0/0	0/0	0/0
ALF1 ECOL6 (+1)	0/3	1/5	0/0	0/0	0/0	0/0	0/0	0/2	0/0	0/1
SECD ECO57 (+1)	8/2	1/1	3/1	0/0	0/0	0/0	0/0	0/0	0/0	0/0
GYRA ECOLI	6/2	3/5	0/0	0/0	0/0	0/0	2/0	4/0	0/0	0/0
BGAL ECOLX	2/2	4/7	0/0	0/0	1/4	2/0	0/0	2/0	0/0	0/0
MCP2 ECOLI	1/1	2/2	6/3	6/9	0/1	0/1	4/4	3/1	0/0	2/2
YQJD ECO57 (+2)	2/1	1/0	0/0	2/1	1/0	2/2	0/0	1/2	0/0	2/2
CHEB ECO57 (+1)	4/1	0/0	0/0	0/0	1/0	0/0	2/0	0/0	0/0	0/0
SECA ECO27	2/1	3/0	0/0	0/0	0/0	0/0	1/2	0/1	0/0	0/1
YEGE ECOLI	0/0	1/1	54/30	36 /25	0/0	0/0	0/0	0/0	0/0	0/0
FLIF ECOLI	0/0	0/0	4/1	7/1	0/0	0/0	0/1	0/0	27/28	25/27
YGAM ECO57 (+2)	2/0	3/3	2/1	3/1	0/0	1/1	0/0	1/1	0/0	1/0
RODZ ECO24	0/0	0/1	2/1	3/1	0/0	0/0	1/0	0/0	0/0	1/0
ACRB ECOLI	0/0	0/0	4/1	2/2	0/0	0/0	0/0	0/0	0/0	0/0
CYCA ECO57 (+1)	0/0	0/0	2/0	2/3	0/1	0/0	0/0	0/0	0/0	0/1
HEMX ECOLI	0/0	0/0	2/1	2/1	0/0	0/0	0/0	0/0	0/0	0/0
ELAB ECO57 (+2)	2/0	3/3	1/0	0/3	0/1	1/1	1/1	2/1	1/1	2/1

teins at both temperatures. Similarly, the N-terminal YegE fusion interacted with HflKC. The interaction between YjdA and HflKC could also be confirmed, with the C-terminal YjdA-T25 fusion complementing T18-HflKC. Since the GTPase mutant YjdA-T103D was not functional in swarm and biofilm assays (see figures 9.1 and 9.2), I checked its interaction with YegE and HflKC (see figure 9.8). As expected, the interaction between HflKC and YjdA was abolished when the GTPase domain was mutated. However, YjdAT103D still showed an interaction with YegE, which does not match the complementation data in swarm plates and biofilms, where GTPase activity was required. Nevertheless, together with the localization, FRET and pull-down data, I propose a possible model, in which the YjdA-YjcZ complex regulates YegE activity via the flotillins HflKC in a so far unknown manner (see figure 9.7 C).

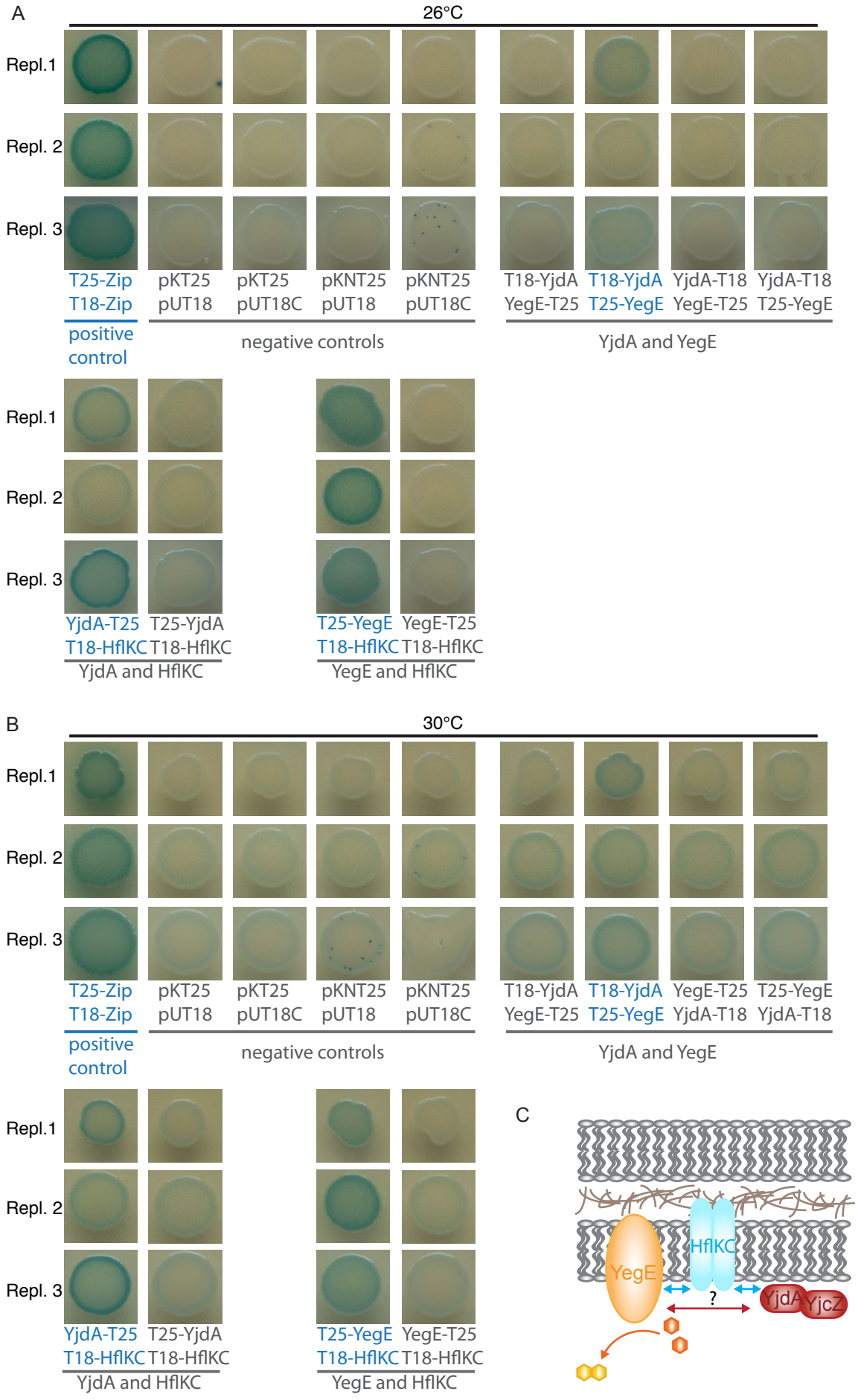

Fig. 9.7. Bacterial Adenylate Cyclase-based Two-Hybrid (BACTH) assay to test interactions between YegE and YjdA, YjdA and HflKC and YegE and HflKC:
(*Continued on the following page.*)

Fig. 9.7. (*Continued from previous page.*)
Cya$^-$ *E. coli* BTH101 were transformed with plasmids encoding the T25 (pKT25 or pKNT25) or T18 (pUT18 or pUT18C) adenylate cyclase fragment and tested on LB-X-Gal-IPTG-Strp-Amp-Kan plates for the Cya$^+$ or Cya$^-$ phenotype.
(A, B) BACTH assay was performed at 26°C (A) and 30°C (B). Positive (T25-Zip/T18-Zip) and negative (pKT25/pUT18, pKT25/pUT18C, pKNT25/pUT18, pKNT25/pUT18C) controls indicate Cya$^+$ (blue) and Cya$^-$ (white) phenotypes. YjdA and YegE interaction was tested with C- and N-terminal fusions to the proteins with T18-YjdA and T25-YegE resulting in the Cya$^+$ phenotype. N- and C-terminal T25 fusions to YjdA and YegE were tested for interaction with T18-HflKC with positive interactions for YjdA-T25 and T25-YegE.
(C) Model showing the interactions between YegE, HflKC and YjdA, potentially including the small protein YjcZ, which interacts with YjdA.

9.2 Characterization of the flotillin-cyclase-dynamin interaction

Speculating that HflKC interact with YjdA and YegE, I checked colocalization of plasmid-encoded fluorescent fusions to these proteins (see figure 9.9 A). All three protein fusions, YegE-CFP, mCherry-HflKC and CFP-YjdA, localized to the plasma membrane. I speculated that if YjdA and YegE are part of HflKC-dependent membrane domains, HflKC might be required for their correct localization. Therefore, I checked localization of YjdA and YegE in the absence of HflK and HflC (see figures 9.9 B, 9.10 B, A.25 A, B and A.26 B). YegE localized at the cell membrane forming small clusters that were present in both wild-type and *hflK/hflC* deletion strains. This was true for both the plasmid-encoded (figure 9.9 B) and a genomic YegE-YFP fusion (figure 9.10 B). Functionality of the genomic YegE-YFP fusion was verified in a swarm plate assay (see figure 9.10 A). The YegE clusters were dynamic and dynamics were similar in the wild-type and *hflK/hflC* deletion strains (see time-lapse pictures in figures A.25 A, B and A.26 B). The same was true if *yjdA* was deleted in the strain with the genomic YegE-YFP fusion (figures 9.10 A and A.26 A). Similarly, HflKC were not required for YjdA localization (see figures 9.9 B and A.25 B). Consistently, deletion of *yjdA* and *yegE* did not abolish HflKC localization no change its dynamics (see figures 9.9 C and A.25 C).
Although the localization data do not support the theory that HflKC is the link between YjdA and YegE, I checked whether HflKC might influence the c-di-GMP dependent interaction between MotA and YcgR, which would mean a change in YegE diguanylate cyclase activity (see figure 9.11 A). Deletion of the PDE YhjH served as a control. In the *yhjH* deletion strain, c-di-GMP levels are increased in comparison to wild type, which is reflected by the increased FRET (1.8 % in wild type and 6 % in $\Delta yhjH$). Deletion of *hflK* and *hflC* in contrast seems to decrease FRET between YcgR and MotA, which means that c-di-GMP production by YegE might indeed depend on HflKC (see figure 9.11 B).

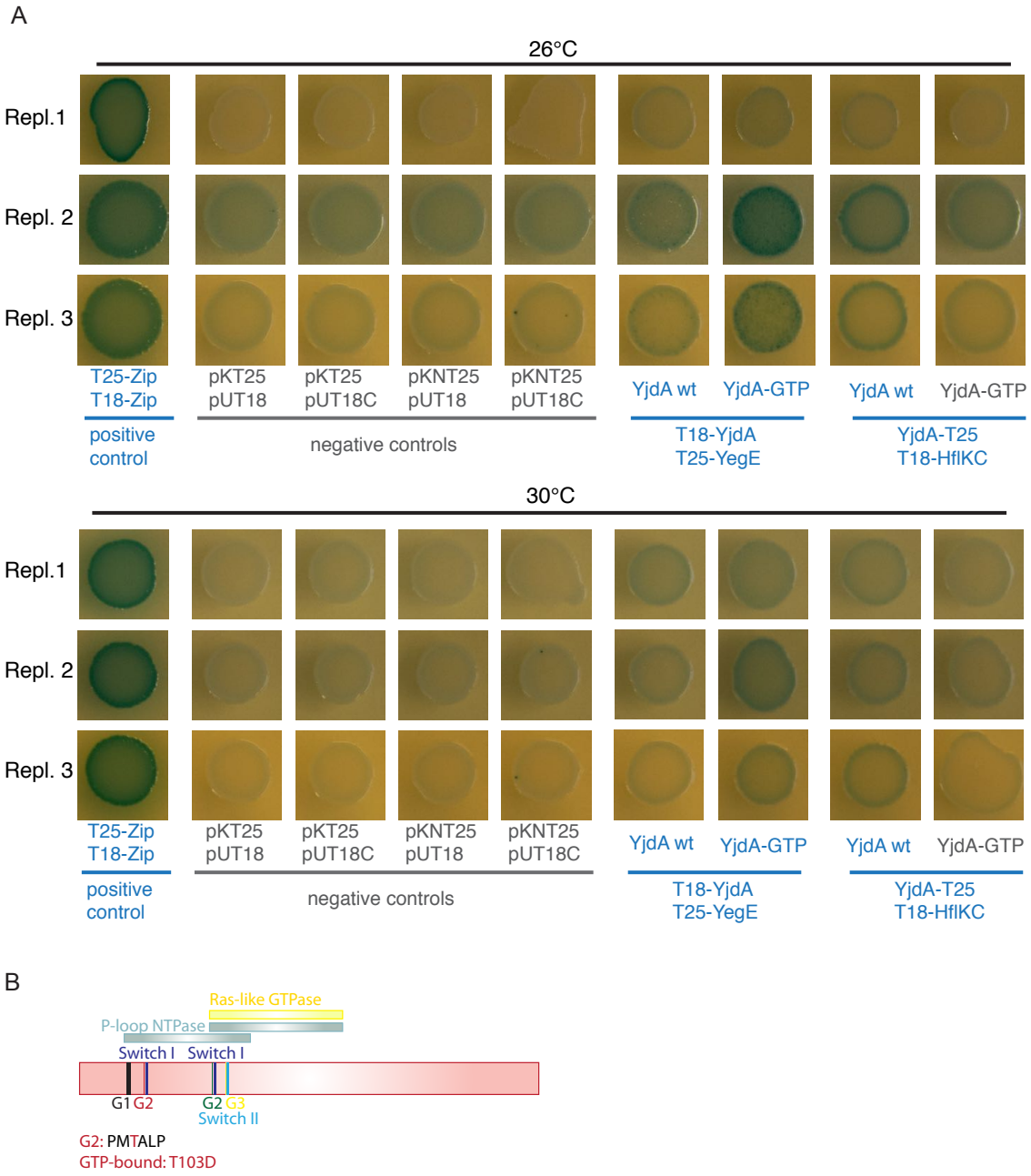

Fig. 9.8. Bacterial Adenylate Cyclase-based Two-Hybrid (BACTH) assay to test the interaction of YjdA-GTP with YegE and YjdA-GTP with HflKC:
Similar to figure 9.7, Cya$^-$ *E. coli* BTH101 were transformed with plasmids encoding the T25 (pKT25 or pKNT25) or T18 (pUT18 or pUT18C) adenylate cyclase fragment and tested on LB-X-Gal-IPTG-Strp-Amp-Kan plates for the Cya$^+$ or Cya$^-$ phenotype.
(A) BACTH assay was performed at 26°C and 30°C. Positive (T25-Zip/T18-Zip) and negative (pKT25/pUT18, pKT25/pUT18C, pKNT25/pUT18, pKNT25/pUT18C) controls indicate Cya$^+$ (blue) and Cya$^-$ (white) phenotypes. The GTPase mutant YjdA T103D interacts with YegE, whereas the interaction between YjdA and HflKC is abolished in the YjdA T103D mutant.
(B) Schematic drawing showing the mutation site in the G2 region in YjdA.

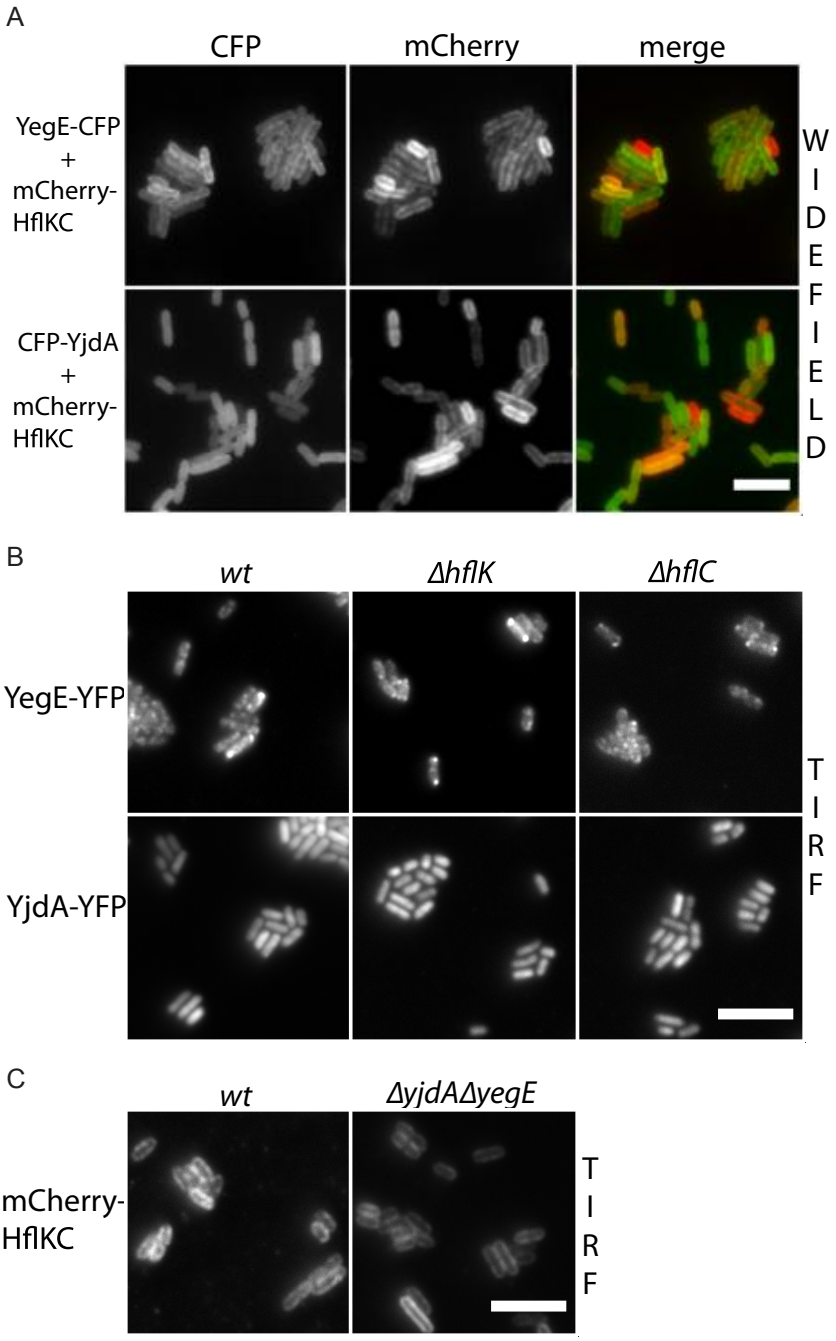

Fig. 9.9. Localization of YegE, YjdA and HflKC:
Widefield and TIRF images of a W3110^{RH} wild-type strain expressing YegE-YFP, YjdA-YFP or mCherry-HflKC from plasmids at OD_{600} 0.6.
(A) Localization of plasmid-encoded YFP- and CFP-fusions of YegE and YjdA with mCherry-HflKC in the W3110^{RH} wild-type background by widefield microscopy.
(B) Localization of plasmid-encoded YFP-fusions of YegE and YjdA in W3110^{RH} wild-type, Δ*hflK* and Δ*hflC* by TIRF microscopy.
(C) Localization of mCherry-HflKC in W3110^{RH} wild-type and Δ*yjdA*Δ*yegE* by TIRF microscopy.
Scalebar: 5 μm.

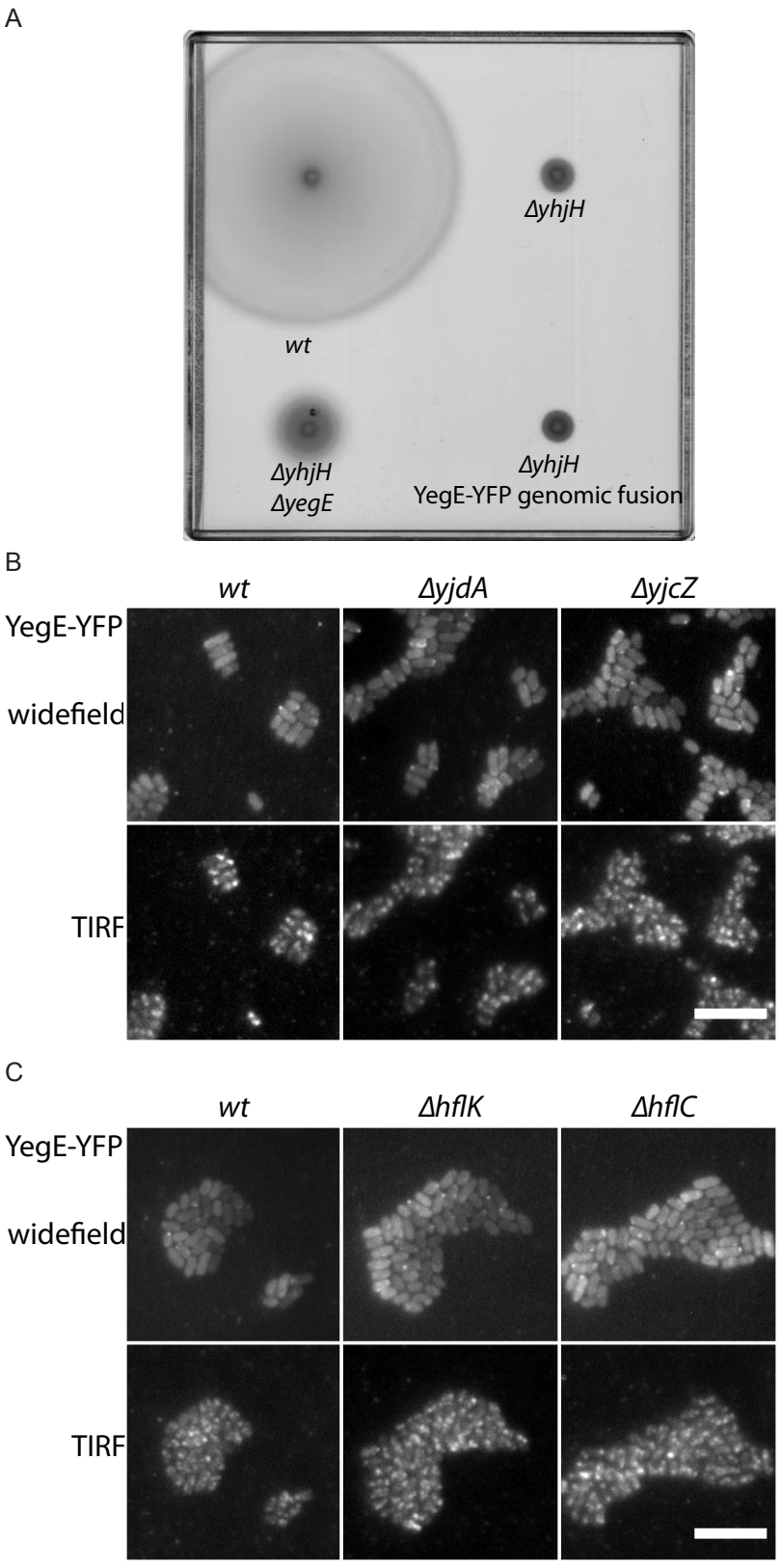

Fig. 9.10. YjdA, YjcZ and HflKC do not influence YegE localization:
Widefield and TIRF images of a W3110^{RH} strain expressing a genomic YegE-YFP fusion from the native locus at OD_{600} 1.7. Wild-type, Δ*yjdA*, Δ*yjcZ*, Δ*hflK* and Δ*hflC* strains were imaged.
(A) Soft agar plate showing functionality of the genomic YegE-YFP fusion. Swimming of W3110^{RH} wild-type, Δ*yhjH*, Δ*yhjH*Δ*yegE* and Δ*yhjH* in the YegE-YFP background was assayed on TB soft agar plates at 34°C.
(B) Localization of YegE-YFP in W3110^{RH} wild-type, Δ*yjdA* and Δ*yjcZ*.
(C) Localization of YegE-YFP in W3110^{RH} wild-type, Δ*hflK* and Δ*hflC*.
Scalebar: 5 μm.

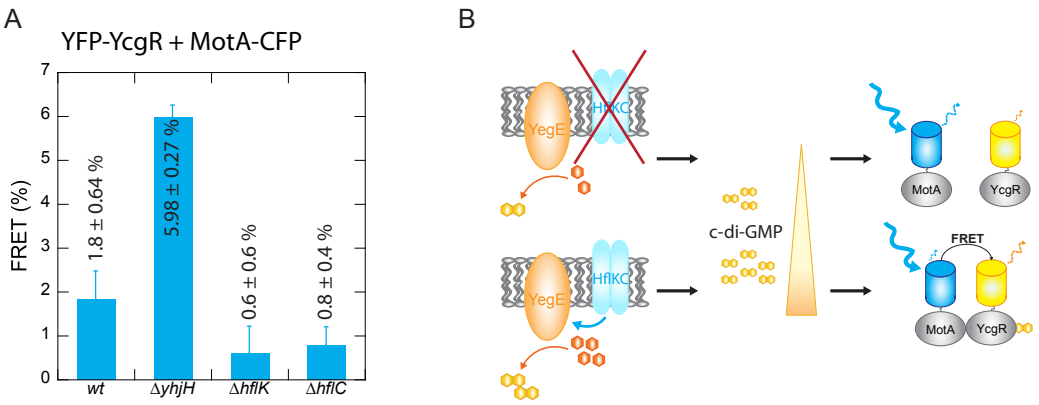

Fig. 9.11. HflKC influences c-di-GMP levels:
FRET between YFP-YcgR and MotA-CFP was measured as a read-out of relative c-di-GMP levels in W3110^{RH} wild-type, Δ*yhjH*, Δ*hflK* and Δ*hflC* strains.
(A) FRET efficiency of the interaction between YcgR and MotA. Mean and standard error of three replicates are shown.
(B) Model showing decreased c-di-GMP production by YegE in the absence of HflKC, which can be detected as a decrease in FRET between YcgR and MotA.

Part V

DISCUSSION

10. WHAT ARE THE ROLES OF MOTILITY IN *E. COLI* BIOFILMS?

The discovery of multicellular bacterial growth in biofilms has brought about many challenges and open questions. Biofilms constitute a severe problem in both healthcare and industrial settings. Biofilm-related diseases are difficult to treat and are a major cause of morbidity of hospital-acquired diseases. Examples for biofilms in industrial settings are biofilm formation on manufacturing plants, e. g. in food industry, and biofilms in water systems, both causing hygienic problems. A major challenge in basic research lies in understanding the way biofilms form and the physiological processes required for successful biofilm formation. In their planktonic state, most bacteria are motile and move forward using different types of motility systems, with flagella-driven swimming motility being the most common. This raises the question of how the transition from a motile planktonic state to a sessile biofilm state is achieved and what the key signaling events are that lead to this drastic lifestyle switch. A major player in this process is the second messenger c-di-GMP that acts as a biofilm-promoting signal juggling between inhibition of motility and upregulation of biofilm matrix production.
In my PhD thesis, I aimed to get a deeper insight into the roles of flagella-driven motility during biofilm formation of *E. coli* by investigating how chemotaxis as well as c-di-GMP signaling orchestrate motility during the different stages of biofilm formation.

10.1 Motility during attachment in *E. coli* biofilms

To analyze motility in *E. coli* biofilms, I used submerged biofilms as a model system since their biomass can be easily quantified with the fast crystal violet staining method. The first step was to systematically delete motility and chemotaxis genes in the two *E. coli* W3110 strains, W3110 and W3110^{RH}, and to test the mutant strains for their biofilm formation capacity. The difference between the two W3110 strains lies in the expression of RpoS, the stationary phase σ-factor. σ^S regulates many biofilm-relates genes, especially during the later stages, when biofilm matrix becomes important for 3-D structure formation. W3110 does not have a functional σ^S and is thereby a good model for early biofilm formation. In contrast, W3110^{RH} expresses σ^S and, to gain a more complete picture of the role of motility in biofilms, was used to analyze the effect of motility both on attachment and on 3-D structure formation. In both strains, my results show that flagella-driven motility is an absolute requirement for successful submerged biofilm formation (see figures 6.2 and 6.12). Deletion of flagella abolishes surface attachment, suggesting the requirement of flagella for

biofilm formation, either due to their function in motility or because of additional roles in biofilms. To prove motility is required for biofilm formation, I deleted the motor gene *motA* and the phosphatase gene *cheZ* to receive flagellated strains with impaired motility, and tested their effect on biofilm formation. Both, *motA* and *cheZ* deletion strains, could not form biofilms. This was true for both W3110 strains used in this work and could be shown throughout different stages of biofilm formation (see figures 6.2, 6.6 and 6.12). Thereby, I concluded that the motility function of flagella strongly promotes biofilm formation. A requirement for flagellar motility in *E. coli* as well as in *P. aeruginosa*, together with twitching motility, for submerged biofilm formation has been published in previous literature [18, 21, 20]. Furthermore, previous literature suggests that flagella might have additional roles during biofilm formation, such as functioning as adhesins, e. g. in *E. coli* or *Salmonella* [167, 127, 128, 129] or as surface sensors that trigger expression of biofilm-specific genes [130, 131, 132, 133]. Although previous work [167, 127, 128, 129] reported that flagella function as adhesins in biofilm formation, my data showed contradictory results, as I could show in figure 6.4 and I concluded that in W3110, flagella are no major adhesins during submerged biofilm formation. When circumventing the necessity of swimming for attachment by centrifuging the bacteria to the surface, flagella-less cells can attach, meaning that flagella per se are not required to adhere to a surface ruling out flagella-mediated adhesion [128]. Furthermore, I could not find any evidence for a specific surface sensing function of flagella in W3110, that would regulate synthesis of surface structures, which mediate cell attachment. Even in the wild type, I could not observe any surface sensing (see figures 6.3 and A.4), which argues against a specific surface sensing role of flagella. Instead, my results suggest that the main factor for attachment is smooth swimming at a surface. Smooth swimming mutants cannot perform tumbles to change their swimming direction and are obtained by deletion of the chemotaxis kinase CheA or the response regulator CheY. With both smooth swimming mutants I observed increased attachment at early biofilm stages (figure 6.6). A clear advantage of smooth swimming for attachment could be demonstrated with planktonic cells of both W3110 and W3110^{RH} (figures and 6.8, 6.12). When cells approach a surface for attachment, they swim for some time along this surface. Surface swimming ends when cells either attach to the surface or change their swimming direction with a tumble in a way, which leads their swimming path away from the surface. Therefore, smooth swimming cells might spend a prolonged time swimming at the surface, since they cannot escape with a tumble. This prolonged time at the surface might increase the chance to attach. Indeed, previous studies have suggested that smooth swimming bacteria become trapped at the surface by hydrodynamic forces and can only efficiently escape by tumbles [168, 143, 169]. It can hence be proposed that such hydrodynamic entrapment may be a general mechanism promoting bacterial attachment at abiotic and biotic surfaces [168, 170]. By measurement of trajectory length and duration of planktonic cells at the surface, we could show this entrapment for the smooth swimming *cheY* deletion strain in W3110 and W3110^{RH} strains (figures 6.7 and 6.12). If entrapment can be regulated by chemotaxis, attachment could be modulated by the

presence of attractants on or near a surface. Chemotactic stimulation at the surface would promote smooth swimming and thereby could enhance attachment. However, in concordance with previous results [18], we could not demonstrate a requirement of chemotaxis in biofilm formation (see figures 6.5 and 6.6).

Hydrodynamic entrapment might as well be influenced by swimming speed [168]. This opens the questions whether modulating swimming speed might change attachment and biofilm formation in *E. coli*. One way how swimming speed is controlled is through the bacterial brake YcgR. YcgR, in response to c-di-GMP, interacts with the flagellar motor [51, 52, 57, 58, 56] (see also figures 6.10 A and 6.14 A) and reduces swimming speed of the cells [58, 56]. With c-di-GMP being a key player in the transition from a motile to a sessile lifestyle, I aimed to identify a causal relationship between its role in regulating swimming speed and the attachment during biofilm formation. Since c-di-GMP production is largely influenced by σ^S-dependent processes, using only W3110 as a model strain for attachment would not have revealed a satisfying insight into the influence of c-di-GMP in early biofilms. Therefore, relating results obtained with both W3110 and W3110^{RH} was crucial for this part of the thesis. I observed that in contrast to its generally assumed role as a biofilm-promoting factor, c-di-GMP inhibits attachment during W3110 biofilm formation and this inhibition was mediated by YcgR (figure 6.9 B-E). This observation is not entirely new though, since low levels of c-di-GMP have been reported to enhance early biofilm formation [171]. I also observed increased attachment at lowered c-di-GMP levels in the σ^S-positive W3110^{RH} strain. However, in contrast to W3110, this advantage of lowered c-di-GMP was only observed during early stages of biofilm formation. At later stages, the effect was even reversed, with strains having lower c-di-GMP forming less biofilm (figure 6.13 A, B), as would be expected considering the general view of c-di-GMP as a biofilm promoting factor (see e. g. [12]). This phenomenon can be explained by the fact that the enhanced initial cell attachment subsequently becomes outweighed by the reduced production of the biofilm matrix (curli), which prevents formation of structured biofilms. This hypothesis is supported by my data in chapter 7, where lowered c-di-GMP levels decrease 3D-structure formation, which depends on biofilm matrix (see also section 10.2). I therefore suggest a dual role of c-di-GMP during biofilm formation, inhibiting initial cell attachment in early biofilm phases by negatively influencing motility and promoting later biofilm stages through positive regulation of biofilm matrix production (see figure 10.1). Thus, c-di-GMP levels need to be tightly regulated over the course of biofilm formation, being low during biofilm initiation and high at the later stage to allow for biofilm maturation.

In my thesis, I further aimed to elucidate why increased motility would increase initial cell attachment. I hypothesized that if hydrodynamic entrapment supports attachment, and entrapment is influenced by swimming speed, cells with lowered c-di-GMP levels and increased swimming speed would get entrapped at the surface. Trajectories of planktonic cells swimming at the surface, however, were not significantly different if c-di-GMP levels

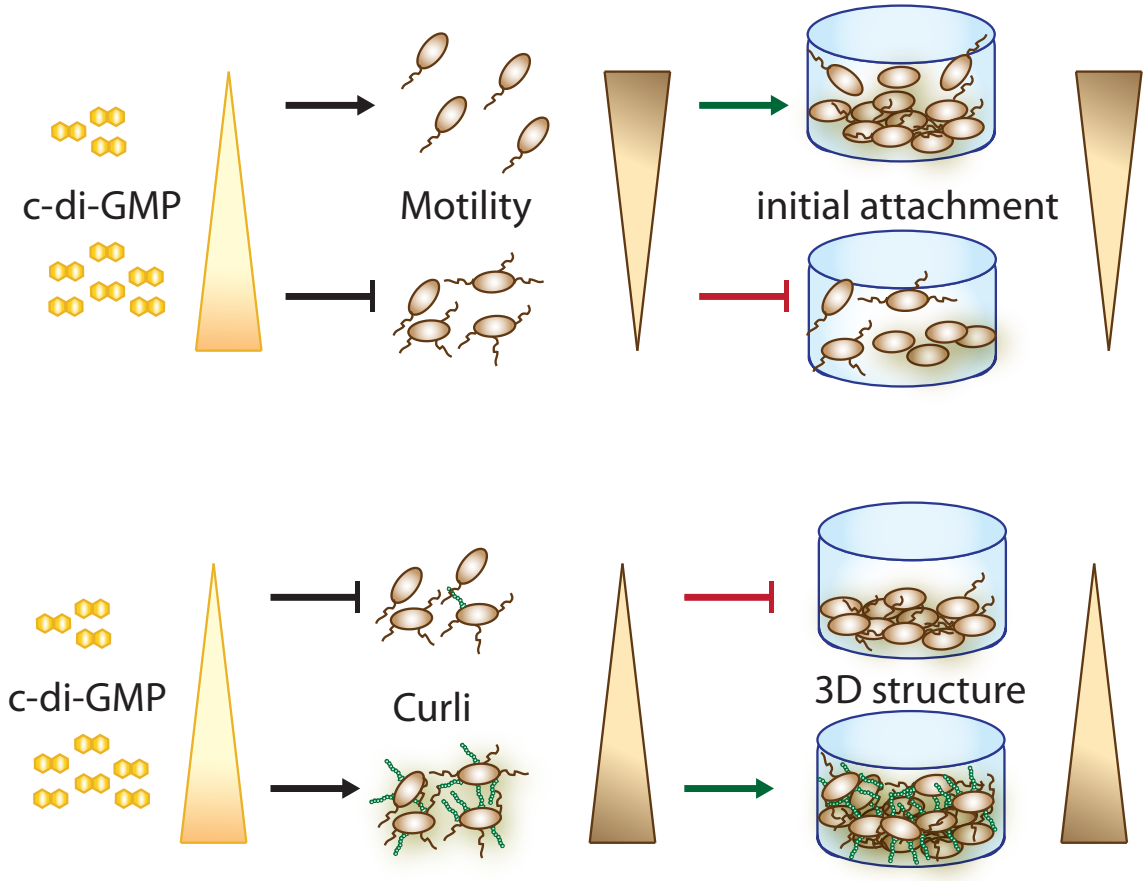

Fig. 10.1. A dual role of c-di-GMP:
Model of the effects of c-di-GMP during submerged biofilm formation in the *E. coli* strain W3110^{RH}. C-di-GMP inhibits motility through the PilZ-domain protein YcgR and thereby negatively interferes with initial attachment. Curli production and thereby 3D-structure formation is positively regulated by c-di-GMP, meaning that c-di-GMP levels need to raise in the course of biofilm formation. Thereby, c-di-GMP levels need to be tightly regulated throughout biofilm formation, being low for efficient initial attachment and being high for biofilm maturation.

were changed (see figures 6.10 B and 6.14 B) and I was not able to explain the changes in cell attachment that I observed in the biofilm assays. Thus, a simple model, where attachment is solely dependent on hydrodynamic entrapment regulated by c-di-GMP levels has to be neglected. An alternative explanation to why increased swimming speed might enhance attachment in our assays is that swimming speed could influence the strength of attachment. In the standard attachment experiments, non-attached and supposedly loosely attached cells are washed away and thereby not taken into account. To investigate this hypothesis I performed an experiment, where I compared attachment before and after washing. Primary data in figure 6.11 show a trend that attachment strength is indeed influenced by swimming speed.

The above described theory of the dual role of c-di-GMP with a requirement for low c-di-GMP levels during initial attachment coincides well with the commonly described two

phases of attachment - reversible and irreversible attachment. In literature, reversible attachment is usually described to require motility, whereas irreversible attachment requires the production of cell surface molecules that stick to the substratum [9]. Therefore, reversible attachment would require low c-di-GMP levels for cell motility and irreversible attachment would require high c-di-GMP levels for the production of biofilm matrix. For *E. coli* submerged biofilm formation, this is shown in the model in figure 10.1. Low c-di-GMP levels promote swimming motility, which is required for efficient initial cell attachment (figure 10.1, upper panel). When attachment becomes irreversible, adhesion factors need to be synthesized. W3110 requires the production of curli fibers to form a mature biofilm with elaborate 3D-structures, which depends on high c-di-GMP levels (figure 10.1, lower panel). The model of the dual role of c-di-GMP can be transferred to other bacterial species, such as *P. aeruginosa*. In *P. aeruginosa*, for example, motility is required to overcome surface repulsion [20, 172, 173] in the reversible attachment phase. Later, during the transition from reversible to irreversible attachment, c-di-GMP production is induced and motility is inhibited [172]. An important player in this transition is the c-di-GMP binding transcription factor FleQ, which causes downregulation of flagellar genes and upregulation of EPS at rising c-di-GMP [174, 175, 176, 177]. The transition from reversible to irreversible attachment and the coinciding requirement of downregulation of flagellar motility and upregulation of adhesion factors is also described in a recent review from Ha and O'Toole [173]. This model of reversible and irreversible attachment can thereby be used to refine the commonly described phenomenon of the motile-to sessile transition in *E. coli*, which is regulated by c-di-GMP. This means that the dual role of c-di-GMP in the motile-to-sessile transition is inhibition of reversible and promotion of irreversible attachment.

10.2 3D-structure formation

In the first part of my thesis, I concentrated on the early phases of biofilm formation when initial cell attachment occurs. There, I observed that flagella are required for attachment because of their motility function and not because of additional roles as surface sensors or adhesins. In the following part, I observed that beyond attachment, flagella are also required for formation of the 3D-structure in static submerged biofilms of the σ^S-positive strain W3110^{RH} (see figure 10.2). Flagella-less cells could form microcolonies on the surface when surface attachment was established by centrifugation (see figure 6.4), however, they were not able to arrange the microcolonies 3-dimensionally (see figures 7.4, A.10 and A.11). A structural role of flagella within the matrix and a contribution to the overall biofilm architecture, has been suggested in previous publications in other types of biofilms, such as flow cell biofilms and biofilm macrocolonies on agar plates [24, 27, 178]. In the submerged biofilms studied in my thesis, this structural role appears to be indispensable (see figures 7.4, A.10 and A.11). With the use of the flagellar motor mutant $\Delta motA$, I could show that rotation of flagella is not a requirement of biofilm formation (see figures 7.4,

A.10 and A.11). However motility does have an effect on the overall shape of the biofilm as *motA* and *cheZ* (reduced motility, but flagellated) deletion strains showed an impaired biofilm structure compared the the wild type strain. This findings are in agreement with a previous publication, in which 3D-structures of flow cell biofilms depended on motility [24] and could be shown for both the curli$^+$ strain W3110^{RH} and the curli$^+$/cellulose$^+$ strain AR3110 (see figures 7.4, 7.7, A.10, A.11, A.19 and A.20).

Biofilms are a dynamic environment, in which many bacterial communities may interact with each other. I hence tested the hypothesis if a subpopulation of flagellated cells may be sufficient to rescue overall 3D-structure by providing a scaffold for the mutant macrocolonies. To elucidate this idea, flagellated cells were co-cultured with flagella-less cells. I could observe that microcolonies of flagella-less cells were incorporated into the structures formed by the wild type cells, confirming our hypothesis that expression of flagella by only one of the microcolonies is sufficient to establish the connection (see figures 7.5, A.13 and A.14). This further suggests that connections within the structure are mediated through attachment of microcolonies to flagella protruding from other microcolonies, rather than through intertwining of flagella, as has been proposed in reference [27]. However, which structure on the cell surface binds to the flagella remains to be elucidated. Preliminary results using mass spectrometry to identify potential binding partners on sheared flagella from biofilm structures (not shown in this thesis) did not answer that question and more experiments need to be conducted. If flagella-less cells are not able to arrange microcolonies on their own, but only when in co-culture with wild type cells, there is a possibility that wild type cells induce the production of surface molecules making the flagella-less cells stickier. Transcriptomic analyses of wild type and flagella-less cells from mixed biofilm cultures could be performed to test that hypothesis. Another possibility is that it is pure chance that microcolonies of flagella-less cells get entrapped by growing microcolonies of wild-type cells while the wild type microcolonies start to arrange 3-dimensionally. This would also explain why the 3-dimensional distribution of flagella-less microcolonies in mixed biofilm cultures remains more or less restricted to the lower part of the biofilm. Importantly, I observed that expression of the curlin genes *csgBA* on population level was lower in the *fliC* and *motA* deletion strains than in wild type (see figure A.12) and unpublished data from our laboratory (O. Besharova) suggest that heterogeneity of curli gene expression is affected in the mutant strains. For the $\Delta motA$ strain, high curli expression is observed in the 3-D clumps, however, low or none expression is observed in the non-arranged cells. Thereby, transcriptomic analyses of wild type, $\Delta fliC$ and $\Delta motA$ might indeed be useful to elucidate the matrix expression patterns and to be able to solve the contribution of flagella to the biofilm structure.

Apart from flagella, the major structural component of the W3110^{RH} submerged biofilms seems to be curli (see figures 7.2, A.5, A.6 and 10.2). This might explain the attachment experiments from figure 6.13, where I demonstrated a possible dual role of c-di-GMP. The cyclase deletion strain $\Delta yegE$, which has decreased c-di-GMP levels, initially had an advantage attaching efficiently to the surface due to its increased motility, but showed im-

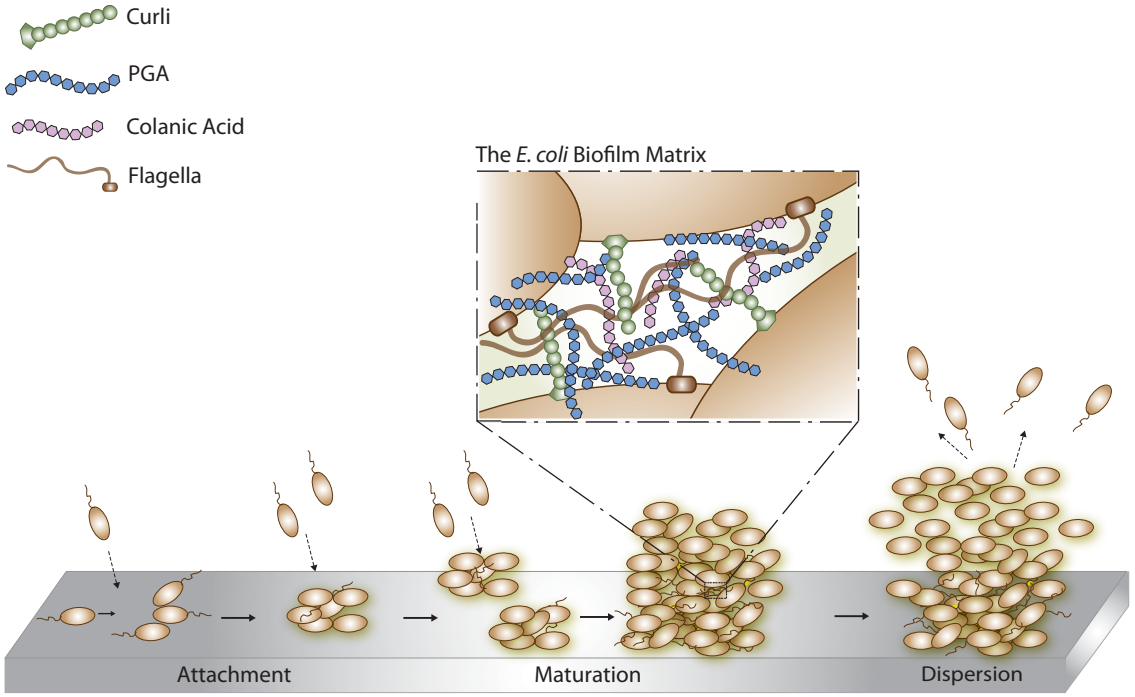

Fig. 10.2. The players for 3D-structure formation:
Phases of biofilm formation in *E. coli* are shown. In submerged biofilm formation of the *E. coli* strain W3110^{RH}, curli and flagella appear to be the major players for shaping biofilm architecture whereas PGA and colanic acid were dispensable.

paired biofilm formation at the later time-points. Curli expression depends on c-di-GMP (see chapter 3.4) and if curli is the main matrix determinant, decreased mature biofilm formation is expected at lowered c-di-GMP levels. Indeed, my analyses of 3-D structures in the c-di-GMP mutant strains confirmed this hypothesis (see figures 7.6, A.15, A.16, A.17 and A.18). If c-di-GMP is lowered, 3D-structure formation is impaired. This was independent of YcgR, since the structures of the *ycgR* deletion strain were similar to wild type structures, meaning that c-di-GMP dependent effects on structures are uncoupled from the motility control. These results are in agreement with studies in other types of biofilms that depend on curli and/or cellulose [27, 86]. If c-di-GMP levels are permanently increased, I observed decreased initial attachment, but no defects in 3D-structures. This can be explained as well by the dual role of c-di-GMP, inhibiting initial cell attachment and promoting matrix production for biofilm maturation. Thus, c-di-GMP levels need to be tightly regulated over the course of biofilm formation, establishing low levels during initiation and high levels during maturation. This could as well explain why the PDE YhjH is expressed in *E. coli* as a part of the flagellar regulon whereas the cyclase YegE is positively regulated by the stationary phase σ factor RpoS.

In addition to the requirement of the c-di-GMP dependent matrix component curli, the *E. coli* adhesins *yfaL* and *ycgV* play a role in 3D-structure formation in submerged biofilms (figures 7.3, A.7). In contrast to biofilms of MG1655 [159], deletions of the two adhesins in W3110^{RH} impaired attachment, as shown by CV staining (unpublished results from O.

Besharova). However, overexpression of *yfaL* and *ycgV* genes has been shown to increase MG1655 attachment and mature biofilm formation in microfermenters [159]. Importantly, in my work, I showed that $\Delta yfaL$ and $\Delta ycgV$ have impaired swimming motility (see figure A.9). The authors of the reference above [159] did not look into motility of their strains and propose a possible adhesin function for YfaL and YcgV based on their overexpression data. It therefore remains to be shown in future work whether these adhesins are actually required for biofilm initiation and maturation because of a structural function or whether the impaired motility of the deletion strains is the reason for the defect in biofilm initiation and architecture. Altogether, my results on 3D-structure formation propose that curli and flagella are the main cell surface structures that help to shape the 3-D structures (see figure 10.2).

11. YJDA IS A NEW REGULATOR OF C-DI-GMP SIGNALING

C-di-GMP signaling has been studied very extensively in the past years and the molecules that make and break this second messenger have been identified in many bacterial species. Commonly, a whole set of cyclases and diesterases are responsible for the production and turnover of c-di-GMP, which in turn regulates a vast variety of processes, including motility and biofilm formation. In my thesis, I adressed one of the remaining questions, namely, in which ways signal specificity of c-di-GMP signaling is achieved. One possibility of generating specific responses to c-di-GMP levels is a dose-dependent regulation of downstream processes by sensing of distinct c-di-GMP concentrations through different types of c-di-GMP receptors, such as protein receptors or riboswitches [79] (see also introduction, section 3.2). Another possibility is the regulation of c-di-GMP production by diguanylate cyclases, which I considered in my thesis. Based on results from a previous publication, I looked into the effects of a potential new regulator of c-di-GMP production, YjdA.
As described in the introduction and results section, YjdA together with the small protein YjcZ were discovered in a motility screen as suppressors of the YhjH-mediated motility regulation [50]. A strain deleted for the major PDE YhjH has elevated c-di-GMP levels, which results in inhibition of swimming motility. Additional deletion of the DGC YegE suppresses this motility defect, since YegE is one of the major cyclases contributing to the c-di-GMP pool sensed by the motility regulator YcgR and degraded by YhjH (for an overview of the mechanism refer to figure 3.1). Similarly to the *yegE* deletion, the *yjdA* and *yjcZ* deletions are able to suppress this defect in the $\Delta yhjH$ background, suggesting that YjdA regulates c-di-GMP production (see also figure 8.1). YjdA is a homolog to the eukaryotic dynamin and is expressed together with the uncharacterized protein YjcZ from one operon, which supposedly is regulated by the flagellar σ factor FliA. The regulation by FliA may also hint towards a role of YjdA and YjcZ in motility control.
In an epistasis experiment, I could confirm the action of YjdA and YjcZ on swimming motility and my data suggest that they act via the cyclase YegE (see figure 8.1). Based on those results, I aimed to investigate the effects of YjdA on YegE and to put the regulation in the physiological context.

11.1 YjdA regulates motility and biofilm formation via the c-di-GMP signaling pathway

Based on the confirmation of the published results that YjdA and YjcZ affect motility and the observation that this might be due to an impact on c-di-GMP production by the

diguanylate cyclase YegE (see figure 8.1), I speculated that YjdA and YjcZ would play a role in biofilm formation. Hence, I tested the regulation of biofilm formation by YjdA and YjcZ during attachment and 3D-structure formation. YjdA and YjcZ both affect biofilm formation in a similar way as YegE, meaning inhibiting initial attachment and promoting biofilm maturation, as shown in my attachment experiments (see figure 8.2 A-D) and 3D-structure experiments (see figures 8.3, 8.4, A.21, A.22, A.23 and A.24). These effects are indeed apparently mediated by changes in c-di-GMP production by YegE, as shown by the decrease of the c-di-GMP dependent interaction between YcgR and MotA (see figure 8.2 E-G).

With the membrane modulating function of dynamins and the apparent regulatory effect of YjdA on the membrane protein YegE, I expected the bacterial dynamin YjdA to localize at the plasma membrane. Although Ozaki and colleagues [109] describe a localization of YjdA (or CrfC, as they renamed it) in foci at the midcell and quarter cell positions, I mainly observed localization at the plasma membrane (see figure 9.3). Localization was influenced by the growth phase with more homogeneous distribution at lower optical density and localization in foci close to the poles at higher optical density. Notably, this localization on foci depends on the GTPase function of YjdA. In the W3110 strain, a GTPase defective YjdA localizes in elongated clusters that resembled chains of proteins being associated with the membrane. This might reflect membrane decoration by YjdA oligomers and might allow speculations for a membrane-remodeling function of the bacterial dynamin. Possibly, this would affect activity of YegE, meaning an indirect regulation of YegE by YjdA. This would also explain, why I could not observe clear colocalization of YjdA/YjcZ with YegE and why no interaction with the cyclase was measured with FRET (see figures 9.4 and 9.5). YjdA seems to act in complex with YjcZ, as suggested by the colocalization and FRET data and the effects of YjcZ on biofilms (figures 9.5, 8.2 - 8.4 and A.21 - A.24). The question is, whether there is a third protein or a protein complex connecting YjcZ/YjdA with YegE and thereby allowing for an indirect regulation of the cyclase by YegE.

11.2 A regulation of c-di-GMP signaling by flotillins?

In the course of trying to elucidate the mechanism by which YjdA regulates the cyclase YegE, potential interactors that might connect YjdA and YegE were searched for in a mass spectrometry approach. We could identify the flotillin pair HflK/C in the mass spectrometry data and confirm the interaction with YjdA and YegE in BACTH assays (see figures 9.6 and 9.7). In general, flotillins are associated with a variety of membrane dynamics and thus, a link to dynamins does seem plausible. Flotillins have indeed been implicated in functioning with bacterial dynamins in previous work in *B. subtilis* [179], though in a different cellular setting, namely cell division and cell shape maintenance. The authors, however, report a synthetic effect on motility on soft agar plates in a flotillin/dynamin double mutant, which they did not investigate further. In my work, I did not include

swimming assays of flotillin mutants, but FRET data with the c-di-GMP dependent interaction of MotA and YcgR point towards a reduction of c-di-GMP levels in the absence of flotillins, which in turn would increase swimming speed (see figure 9.11). However, since I did not measure swimming speeds, this is speculation and needs to be confirmed. Nevertheless, the results would support the idea that HflK/C influence the activity of YegE in a similar way as the dynamin YjdA. With microscopy experiments, I was not able to detect colocalization of YegE with the flotillins, neither did I observe a dependence of YjdA or YegE localization and dynamics on flotillins nor vice versa. It therefore remains to be elucidated, with which mechanism the regulation of YegE by YjdA works and which contributions the flotillins have. A plausible idea is that flotillins change the lipid composition in membranes, thereby changing membrane fluidity [179]. The cyclase YegE might reside in membrane regions that due to the action of the flotillins HflK/C contains lipids that allow for easier membrane bending and the dynamin YjdA might be responsible for changing membrane curvature. This would be a new phenomenon in bacteria, however, is well established in eukaryotic cells, where induction of membrane curvature is an important process, e.g. in the formation of vesicles in the secretory pathway. In turn, activity of YegE could be regulated by the changes in the membrane rather than by direct interactions with the dynamin or the flotillins. Speculatively, the membrane bending implemented by the dynamin and facilitated through adapted lipid composition in the membrane by the flotillins, could create microcompartments in the cell, to which YegE-dependent c-di-GMP processes are located, thereby ensuring signal specificity.

12. CONCLUSION AND OUTLOOK

The transition from a motile planktonic to a sessile biofilm lifestyle includes many regulatory processes, including the downregulation of bacterial motility and the upregulation of adhesion factors by the second messenger c-di-GMP. In my thesis, I have investigated roles of flagellar motility in the formation of submerged biofilm formation of *E. coli* and described multiple roles of flagella in biofilms. First and foremost, flagella are required for initial attachment due to their motility function. I could show that smooth swimming leads to surface trapping of cells and promotes initial cell attachment. This requirement of swimming motility in early biofilm formation is reflected by a dual role of c-di-GMP inhibiting early attachment and promoting biofilm maturation. Thus, my results suggest that c-di-GMP levels need to be tightly regulated throughout the course of biofilm formation, being low at biofilm initiation and being high in mature biofilms. The observed advantage for attachment at lower c-di-GMP, causing elevated swimming speed, requires further investigation since I could not explain why faster swimming causes increased cell attachment. My hypothesis that enhanced swimming speed might strengthen the initial attachment could be investigated in microfluidics systems where already attached cells are subjected to a flow of medium or buffer. Alternatively, attachment under flow conditions could be investigated.

In addition to the requirement of flagellar motility for attachment, flagella appear to play a structural role in shaping the architecture of mature submerged biofilms. I could show that flagella-less cells fail to arrange 3-dimensionally and thereby cannot form elaborate biofilm structures. In mixed cultures with wild type cells, flagella-less cells are able to partially integrate into the wild type structures by a so far unknown manner. Possibly, flagella from wild type microcolonies attach to the surface of cells in the flagella-less microcolonies, which allows incorporation of the flagella-less microcolonies into the biofilm. In future experiments, we could investigate the structural role of flagella further in an experiment where flagella synthesis is stopped in a wild type biofilm. Additionally, flagella on the cell surface containing a protease recognition site could be cleaved of and the following events could be monitored by live-cell imaging.

In the last part of the thesis, I describe a new regulator of c-di-GMP, the bacterial dynamin YjdA. YjdA together with the small protein YjcZ positively regulates c-di-GMP production by the diguanylate cyclase YegE, affecting swimming motility, cell attachment and biofilm maturation. This regulation includes interaction with the flotillins HflK/C in a so far unknown mechanism. Speculatively, the dynamin alters membrane curvature of membrane regions containing flotillins, which in turn affects the activity of the membrane

protein YegE. The role of flotillins in this regulation might be altering lipid composition of the membrane in a way that facilitates membrane deformation. In future work, membrane fractions containing YegE could be purified and c-di-GMP production could be monitored with increasing concentrations of titrated YjdA. Since c-di-GMP is produced from GTP, c-di-GMP production could be quantified with a spectroscopic assay detecting GTP. This experiment could prove that c-di-GMP production by YegE is indeed influenced by YjdA, as I concluded from my biofilm phenotypes and FRET of the c-di-GMP dependent MotA-YcgR interaction. Additionally, electron microscopy of YjdA-decorated membranes could shed light into the actions of the dynamins, hopefully showing membrane deformation.

Part VI

MATERIALS AND METHODS

13. MATERIALS

13.1 Chemicals and consumables

Chemicals used in this work are listed in the appendix in table B.1.

13.2 Reaction kits

Tab. 13.1. Reaction kits

Kit	**Company**
NucleoSpin® Gel and PCR Clean-up kit:	Macherey-Nagel
GenElute^{TM} HP Plasmid Miniprep Kit:	Sigma-Aldrich

13.3 Well plates

Tab. 13.2. Well plates

Plate	**Order number**	**Company**
24-Well Clear TC-Treated Multiple Well Plates, Sterile	Product 3527	Corning® Costar® (Corning Inc.)
96-Well Clear Flat Bottom TC-Treated Microplate, Sterile	Product 3585	Corning® Costar® (Corning Inc.)
μ-Slide 8 Well, Uncoated, 1.5 polymer coverslip, hydrophobic, sterilized	Product 80821	ibidi® (ibidi GmbH)
μ-Plate 96 Well Uncoated, 1.5 polymer coverslip, hydrophobic, sterilized	Product 89621	ibidi® (ibidi GmbH)
96-Well Tissue Culture Black/Clear Flat-bottom Plates	Product 353219	BD Falcon^{TM} (Becton, Dickinson and Co.)

13.4 Media

Tab. 13.3. Media for bacteria

LB (Luria broth) medium:	10 g bacto tryptone
	5 g bacto yeast extract
	5 g NaCl
	H_2O ad 1 l; pH 7 with NaOH
	autoclaved
LB agar plates:	1.5 % agar in LB medium
	autoclaved
TB (Tryptone broth):	10 g bacto tryptone
	5 g NaCl
	H_2O ad 1 l; pH 7 with NaOH
	autoclaved
M9 minimal medium:	47.7 mM $Na_2HPO_4x7H_2O$
	22 mM KH_2PO_4
	8.55 mM NaCl
	18.7 mM NH_4Cl
	2 mM $MgSO_4$
	0.1 mM $CaCl_2$
	0.4 % ribose
Congo red plates:	10 g bacto tryptone
	5 g yeast extract
	2 % agar
	900 ml H_2O
	autoclave, then add:
	80 ml congo red/coomassie solution
	20 ml H_2O
	(c [congo red]= 40 μg/ml; c [coomassie]= 20 μg/ml)

13.5 Buffers

Tab. 13.4. Buffers for bacteria

Tethering buffer:	10 mM KPO_4
	0.1 mM EDTA
	1 μM methionine
	10 mM lactic Acid
	pH 7.0
	sterile filtered
Motility buffer:	10 mM KPO_4
	0.1 mM EDTA
	67 mM NaCl
	0.5 % glucose
	pH 7.0
	sterile filtered
P1 buffer:	10 mM $MgSO_4$
	5 mM $CaCl_2$
	sterile filtered
Tss solution:	5 g polyethyleneglycol (PEG) 8000
	0.3 g $MgCl_2x6H_2O$
	2.5 ml DMSO
	LB ad 50 ml
	sterile filtered

Tab. 13.5. Buffers for agarose gel electrophoresis

TAE buffer:	242 g Tris base
	100 ml 0.5 M EDTA (pH 8)
	57.1 ml glacial acetic acid
	H_2O ad 1 l
6x DNA loading dye:	30 % glycerol
	0.25 % bromphenol blue
	0.25 % xylene cyanol

Tab. 13.6. Buffers for Pull-Down and SDS PAGE

3x SDS Laemmli buffer:	6 % SDS
	30 % glycerol
	15 % β-mercaptoethanol
	0.006 % bromphenol blue
	0.25 M Tris
	pH 6.8
10X SDS running buffer:	144.2 g glycine
	30.3 g Tris base
	10 g SDS
	H_2O ad 1 l
10 ml 10 % SDS resolving gel:	4 ml H_2O
	3.3 ml 30 % acrylamide mix
	2.5 ml 1.5 M Tris, pH 8.8
	100 μl 10 % SDS
	100 μl 10 % APS
	10 μl TEMED
6 ml 5 % SDS stacking gel:	4.2 ml H_2O
	1 ml 30 % acrylamide mix
	760 μl 1 M Tris, pH 6.8

	60 μl 10 % SDS
	60 μl 10 % APS
	6 μl TEMED
Blue Silver staining [180]:	100 ml H_2O
	117 ml H_3PO_4
	100 g $(NH_4)_2SO_4$
	1.2 g coomassie Brilliant Blue G-250
	H_2O ad 800 ml
	200 ml methanol
Buffer TN:	20 mM Tris-HCl, pH 8.0
	NaCl 0.2 M

Tab. 13.7. Antibiotic stock solutions

ampicillin:	100 mg/ml in H_2O
kanamycin:	50 mg/ml in H_2O
chloramphenicol:	34 mg/ml in H_2O
streptomycin:	100 mg/ml in H_2O

Tab. 13.8. Inducers and other stock solutions

IPTG:	0.1 M in H_2O
arabinose:	10 % in H_2O
X-Gal:	40 mg/ml in DMF
lysozym:	50 mg/ml in H_2O
congo red/coomassie solution:	200 mg congo red
	100 mg coomassie Brilliant Blue
	70 % ethanol ad 100 ml
DNase:	100 μg/ml

14. METHODS

14.1 Molecular Cloning

14.1.1 Polymerase chain reaction

Genes for cloning were amplified by Polymerase chain reaction (PCR) using either Taq polymerase or Phusion polymerase (ThermoFisher) according to the reaction setup in tables 14.1 and 14.2 and the PCR program shown in tables 14.3 and 14.4. For the amplification of wild type genes, freshly grown colonies of strains W3110 or W3110^{RH} were used. PCR primers were ordered from Eurofins Genomics or from Sigma-Aldrich, and used at concentrations of 10 pmol/μl. PCR products were analyzed by agarose gel electrophoresis on a 1 % agarose gel in TAE and purified using the Macherey-Nagel NucleoSpin® Gel and PCR Clean-up kit according to the manufacturer's instructions.

Tab. 14.1. PCR reaction set-up for amplification using Taq polymerase

DreamTaq Green PCR Master Mix (2x)	**forward primer**	**reverse primer**	**H_2O**
25 μl	2.5 μl	2.5 μl	20 μl

Tab. 14.2. PCR reaction set-up for amplification using Phusion polymerase

Phusion HF buffer (5x)	**forward primer**	**reverse primer**	**dNTPs (1.25 mM)**	**DMSO**	**Phusion Polymerase**	**template**	**H_2O**
10 μl	2.5 μl	2.5 μl	8 μl	2.5 μl	0.5 μl	1 μl	23 μl

Tab. 14.3. PCR program for Taq polymerase

Step	Temperature	Time	Cycle(s)
Precycle	95°C	10 min	1
Denaturation	95°C	30 sec	25
Annealing	55 − 57°C	30 sec	
Extension	72°C	60 sec/bp	
Post-Extension	72°C	10 min	1
Cooling	16°C	forever	1

Tab. 14.4. PCR program for Phusion polymerase

Step	Temperature	Time	Cycle(s)
Precycle	98°C	5 min	1
Denaturation	98°C	20 sec	25
Annealing	55 − 57°C	30 sec	
Extension	72°C	30 sec/bp	
Post-Extension	72°C	10 min	1
Cooling	16°C	forever	1

14.1.2 Restriction digest

PCR products and vectors for cloning were digested with restriction enzymes from New England Biolabs Inc. or Thermo Scientific^{TM}. Preparative digests were performed in 30-40 μl reaction volumes for 2-4 h at 37°C and purified with the Macherey-Nagel NucleoSpin® Gel and PCR Clean-up kit. Analytic digests were performed in 20 μl reaction volumes for 1 h at 37°C. Reaction set-ups were as described in table 14.5.

Tab. 14.5. Restriction digest reaction set-up

	Preparative digest	Analytical digest
DNA	10-15 μl	5 μl
Enzyme 1	1 μl	0.3 μl
Enzyme 2	1 μl	0.3 μl
10x reaction buffer	3 μl	2 μl
H_2O	ad 30 μl	ad 20 μl

14.1.3 Ligation

For ligation, 1 μl vector was ligated with 3 μl insert DNA using 0.5 μl Thermo Scientific^{TM} DNA ligase and 1.5 μl 5xligation buffer in a 15 μl reaction volume. Ligations were per-

formed at RT for 30 min or at 16°C ON.

14.1.4 Competent cells and transformations

Cells were made competent for transformations using either the chemical approach with $CaCl_2$ or the one-step TSS-method [181]. For chemically competent cells, an overnight culture was grown in 5 ml LB at 37°C. 3 ml overnight culture were diluted in 300 ml fresh LB medium and cells were grown to an OD_{600} of 0.5-0.7. The following steps were performed on ice or at 4°C using ice-cold buffers. Cells were pelleted at 3,200 g for 10 min and resuspended in 100 ml 0.1 M $MgCl_2$. After 30-45 min incubation on ice, cells were pelleted at 1,800 g for 10 min and pellets were resuspended in 50 ml 0.1 M $CaCl_2$. After 10 min centrifugation at 1,800 g, pellets were resuspended in 1.5 ml 0.1 M $CalCl_2$/18 % glycerol, aliquoted in 100 μl portions, frozen in liquid nitrogen and stored at −80°C. For transformations, 30-50 μl cells were mixed with 0.3 μl DNA and transformed as described below. For the TSS-method, overnight cultures in 5 ml LB were grown at 37°C, diluted 1:100 in fresh LB and grown for 3-4 h at 37°C. 1 ml culture was centrifuged at 13,000 rpm in a tabletop centrifuge and resuspended in 50 μl ice-cold TSS solution. Cells were mixed with 0.5-1 μl DNA and transformations were performed as described below.

14.1.5 Transformation of ligation mixtures

5 μl Ligation mixture were transformed into 50 μl chemically competent *E. coli* DH5α. For that, cells and DNA were mixed and incubated on ice for 15 min followed by a 1 min heatshock at 42°C. After additional 15 min incubation on ice, 1 ml LB medium was added to the cells and they were incubated for 1 h at 37°C on a rotary shaker at 450 rpm. After 1 min centrifugation at 11,000 rpm, transformed cells were plated on LB plates containing appropriate antibiotics for selection and incubated ON at 37°C.

14.1.6 Screening for positive clones and DNA isolation

Clones obtained after transformation were screened for correct inserts by PCR using vector-specific primers. DNA of positive clones was isolated using the Sigma-Aldrich GenElute^{TM} HP Plasmid Miniprep Kit according to the manufacturer's instructions. Alternatively, clones were screened for correct inserts by analytical digestions (see table 14.5).

14.1.7 Sequencing

Positive clones were confirmed by sequencing at GATC Biotech, Konstanz or Eurofins Genomics, Ebersberg. Primers for sequencing were designed as recommended by the companies. The obtained sequences were analyzed using Serial Cloner 2.1.

14.2 Biochemical methods

14.2.1 Immunoprecipitation

Pull-down experiments were performed by Hui Li. Strains were grown as described in section 14.4.1 at 200 rpm and 30°C for 5 h and 14 h. 10 ml culture were harvested for 5 min at 3,200 g and washed once in 10 ml buffer TN. Pellets were resuspended in 800 μl buffer TN supplemented with 100 μg/ml DNase, 50 μg/ml lysozyme and 32 μl 25x protease inhibitors cocktail. Cells were lysed by four times sonication on ice for 10 s and 50 % power. 0.2 % Nonidet P-40 was added to the lysate, which subsequently was incubated at 4°C for 18 h. The lysate was centrifuged for 15 min at 14,000 g and the supernatant was transferred into a pre-cooled tube. 25 μl GFP-Trap®_A beads were washed three times with ice-cold TN buffer to equilibrate. The beads were mixed with the cell lysate and incubated at 4 ° C for 1 h gently rotating. The beads were washed three times with ice-cold TN buffer and were transferred into a clean tube. The beads were resuspended in 70 μl 1x Laemmli buffer (4x Laemmli diluted in TN buffer) and the samples were boiled at 98 ° C for 20 min.

14.2.2 SDS-PAGE (Sodiumdodecylsulfate polyacrylamide gel electrophoresis)

Proteins were separated by SDS-PAGE using the discontinuous buffer system according to Laemmli [182]. Therefore, protein samples in Laemmli sample buffer were boiled at 70°C - 98 ° C for 5 -20 min and separated on a SDS-polyacrylamide gel at 70 V (stacking gel) and at 120 V (separating gel). 5 μl molecular weight marker (PageRuler^{TM} Plus Prestained Protein Ladder, 10 to 250 kDa, ThermoScientific) were loaded as a standard. Gels were stained with Blue Silver [180].

14.2.3 Mass spectrometry

Mass spectrometry was performed at the ZMBH Core facility for mass spectrometry and proteomics. Data were analyzed using softwares Scaffold_4.4.1 (Proteome Software Inc.), Microsoft® Excel® 2008 for Mac (version 12.3.6), KaleidaGraph (version 4.0.3) and R (version 2.15.2 GUI 1.53 Leopard build 32-bit).

14.3 *E. coli* strains

All strains used in this work are listed in table B.4. *E. coli* strains used in this work were derived from W3110 or W3110^{RH}. Knockout strains were made either following the one-step method for inactivation of genes ([183]; see section 14.3.2) or by P1 transduction (see section 14.3.3) using strains of the Keio collection [142] as donors. FLP recombinase expressed from the plasmid pCP20 [184] (see section 14.3.5) was used to excise the kanamycin cassette.

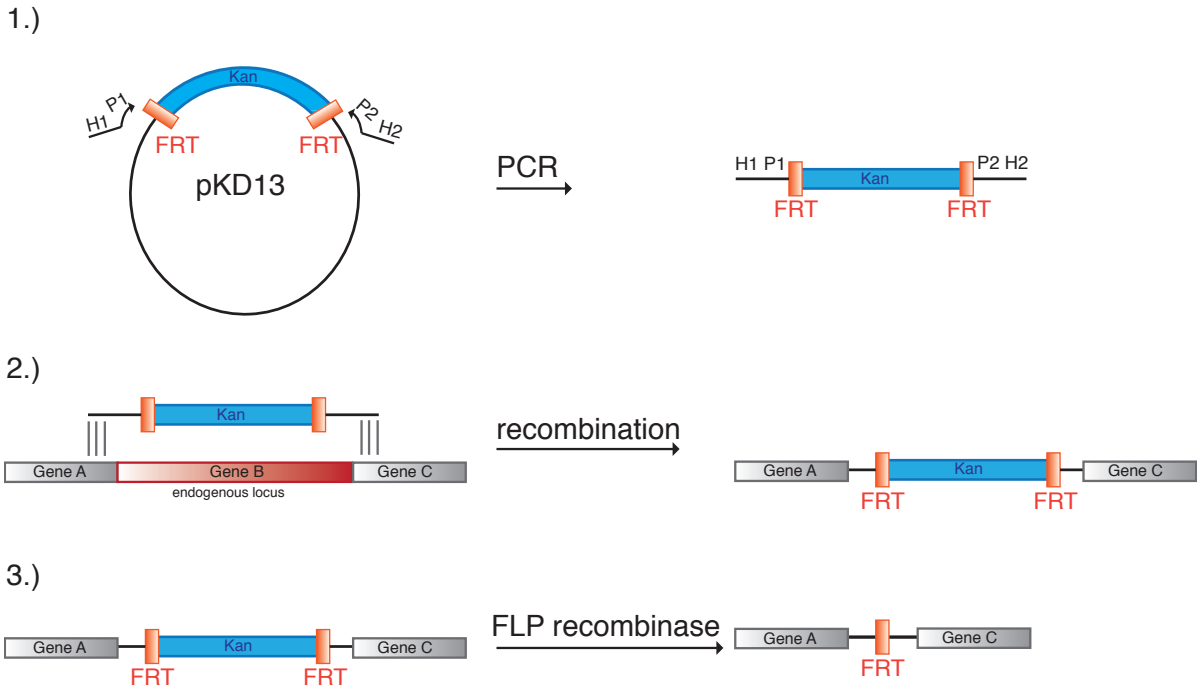

Fig. 14.1. Schematic overview of the one-step method for inactivation of genes according to Datsenko and Wanner [183]:
1.) Kanamycin resistance cassette from plasmid pKD13 was amplified with primers containing overhangs that are homologous to flanking sequences of the target gene (H1, H2).
2.) PCR products were introduced in the receptor strain expressing λ Red recombinase.
3.) Kanamycin cassette was excised expressing FLP recombinase from plasmid pCP20.
H1/H2: homology regions; P1/P2: priming sites.

14.3.1 Freezing and storage of bacterial strains

5 ml overnight cultures of strains were pelleted and resuspended in ice-cold 1 ml LB/18 % glycerol. Cells were frozen and stored at −80°C.

14.3.2 One-step method for inactivation of genes

For the indicated strains in table B.4, gene deletions were made using the one-step method for inactivation of genes developed by Datsenko and Wanner [183] (see Figure 14.1). Briefly, the gene on the chromosome was replaced with a kanamycin resistance cassette that was amplified by PCR from plasmid pVS906 using primers with homology extensions (H1 and H2; for primers see Appendix, table B.2). The PCR product was purified via gel extraction and electroporated into electrocompetent W3110^{RH} cells expressing phage λ Red recombinase. For that, W3110^{RH} cells transformed with plasmid pKD46 were grown ON at 30°C in LB medium containing 100 μg/ml ampicillin. 3 ml ON culture were diluted in 300 ml fresh LB medium supplemented with 100 μg/ml ampicillin and 1 mM arabinose. The culture was grown at 30°C and 200 rpm until an OD_{600} of approx. 0.7, incubated on ice for 20 min and harvested at 3,200 g for 10 min at 4°C. The pellet was washed four times with 1.) 150 ml, 2.) 150 ml, 3.) 150 ml and 4.) 60 ml 10 % glycerol by resuspension fol-

lowed by centrifugation at 3,200 g for 10 min at 4°C. The resulting pellet was resuspended in 1.8 ml 10 % glycerol, frozen in liquid nitrogen and either stored at −80°C or used for electroporation immediately. For electroporation, 75 μl competent cells were mixed with 10 μl purified PCR product and incubated on ice for 20 min. Electroporation was perfomed with a Biorad Micropulser^{TM} using program Ec1 (gap width 1 mm, approx 2 kV and 5.2 ms). Directly after electroporation, 1 ml pre-warmed LB medium was added and the cells were incubated at 37°C and 450 rpm. Cells were pelleted, plated on LB plates containing 50 μg/ml kanamycin and incubated at 37°C ON. Received clones were restreaked on LB plates containing 50 μg/ml kanamycin and incubated at 37°C ON. Correct clones were verified by PCR and kanamycin cassette was excised using FLP recombinase ([184]; see section 14.3.5).

14.3.3 P1 transduction

P1 transductions were performed to transfer knockouts from the Keio collection [142] into W3110 and W3110^{RH}, or to transfer self-made knockouts or genomically tagged genes within a strain background. Donor and acceptor strains were grown overnight in 5 ml LB supplied with 50 μg/ml kanamycin (for donor strains). 1 ml of acceptor culture was centrifuged at 2700 rpm for 5 min in a tabletop centrifuge and the pellet was resuspended in 500 μl P1 buffer. Overnight cultures of donor strains were diluted 1:100 in two cultures with 5 ml fresh LB supplied with 50 μg/ml kanamycin, 5 mM $CaCl_2$ and 0.2 % glucose and grown at 37°C in a rotary shaker. After 30 min, one donor culture was mixed with 100 μl P1 lysate from a previous P1 transduction. After additional 3 h at 37°C, the lyzed donor culture was sterile-filtered. 100 μl lysate were mixed with 100 μl pre-treated acceptor cell suspension and incubated at 37°C and 250 rpm. After 30 min, 1 ml LB containing 10 mM sodium citrate were added to the cell suspension and cells were incubated at 37°C and 250 rpm for additional 30-60 min. Cells were pelleted at 13,000 rpm in a tabletop centrifuge, resuspended in 50-100 μl 1 M sodium citrate, plated on LB plates containing 50 μg/ml kanamycin and incubated at 37°C overnight. Received clones were restreaked on LB plates containing 50 μg/ml kanamycin and incubated at 37°C ON. Correct clones were verified by PCR and kanamycin cassette was excised using FLP recombinase ([184]; see section 14.3.5).

14.3.4 Genomic tagging

Genomic fusions of YjdA and YegE to YFP were made using plasmids pKD13-YjdA-YFP and pKD13-YegE-YFP from H. Li according to a protocol derived from [185]. Briefly, receiver strains were co-transformed with the pKD13-derivative plasmids and the helper plasmid pACBSR using the TSS method. Transformants were selected at 37°C ON on LB plates containing 50 μg/ml kanamycin, 100 μg/ml ampicillin and 34 μg/ml chloramphenicol. One colony was resuspended in 1 ml LB containing 0.2 % arabinose, 50 μg/ml kanamycin and 34 μg/ml chloramphenicol. The cell suspension was incubated at 37°C on

a rotating wheel for 8-10 h. Cells were pelleted by centrifugation at 13,000 rpm in a table-top centrifuge and plated on LB plates containing 0.01 % arabinose, 50 μg/ml kanamycin and 13.3 μg/ml chloramphenicol. Recombinants were selected at 37°C ON, restreaked on LB plates containing 50 μg/ml kanamycin and incubated at 37°C ON. Correct clones were verified by PCR and kanamycin cassette was excised using FLP recombinase ([184]; see section 14.3.5). pACBSR was lost during sequential growth under non-selective conditions at 42°C. Loss of resistances was confirmed by growth at 30°C.

14.3.5 Cross-out of kanamycin resistance cassette

To cross out the kanamycin resistance cassette introduced by the one-step method for inactivation of genes or by P1 transduction, Kan^R-strains were transformed with plasmid pCP20 [184] and grown at 30°C. pCP20 was lost during sequential growth under non-selective conditions at 42°C. Loss of resistances was confirmed by growth at 30°C.

14.4 Growth conditions

14.4.1 Planktonic cultures

For experiments with planktonic cultures, overnight cultures of W3110 and $W3110^{RH}$ were grown at 30°C and 200 rpm in 10 ml TB or in on a rotary wheel in 5 ml TB supplemented with appropriate antibiotics, if required. Overnight cultures were diluted 1:50 or 1:100 in 10 ml fresh TB supplemented with appropriate antibiotics and indicated IPTG or arabinose concentrations for induction, if required. Cells were grown at 30°C and 200 rpm until they reached the indicated OD_{600}. Cells were harvested at 3,200 g for 5 min, washed once in Tethering buffer by resuspension in buffer followed by centrifugation, and incubated for 20 min at 4°C in Tethering buffer. Alternatively, cells were harvested as described above and resuspended in Motility buffer (for attachment experiments) and incubated for 20 min at 4°C.

14.4.2 Static biofilm growth

For biofilms of W3110 and $W3110^{RH}$, precultures were grown in 1 ml TB / well in 24-well plates from Corning® Costar® (Corning Inc.) at 30°C or 26°C for 48 h under static conditions. OD_{600} of precultures was determined and cultures were diluted to an OD_{600} of 1 in TB. W3110 cultures were further diluted to an OD_{600} of 0.1 in M9 medium, $W3110^{RH}$ cultures to an OD_{600} of 0.05 in TB. For mixed culture experiments, differently labeled strains were mixed at indicated ratios. 125 μl cells were seeded per well in 96-well plates from Corning® Costar® (Corning Inc.), ibidi® (ibidi GmbH) or BD Falcon^{TM} (Becton, Dickinson and Co.). For confocal imaging, 125 μl cells were seeded into wells of 8-well slides from ibidi® (ibidi GmbH), which were placed into sterile petridishes containing moist tissue. On plates / slides used for imaging, additional 175 μl medium were added to the cells. On plates used for CV staining, outer wells of plates were filled with 200 μl sterile

H_2O. 96-well plates and petridishes were sealed with parafilm and biofilms were grown at 30°C or 26°C for the indicated time. Media were supplied with appropriate antibiotics and/or IPTG or arabinose.

14.4.3 Attachment of planktonic cells

Cells were grown and harvested as described in section 14.4.1. OD_{600} of cells in Motility buffer was adjusted to 0.4 and differently labeled wild type and mutant cells (or wild type control) were mixed 1:1. 200 μl cells were seeded in 96-well plates from ibidi® (ibidi GmbH) and cells were allowed to attach to the surface of the well for the indicated time (2 min - 1 h). Unattached cells were removed by washing three times with Motility buffer. Attached cells were imaged in 200 μl Motility buffer and the number of attached cells was quantified as described in 14.5.4.

14.4.4 Centrifugation-enforced cell attachment

Both, cells of mixed cultures labeled with different fluorophores prepared as for biofilm experiments (see section 14.4.2) and 1:1 mixtures of cells from planktonic cultures, grown as described in section 14.4.1 were centrifuged on 96-well plates from ibidi® (ibidi GmbH) or BD Falcon^{TM} (Becton, Dickinson and Co.) for 2 min at 650 g. For centrifugation, OD_{600} of planktonic cells in motility buffer was adjusted to 0.1. After centrifugation, cells were either washed with tethering buffer (biofilm cells) or motility buffer (planktonic cells), and imaged directly. Alternatively, biofilm culture cells were washed with the respective medium and incubated for 24 h at 30°C in medium supplied with ampicillin and IPTG before being washed and imaged in tethering buffer.

14.4.5 Soft agar plates

To analyze swimming of cells in soft agar, 3 μl overnight culture grown in LB at 37°C were spotted on plates containing TB with 0.3 % agar. If required, soft agar was supplied with 100 μg/ml ampicillin and IPTG as indicated. Plates were incubated at 34°C for 6-8 h.

14.5 Quantification of biofilm growth and surface attachment

14.5.1 Crystal violet staining of biofilms

Biofilms were washed three times with 200 μl sterile H_2O and stained with 200 μl 1 % crystal violet (CV) for 20 min at RT. CV was removed and biofilms were washed sequentially with with 200 μl sterile H_2O until no further destaining was visible. Plates were dried ON at RT and CV was dissolved in 200 μl 96 % ethanol for 1 h at 150 rpm. Absorption was measured in a plate reader (Appliskan®, Thermo Scientific; Omega, BMG LABTECH; Tecan infinite® M1000 or Tecan infinite® M1000PRO, Tecan) at 600 nm. Blank values were obtained from wells with an empty medium control, which was treated the same way as the samples. Blank values were subtracted from the raw values of the

samples, which were then normalized to the wild-type control. For normalization of CV values to the OD_{600} of the biofilm culture, OD_{600} was measured before washing and staining with CV. Blank OD_{600} values were subtracted and $\frac{CV-blank}{OD_{600}-blank}$ were calculated.

14.5.2 Staining with wheat-germ agglutinin (WGA)

The protocol for biofilm staining with fluorescently labeled WGA was adapted from references [186, 187]. Biofilms grown in 96-well plates were washed three times with PBS. 200 μl WGA-Alexa488 conjugate (Molecular Probes; 5 μg/ml in PBS) were added to the attached cells and plates were incubated at 2 h and 4°C in darkness. Unbound dye was removed by pipetting and three times washing with PBS. Plates were air-dried for 15 min at RT and the probe was solubilized with 200 μl 33 % acetic acid. Plates were thoroughly sealed with parafilm and sonicated for 30 sec in a waterbath. Plates were incubated for 1 h at 37°C followed by a second 30 sec sonication step. 150 μl were transferred in a black glass bottom plate (Matrical Bioscience) and fluorescence was measured at Ex495/Em520 in a plate reader.

14.5.3 BacTiter Glo

Cell viability was assessed using the Promega BacTiter-Glo^{TM} Microbial Cell Viability Assay. With this assay, relative ATP content of cells is measured with a luminescent signal. BacTiter-Glo^{TM} buffer and substrate were thawed and equilibrated to RT. Buffer was mixed with substrate and vortexed gently to mix reagents homogeneously. Biofilms were grown in white 96-well plates (Greiner) and washed three times with PBS. 100 μl fresh growth medium and 100 μl BacTiterGlo solution were added. Plates were incubated shortly on an orbital shaker to mix the solutions and incubated at RT for 5 min in darkness. Luminescence was measured in a plate reader.

14.5.4 Quantification of attached cells by microscopy

Attachment to the surface of microscopy plates was quantified both for biofilms and for attachment experiments with planktonic cultures. For that, wild-type and mutant strains were labeled with two different fluorescence proteins and mixed 1:1. As a control, wild type cells with one label and wild type cells with the other label were used. Two different methods were applied for quantification: Quantification of cell numbers and quantification of the area covered by attached cells (see also Fig. 14.2).
For quantification of cell numbers, cells were identified in brightfield images using a self-written macro in ImageJ (http://imagej.nih.gov/ij/). Briefly, brightfield images were tranformed to 8-bit images, smoothed with a mean filter, and thresholded with Otsu's threshold clustering algorithm [188]. Cells were identified in the thresholded image with the Analyze particle-function using the following settings: $size = 30 - 170$ pixel $circularity = 0.40 - 1.00$. Selections were checked in the brightfield images and, if required, faulty structures were excluded from the analysis. ROIs (regions of interest, i. e. the segmented

cells) were overlaid on the fluorescence images and fluorescence intensities were measured. Additionally, background fluorescence in all channels was measured. Further analysis was performed in Microsoft® Excel® 2008 for Mac (version 12.3.6) and KaleidaGraph (version 4.0.3). Background fluorescence was subtracted and ratios of fluorescence intensities in the two channels corresponding to mutant (or wild type control) in channel 1 and the wild type in channel 2 were calculated. Based on the ratios, segmented cells could be assigned to either one of the channels: $\frac{channel1}{channel2}>1$ and $\frac{channel1}{channel2}<-1 \implies$ cell belongs to channel 1; $1>\frac{channel1}{channel2}>-1 \implies$ cell belongs to channel 2. Values >0 occur, when the background value of the selected ROI used for background measurement is below the mean fluorescence value of a segmented cell in that channel. Ratios of $\frac{mutant}{wildtype}$ were further normalized to the ratio of $\frac{wildtype}{wildtype}$, meaning that in the quantification, wild type corresponds to 1.

For quantification of the area covered by attached cells, a threshold was computed for fluorescence images. For that, either the Otsu's method for thresholding [188] or the Minimum white-method [189] were used. Cells were identified in the thresholded image with the Analyze particle-function using the following settings: $size = 0 - Infinity$ $circularity = 0.00 - 1.00$. In this way, all structures, including single cells and cell aggregates, were identified and their total area was measured. The selections were checked in the fluorescence images. Further analysis was performed in Microsoft® Excel® 2008 for Mac (version 12.3.6) and KaleidaGraph (version 4.0.3). Ratios of the area covered by cells to the total area of the image were calculated and area fractions of mutants to wild type were calculated. As above, $\frac{mutant}{wildtype}$ were further normalized to the ratio of $\frac{wildtype}{wildtype}$, meaning that in quantification, wild type corresponds to 1.

Exception: In figure 6.11, attached cells were identified and segmented in the fluorescence channels as described above, however, identification of single cells with the Analyze particle-function was performed with settings similar to the identification of cells in the brightfield image.

14.6 Measurements of swimming speeds and tracking

14.6.1 Tracking experiments

All tracking experiments were performed and analyzed by Remy Colin according to his protocol, as follows: Cells were grown as described in section 14.4.1 and harvested at OD_{600} of approx. 0.6 and 1.0 by centrifugation at 1,300 rcf for 5 min. Cells were resuspended in motility buffer and stored at 4°C for 20 min. Cell suspensions were diluted to OD_{600} of 0.02 and 0.005. A small droplet of 4 μl cell suspension was trapped between a slide and a coverslip sealed with grease in a way, that sufficient air was between the slide and the coverslip. Swimming bacteria were observed and recorded at the bottom surface of the sample, which is hydrophilic, using a phase contrast microscope at 10x magnification (NA 0.3) and a Mikrotron Eosens camera (1 px = 0.7 μm) running at 100 frames per seconds (fps) for 30 seconds. Tracking was done with the Mosaic analysis program [190] running as

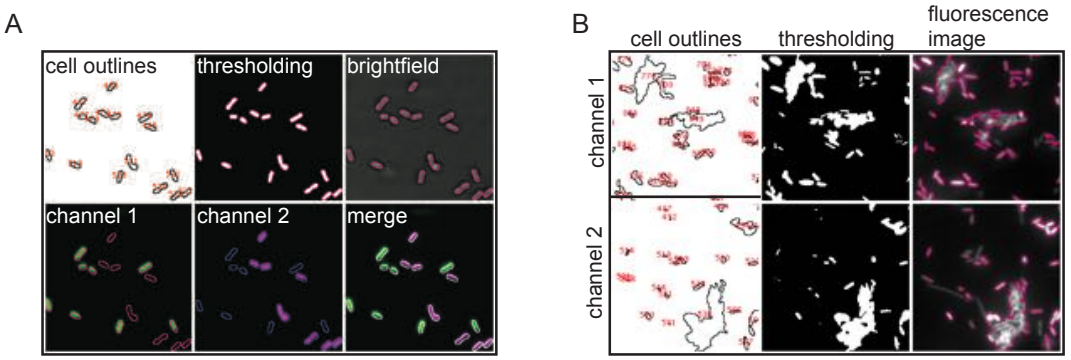

Fig. 14.2. Image analysis to quantify cell attachment:
(A) Exemplary images to demonstrate segmentation of single cells. Cells were identified in brightfield images and cell outlines were overlaid on fluorescence channels. Fluorescence intensities of selected cells were measured in each channel.
(B) Exemplary images demonstrating segmentation of cells and cell aggregates. Cells and aggregates were identified in each fluorescence channel and area of segmented objects was measured. Segmented areas were overlaid on fluorescence images.

an ImageJ plugin, trajectories were extracted and analyzed using custom-made algorithms running as ImageJ plugins, to evaluate tumbling rate, run speeds, trajectory duration and lengths.

14.7 Bacterial Two-Hybrid Assay

Bacterial two-hybrid assays were performed with the adenylate cyclase deficient *E. coli* strain BTH101 from the Euromedex bacterial two-hybrid (Bacterial Adenylate Cyclase-based Two-Hybrid, BACTH) system. The system is based on the reconstruction of the catalytic domain of adenylate cyclase (CyaA) from *Bordetella pertussis* consisting of two adenylate cyclase fragments (T18 and T25) [165, 166]. These fragments are fused to two proteins of interest. If the proteins interact, adenylate cyclase activity can be detected. If the two proteins do not interact, the T18 and T25 fragments are physically separated and adenylate cyclase activity cannot be reconstructed (see Figure 14.3). In case of positive interactions, cAMP is produced and binds to the catabolite gene activator protein (CAP). The cAMP-CAP complex leads to the transcription of cAMP-CAP-dependent genes, such as *lacZ* in *E. coli*. Therefore, β-Galactosidase expression is dependent on the interaction of the two proteins of interest and can be used as a reporter.
Plasmids pKT25-zip and pUT18C-zip, in which the leucine zipper of GCN4 is fused to the T25- and T18-fragments, were used as positive controls. To test the interactions between YjdA and YegE, YjdA and HflKC, YegE and HflKC, YjdA and YcgR, and YegE and FliF, the genes were cloned into pKT25, pKNT25, pUT18 and pUT18C vectors, respectively (pVM65-pVM79, for details see Appendix, table B.3 for plasmids). T25- and T18-plasmids were co-transformed into strain BTH101 and grown ON at 37°C on LB-plates containing 100 μg/ml ampicillin and 50 μg/ml kanamycin. Empty vectors were used as negative controls, pKT25-zip and pUT18C-zip as positive controls. Transformants were

restreaked on LB-plates containing 100 μg/ml ampicillin, 50 μg/ml kanamycin, 100 μg/ml streptomycin, 40 μg/ml X-Gal (5-bromo-4-chloro-3-indolyl-β-D-galacto-pyranoside) and 500 μM IPTG in a way, that 1 strain covered a quarter of an agar plate. After growth ON at 30°C, cells were scratched from agar plates and resuspended in 1 ml LB-medium. Cell suspensions were diluted to an OD of 0.1 and 10 μl were spotted on LB-plates containing 100 μg/ml ampicillin, 50 μg/ml kanamycin, 100 μg/ml streptomycin, 4 μg/ml X-Gal and 500 μM IPTG. Plates were incubated at 30°C and 26°C for 48h. Plates were imaged using a Nikon 5300d camera.

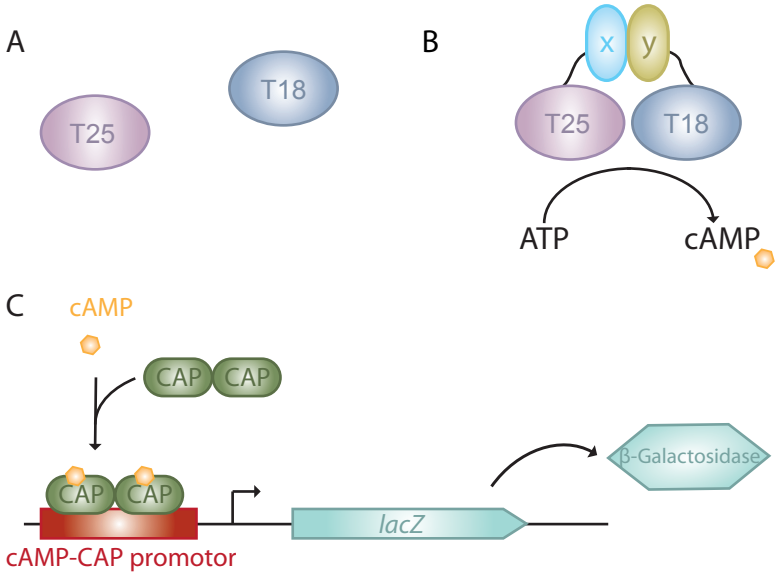

Fig. 14.3. Overview of the principle of the BACTH-assay:
(A) If the two domains T25 and T18 of the *Bordetella pertussis* adenylate cyclase CyaA are expressed as separate polypeptides in a *cya* deficient *E. coli* strain, no cAMP can be produced.
(B) If the T25 and T18 domains are fused to two interacting proteins x and y, CyaA activity is reconstructed and cAMP is produced.
(C) cAMP binds to the catabolite gene activator protein (CAP) and the cAMP-CAP complex binds to cAMP-CAP-dependent promoters. Amongst other genes, *lacZ* in *E. coli* is under the control of cAMP-CAP complex, which allows the use of β-Galactosidase activity as a readout for protein interactions.

14.8 Microscopy

14.8.1 Widefield microscopy

Widefield microscopy was used to investigate expression and localization of fluorescent fusion proteins, to monitor promoter activation, and to quantify surface attachment.
Widefield microscopy experiments were performed on a Zeiss Observer Z1 microscope equipped with an ORCA CCD camera (Hamamatsu) and 40x NA 0.75 and 100x NA 1.46 objectives, using mCherry (Ex572/25, Em645/90), GFP (Ex470/40, Em525/50), YFP (Ex500/25, Em535/30) and CFP (Ex436/25, Em480/40) filter sets. Images were taken with the AxioVision software. Alternatively, an IX81 microscope equipped with an EM-

CCD camera (Hamamatsu C9100), 20x (Olympus UPLSAPO NA 0.75) or 40x (Olympus UPLSAPO NA 0.95) objectives, and mCherry (Ex562/40, Em641/75), GFP (Ex474/23, Em525/45), YFP (Ex504/12, Em535/22) and CFP (Ex434/17, Em479/40) filters, or on an Olympus IX81 microscope equipped with an ORCA-R2 camera (Hamamatsu), a 40x (UPLSAPO NA 0.95) objective, and mCherry (Ex572/35, Em641/75) and GFP (Ex470/40, Em520/35) filters was used. For Olympus microscopes, the Xcellence rt software (Olympus) was used. Images were analyzed using ImageJ (http://imagej.nih.gov/ij/).

Quantification of expression levels of CFP fusions: Fluorescence microscopy was used to quantify expression levels of protein fusions to CFP. Briefly, cells were grown as described in section 14.4.1 until OD_{600} 0.6 and 1 ml culture was washed three times in tethering buffer and resuspended in 1 ml buffer. After 20 min in the fridge, 2-5 μl cells were imaged on a 1 % agar pad (prepared in tethering buffer) on a microscopy slide. A strain with known CFP levels at given induction (HCB33 with plasmid pDK2, [191]) was used as a positive control, the wild type strain as a negative control. To quantify expression levels, cells were segmented in the brightfield image as described in section 14.5.4. Masks were overlaid on fluorescence images and mean fluorescence of cells was measured. Following analyses were carried out in Microsoft® Excel® 2008 for Mac (version 12.3.6). Expression levels were chosen to have between 4000 and 9000 fusions per cell, if possible (see table 14.6). At least two biological replicates were used to determine induction conditions.

Tab. 14.6. Quantification of CFP-fusion expression levels

Plasmid	Strain	Fusion protein	Arabinose	Mean fusion number ± StDev
CFP-YjdA-pDK6	$W3110^{RH}$	CFP-YjdA	0.005 %	6287 ± 380
pVM15	$W3110^{RH}$	CFP-YjcZ	0.005 %	5385 ± 1370
pVM18	$W3110^{RH}$	YjcZ-CFP	0.001 %	4424 ± 823
pHL14	$W3110^{RH}$	MotA-CFP	0.001 %	8926 ± 480
pVM41	$W3110^{RH}$	YegE-CFP	0.01 %	8267 ± 1378

Imaging of planktonic cells: Planktonic cultures were grown as described in 14.4.1. 1 ml planktonic culture was washed three times in tethering buffer, resuspended in 1 ml buffer and 2-5 μl imaged on a 1 % agar pad (prepared in tethering buffer) on a microscopy slide.

Imaging of attached cells: Biofilms were grown in 96-well plates from BD Falcon^{TM} or ibidi® as described in section 14.4.2. Biofilms were washed three times in 200 μl tethering buffer and imaged in 200 μl fresh tethering buffer. Cells for attachment of planktonic cultures were prepared as described in 14.4.3.

Promotor activation assays: Biofilms were grown in 96-well plates from ibidi® as described in section 14.4.2. Biofilm supernatant cells were removed and washed in tethering buffer. SN cells were imaged on on a 1 % agar pad (prepared in tethering buffer) on a microscopy slide. Biofilms were washed three times in 200 μl tethering buffer and imaged in 200 μl fresh tethering buffer.

14.8.2 Confocal microscopy

Confocal microscopy was used to investigate the three-dimensional structure of static biofilms.
Biofilms for confocal imaging were grown as described in section 14.4.2 in 8-well slides from ibidi® for 48 h. Unwashed biofilm cultures were imaged directly. Confocal imaging was performed on a Zeiss LSM 780 confocal microscope using a C-Apochromat 40x/1.2 W Korr-UV-VIS-IR objective and the Zeiss ZEN2012 software. Biofilms labeled with GFP or mCherry were recorded as z-stacks with dimensions of x=142 μm, y=142 μm and z=80 μm using a 561 nm and a 488 nm laser and 493-556 and 578-696 filters. Images were analyzed using the Zeiss ZEN2010 software.

14.8.3 TIRF microscopy

TIRF (Total internal reflection fluorescence microscopy) was used to analyze the interactions between YegE, HflKC and YjdA in more detail.
For TIRF, cells were grown in planktonic cultures as described in section 14.4.1 and washed three times with tethering buffer. 2-5 μl cell suspension were imaged on a 1 % agar pad (prepared in tethering buffer) on a microscopy slide. TIRF imaging was performed on a Olympus IX81 inverted microscope equipped with an Olympus cellTIRF 4-Line Motorized TIRF Combiner, an Olympus XM10 camera, a Cell$*$ 488 nm/100 mW laser controlled by the Xcellence rt software (Olympus) and a 561 nm Lambda 1 100 mW laser controlled by Omicron Control Center, and a PLAPO 100x/1.45 Oil DIC objective using a TIRF Quadband filter. Images were acquired with the Xcellence rt software (Olympus) and analyzed using ImageJ (http://imagej.nih.gov/ij/). Bleaching during time-lapse movies was corrected with the Histogram matching method from the Bleach corrector-ImageJ plugin developed by Kota Miura from the EMBL, Heidelberg (http://cmci.embl.de/downloads/bleach_corrector).

14.8.4 FRET

Acceptor photobleaching Fluorescence resonance energy transfer (FRET) was used to investigate protein interactions (see figure 14.4).
Cells were grown as described in section 14.4.1 until OD_{600} 0.6 and 10 ml culture were washed and resuspended twice in 10 ml tethering buffer. After 20 min in the fridge, 1

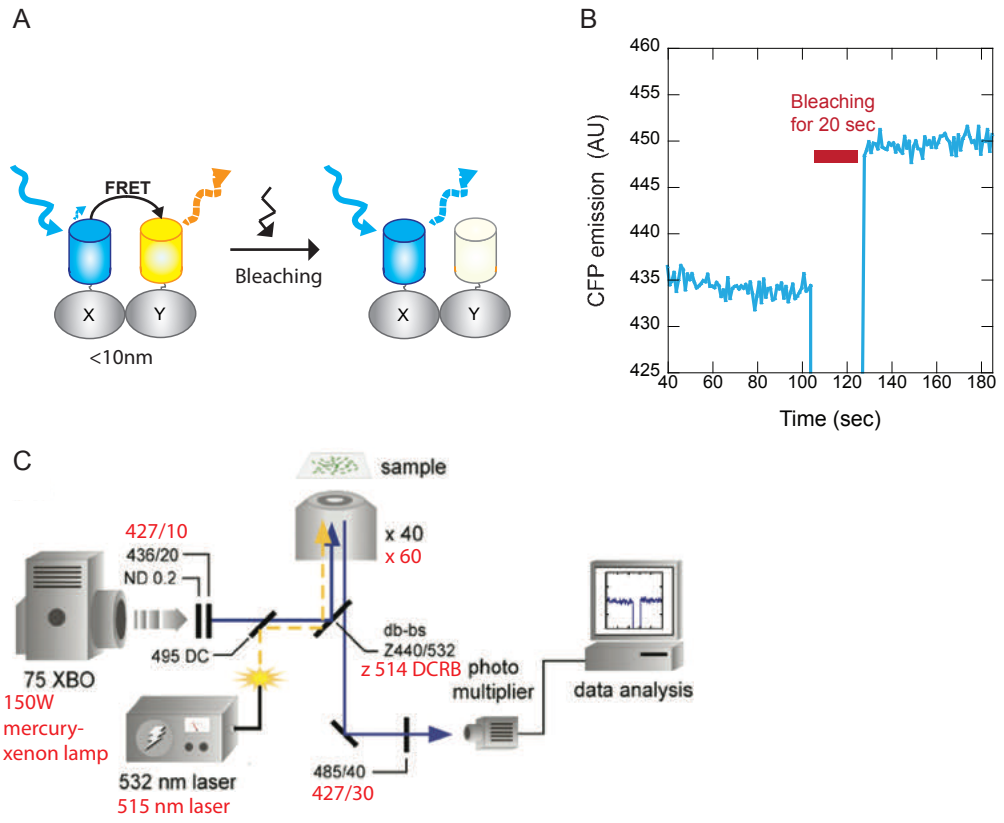

Fig. 14.4. Overview of acceptor photobleaching FRET:
(A) FRET occurs upon CFP excitation between CFP and YFP if the distance between the fusion proteins is <10 nm. In acceptor photobleaching FRET, the YFP is bleached with a laser, which leads to dequenching of the CFP resulting in an increase in CFP emission.
(B) Example of a typical FRET measurement showing CFP emission before and after bleaching of YFP.
(C) Set-up of the used microscope. In black, settings of the Zeiss Axiovert setup are shown, in red settings of the Olympus IX81 microscope (Image was adapted from [193]).

ml cell suspension was concentrated and applied on a thin 1 % agarose pad prepared in tethering buffer. FRET of a monolayer of cells was measured on a Zeiss Axiovert 200 microscope equipped with a 532 nm diode laser (Rapp OptoElectronic) and a H7421-40 photomultiplier (Hamamatsu) and on an Olympus IX81 microscope equipped with an with a 515 nm laser (Cobolt Fandango 100) and a two-photon counter (Hamamatsu) using the Xcellence rt software (Olympus) and LabView 7.1 (National Instruments) as described previously [192]. CFP emission was measured with 1 sec integration time before and after bleaching of YFP for 20 sec with a 515 nm or 532 nm laser and FRET efficiency was calculated as the increase in CFP signal divided by the CFP signal after bleaching (see equation 14.4).

14.9 FACS

Flow cytometry was used to quantify YFP expression levels of protein fusions to YFP or to monitor activity of promoters using GFP-reporters.

14.9.1 Quantification of expression levels of YFP fusions

YFP fluorescence of protein fusions was measured either on a FACScan (BD Biosciences) or on a BD FACS Canto® II equipped with a 488 nm laser. For FACS, strains with YFP-fusions were grown as described in section 14.4.1 until OD_{600} 0.6 and 1 ml culture was washed three times in tethering buffer and resuspended in 1 ml buffer. The cell suspension was incubated at 4°C for 20 min and diluted 1:20 in 2 ml tethering buffer. Fluorescence of 55,000 counts was measured on the FACScan using the CellQuestTM Pro 4.0.1 software (BD Biosciences) or 10,000 counts on the BD FACS Canto® II using the FACSDiva® Software. To quantify YFP levels, a strain with known fusion levels was used as a positive control (HCB33 with plasmid pVS18) and the wild type strain served as a negative control. For all plasmids, at least two independent biological replicates were used for quantification. Subsequently, inductions for microscopy were chosen in a way that the number of fusions per cell was approx. between 4000 and 9000 (see table 14.7).

Tab. 14.7. Quantification of YFP-fusion expression levels

Plasmid	Strain	Fusion protein	IPTG	Mean fusion number ± StDev
pVM13	W3110	YegE-YFP	1 μM	5975 ± 371
pVM13	W3110^{RH}	YegE-YFP	1 μM	4165 ± 247
YFP-YjdA-pDK4	W3110^{RH}	YFP-YjdA	15 μM	7093 ± 515
YjdA-YFP-pDK66	W3110^{RH}	YjdA-YFP	0 μM	9321 ± 1387
YjdA-YFP-pDK66	W3110^{RH} Δ*yjdA*	YjdA-YFP	0 μM	9263 ± 2656
pVM38	W3110^{RH} Δ*yjdA*	YjdA*T103D*-YFP	0 μM	7447 ± 1475
pVM39	W3110^{RH} Δ*yjdA*	YjdA*K72A*-YFP	0 μM	7093 ± 1113
YjcZ-YFP-pDK66	W3110^{RH}	YjcZ-YFP	15 μM	5505 ± 687
pHL55	W3110^{RH}	YFP-YcgR	20 μM	6539 ± 1520

14.9.2 Promotor activation assays

To quantify expression of biofilm matrix genes, promotor activity was measured using GFP reporters on the BD FACS Canto® II using the FACSDiva® Software. Planktonic cultures were grown as described in section 14.4.1 until OD_{600} 0.6, 1 or 2. Planktonic cultures were washed and samples were prepared as described above, except that cells at OD_{600} 1 and 2 were diluted 1:40 and 1:80. Biofilms were grown as described in 14.4.2 on ibidi® 96-well plates. Biofilm cells were collected (supernatant and attached cells) and

washed three times in Tethering buffer. After 20 min at 4°C, cells were diluted 1:20 and fluorescence was measured on the BD FACS Canto® II using the FACSDiva® Software.

14.10 Data analysis

All experiments were performed in at least two biological replicates. Mean values of replicates were calculated with Eq. 14.1.

$$\bar{x} = \frac{1}{n}\sum_{i=1}^{n} x_i \tag{14.1}$$

The differences between replicates were calculated with the standard deviation (see Eq. 14.2) or the standard error (see Eq. 14.3).

The standard deviation is defined as:

$$s = \sqrt{s^2} = \sqrt{\frac{1}{n-1}\sum_{i=1}^{n}(x_i - \bar{x})^2} \tag{14.2}$$

The standard error is defined as:

$$s_{\bar{x}} = \frac{s}{\sqrt{n}} \tag{14.3}$$

FRET efficiency in acceptor photobleaching experiments was calculated as follows:

$$E_{FRET} = \frac{\Delta C}{C_0} \tag{14.4}$$

with ΔC being defined as

$$\Delta C = C_0 - C \tag{14.5}$$

with C_0 being the CFP signal after bleaching (=CFP without FRET) and C the CFP signal before bleaching. For more detail about FRET efficiencies see reference [194].

APPENDIX

A. SUPPLEMENTARY DATA

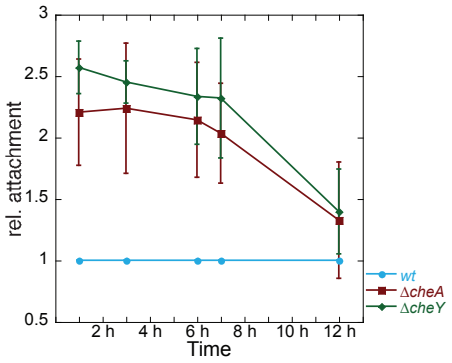

Fig. A.1. Smooth swimming promotes early biofilm formation:
Early biofilm formation of mixed cultures of W3110 wild type, Δ*cheA* and Δ*cheY* on ibidi imaging plates. Wild type cells were mixed with wild type or mutant cells 1:1 and mixed biofilm cultures were grown in M9 at 30°C for the indicated time. Non-attached cells were removed and attached cells were imaged. Experiment is the same as in figure 6.6 C, but attached cells were quantified as in figure 6.9 E.

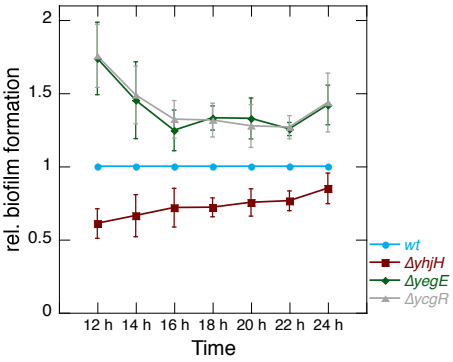

Fig. A.2. Motility regulation by c-di-GMP alters biofilm formation in W3110:
Early biofilm formation of W3110 wild type, Δ*yhjH*, Δ*yegE* and Δ*ycgR* in M9 medium at 30°C. Biofilms were formed on 96-well Corning® Costar®plates and stained with crystal violet (CV). CV was normalized to the OD_{600} of the culture before washing and CV/OD ratios were further normalized to the CV/OD of the wild type. Experiment is the same as in figure 6.9 C.

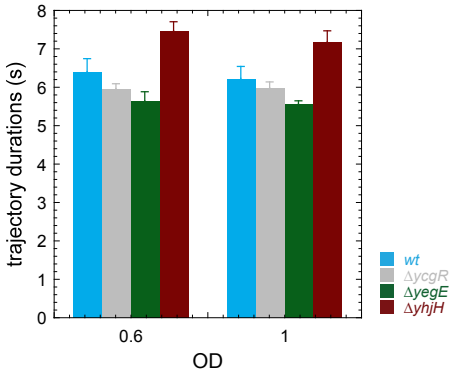

Fig. A.3. Swimming behavior of planktonic W3110 cells with defects in c-di-GMP signaling:
Trajectory duration of W3110 wild-type, Δ*ycgR*, Δ*yegE* and Δ*yhjH* grown in planktonic culture until OD_{600} 0.6 and 1. Shown are mean and standard error of three replicates. Experiment was performed by Dr. Remy Colin.

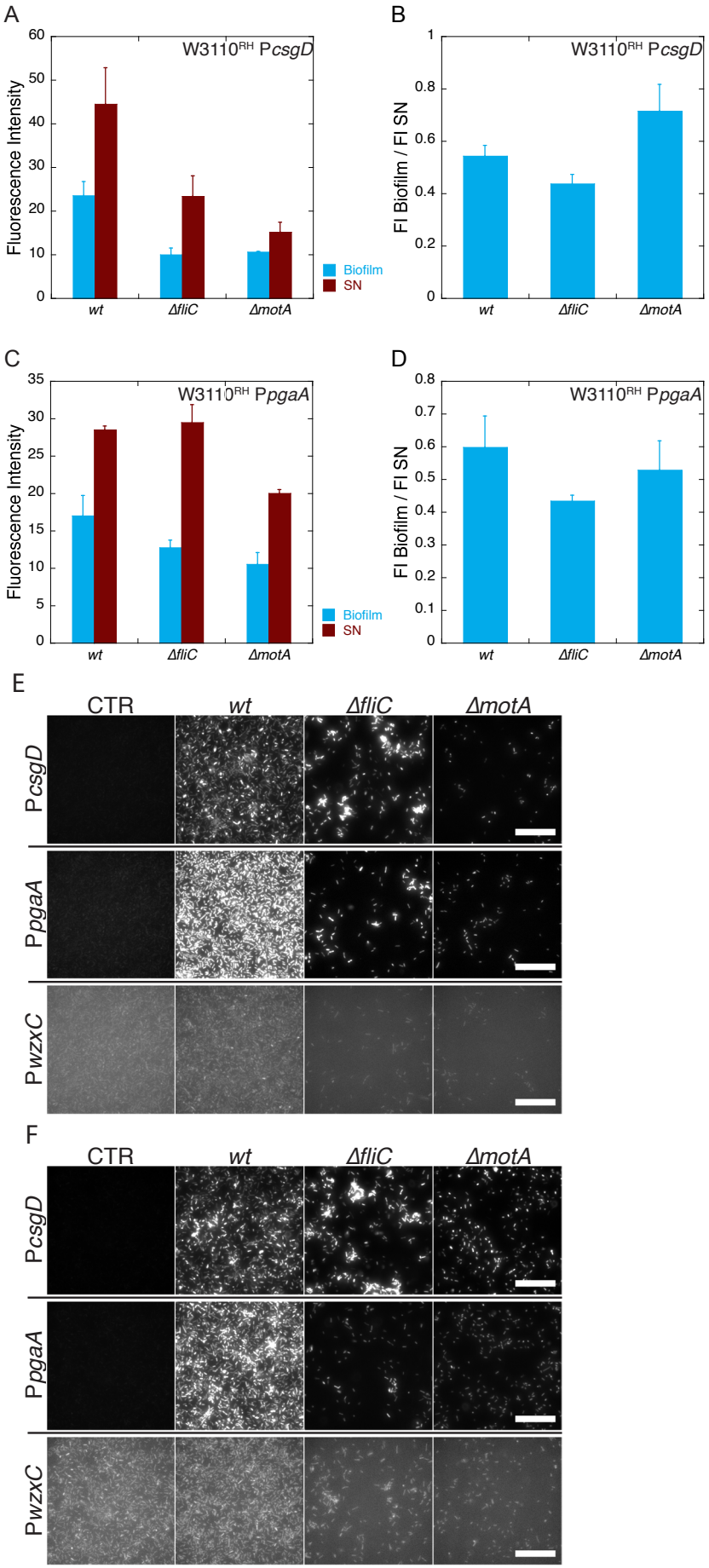

Fig. A.4. In W3110^{RH} early biofilm formation, surface sensing of flagella does not seem to play a role:

(*Continued on the following page.*)

Fig. A.4. (*Continued from previous page.*)
GFP-Reporter activity was quantified in 7 h old biofilms of W3110^{RH} grown in TB medium at 30°C on ibidi imaging plates. Fluorescence intensity (FI) was quantified in attached (biofilm) and supernatant (SN) cells.
(A-B) Activity of the *csgD* promoter expressed from plasmid pVM49. Shown are mean and standard error of three replicates.
(C-D) Activity of the *pgaA* promoter expressed from plasmid pVM53. Shown are mean and standard error of three replicates.
(E-F) Activity of the *csgD*, *pgaA* and *wzxC* (expressed from plasmid pVM55) promoters in 24 h (E) and 48 h (F) old biofilms. Unattached biofilm cells were removed and attached cells were imaged. Control: empty reporter plasmid.

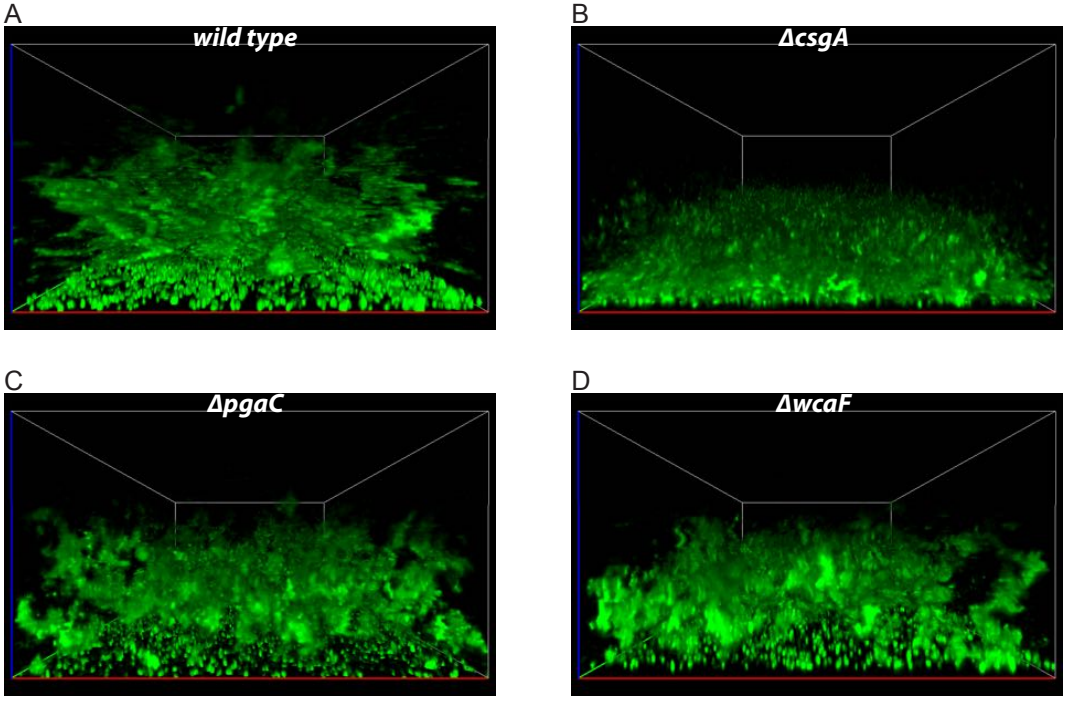

Fig. A.5. Curli is the main structural part of the W3110^{RH} biofilm matrix (additional replicates):
Confocal images of 48 h old biofilms of W3110^{RH} wild type (A), Δ*csgA* (B), Δ*pgaC* (C) and Δ*wcaF* (D). Images of additional biological replicates to replicates in figure 7.2 are shown. Dimensions of bounding box (x:y:z): 142:142:80 μm.

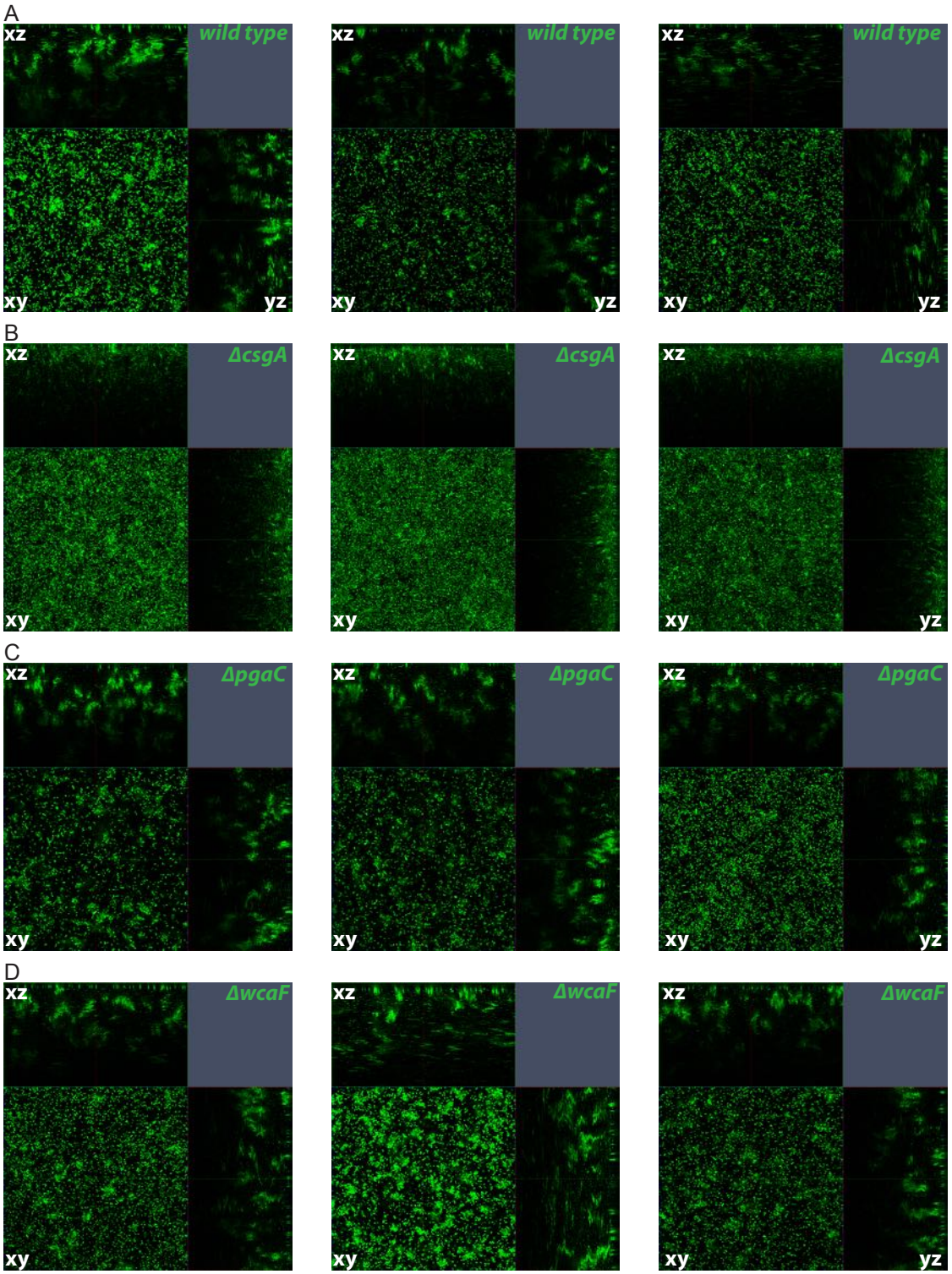

Fig. A.6. Curli is the main structural part of the W3110^{RH} biofilm matrix (orthogonal views):
Confocal images of 48 h old biofilms of W3110^{RH} wild type (A), Δ*csgA* (B), Δ*pgaC* (C) and Δ*wcaF* (D). Orthogonal views of images shown in figures 7.2 and A.5 are shown. Dimensions (x:y:z): 142:142:80 μm.

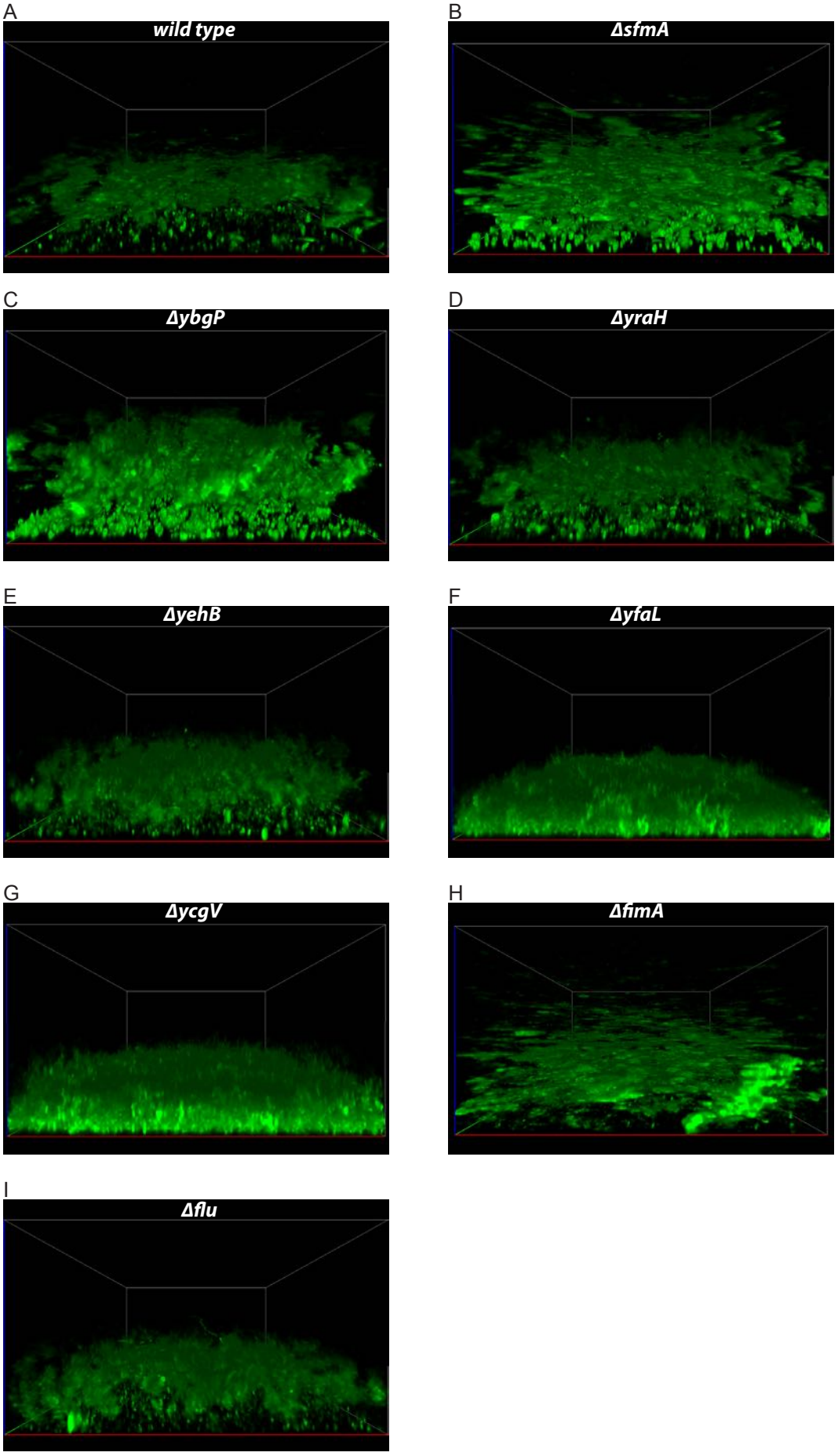

Fig. A.7. Role of *E. coli* adhesins in three-dimensional structure formation (additional replicates):
(*Continued on the following page.*)

Fig. A.7. (*Continued from previous page.*)
Confocal images of 48 h old biofilms of W3110^{RH} wild type (A), Δ*sfmA* (B), Δ*ybgP* (C), Δ*yraH* (D), Δ*yehB* (E), Δ*yfaL* (F), Δ*ycgV* (G), Δ*fimA* (H) and Δ*flu* (I). Images of additional biological replicates to replicates in figure 7.3 are shown. Dimensions of bounding box (x:y:z): 142:142:80 μm.

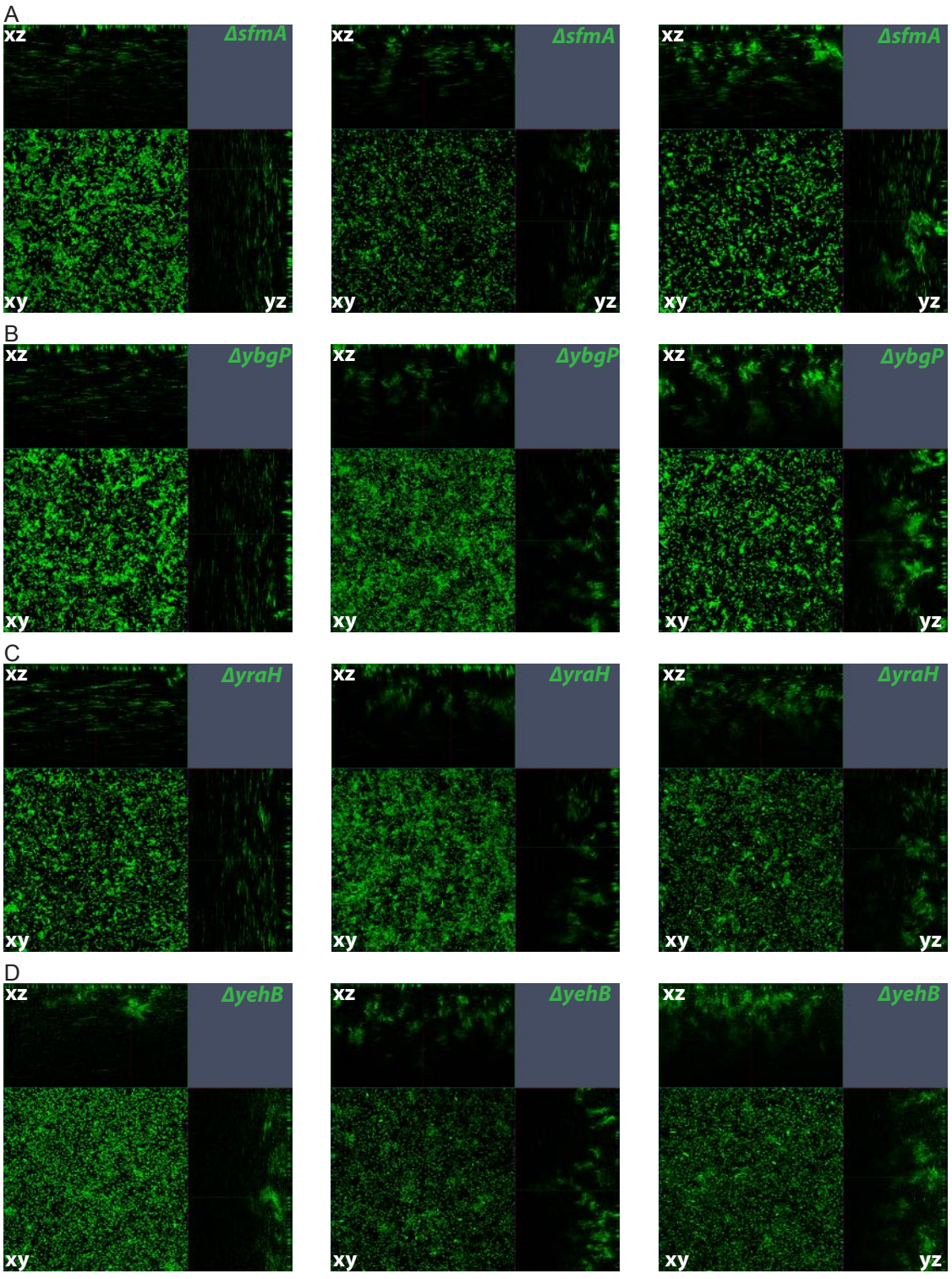

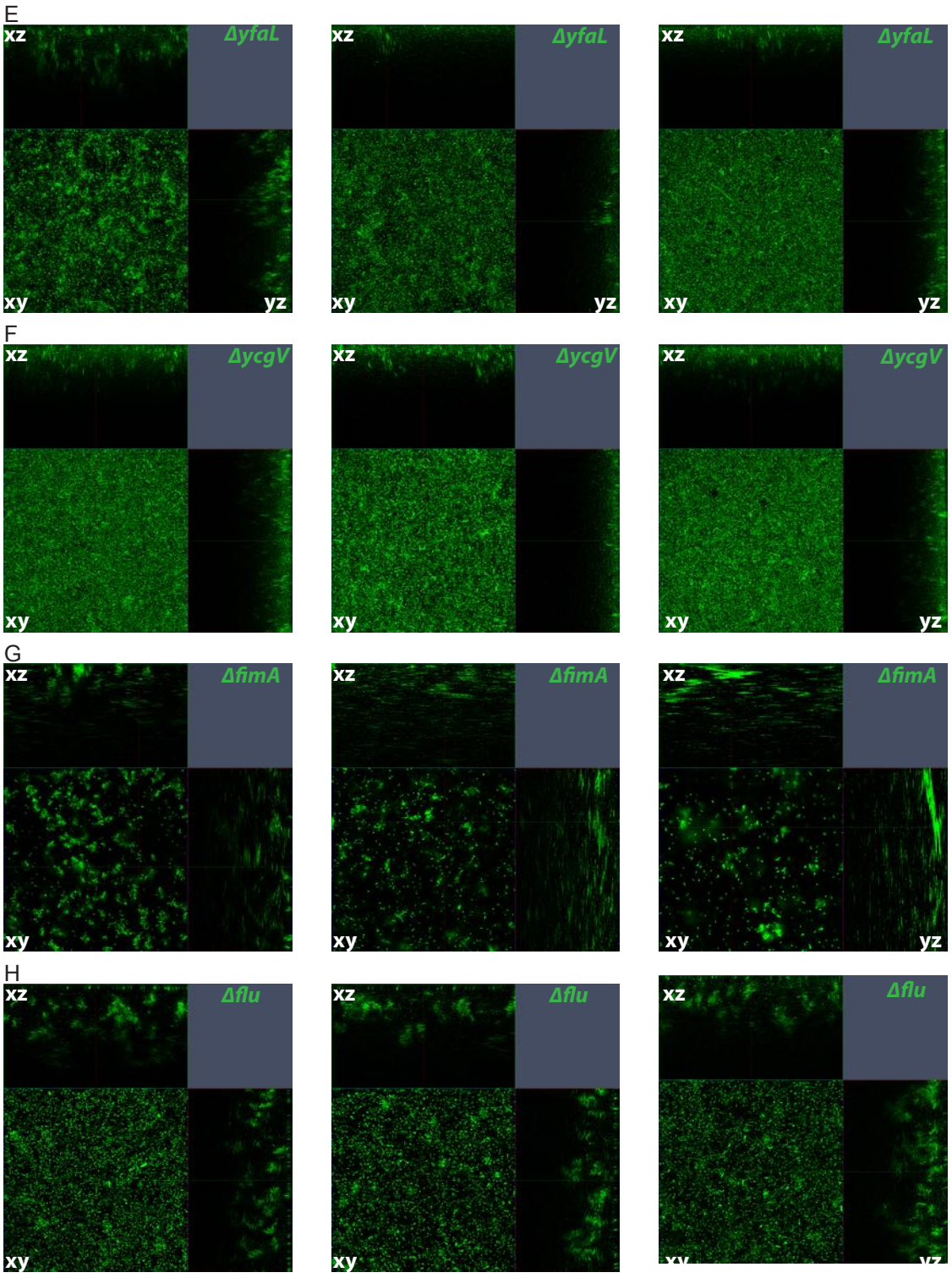

Fig. A.8. Role of *E. coli* adhesins in three-dimensional structure formation (orthogonal views):
Confocal images of 48 h old biofilms of W3110^{RH} Δ*sfmA* (A), Δ*ybgP* (B), Δ*yraH* (C), Δ*yehB* (D), Δ*yfaL* (E), Δ*ycgV* (F), Δ*fimA* (G) and Δ*flu* (H). Orthogonal views of images shown in figures 7.3 and A.7 are shown. Dimensions (x:y:z): 142:142:80 μm. Images of additional biological replicates to replicates in figure 7.3 are shown. Dimensions of bounding box (x:y:z): 142:142:80 μm.

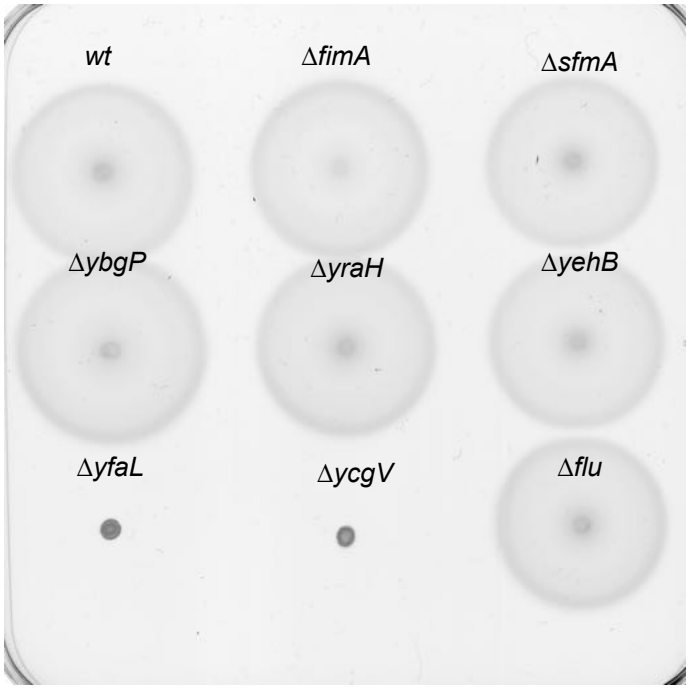

Fig. A.9. Motility of *E. coli* adhesins knockouts:
Swimming of the *E. coli* adhesins knockouts Δ*fimA*, Δ*sfmA*, Δ*ybgP*, Δ*yraH*, Δ*yehB*, Δ*yfaL*, Δ*ycgV* and Δ*flu* on soft agar plates.

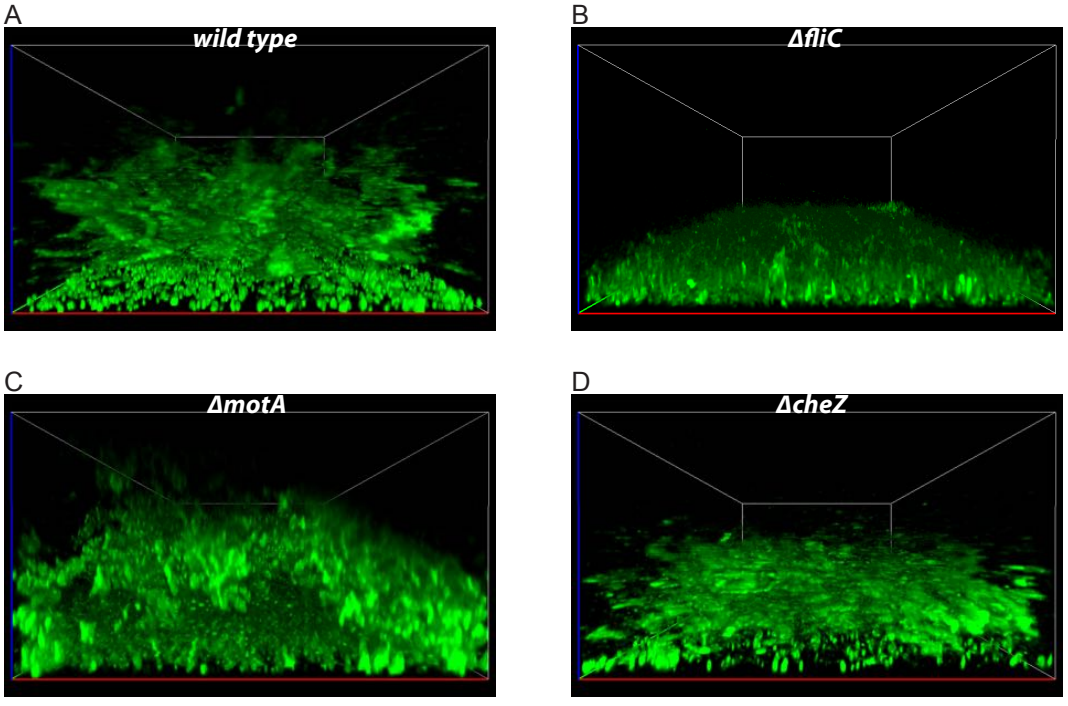

Fig. A.10. Role of motility in three-dimensional structure formation (additional replicates):
Confocal images of 48 h old biofilms of W3110^{RH} wild type (A), Δ*fliC* (B), Δ*motA* (C) and Δ*cheZ* (D). Images of additional biological replicates to replicates in figure 7.4 are shown. Dimensions of bounding box (x:y:z): 142:142:80 μm.

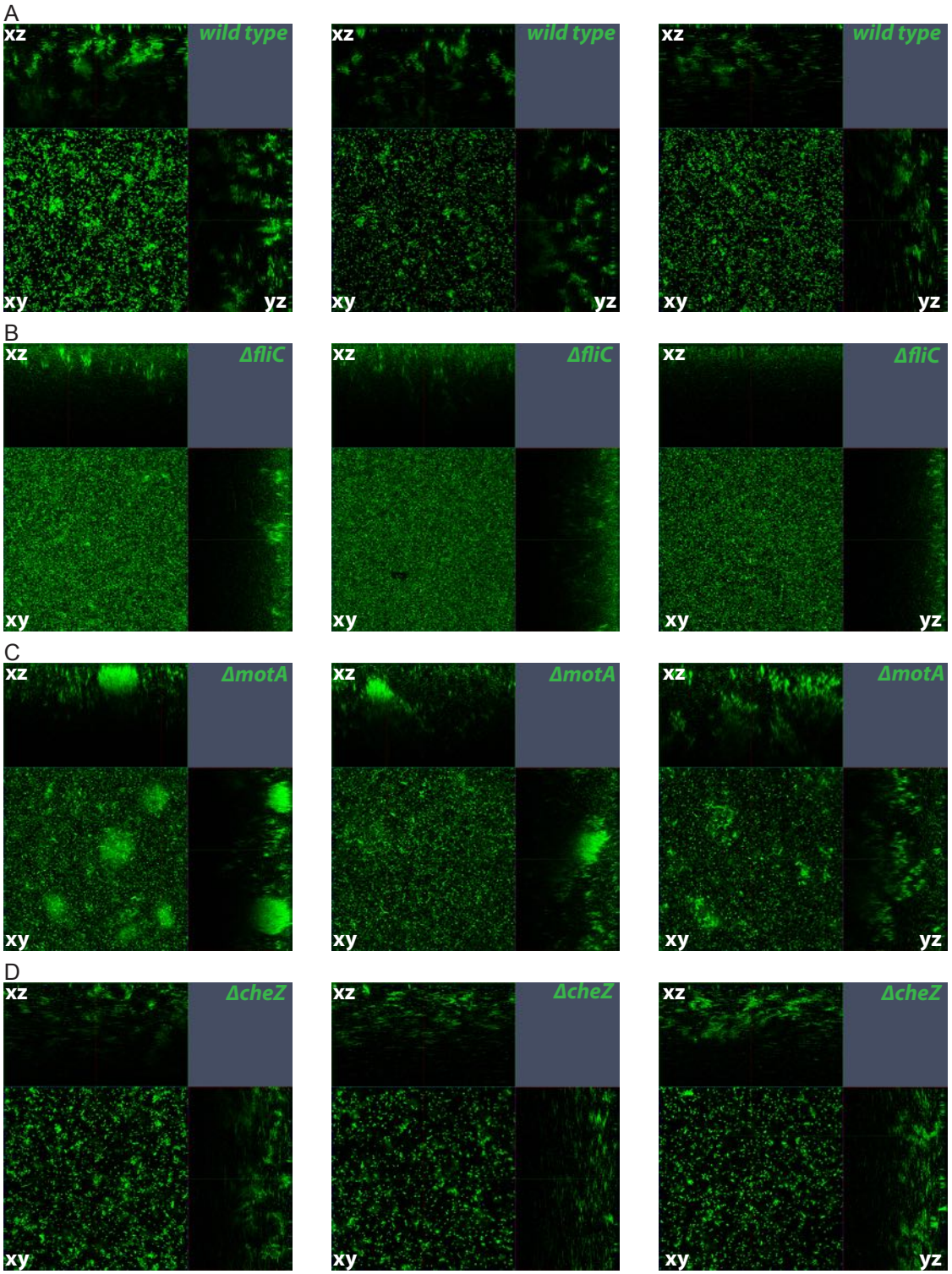

Fig. A.11. Role of motility in three-dimensional structure formation (orthogonal views):
Confocal images of 48 h old biofilms of W3110^{RH} wild type (A), Δ*fliC* (B), Δ*motA* (C) and Δ*cheZ* (D). Orthogonal views of images shown in figures 7.4 and A.10 are shown. Dimensions (x:y:z): 142:142:80 μm.

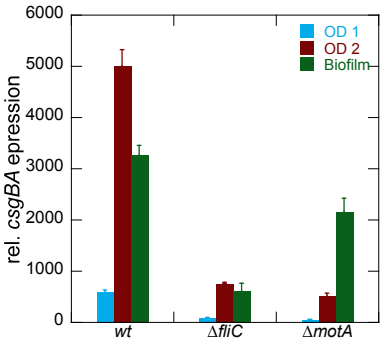

Fig. A.12. Curli expression levels change in W3110^{RH} Δ*fliC* and Δ*motA*:
Relative Curli expression was determined with a genomic *csgBA::STOP::sfgfp*-reporter using flow cytometry. Cells were either grown in planktonic cultures to OD_{600} 1 and 2 or in biofilm cultures for 48 h. Fluorescence was measured in tethering buffer. For biofilms, both surface-attached and unattached cells were measured. Shown are mean and standard error of two (planktonic cultures) and four (biofilm) biological replicates.

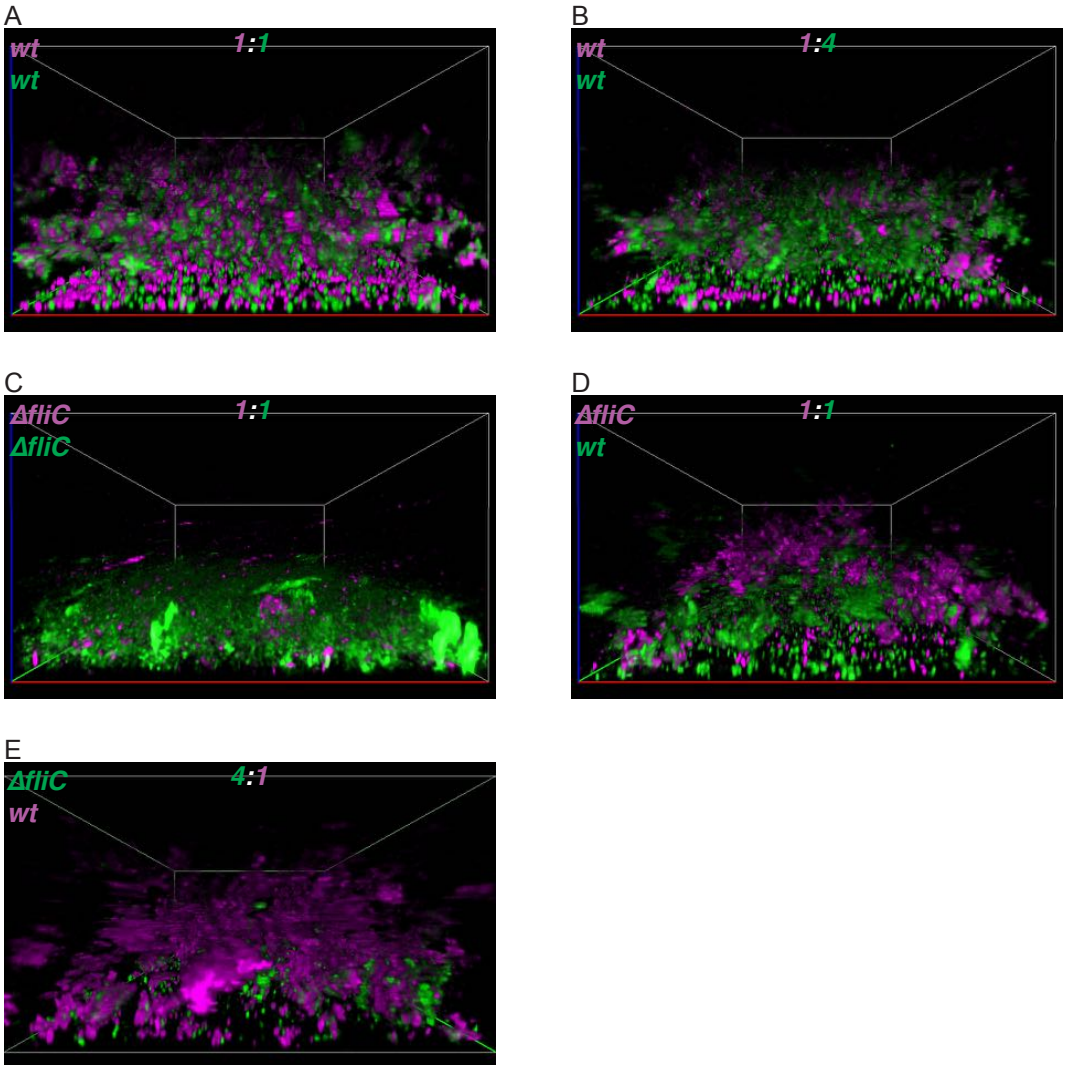

Fig. A.13. Flagella-less cells can partially integrate into three-dimensional structures of W3110^{RH} wild type (additional replicates):
Confocal images of 48 h old biofilms of different mixtures of W3110^{RH} wild type and Δ*fliC*. Wild type and Δ*fliC* cells labeled with different fluorescent proteins were mixed as indicated and biofilms of mixed cultures were grown. Additional replicates to the images shown in figure 7.5 are shown. For (B), only a technical replicate is shown.
(A) Wild type cells labeled with mCherry (magenta) and GFP (green) were mixed 1:1.
(B) Wild type cells labeled with mCherry (magenta) and GFP (green) were mixed 1:4.
(C) Δ*fliC* cells labeled with mCherry (magenta) and GFP (green) were mixed 1:1.
(D) Δ*fliC* cells labeled with mCherry (magenta) and wild type cells labeled with GFP (green) were mixed 1:1.
(E) Δ*fliC* cells labeled with GFP (green) and wild type cells labeled with mCherry (magenta) were mixed 4:1.
Dimensions of bounding box (x:y:z): 142:142:80 μm.

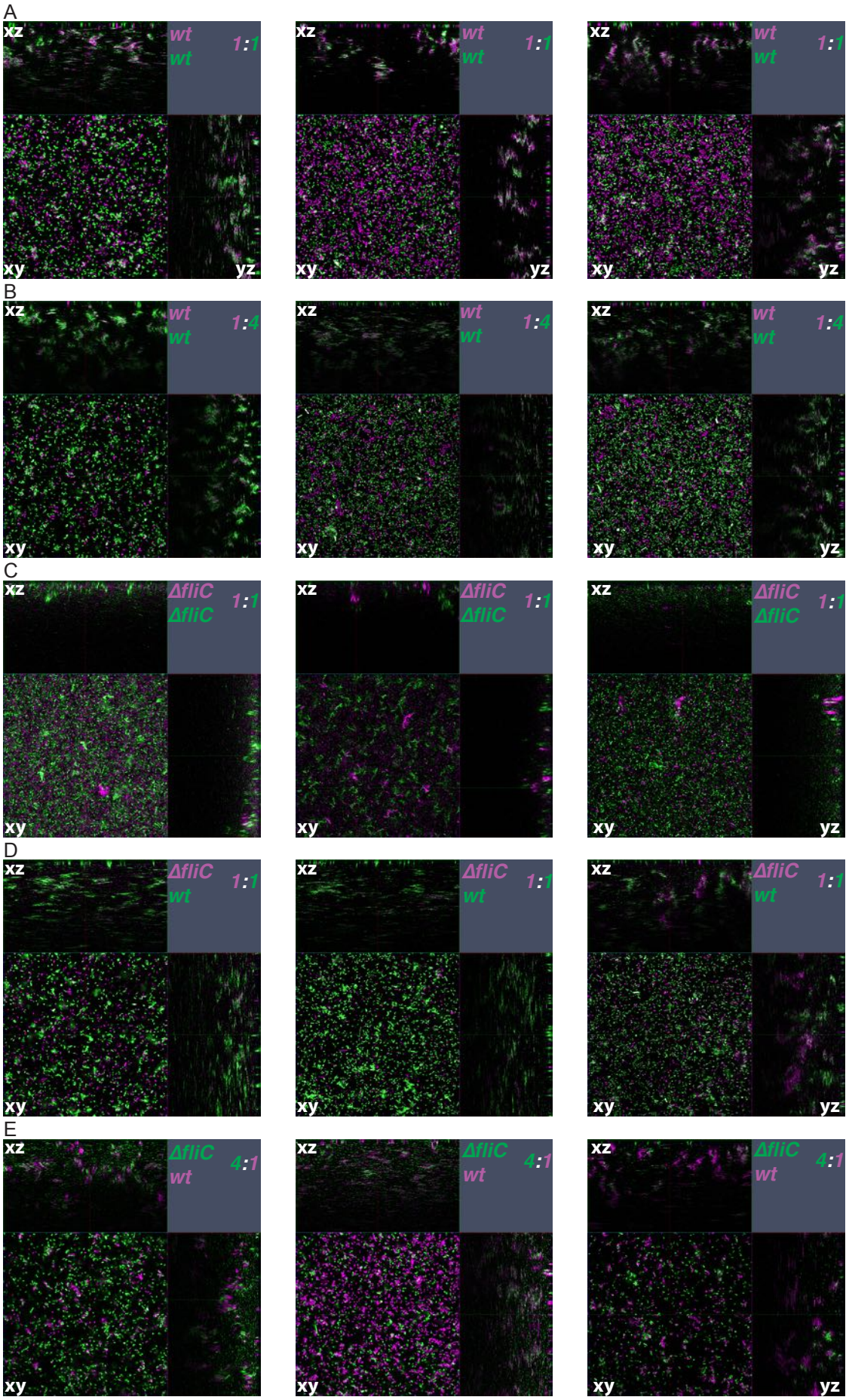

Fig. A.14. Flagella-less cells can partially integrate into three-dimensional structures of W3110^{RH} wild type (orthogonal views):
(*Continued on the following page.*)

Fig. A.14. (*Continued from previous page.*)
Confocal images of 48 h old biofilms of different mixtures of W3110^{RH} wild type and Δ*fliC*. Wild type and Δ*fliC* cells labeled with different fluorescent proteins were mixed as indicated and biofilms of mixed cultures were grown. Orthogonal views of images shown in figures 7.5 and A.13 are shown.
(A) Wild type cells labeled with mCherry (magenta) and GFP (green) were mixed 1:1.
(B) Wild type cells labeled with mCherry (magenta) and GFP (green) were mixed 1:4.
(C) Δ*fliC* cells labeled with mCherry (magenta) and GFP (green) were mixed 1:1.
(D) Δ*fliC* cells labeled with mCherry (magenta) and wild type cells labeled with GFP (green) were mixed 1:1.
(E) Δ*fliC* cells labeled with GFP (green) and wild type cells labeled with mCherry (magenta) were mixed 4:1.
Dimensions (x:y:z): 142:142:80 μm.

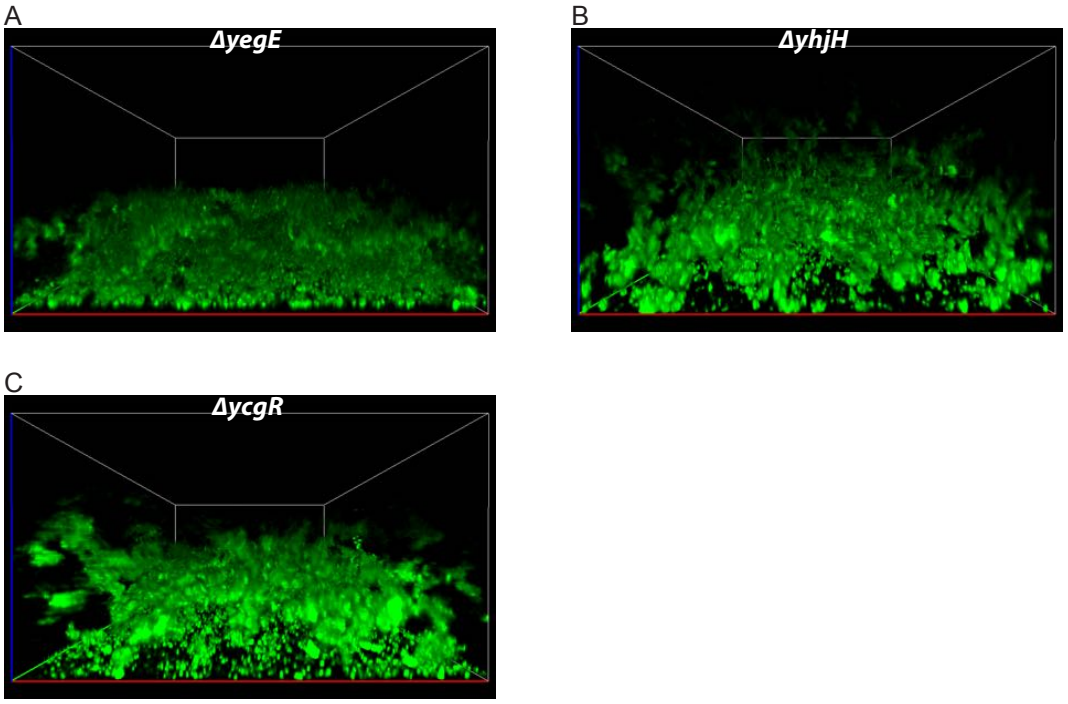

Fig. A.15. Role of c-di-GMP in three-dimensional structure formation (additional replicates):
Confocal images of 48 h old biofilms of W3110^{RH} Δ*yegE* (A), Δ*yhjH* (B) and Δ*ycgR* (C). Additional replicates to images in figure 7.6 are shown. Dimensions of bounding box (x:y:z): 142:142:80 μm.

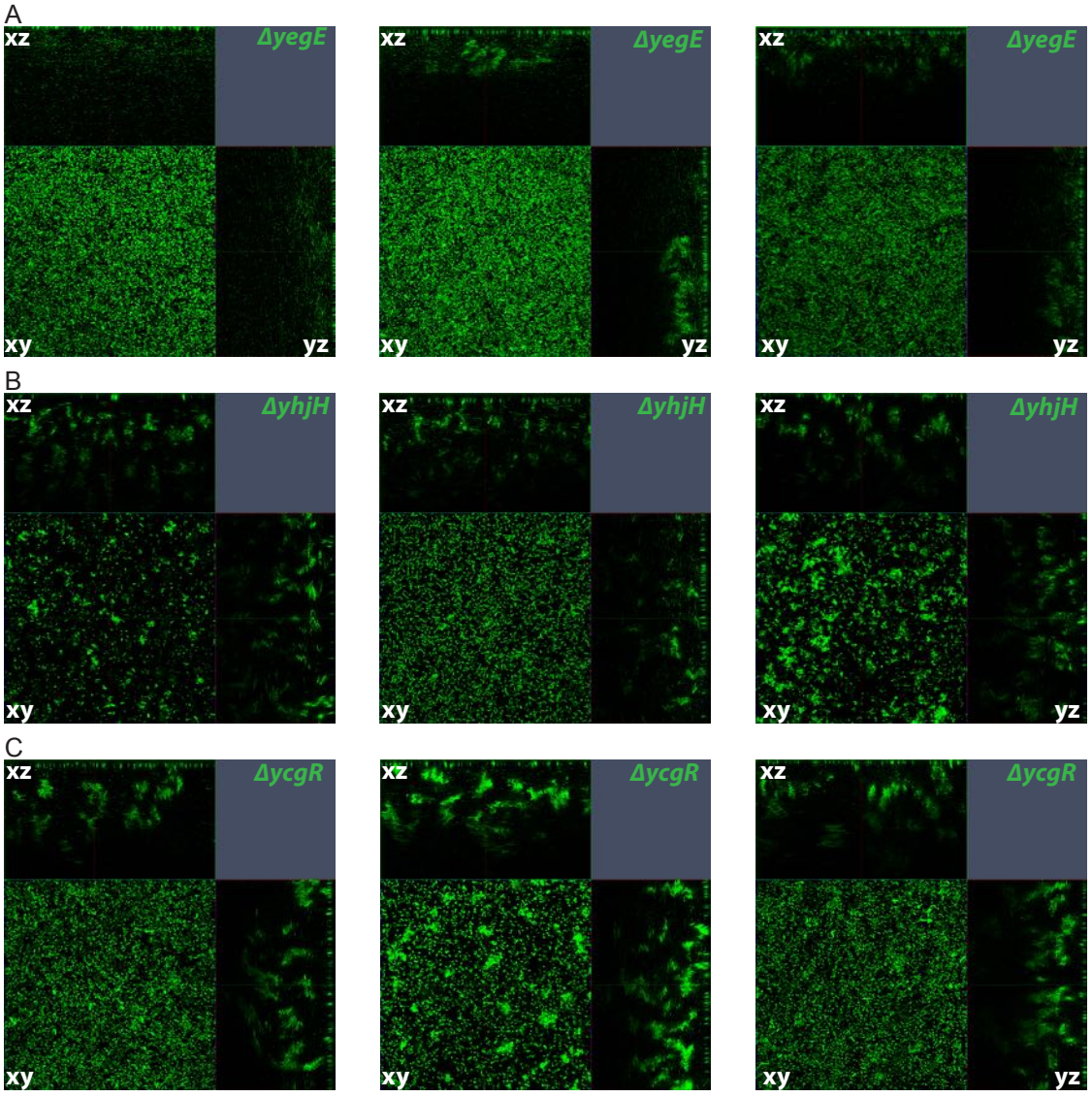

Fig. A.16. Role of c-di-GMP in three-dimensional structure formation (orthogonal views):
Confocal images of 48 h old biofilms of W3110^{RH} $\Delta yegE$ (A), $\Delta yhjH$ (B) and $\Delta ycgR$ (C). Orthogonal views of images shown in figures 7.6 and A.15 are shown. Dimensions (x:y:z): 142:142:80 μm.

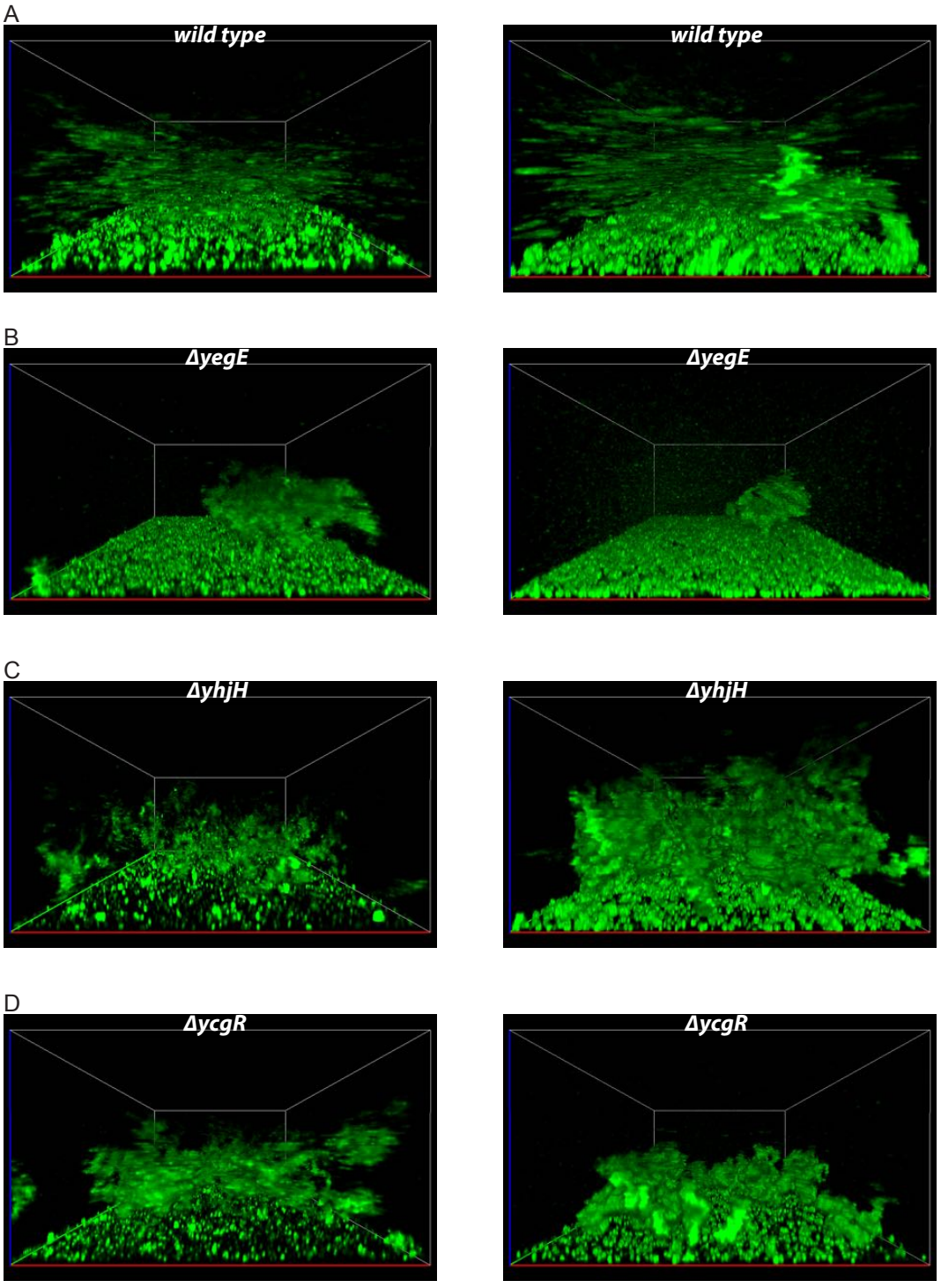

Fig. A.17. Role of c-di-GMP in three-dimensional structure formation (24 h): Confocal images of 24 h old biofilms of W3110^{RH} wild type (A), Δ*yegE* (B), Δ*yhjH* (C) and Δ*ycgR* (D). Images of two biological replicates are shown. Dimensions of bounding box (x:y:z): 142:142:80 μm.

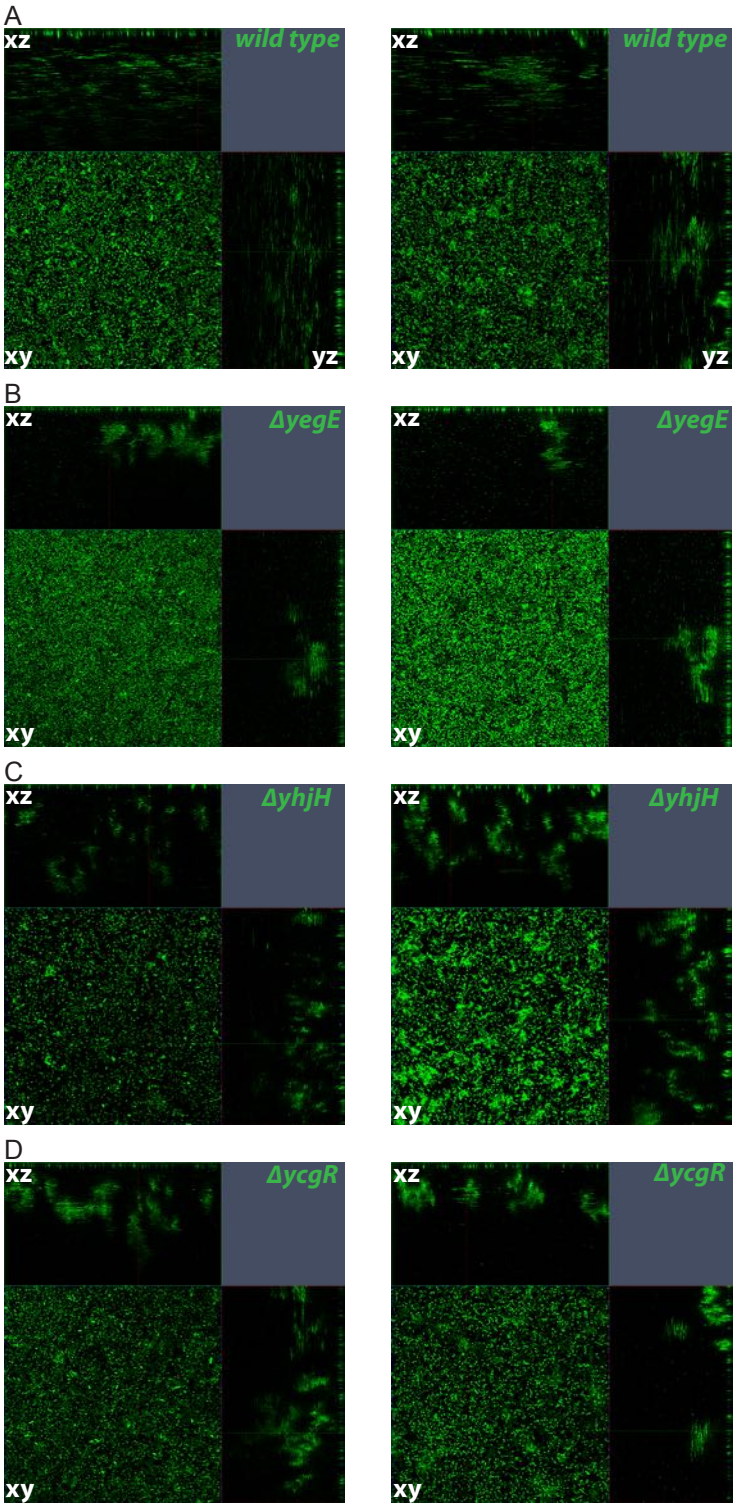

Fig. A.18. Role of c-di-GMP in three-dimensional structure formation (24 h, orthogonal views):
Confocal images of 24 h old biofilms of W3110^{RH} wild type (A), Δ*yegE* (B), Δ*yhjH* (C) and Δ*ycgR* (D). Orthogonal views of images shown in figure A.17 are shown. Dimensions (x:y:z): 142:142:80 μm.

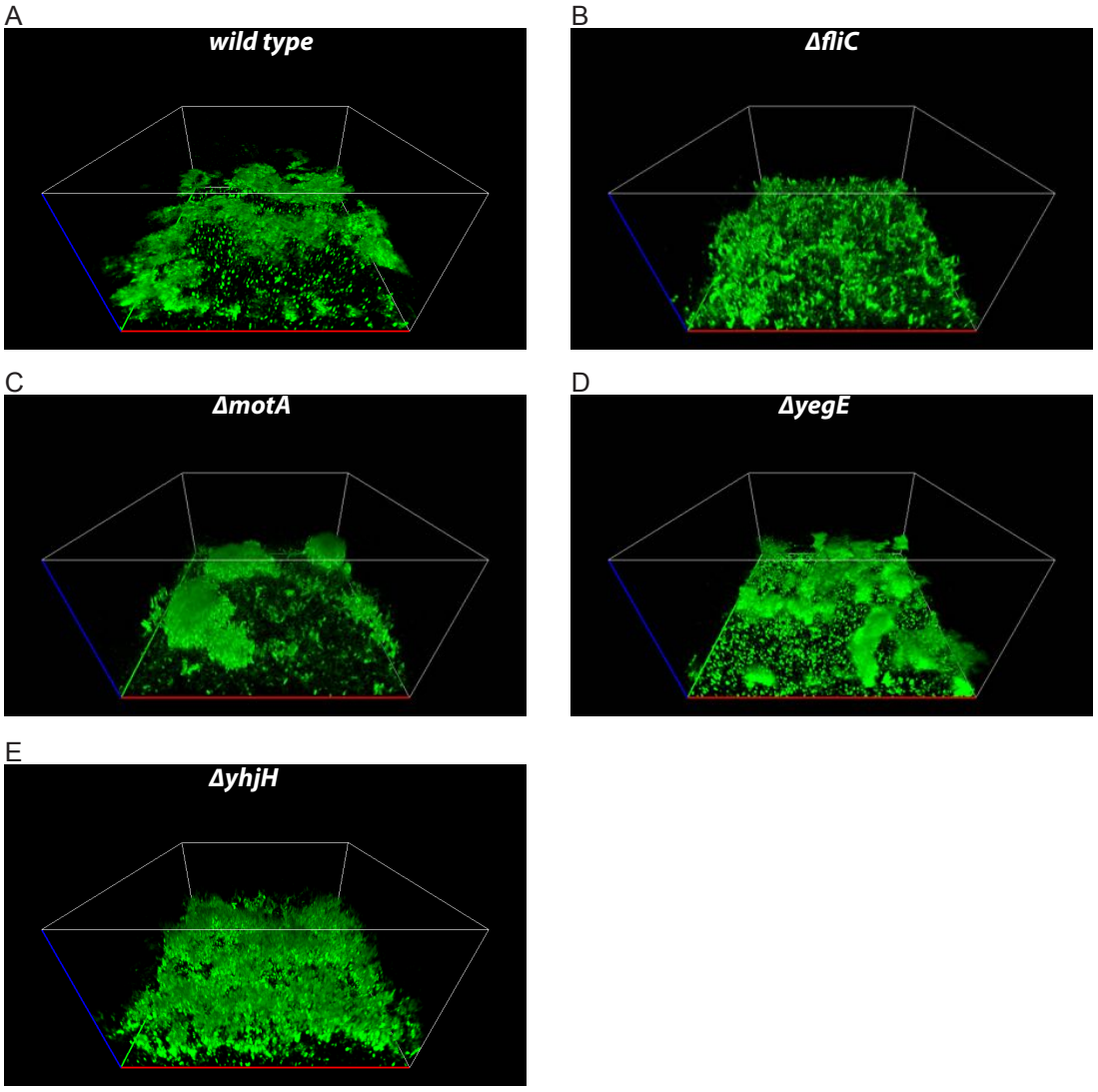

Fig. A.19. Role of motility and c-di-GMP in AR3110 three-dimensional structure formation (additional replicates):
Confocal images of 48 h old biofilms of AR3110 wild type (A), Δ*fliC* (B), Δ*motA* (C), Δ*yegE* (D) and Δ*yhjH* (E). Additional replicates to the images shown in figure 7.7 are shown. Dimensions of bounding box (x:y:z): 142:142:80 μm.

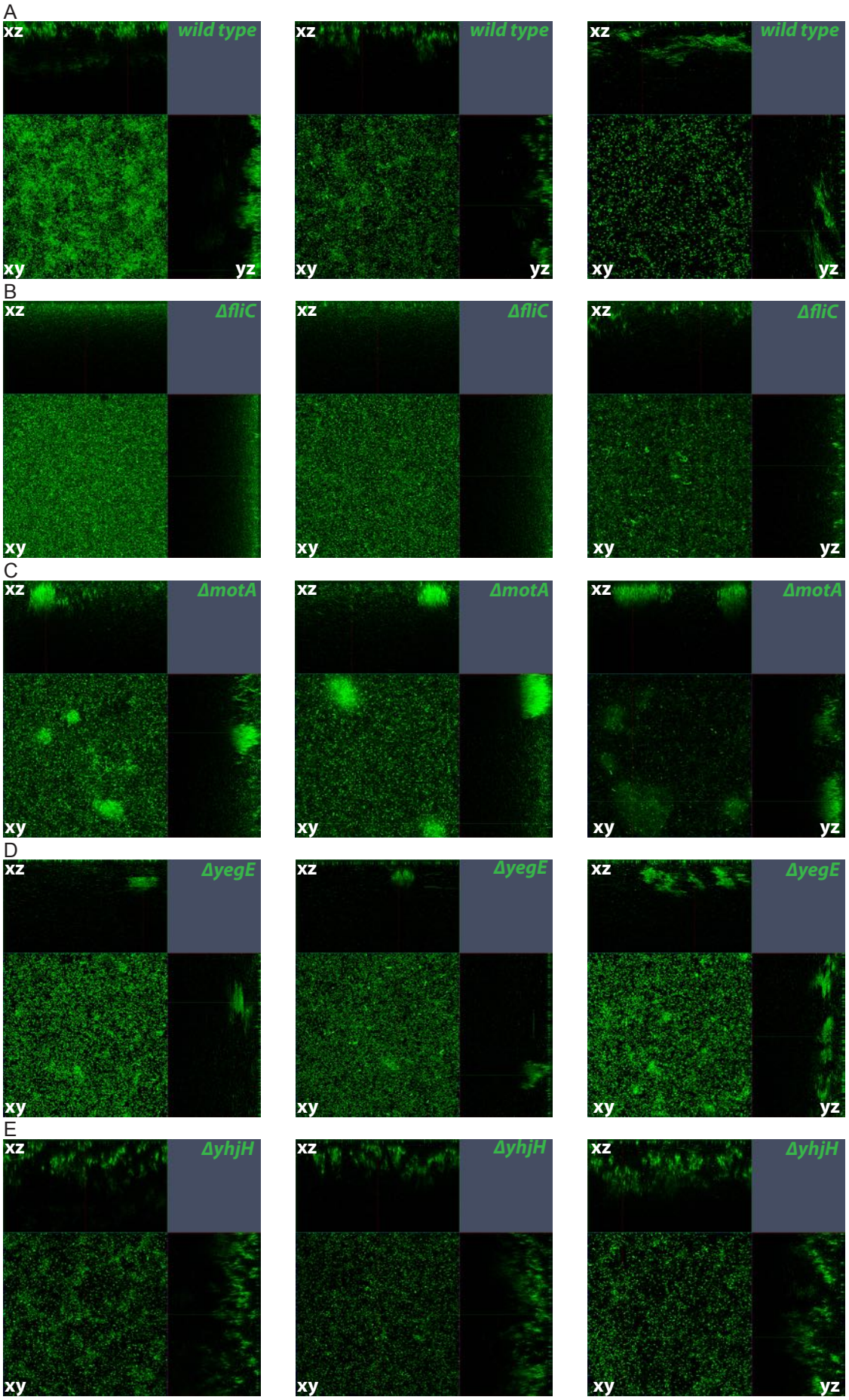

Fig. A.20. Role of motility and c-di-GMP in AR3110 three-dimensional structure formation (orthogonal views):
(*Continued on the following page.*)

Fig. A.20. (*Continued from previous page.*)
Confocal images of 48 h old biofilms of AR3110 wild type (A), Δ*fliC* (B), Δ*motA* (C), Δ*yegE* (D) and Δ*yhjH* (E). Orthogonal views of images shown in figures 7.7 and A.19 are shown. Dimensions (x:y:z): 142:142:80 μm.

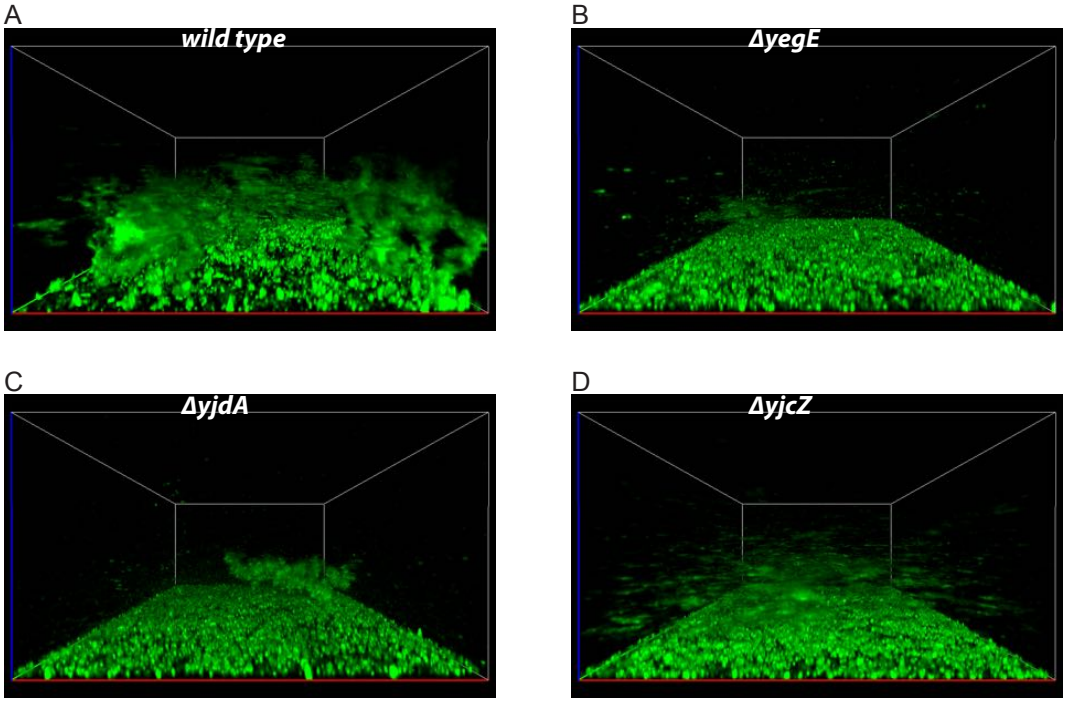

Fig. A.21. YjdA and YjcZ affect 3D-structure formation in static W3110^{RH} biofilms similarly to YegE (additional replicates):
Confocal images of an additional biological replicate to the images in figure 8.3. Static submerged biofilms of W3110^{RH} cells labeled with GFP were grown for 24 h.
(A) wild type, (B) Δ*yegE*, (C) Δ*yjdA*, (D) Δ*yjcZ*. Dimensions of bounding box (x:y:z): 142:142:80 μm.

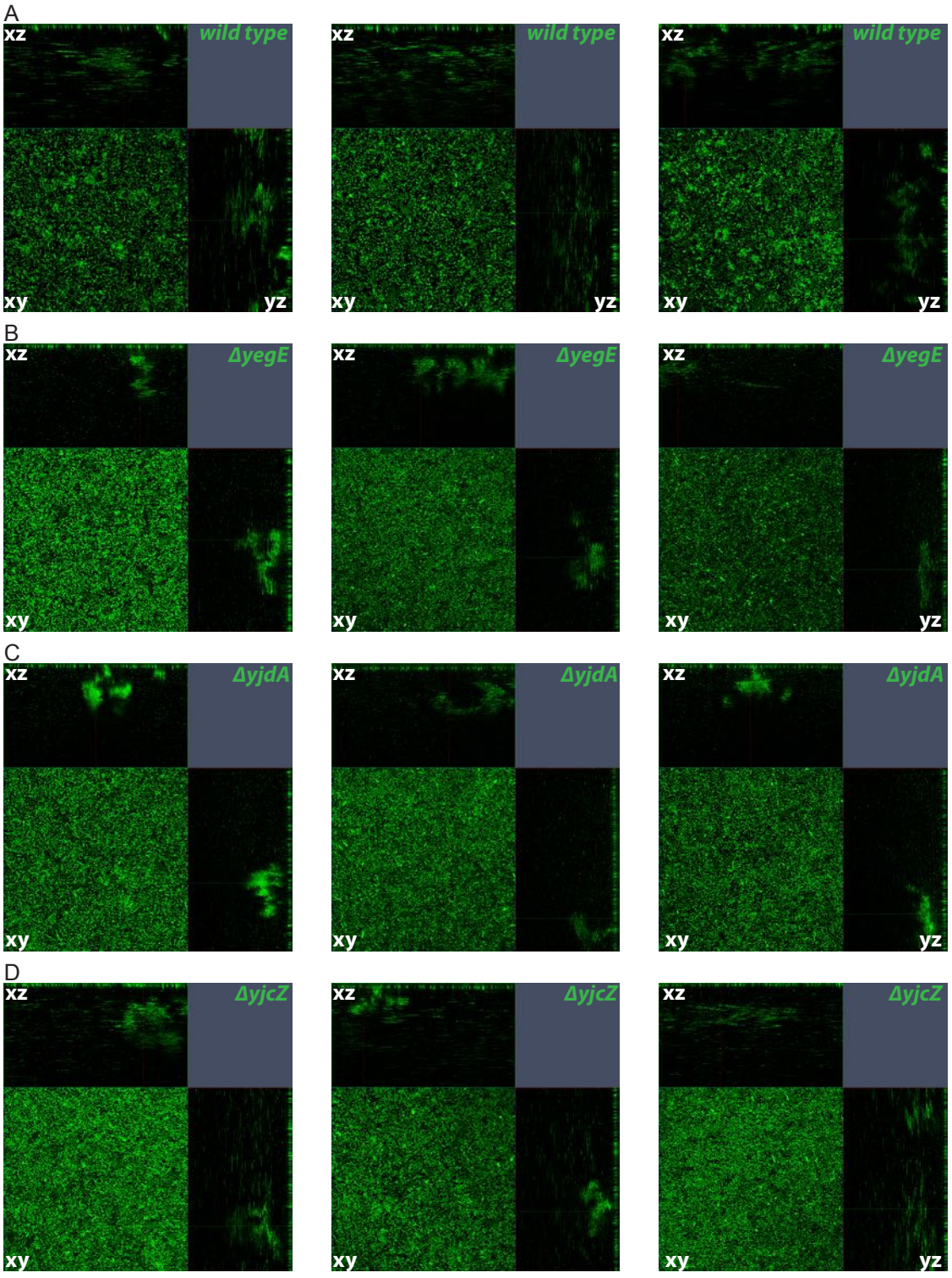

Fig. A.22. YjdA and YjcZ affect 3D-structure formation in static W3110^{RH} biofilms similarly to YegE (orthogonal views):
Orthogonal views (xz-, xy-, yz-planes) of the biofilms shown in Figures 8.3 and A.21. Static submerged biofilms of W3110^{RH} cells labeled with GFP were grown for 24 h.
(A) wild type, (B) Δ*yegE*, (C) Δ*yjdA*, (D) Δ*yjcZ*.
Dimensions (x:y:z): 142:142:80 μm.

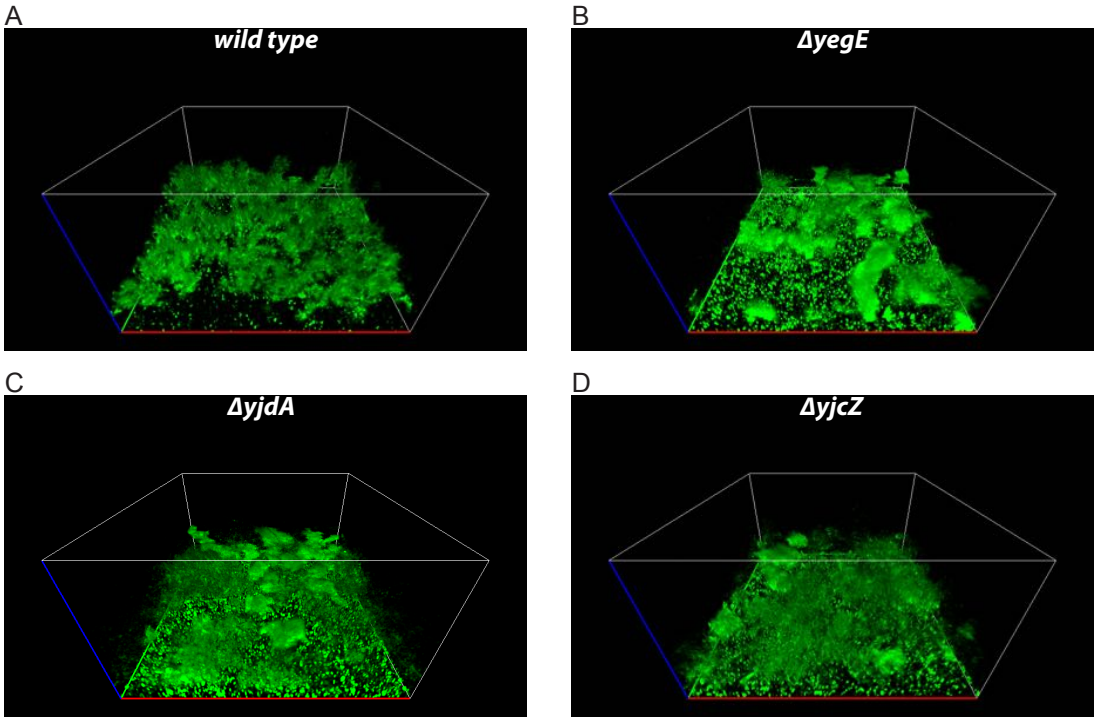

Fig. A.23. YjdA and YjcZ affect 3D-structure formation in static AR3110 biofilms similarly to YegE (additional replicates):
Confocal images of an additional biological replicate to the images in Figure 8.4. Static submerged biofilms of AR3110 cells labeled with GFP were grown for 48 h.
(A) wild type, (B) Δ*yegE*, (C) Δ*yjdA*, (D) Δ*yjcZ*. Dimensions of bounding box (x:y:z): 142:142:80 μm.

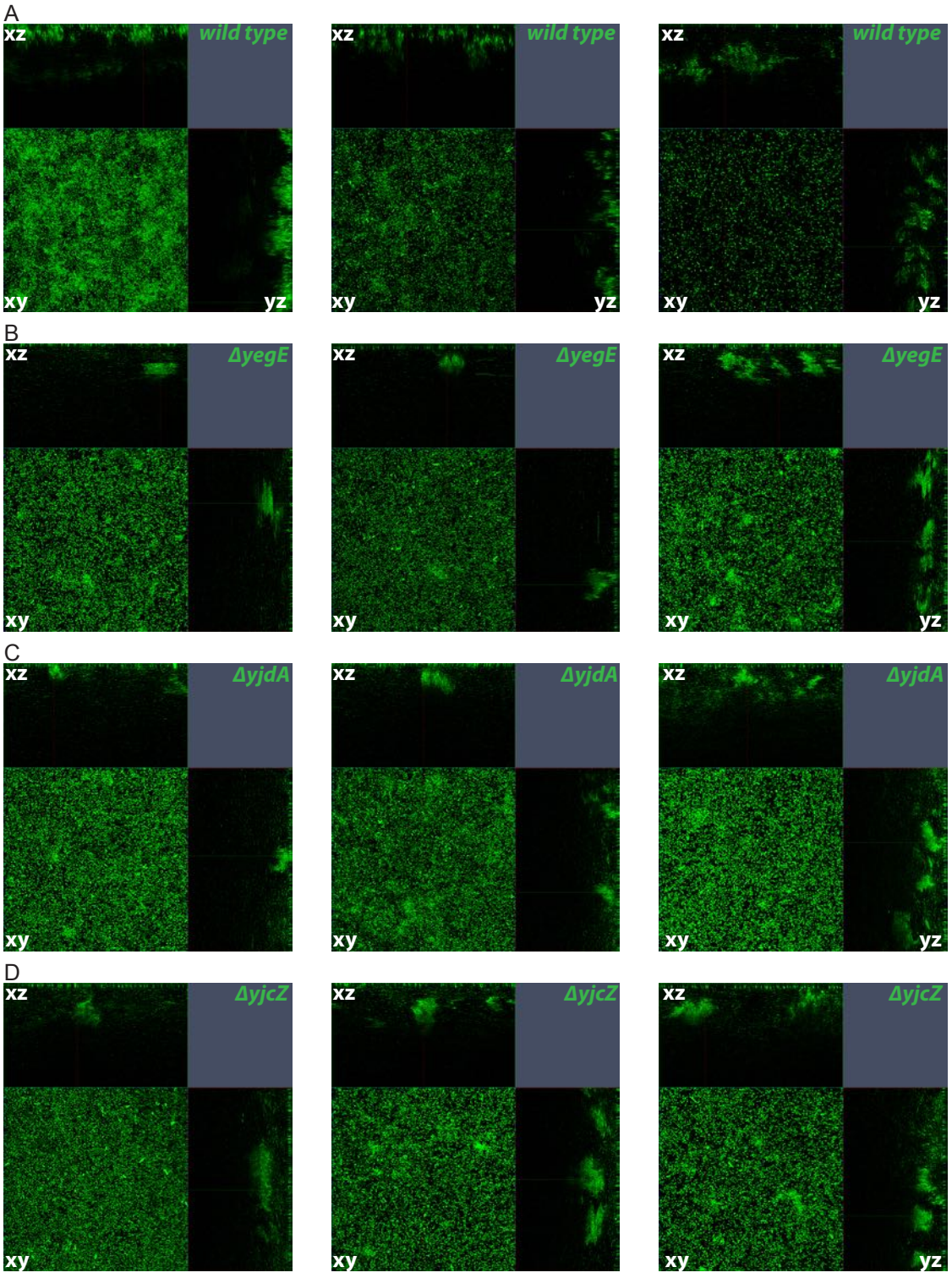

Fig. A.24. YjdA and YjcZ affect 3D-structure formation in static AR3110 biofilms similarly to YegE (orthogonal views):
Orthogonal views (xz-, xy-, yz-planes) of the biofilms shown in Figures 8.4 and A.23. Static submerged biofilms of AR3110 cells labeled with GFP for 48 h.
(A) wild type, (B) Δ*yegE*, (C) Δ*yjdA*, (D) Δ*yjcZ*.
Dimensions (x:y:z): 142:142:80 μm.

Tab. A.1. Extended hit-list for Pull-Downs of YjdA, YegE, YjcZ, YcgR and FliF:

	YjdA	YjdA	YjdA	YjdA	YegE	YegE	YegE	YegE	YjcZ	YjcZ	YjcZ	YjcZ	YcgR	YcgR	YcgR	YcgR	FliF	FliF	FliF	FliF
	5 h	5 h	14 h	14 h	5 h	5 h	14 h	14 h	5 h	5 h	14 h	14 h	5 h	5 h	14 h	14 h	5 h	5 h	14 h	14 h
Accession Number	- 01	- 02	- 01	- 02	- 01	- 02	- 01	- 02	- 01	- 02	- 01	- 02	- 01	- 02	- 01	- 02	- 01	- 02	- 01	- 02
EFTU1_ECO24 (+6)	23	17	19	22	20	11	13	12	16	18	19	14	23	22	23	15	17	17	17	13
CRFC_ECOLI	58	37	48	61	0	0	0	0	0	0	0	0	0	0	0	0	0	0	0	0
ATPB_ECO24 (+19)	20	18	15	24	17	7	10	7	15	5	13	3	28	24	25	22	17	17	17	11
ACEA_ECOL6 (+1)	11	14	19	19	11	13	13	6	16	18	13	5	15	15	12	17	16	17	11	5
CATE_ECOLI	18	15	15	14	12	8	7	4	15	23	25	8	20	20	18	15	17	18	18	7
FLIF_ECOLI	0	0	0	0	4	1	7	1	0	0	0	0	0	1	0	0	27	28	25	27
YEGE_ECOLI	0	0	1	1	54	30	36	25	0	0	0	0	0	0	0	0	0	0	0	0
TNAA_ECO24 (+14)	22	7	12	16	17	3	9	4	16	10	16	7	23	21	10	5	17	10	8	5
RL5_ECO24 (+20)	15	11	6	9	8	3	1	4	8	7	5	0	17	11	11	11	7	5	6	5
GLPK_ECO24 (+12)	27	10	7	9	13	5	2	4	8	6	5	2	30	20	17	12	12	9	5	4
RL6_ECO24 (+20)	13	12	9	10	9	4	4	6	11	9	6	4	12	11	10	8	8	8	5	4
LACI_ECOLI	12	12	8	9	15	9	12	4	10	7	9	6	14	15	12	7	10	11	8	8
FTSH_ECOLI	2	7	11	6	27	20	20	21	1	0	0	0	9	10	7	8	4	5	8	7
FLIC_ECOLI	8	6	6	5	9	5	4	4	14	19	18	16	14	14	8	5	13	9	10	9
OMPA_ECO57 (+1)	5	13	5	7	18	9	12	14	4	6	10	9	12	9	4	7	6	7	4	10
AHPC_ECO57 (+2)	8	10	0	0	7	4	0	2	9	7	3	3	9	8	4	1	8	7	1	1
SDHA_ECO57 (+2)	8	8	5	5	8	8	2	4	17	15	12	9	16	14	7	6	13	14	7	6
RS5_ECO24 (+8)	10	10	7	7	7	6	5	5	5	4	5	2	8	7	9	9	3	4	4	3
LPP_ECO57 (+2)	3	3	4	4	3	3	3	4	3	4	4	4	4	3	3	3	3	3	4	4
ACSA_ECOLI	13	8	12	12	3	6	3	0	9	6	7	0	16	17	14	13	6	6	6	2
HFLK_ECO57 (+1)	1	6	7	3	18	16	17	20	1	0	0	0	2	5	3	6	6	4	7	10
PFLB_ECOLI	2	5	12	13	0	3	4	4	1	2	9	1	11	9	21	20	1	2	6	5
YCGR_ECOLI	3	0	0	0	0	0	0	0	0	0	0	0	15	13	14	7	0	0	0	0
PPSA_ECOLI	23	4	10	18	6	0	0	0	0	0	1	0	27	13	25	18	1	0	3	0
IDH_ECOLI	15	2	8	10	4	0	0	0	5	0	7	0	18	13	14	8	6	3	3	1
YEAG_ECO57 (+2)	5	1	15	21	1	0	0	0	2	0	0	0	16	6	27	21	0	0	2	0
ENO_ECO24 (+20)	5	4	6	10	2	0	1	4	5	6	7	4	10	9	13	7	5	5	6	7
PT1_ECOLI	18	3	11	15	4	0	0	0	2	0	3	0	19	11	22	14	3	1	6	2
PUTA_ECOLI	29	2	2	5	11	0	0	0	3	0	0	0	42	5	16	6	5	0	0	0
CH601_ECOK1 (+19)	10	6	9	7	0	0	7	5	10	5	9	4	10	5	15	20	0	1	4	5
ALDB_ECOLI	10	3	12	14	2	0	4	0	0	0	2	0	15	12	13	9	0	0	1	1
TPX_ECO57 (+2)	7	8	2	3	3	1	2	7	7	7	7	6	6	8	4	6	4	3	6	7
ALDA_ECOLI	6	6	9	8	4	4	5	5	8	9	9	4	13	13	15	7	4	8	6	6
G3P1_ECO57 (+2)	6	16	1	0	6	5	0	0	6	10	2	0	9	11	1	0	5	8	2	0
ADHE_ECO57 (+1)	4	5	5	9	3	2	4	1	5	5	9	7	18	8	10	6	3	2	2	1
MREB_ECOL6 (+1)	8	3	4	11	4	0	1	0	1	0	1	0	11	6	13	13	1	1	2	1
PURA_ECO24 (+20)	19	2	1	3	6	0	0	0	10	0	8	1	19	9	7	2	9	2	1	1
DPS_ECO24 (+18)	5	9	1	3	4	2	3	3	9	8	4	1	9	10	4	3	6	8	1	1
FADB_ECOHS	13	3	2	7	1	0	0	0	0	0	1	0	18	5	21	8	3	2	4	2
HFLC_ECO57 (+2)	1	9	2	4	14	2	5	8	0	0	1	0	2	3	0	2	2	4	2	4
RL11_ECO24 (+19)	5	5	3	2	3	2	3	3	4	4	4	2	4	4	4	4	4	4	4	4
PTA_ECOLI	12	4	10	12	4	1	1	1	1	0	0	0	15	6	19	6	0	1	3	0
SDHB_ECOLI	4	6	0	1	1	0	1	6	6	6	4	4	9	5	7	4	6	2	4	4
ATPA_ECO24 (+19)	8	9	5	4	12	3	6	4	3	0	1	0	8	21	3	2	2	4	1	3
RPOB_ECO24 (+18)	17	3	2	3	1	0	0	1	1	1	1	0	41	8	9	9	1	2	0	0
RS10_ECO24 (+20)	7	5	0	4	5	0	0	3	4	3	1	2	5	4	9	5	3	3	4	1
DNAK_ECO24 (+7)	2	1	2	9	0	2	3	7	4	2	6	4	3	2	5	4	3	4	5	5
RL14_ECO24 (+20)	7	3	2	6	2	1	0	0	2	0	0	0	4	4	6	4	2	1	2	0
RS2_ECO27 (+15)	9	4	5	2	4	1	0	0	1	1	3	0	10	6	4	6	1	0	0	0
TIG_ECO24 (+15)	2	1	1	2	1	2	1	2	4	9	11	6	7	8	2	4	3	4	6	6
OSME_ECO57 (+1)	4	4	3	3	3	0	3	4	4	2	5	5	3	3	4	3	2	2	4	4
RL10_ECO24 (+20)	5	4	2	6	1	0	1	3	2	1	3	1	7	3	4	4	2	3	4	3
DLDH_ECO57 (+2)	4	1	14	12	1	0	3	0	1	0	6	0	11	3	15	9	0	0	3	1
DPPF_ECOLI	3	2	5	6	4	0	3	2	3	0	8	4	3	2	3	4	4	2	5	7
SYGB_ECOBW (+4)	17	1	2	2	5	0	0	0	0	0	0	0	31	6	5	5	0	0	1	0
NUOG_ECOLI	8	2	5	5	4	2	2	0	1	2	11	0	12	5	9	8	4	1	5	3
RHO_ECO57 (+2)	14	7	2	1	7	0	0	0	0	0	2	0	14	10	4	2	4	3	0	0
RECA_ECO24 (+18)	11	0	8	6	4	0	0	0	0	0	1	0	12	7	13	7	1	0	1	0
ARCA_ECO57 (+2)	6	3	0	0	0	0	0	0	3	0	0	0	12	8	4	0	1	0	1	0
RS3_ECO24 (+19)	3	5	3	2	3	1	0	2	1	0	0	0	7	9	5	3	1	1	2	0
MIND_ECO57 (+2)	12	3	2	4	3	0	0	0	1	0	3	0	11	1	10	3	2	1	1	0
ODO2_ECO57 (+1)	10	2	8	11	1	1	0	1	1	1	2	0	5	3	9	6	1	0	2	2
EFG_ECO24 (+20)	2	7	4	1	1	3	5	4	0	2	4	2	4	8	8	5	1	1	1	1
CRP_ECO57 (+2)	10	3	1	1	4	0	0	0	4	0	0	0	9	6	4	3	3	2	3	1
RL4_ECO24 (+20)	6	4	1	1	1	0	0	4	0	1	2	0	5	5	4	4	0	1	2	0
RS11_ECO24 (+20)	7	5	4	3	4	1	1	1	1	1	4	0	6	4	5	4	3	2	3	0
RPOA_ECO24 (+7)	3	3	2	3	2	1	3	1	3	4	4	2	10	5	5	2	4	3	3	1

RL1_ECO24 (+19)	5	5	3	4	3	3	4	5	1	2	2	4	5	3	5	4	3	2	3	2
USPF_ECOLI	3	2	2	2	2	0	2	3	3	2	3	3	3	3	3	3	3	2	2	2
OMPF_ECOLI	1	6	2	2	8	3	5	3	1	3	2	3	7	2	1	1	4	3	5	3
PAL_ECO57 (+1)	6	3	2	3	4	0	1	6	6	3	2	4	5	4	4	2	2	2	3	3
ODP1_ECO57 (+1)	5	5	4	2	2	1	3	0	2	1	2	0	13	9	5	4	2	2	2	2
NQOR_ECO24 (+17)	8	11	2	2	2	3	1	0	1	2	2	2	9	9	3	2	1	6	1	0
GCST_ECO27 (+4)	3	4	1	1	3	3	2	2	4	6	2	1	5	5	0	1	5	4	1	1
RS17_ECO24 (+20)	5	6	1	3	3	1	0	2	2	2	2	2	2	3	3	3	3	1	3	2
DEOB_ECO24 (+20)	4	3	2	5	2	2	1	0	5	1	2	0	8	7	8	6	2	3	2	0
SPEA_ECOLI	6	2	3	6	0	0	0	0	0	0	1	0	18	3	10	4	0	1	1	0
RS7_ECOBW (+2)	5	3	4	5	1	1	2	2	0	0	1	0	7	6	4	4	0	3	2	1
ACCC_ECO57 (+1)	7	2	0	2	2	0	1	0	5	0	2	0	13	7	5	0	3	0	4	1
YGAU_ECOL6 (+1)	1	1	3	2	1	0	2	8	2	2	8	7	2	2	5	7	1	1	6	4
YGAU_ECOL6 (+1)	1	1	3	2	1	0	2	8	2	2	8	7	2	2	5	7	1	1	6	4
KPRS_ECO57 (+2)	8	3	1	3	1	0	0	0	0	0	0	0	10	4	9	6	1	0	1	0
SUCC_ECO24 (+13)	9	2	1	2	4	1	1	1	3	6	1	0	13	5	6	2	5	3	1	0
OMPR_ECO57 (+2)	9	2	0	1	2	0	0	0	5	0	0	0	11	5	6	3	0	0	0	0
FABI_ECO57 (+1)	6	2	2	2	2	1	1	0	1	1	1	0	9	5	3	1	1	1	2	2
MCP2_ECOLI	1	1	2	2	6	3	6	9	0	1	0	1	4	4	3	1	0	0	2	2
DPPD_ECO57 (+1)	0	1	1	4	0	0	4	3	0	0	8	5	0	0	6	6	1	0	2	3
GYRB_ECO57 (+1)	11	0	3	6	1	0	0	0	0	0	0	0	18	1	13	4	0	0	0	0
PHNB_ECOLI	2	2	2	4	0	0	2	3	0	0	4	3	0	1	3	2	1	0	3	3
HSLU_ECO27 (+9)	4	2	4	3	1	0	0	0	0	0	0	0	11	5	10	6	0	0	1	0
EFTU2_ECO24	2	2	2	1	2	1	2	2	0	0	0	0	1	1	1	1	1	2	2	1
PTW3C_ECOLI	7	5	2	4	9	5	2	2	0	0	0	0	5	2	4	2	0	1	1	1
ETTA_ECO57 (+1)	9	1	4	2	2	0	0	0	0	0	0	0	14	6	5	8	0	0	0	0
FTSZ_ECO57 (+2)	5	1	1	1	1	1	2	1	1	0	0	0	13	4	7	4	3	1	3	2
GATZ_ECO24 (+2)	11	3	2	3	5	0	0	0	3	0	2	0	12	2	9	3	2	0	2	0
GLYA_ECO24 (+19)	3	3	2	1	2	3	0	1	4	3	4	1	5	5	1	1	3	2	1	3
FLGI_ECOSE	0	1	0	0	2	1	1	0	0	0	0	0	1	1	0	0	10	10	5	5
GATY_ECOL6	5	2	1	3	1	0	0	0	0	0	0	0	4	1	5	2	1	1	0	0
YBAY_ECOLI	1	1	0	2	0	0	2	6	2	1	2	3	3	2	0	2	0	0	3	6
RL2_ECO24 (+20)	3	2	2	2	3	0	0	1	0	0	0	1	0	4	4	3	3	2	3	1
NUOCD_ECODH	1	0	0	2	2	0	1	0	2	0	1	0	13	7	6	4	0	0	1	2
CSGD_ECOLI	0	0	1	2	0	0	0	0	0	0	0	0	6	0	11	6	0	0	1	0
PFKA_ECO24 (+16)	3	8	1	1	1	2	0	0	1	4	1	0	4	2	0	0	3	3	1	0
OMPC_ECOLI	0	5	0	1	7	0	4	4	1	1	4	4	2	2	1	2	0	0	6	7
RS4_ECO24 (+20)	5	3	3	2	0	0	0	0	0	0	0	0	3	3	1	3	1	1	1	1
FADH_ECOLI	8	1	3	6	1	0	0	0	1	0	1	0	8	3	7	4	0	0	2	0
ODP2_ECOLI	1	1	12	5	0	0	3	0	0	0	0	0	3	0	15	7	0	0	2	1
LOIP_ECOLI	1	1	2	3	0	0	2	3	2	1	1	3	1	1	5	3	0	1	4	1
CHEA_ECOLI	6	2	0	0	2	1	0	0	0	0	0	0	16	9	0	0	0	0	0	0
RL13_ECO24 (+20)	4	3	3	1	3	0	0	2	0	0	2	1	5	2	3	2	0	0	3	0
DADA_ECO24 (+13)	10	0	0	0	2	0	0	0	2	0	0	0	12	2	5	0	2	0	0	0
YGFZ_ECOSE	1	1	2	5	2	0	1	0	2	0	8	0	1	2	4	4	2	0	3	3
PHOL_ECO57 (+2)	6	2	4	8	2	1	0	0	1	0	1	0	1	5	6	5	0	0	1	0
STHA_ECO24 (+12)	8	0	4	4	1	0	2	0	0	0	1	0	13	1	4	0	1	0	2	0
SYGA_ECOLI	5	2	2	4	1	0	0	0	0	0	0	0	9	2	7	4	0	1	1	0
RL9_ECO24 (+20)	3	3	2	1	0	0	2	5	3	2	2	3	4	3	4	4	2	2	4	3
QUEF_ECOBW (+4)	2	4	0	1	0	0	0	0	2	3	3	0	1	1	0	3	1	2	0	0
RS12_ECO24 (+18)	5	3	3	3	2	2	0	0	0	0	0	0	4	3	4	3	2	2	1	0
KBL_ECO57 (+1)	9	2	3	3	1	0	0	0	0	0	0	0	11	7	3	1	2	1	1	0
FABG_ECOLI	7	5	0	0	2	1	2	1	0	0	1	0	8	7	0	1	0	1	0	0
RL19_ECO24 (+20)	3	3	2	2	2	0	0	1	0	0	1	0	1	2	2	2	1	1	1	0
DNAJ_ECODH (+1)	5	1	2	3	2	0	0	0	2	0	0	0	8	5	6	2	3	1	1	0
RPOC_ECOK1 (+2)	3	3	1	1	2	1	1	0	0	1	0	0	11	2	2	1	1	0	1	0
GALF_ECO57 (+1)	6	1	1	1	2	0	1	0	2	0	1	0	6	2	1	1	1	1	1	1
FABH_ECO24 (+6)	2	2	0	2	1	0	0	1	1	0	4	0	9	1	2	4	1	0	0	1
SYN_ECO24 (+6)	2	3	1	1	5	0	1	0	7	0	0	0	11	5	1	0	5	2	0	0
FABB_ECOL6 (+1)	1	0	2	3	2	0	2	0	0	0	6	0	5	0	5	3	1	0	5	3
NANE_ECO45 (+12)	6	0	1	1	2	0	1	0	4	1	3	0	4	2	4	1	3	2	2	1
RS8_ECO24 (+20)	2	3	2	1	1	1	1	3	2	3	0	0	2	4	2	3	0	3	1	1
YRAP_ECO57 (+2)	3	2	2	3	4	1	2	3	2	0	1	0	1	2	2	2	2	1	1	1
ACRA_ECO57 (+1)	1	2	0	1	3	2	3	3	1	0	0	0	0	0	0	0	0	0	0	1
FKBB_ECOLI	4	5	1	0	1	1	2	1	4	2	1	0	4	4	3	3	3	4	0	0
CARB_ECOLI	1	0	1	4	0	0	0	0	0	0	0	0	6	0	20	8	0	0	0	0
SEQA_ECOL6 (+1)	3	6	0	0	1	2	0	1	5	3	0	0	4	5	0	0	1	2	0	0
NUOB_ECO24 (+20)	2	3	1	2	3	2	3	2	3	1	1	0	3	2	0	0	0	0	0	0
RS9_ECO24 (+20)	4	2	4	3	1	0	0	2	0	0	2	0	1	2	3	3	0	2	2	1
MURA_ECO24 (+16)	3	1	1	2	0	0	0	0	0	0	0	0	6	3	7	1	0	1	0	0
GLMS_ECO57 (+2)	6	0	0	0	0	0	0	0	1	0	0	0	15	1	4	1	0	0	0	0
FUR_ECO57 (+2)	1	3	1	2	2	1	0	3	2	1	3	2	2	1	1	2	2	2	2	1
FADL_ECOLI	1	1	1	3	1	1	2	1	1	2	4	3	1	1	1	0	2	2	4	4
EFTS_ECO24 (+19)	0	5	0	0	0	1	1	2	0	1	2	0	4	5	1	2	0	1	0	0
HNS_ECO57 (+2)	0	2	0	0	1	0	0	4	3	3	3	2	3	0	2	1	0	1	1	2
CISY_ECOL6 (+1)	1	0	2	1	0	0	3	3	0	0	3	2	1	0	2	2	0	0	3	1

PYRG_ECO24 (+19)	10	0	1	0	1	0	0	0	5	0	0	0	16	2	4	1	1	0	0	0
IADA_ECOLI	0	1	2	1	1	2	2	1	2	3	3	2	0	1	0	0	3	3	2	2
HLDE_ECO24 (+17)	5	1	2	2	1	0	0	0	0	0	0	0	8	2	8	2	0	0	0	0
IF2_ECOSM	6	0	0	0	0	0	0	0	0	0	0	0	16	2	1	0	0	0	0	0
DHG_ECOLI	0	0	3	1	0	0	0	3	0	0	0	0	0	0	3	3	0	0	5	6
RL3_ECO24 (+20)	2	4	2	2	1	1	1	2	1	1	2	0	4	2	2	1	1	1	2	1
USPA_ECO57 (+2)	3	0	0	0	0	0	0	1	1	0	0	0	4	3	1	1	1	0	1	0
BGAL_ECOLX	2	2	4	7	0	0	0	0	1	4	2	0	0	0	2	0	0	0	0	0
LOLB_ECO24 (+11)	1	0	1	1	1	0	1	5	1	0	1	3	1	0	5	0	1	1	1	1
BLC_ECO57 (+1)	2	0	1	4	0	0	1	2	0	0	1	0	1	1	5	3	0	0	2	0
YAJC_ECO57 (+2)	1	2	0	0	3	0	2	3	0	0	0	0	1	2	2	1	3	3	1	1
RS1_ECO57 (+2)	0	3	2	1	0	0	0	0	0	0	3	0	2	5	2	1	0	2	0	0
YGAM_ECO57 (+2)	2	0	3	3	2	1	3	1	0	0	1	1	0	0	1	1	0	0	1	0
UPP_ECO24 (+19)	4	1	0	0	0	0	1	1	0	0	0	0	7	3	4	1	1	1	2	0
CLPB_ECO57 (+2)	7	0	0	0	0	0	0	0	0	0	0	0	10	6	0	0	0	0	1	0
GLRX3_ECO57 (+2)	2	3	0	0	1	0	0	2	3	3	3	3	3	4	0	0	2	2	0	0
GSA_ECOBW (+2)	4	1	2	2	0	0	0	0	1	0	1	0	7	1	7	3	0	0	1	0
RPOD_ECOLI	5	0	0	0	0	0	0	0	0	0	0	0	8	1	0	0	0	0	0	0
ELAB_ECO57 (+2)	2	0	3	3	1	0	0	3	0	1	1	1	1	1	2	1	1	1	2	1
ACCA_ECO24 (+11)	4	0	0	0	0	0	0	0	2	0	0	0	7	1	1	0	2	1	0	0
NUOE_ECOL6 (+1)	1	1	0	1	0	0	1	4	1	1	1	2	0	1	3	1	1	0	2	0
ATPF_ECO24 (+11)	1	0	0	0	0	0	0	3	0	0	2	0	1	1	3	0	2	0	3	2
KPYK2_ECOLI	6	1	0	0	1	0	0	0	1	0	0	0	6	6	2	0	0	0	0	0
MDH_ECO7I (+2)	4	1	1	1	1	1	1	1	0	0	0	0	6	4	1	0	0	1	0	0
MCP3_ECOLI	2	3	1	1	4	4	3	4	0	0	0	0	2	1	0	0	0	0	0	0
NUSG_ECOLI (+1)	7	2	0	1	2	0	0	0	0	0	0	0	8	4	2	1	0	0	0	0
FLGH_ECO27 (+1)	2	1	1	0	1	0	1	1	1	1	2	0	5	4	3	1	5	5	2	1
LEPA_ECO27 (+4)	3	0	0	0	1	0	0	0	1	0	0	0	13	0	1	0	0	0	0	0
BTUE_ECOLI	1	1	1	2	0	0	1	0	0	0	0	0	2	1	3	1	0	0	0	0
YEDD_ECOLI	2	2	1	3	1	0	1	3	2	0	1	1	2	1	2	2	2	0	2	2
GLNQ_ECOLI	2	0	0	2	0	0	0	0	2	1	0	0	3	0	3	2	1	1	0	0
CYOA_ECOL6 (+1)	1	1	0	1	3	1	1	3	0	0	1	0	2	0	2	1	0	0	2	1
GSH1_ECO7I (+1)	0	1	0	4	1	0	1	0	2	2	7	0	0	2	0	0	2	0	2	0
GYRA_ECOLI	6	2	3	5	0	0	0	0	0	0	0	0	2	0	4	0	0	0	0	0
SECB_ECO24 (+20)	2	2	1	1	1	1	1	1	2	1	1	1	2	2	2	1	1	1	0	0
SLYB_ECO57 (+1)	1	2	1	1	3	1	2	3	1	0	0	1	2	2	1	1	2	1	1	0
POXB_ECOLI	3	0	1	1	0	0	0	0	0	0	1	0	11	1	5	0	0	0	0	0
NDK_ECO24 (+11)	2	4	0	0	0	0	0	1	4	3	0	0	4	4	0	1	2	1	0	0
LUXS_ECO24 (+10)	1	1	0	1	0	0	0	3	0	3	2	1	1	2	3	2	1	0	1	0
FUMA_ECO57	1	2	0	0	0	3	0	0	4	3	0	0	2	4	0	1	3	3	1	0
NUSA_ECO57 (+2)	2	1	0	0	0	0	0	0	3	1	0	0	4	3	2	1	0	0	0	0
ATPG_ECO24 (+20)	2	1	0	1	3	1	0	0	3	1	0	0	3	1	1	1	1	1	0	0
SLYA_ECO27 (+6)	1	1	2	2	1	0	2	3	0	0	2	2	0	1	2	3	1	1	3	1
SELD_ECOHS (+1)	4	0	0	2	0	0	0	0	0	0	0	0	7	1	7	2	0	0	0	0
SUBI_ECOLI	1	0	1	0	1	0	2	1	0	1	0	1	0	0	1	0	0	0	0	0
ACTP_ECO24 (+19)	3	1	2	3	4	1	3	1	1	0	1	0	2	2	1	2	1	1	3	1
SLP_ECOLI	1	2	2	1	1	0	2	3	0	0	3	0	2	0	2	2	0	0	2	2
GALU_ECO57 (+2)	4	0	0	0	1	0	0	0	1	0	0	0	6	4	1	1	1	0	0	1
CHEW_ECO57 (+2)	7	3	0	0	1	0	0	0	1	0	0	0	3	3	2	1	0	1	0	0
CRA_ECO57 (+2)	4	0	0	0	0	0	0	0	0	0	0	0	4	0	4	1	0	0	0	0
RIR1_ECOLI	2	1	1	3	0	0	0	0	0	0	0	0	6	1	2	2	0	0	0	0
YIAF_ECO57 (+2)	2	1	1	1	1	0	1	3	2	0	1	1	1	1	2	2	1	1	2	2
PUR7_ECO24 (+18)	3	0	0	0	0	0	0	0	1	0	2	0	5	0	6	2	0	0	1	1
GUAC_ECO24	4	1	1	2	1	0	0	0	1	0	1	0	3	1	1	1	1	1	1	1
YCFP_ECO24 (+18)	3	1	1	1	1	0	0	0	5	0	1	0	2	1	2	2	3	0	0	0
LAMB_ECOSE	0	0	1	1	1	0	2	0	0	0	4	4	1	1	0	0	1	0	1	3
DOSC_ECO57 (+1)	0	0	1	3	0	0	0	0	0	0	0	0	2	0	9	1	0	0	0	0
YQJD_ECO57 (+2)	2	1	1	0	0	0	2	1	1	0	2	2	0	0	1	2	0	0	2	2
ISCU_ECO57 (+2)	1	1	0	0	1	0	0	3	2	3	0	1	2	1	1	1	2	1	0	0
MAP1_ECO57 (+2)	1	5	0	0	1	1	0	0	2	1	1	0	1	1	0	0	1	1	0	0
YBJP_ECOLI	0	0	0	1	0	0	1	2	0	0	1	4	0	0	2	0	0	0	2	1
YADG_ECOLI	2	0	0	0	0	0	0	0	0	0	0	0	3	0	5	1	0	1	0	0
LPOB_ECO57 (+1)	1	2	2	3	2	0	1	2	2	1	1	1	2	1	2	1	1	0	1	1
SYT_ECO27 (+12)	2	1	2	1	2	0	0	0	1	1	1	0	2	2	2	0	1	1	1	1
LPTB_ECO57 (+2)	3	0	0	2	0	0	0	0	1	0	0	0	2	0	4	2	0	0	2	0
RL15_ECOBW (+4)	2	0	1	1	0	0	0	1	0	0	0	0	2	2	5	3	1	1	1	0
DCRB_ECOLI	1	1	1	2	0	0	0	2	2	0	1	0	0	1	1	1	0	0	2	1
CLPX_ECO24 (+20)	3	0	1	1	1	0	0	0	0	0	0	0	10	2	1	3	0	0	0	0
RL7_ECO24 (+19)	3	2	1	2	0	0	1	2	0	1	2	2	3	1	3	1	0	0	2	2
ASTE_ECOLU	2	1	0	0	0	0	0	0	2	0	0	0	1	1	2	2	1	0	0	0
FABZ_ECO24 (+17)	0	2	0	0	0	0	0	0	1	3	0	2	3	3	0	0	1	1	0	0
GLRX4_ECO57 (+2)	1	1	0	0	0	0	0	4	2	1	3	3	2	1	1	1	1	0	1	0
TYPA_ECO27 (+3)	1	2	2	0	0	0	0	0	0	0	0	0	4	2	0	1	0	0	0	0
MUKB_ECOHS	3	0	0	0	0	0	0	0	0	0	0	0	4	1	0	0	0	0	0	0
NUOA_ECO24 (+10)	2	2	0	2	2	0	1	1	1	1	1	0	2	1	0	0	1	0	1	1
ABDH_ECO24 (+3)	0	1	2	0	0	1	2	1	0	0	1	0	1	3	2	1	0	1	1	1
NFUA_ECO7I	1	0	2	0	0	0	0	2	0	1	2	2	2	0	2	3	0	1	0	0

GLK_ECO24 (+19)	3	2	0	0	2	0	0	0	3	0	0	0	3	2	0	0	2	1	0	0
F16PA_ECO24 (+9)	3	1	0	0	0	0	0	0	0	0	0	0	2	2	2	1	0	0	1	0
DAPA_ECO24 (+12)	1	4	0	0	0	0	0	0	1	2	0	0	2	1	0	0	0	0	0	0
RL17_ECO24 (+20)	0	0	0	1	1	0	1	2	0	0	0	2	0	0	1	1	1	0	0	1
YGDI_ECOL6 (+1)	0	0	0	2	0	0	1	2	0	0	2	1	0	0	2	2	0	0	2	2
SECA_ECO27	2	1	3	0	0	0	0	0	0	0	0	0	1	2	0	1	0	0	0	1
MGLA_ECOLI	3	0	1	0	0	0	0	0	0	0	0	0	6	0	1	0	0	0	0	0
MCP1_ECOLI	1	1	1	1	0	3	2	4	0	0	0	0	1	1	1	1	0	1	1	1
YAJG_ECOL6 (+1)	3	0	1	2	0	0	0	1	2	0	1	1	1	1	3	1	0	0	0	1
MENB_ECOL6 (+1)	0	2	0	0	0	0	0	0	0	4	0	0	0	0	0	0	0	3	0	0
SECD_ECO57 (+1)	8	2	1	1	3	1	0	0	0	0	0	0	0	0	0	0	0	0	0	0
RS14_ECO24 (+15)	2	0	1	0	1	0	0	1	0	1	2	1	2	2	1	1	1	1	1	0
ERPA_ECO24 (+20)	0	0	0	2	0	0	0	1	1	0	0	1	0	1	3	2	2	0	2	1
YAEH_ECO24 (+20)	1	2	0	0	0	0	0	2	3	3	1	1	2	1	2	0	0	0	1	1
KATG_ECOUT (+4)	1	1	1	3	0	0	0	0	0	0	2	0	0	0	0	0	0	0	0	1
NIFJ_ECOLI	1	0	2	1	0	0	0	0	0	0	0	0	5	0	8	2	0	0	0	0
RCSB_ECO57 (+3)	3	1	0	0	0	0	0	0	0	0	0	0	6	1	0	0	0	0	0	0
PUR8_ECOLI (+1)	4	0	0	0	0	0	0	0	0	0	0	0	10	1	0	0	0	0	0	0
GCSP_ECOSM	2	3	0	0	1	1	0	0	0	0	0	0	2	1	0	0	1	0	0	0
CSGG_ECO57 (+2)	0	0	0	0	0	0	0	4	0	0	0	0	2	1	1	1	0	0	0	0
RRAA_ECO24 (+19)	1	0	0	2	1	0	0	1	1	1	0	0	2	1	3	1	0	2	0	0
GABD_ECOLI	2	0	0	0	1	0	0	0	0	0	0	0	1	1	0	0	1	0	0	0
BAMA_ECO24 (+19)	0	0	0	0	0	0	2	0	0	0	2	0	0	0	0	1	0	0	2	2
ALF1_ECOL6 (+1)	0	3	1	5	0	0	0	0	0	0	0	0	0	0	0	2	0	0	0	1
CYCA_ECO57 (+1)	0	0	0	0	2	0	2	3	0	1	0	0	0	0	0	0	0	0	0	1
MAO1_ECO57 (+6)	2	0	0	0	0	0	0	0	1	0	0	0	6	2	0	0	1	0	0	0
ACCD_ECOUT (+9)	3	2	0	0	0	0	0	0	0	0	0	0	4	3	0	0	0	0	0	0
FLII_ECOLI	2	1	1	0	0	0	0	0	0	0	0	0	6	0	1	0	0	0	0	0
ASSY_ECO45 (+2)	2	0	0	0	0	0	0	0	0	0	0	0	6	0	0	0	0	0	0	0
CARA_ECO57 (+1)	0	0	0	2	0	0	0	0	0	0	0	0	0	0	7	1	0	0	0	0
MINE_ECO24 (+20)	2	2	0	1	1	0	0	1	1	1	1	0	2	1	2	2	2	1	1	1
AROB_ECO81	1	1	0	2	1	0	1	1	0	0	0	0	2	2	1	1	1	2	2	2
OPPF_ECOLI	4	0	0	0	0	0	0	0	0	0	0	0	3	0	7	1	0	0	0	0
GPMA_ECO24	0	1	1	0	0	0	0	3	0	1	1	0	0	1	1	2	0	1	0	0
FLAV_ECO57 (+2)	0	2	0	0	1	0	0	1	2	3	0	0	1	1	0	0	1	1	0	0
FADA_ECO24	2	0	0	0	0	0	0	0	1	0	0	0	5	2	0	0	0	0	0	0
YQEF_ECOLI	2	0	0	0	0	0	0	0	0	0	0	0	3	0	1	0	0	0	0	0
KDPD_ECOLI	0	0	0	0	5	0	0	0	0	0	0	0	0	0	0	0	0	0	0	0
OMPX_ECO57 (+2)	0	0	0	0	1	0	1	4	0	0	0	1	2	0	1	0	0	0	0	0
RODZ_ECO24	0	0	0	1	2	1	3	1	0	0	0	0	1	0	0	0	0	0	1	0
AK1H_ECOLI	3	1	0	0	0	0	0	0	0	0	0	0	3	0	7	1	0	0	0	0
HTPG_ECOK1 (+1)	2	1	0	0	1	0	0	0	0	0	0	0	4	3	0	0	0	0	0	0
YIDC_ECOUT (+19)	0	0	0	0	2	0	1	1	0	0	0	0	0	0	0	0	0	0	0	0
CLPA_ECO57 (+2)	3	0	0	0	1	0	0	0	0	0	0	0	11	0	0	0	0	0	0	0
MALT_ECOBW (+4)	4	0	0	0	0	0	0	0	0	0	0	0	5	0	0	0	0	0	0	0
BAMB_ECOLI	0	2	1	1	0	0	1	0	1	1	2	0	0	0	0	0	1	1	1	2
YCIO_ECOLI (+1)	2	0	1	1	0	0	0	0	1	0	0	0	3	1	3	0	1	0	0	0
PHOP_ECOLI (+2)	3	1	0	1	0	0	0	0	0	0	0	0	3	2	2	1	0	0	1	1
YAJO_ECOLI	2	0	1	3	0	0	0	0	0	0	0	0	5	0	3	2	0	0	0	0
ALKH_ECO57 (+2)	0	2	0	0	1	1	0	0	2	3	0	0	1	1	0	0	0	1	0	0
UVRY_ECO57 (+1)	3	0	0	0	0	0	0	0	0	0	0	0	3	0	2	0	0	0	0	0
SUCD_ECOLI (+2)	0	4	0	0	0	0	0	0	0	1	0	0	3	1	0	0	0	0	0	0
YIBN_ECO57 (+2)	1	1	0	1	1	0	0	2	0	0	0	1	0	0	1	1	0	0	1	0
ATPD_ECO24 (+17)	2	1	0	1	2	0	0	1	1	0	0	0	0	0	1	0	0	0	0	0
PTGA_ECOL6 (+1)	0	0	0	0	0	0	1	2	0	0	1	1	0	0	0	0	0	0	1	0
BLAT_ECOLX	0	0	0	0	0	0	0	2	0	0	0	0	0	0	0	1	5	4	2	0
SDHL_ECOLI	2	0	0	0	0	0	0	0	0	0	0	0	4	0	0	0	0	0	0	0
YRAR_ECOLI	0	0	2	1	0	0	0	0	0	0	0	0	1	1	1	0	0	0	1	0
RS20_ECO24 (+19)	1	2	0	0	0	0	0	0	0	1	0	0	2	1	1	0	0	2	0	0
CHEB_ECO57 (+1)	4	1	0	0	0	0	0	0	1	0	0	0	2	0	0	0	0	0	0	0
HEMX_ECOLI	0	0	0	0	2	1	2	1	0	0	0	0	0	0	0	0	0	0	0	0
RISB_ECO24 (+17)	2	1	0	0	0	0	0	0	0	0	0	0	6	3	0	0	0	0	0	0
ACRB_ECOLI	0	0	0	0	4	1	2	2	0	0	0	0	0	0	0	0	0	0	0	0
FLIM_ECOLI	2	0	0	0	0	0	0	0	0	0	0	0	6	0	1	0	0	0	1	0
YDAM_ECOLI	2	0	0	0	0	0	0	0	0	0	0	0	5	0	3	0	0	0	0	0
TYRB_ECOLI	4	0	0	0	0	0	0	0	0	0	0	0	8	0	1	0	0	0	0	0
ENTB_ECO57 (+1)	0	2	1	1	0	0	0	0	0	1	0	0	0	0	1	1	0	1	0	0
PGK_ECO24 (+6)	0	0	0	0	0	0	2	0	1	1	0	0	0	1	0	0	0	0	1	1
PTM3C_ECOLI	0	1	0	0	3	1	0	0	0	0	0	0	0	1	0	0	0	0	0	0
YHCB_ECO57 (+2)	2	0	0	0	1	0	0	0	0	0	0	0	0	0	0	0	0	0	1	0
BAMC_ECOLI	0	1	1	0	0	0	2	0	0	0	0	0	0	0	0	0	0	0	0	0
ASNA_ECOSM	2	0	0	0	0	0	0	0	0	0	0	0	3	1	0	0	0	0	0	0
PTKC_ECO57 (+1)	0	0	0	0	3	0	0	1	0	0	0	0	0	0	0	0	0	0	0	0
IMDH_ECO57 (+1)	1	1	2	2	0	0	0	0	0	1	1	0	0	1	0	0	0	0	0	0
QMCA_ECO57 (+2)	0	0	0	0	3	0	1	2	0	0	0	0	0	0	0	0	0	0	0	0
GMHA_ECOSM (+16)	2	0	0	1	0	0	0	0	0	0	0	0	0	1	3	1	0	0	0	0
LPTE_ECO24 (+14)	0	0	1	1	1	0	2	1	0	0	0	0	0	0	0	0	0	0	0	0

WZZE_ECO57 (+1)	0	0	0	0	3	0	0	0	0	0	0	0	0	0	0	0	0	0	0	0
PDXJ_ECO57 (+1)	0	2	0	0	0	0	0	0	1	1	0	0	1	1	0	0	1	2	0	0
FDOH_ECOL6 (+1)	0	0	0	0	0	0	0	2	0	0	0	1	1	0	1	1	0	0	0	0
PHSG_ECOLI	2	0	0	0	0	0	0	0	0	0	0	0	2	1	0	0	0	0	0	0
FUCM_ECO24 (+20)	0	2	0	0	0	0	0	0	0	3	0	0	0	0	0	0	1	0	0	0
SUFC_ECOLI	3	0	0	0	0	0	0	0	0	0	0	0	1	0	0	0	0	0	0	0
PNTA_ECOLI	0	0	0	0	2	0	0	0	0	0	0	0	0	0	0	0	0	0	0	0
SYW_ECOLI	3	0	0	0	0	0	0	0	0	0	0	0	3	0	0	0	0	0	0	0
HFLX_ECOLI	2	0	0	0	0	0	0	0	0	0	0	0	2	0	0	0	0	0	0	0
OSMC_ECOLI	0	0	0	0	0	0	0	2	0	0	1	0	0	0	0	0	0	0	0	0
NANT_ECOSM (+8)	0	0	0	0	3	1	1	0	0	0	0	0	0	0	0	0	0	0	0	0
CSIE_ECOLI	2	0	0	0	0	0	0	0	0	0	0	0	0	0	3	0	0	0	0	0
RBFA_ECO24 (+20)	2	0	0	0	0	0	0	0	0	0	0	0	3	1	0	0	0	0	0	0
FADE_ECOLI	0	0	0	0	2	0	0	0	0	0	0	0	0	0	0	0	0	0	0	0
SPEB_ECO24 (+10)	0	0	0	0	0	0	0	2	0	0	0	1	0	0	0	0	0	0	0	0
PROB_ECO24 (+20)	2	0	0	0	0	0	0	0	0	0	0	0	1	0	0	0	0	0	0	0
YCAP_ECOLI	0	0	0	0	0	0	0	2	0	0	0	0	0	0	0	0	0	0	0	0

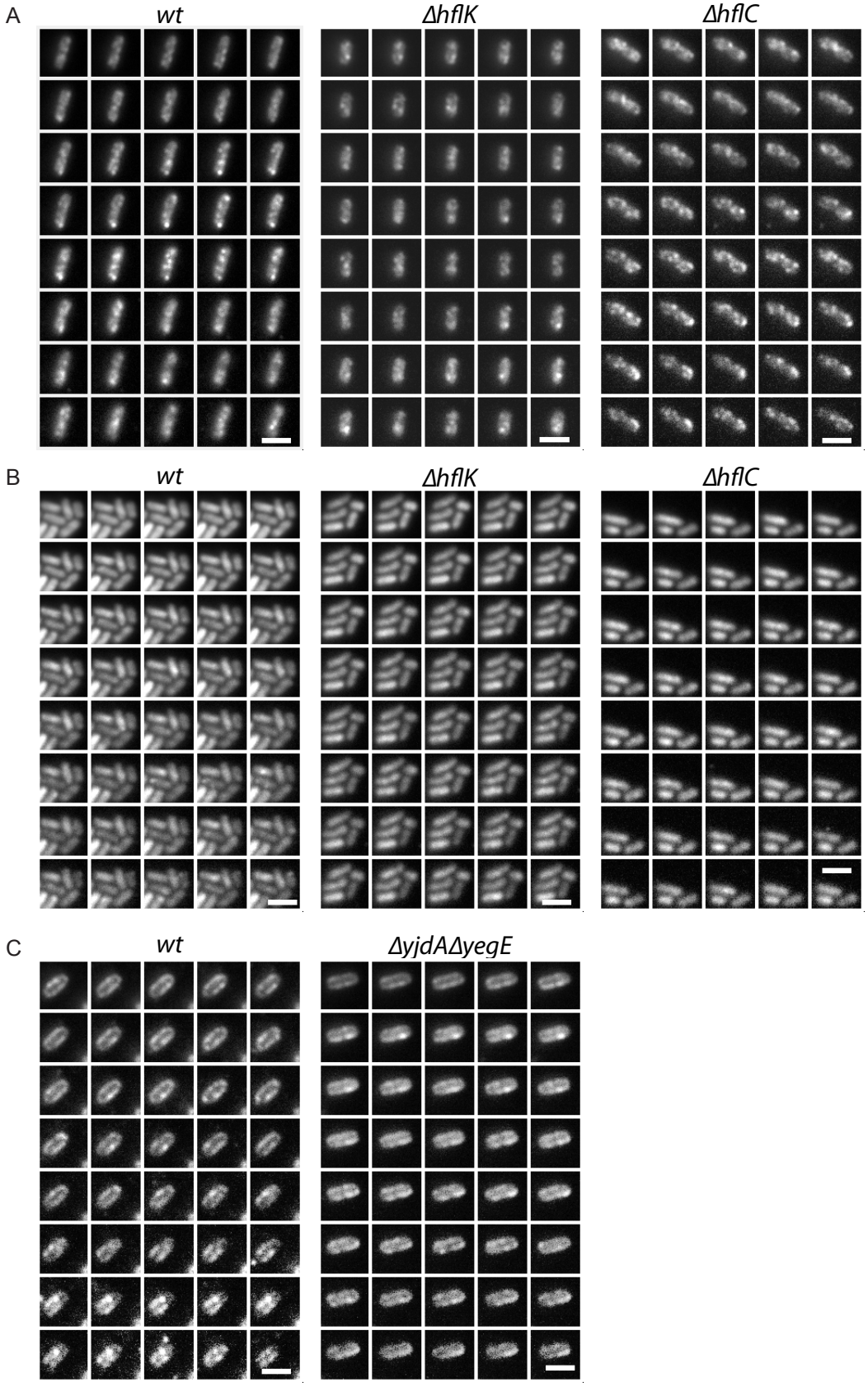

Fig. A.25. Localization of YegE, YjdA and HflKC over time:
TIRF microscopy time-lapse of plasmid-encoded YFP-fusions of YegE and YjdA and mCherry-HflKC W3110^{RH}. Cultures were sampled at OD_{600} 0.6 and images were taken at 2 fps for 20 sec.
(A) Localization of YegE-YFP in W3110^{RH} wild-type, Δ*hflK* and Δ*hflC*.
(B) Localization of YjdA-YFP in W3110^{RH} wild-type, Δ*hflK* and Δ*hflC*.
(C) Localization of mCherry-HflKC in W3110^{RH} wild-type and Δ*yjdA*Δ*yegE*.
Scalebar: 2 μm.

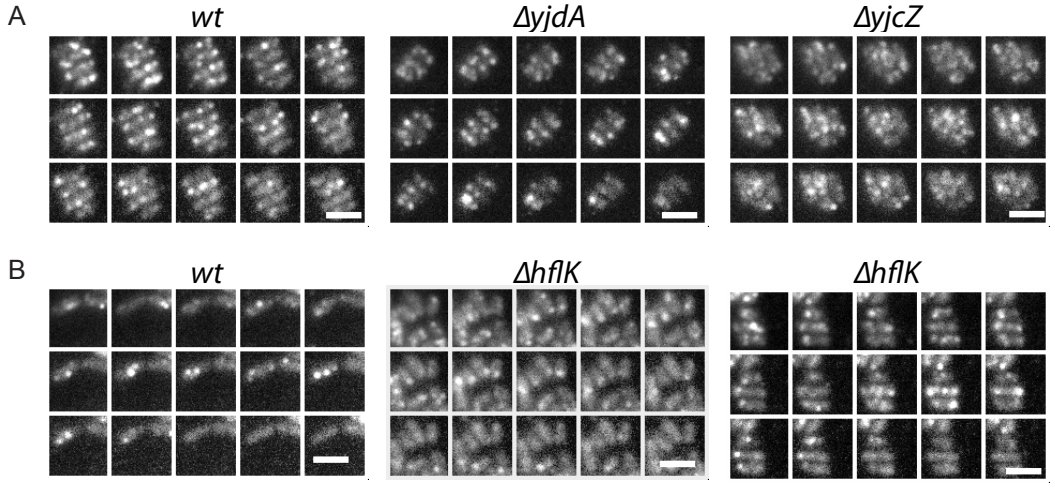

Fig. A.26. Localization of YegE over time:
TIRF microscopy time-lapse of genomic YFP-fusions of YegE in W3110^{RH}. Cultures were sampled at OD_{600} 1.7 and images were taken at 2 fps.
(A) Localization of YegE-YFP in W3110^{RH} wild-type, Δ*yjdA* and Δ*yjcZ*. Exposure time was 200 msec.
(B) Localization of YegE-YFP in W3110^{RH} wild-type, Δ*hflK* and Δ*hflC*. Exposure time was 500 msec.
Scalebar: 2 μm.

B. SUPPLEMENTARY MATERIAL

B.1 Chemicals and consumables

Tab. B.1. Chemicals

Name	Company
1 Kb Plus DNA Ladder	Invitrogen
α-methyl-DL-aspartic acid (MeAsp)	Sigma-Aldrich
Acetic acid	Merck
Agar bacteriology	Applichem
Agarose electrophoresis grade	Invitrogen
Ammoniumpersulfate	Roth
Ammonium sulphate	Applichem
Ampicillin	Applichem
β-mercaptoethanol	Applichem
Bacto tryptone	Difco
Bacto yeast extract	Difco
Bromphenol blue	Applichem
Calcium chloride	Roth
Casein hydrolysate (acid)	Oxoid Microbiology products (Thermo Fisher)
Chloramphenicol	Applichem
Coomassie Brilliant Blue F-250	Applichem
Coomassie R250	Applichem
Congo red	Sigma-Aldrich
Cover slips 46x24 mm, 1.5	Assistent, Glaswarenfabrik Karl Hecht GmbH & Co KG
Crystal violet	Merck
Cuvettes for spectrometry	Sarstedt
D-(+)glucose	Sigma-Aldrich
D-ribose	Sigma-Aldrich
di-Potassium hydrophosphate	Roth
di-Sodium hydrophosphate	Roth
DMF (Dimethylformamid)	Sigma
dNTPs	Invitrogen
EDTA	Merck
Ethanol	Applichem
GenElute^{TM} HP Plasmid Miniprep Kit	Sigma-Aldrich
GFP-Trap®_A beads	Chromotek
Glycerol	Roth
Glycine	Applichem
Hydrochloric acid	Applichem
IPTG	Roth

Continued on next page

continued from previous page

Name	Company
Isopropanol	J.T. Baker
Kanamycin sulphate	Applichem
Lactic acid	Sigma-Aldrich
L-arabinose	Sigma-Aldrich
L-methionine	Sigma-Aldrich
L-serine	Sigma-Aldrich
Lysozyme	Sigma-Aldrich
Magnesium chloride	Merck
Magnesium sulfate	Merck
Microscopy slides 76x26 mm	Thermo Scientific
Midori Green Advanced strain	Nippon Genetics Europe GmbH & Biozym
Methanol	J.T. Baker
α-methyl-D,L-aspartic acid	Sigma
Milk powder, non fat	Applichem
Na-Salicylate	Sigma-Aldrich
Nitrocellulose Hybond-ECL. 0.2 μm	GE Healthcare
Nonidet P-40	Sigma
NucleoSpin®Gel and PCR Clean-up kit	Macherey-Nagel
Pageruler Prestained Protein Ladder	Fermentas
Poly-L-lysine	Sigma-Aldrich
Polyethylenglycol	Sigma-Aldrich
Potassium chloride	Applichem
Potassium di-hydrogen phosphate	Applichem
Di-potassium hydrogen phosphate	Applichem
Protease-inhibitor cocktail complete EDTA-free	Roche
Rotiphorese Gel 30 (Acrylamide mix)	Roth
SDS (Sodium dodecylsulfate)	Applichem
Sodium citrate	Applichem
Sodium chloride	Applichem
Sodium hydroxide	Applichem
Streptomycin sulphate	Applichem
Sulfuric acid	Sigma
TEMED	Applichem
Tris	Roth
Tween 20	Roth
Whatman paper	Whatman GmbH
X-gal (5-bromo-4-chloro-3-indolyl-β-D-galacto-pyranoside)	Bioline
Xylene cyanol	Applichem

B.2 Oligonucleotides

All oligonucleotides used in this work are listed in table B.2. If not otherwise stated, reference of oligonucleotides is this work.

Tab. B.2. Primer

Name	Description	Restriction site	Sequence
VM15	*yjcZ* upstream	NcoI	gagagaCCATGGtgACCAAGACGTTACTTGAC
VM16	*yjcZ* downstream	Bgl II	gagagaAGATCTCGCCAAATTTACAGA GAAGAT
VM17	*yjcZ* upstream	Bgl II	gagagaAGATCTatgACCAAGACGTTACTTG
VM18	*yjcZ* downstream	XbaI	gagagaTCTAGATTACGCCAAATTTAC AGAGAAG
VM19	*yjdA* upstream	NcoI	gagagaCCATGGTGTACACACAGACC CTGTATG
VM20	*yjda* downstream	BamHI	gagagaGGATCCATATCGTTCTGCCGT GAAAAGT
VM33	*trg* upstream to check KO		GAGAGACCATGGTGAATACAACTC CCTCACAG
VM34	*trg* downstream to check KO		GAGAGAGGATCCCACCGTAGC GAAACTAACTG
VM78	*yegE* upstream, to check genomic *yegE-yfp* fusion		GTAGCTTCAGCGATC
VM79	*yjdA* upstream, to check genomic *yjdA-yfp* fusion		GCTGGTTGAATCAGC
VM84	*ycgR* upstream to check KO		GTTAACTGTGACCGATAAACC
VM85	*ycgR* downstream to check KO		GATGCTGACGAGTTCCTCGA
VM91	*yjdA* upstream for YjdA T103D mutation		CGTAATCGCCCAATGgacGCGCTG
VM92	*yjdA* downstream for YjdA T103D mutation		TAAGCGTCGGCAGCGCgtcCATTG
VM93	*yegE* upstream to check KO		gagagaGATGTTAGGAAGGGGGCGACGAAGC
VM94	*yegE* downstream to check KO		gagagaGCTTTGCGTGGCTGGCAGGCGAAAG
VM95	*yjdA* upstream to check KO		gagagaGACGACGATCGTTTTCATTTG
VM96	*yjdA* downstream to check KO		gagagaGATCTGCGTCAGTGCCAGATGAC
VM97	*yjcZ* upstream to check KO		gagagaGAGCATTAAGCGCAGAAGTCG
VM98	*yjcZ* downstream to check KO		gagagaCAGCATAGCTTTCCTCGCAGAG
VM99	*yhjH* upstream to check KO		gagagaGACATAGTCGTGAACCTGATC
VM100	*yhjH* downstream to check KO		gagagaCAGATCGCCACGGATAGCGAAC
VM103	*csgA* upstream to check KO		gagagaGGTTGTTGCGCAAGAAGGTAG
VM104	*csgA* downstream to check KO		gagagaCAAAGCAATGGGTTGATTAGCAG
VM105	*pgaA* upstream to check KO		gagagaGATCCTCATCATTGGAATGG
VM106	*pgaA* downstream to check KO		gagagaGCTTCACGAATTTGAGCAATAC
VM107	*wcaF* upstream to check KO		gagagaCGTTATGACCTGGAATATAAAG
VM109	*fliC* upstream to check KO		gagagaGACCCGACTCCCAGCGATG
VM110	*fliC* downstream to check KO		gagagaGAGTTATCGGCATGATTATCC
VM115	*cheA* upstream to check KO		gagagaCTGCCGATCGGGCCAATGCATC
VM116	*cheA* downstream to check KO		gagagaCGAGATTCAGGACGATAACTAC
VM117	*cheB* upstream to check KO		gagagaCATGAAGGGCTGGTACGCGTGC
VM118	*cheB* downstream to check KO		gagagaCGCTTCTGCAGTCACCATTAAC
VM119	*cheR* upstream to check KO		gagagaCGTGAACGACATTATGGGAG
VM120	*cheR* downstream to check KO		gagagaCAGCTCCAGCGCGCGCAGCGTG
VM121	*chew* upstream to check KO		gagagaCTGTGGAAAGTGTTCAACGTC
VM122	*chew* downstream to check KO		gagagaGCTCTTCTGGCTATGGTGAAGG

Continued on next page

continued from previous page

Name	Description	Restriction site	Sequence
VM123	*cheY* upstream to check KO		gagagaCATCGGCCTTCGGTAGATGTG
VM124	*cheY* downstream to check KO		gagagaCAGTCATCCCAACGTTGGGTTAAC
VM125	*cheZ* upstream to check KO		gagagaGGCGTCGACGCTCTCAATAAG
VM126	*cheZ* downstream to check KO		gagagaGGTGAGGTGTGGGGGCTTCTG
VM127	*cheA* upstream with P1 for gene deletion		ACCGGTCATATTGTTACCTTTTTA CTCATTCAGGCGGCGGTGTTC GCCATATTCCGGGGATCCGTCGACC
VM128	*cheA* downstream with P2 for gene deletion		ACAGGTCAGTGTTCCCACAATG CCATCAGCCGAACCGAGGTGACAGC GTGTGTAGGCTGGAGCTGCTTCG
VM129	*yjdA* upstream for YjdA K82A mutation		ACCATGAAAGCAGGGgcaTCAACC
VM130	*yjdA* downstream for YjdA K82A mutation		CATTAATGGTGGTTGAtgcCCCTG
VM165	*yegE* downstream, complementary to Vic21 (5x linker)		tccgcctccgcctccGTTAATCGCGAAATAACTAC
VM166	*cfp* downstream	HindIII	gagagaaagcttTTACTTGTACAGCTCGTCC
VM169	*yddV* upstream to check KO		CAGTTGAAGAGTGCGATGG
VM170	*yddV* downstream to check KO		CATCGGTTAGCTTCATGATTAC
VM181	*yedQ* upstream to check KO		GGATCACATCCGGCCTGGTG
VM182	*yedQ* downstream to check KO		GATTGTGAAAGGGCTAAATC
VM185	*yfiN* upstream to check KO		CCGAACAAAATACCGAGTGC
VM186	*yfiN* downstream to check KO		CAGTAAATCCATAAGATTGC
VM201	*yjdA* upstream with P1 for gene deletion		ATCTGGCTAAATAAAATAACAAAAT TTGCTTTAAGGAAGAATTTTCTatgA TTCCGGGGATCCGTCGACC
VM202	*yjdA* downstream with P2 for gene deletion		GCGACCGGGGCCGTCAAGTAAC GTCTTGGtcaATATCGTTCTGCCGT GAATGTAGGCTGGAGCTGCTTCG
VM203	*yjcZ* upstream with P1 for gene deletion		CAGCTGTTACGCGATGATATTC AAACACTTTTCACGGCAGAACGAT AttgATTCCGGGGATCCGTCGACC
VM204	*yjcZ* downstream with P2 for gene deletion		GTTTAGGACTCATTGATGTAAC TGATTATttaCGCCAAATTTACAG AGAATGTAGGCTGGAGCTGCTTCG
VM205	*yegE* upstream with P1 for gene deletion		AACACAGAAACGAATACTGGCGA CCAGGTCTTGCGGATAAAGCGGTA atgATTCCGGGGATCCGTCGACC
VM206	*yegE* downstream with P2 for gene deletion		CGTCGCATCAGGCGATGGGGAAGCA CGCCtcaGTTAATCGCGAAATAA CTTGTAGGCTGGAGCTGCTTCG
VM207	*ycgR* upstream with P1 for gene deletion		ACTTGAGCAGGCACTGGACGC GATGTAAAtcaATTCCGGGGA TCCGTCGACC
VM208	*ycgR* downstream with P2 for gene deletion		TGTGACCGATAAACCAAAGAC AGTTTGTCAGTCAGGAGTTTTTGC gtgTGTAGGCTGGAGCTGCTTCGCC
VM209	*yhjH* upstream with P1 for gene deletion		TAGTCCAGCCAGGCGGAAAATGA GGCAGCttaTAGCGCCAGAACCG CCGTATTCCGGGGATCCGTCGACC
VM210	*yhjH* downstream with P2 for gene deletion		CTTTGTCGAGTCCGGGCAGCAT CACTTTTAAACACAGGACATCTTTG atgTGTAGGCTGGAGCTGCTTCG
VM211	*fliC* upstream with P1 for gene deletion		GTCAGTCTCAGTTAATCAGGTTA CAACGAttaACCCTGCAGCAGAG

Continued on next page

continued from previous page

Name	Description	Restriction site	Sequence
			ACAGATTCCGGGGATCCGTCGACC
VM212	*fliC* downstream with P2 for gene deletion		GGAAACCCAATACGTAATCAACGA CTTGCAATATAGGATAACGAATC atgTGTAGGCTGGAGCTGCTTCG
VM213	*motA* upstream with P1 for gene deletion		GACGACAATAATCGGATGCGCTT GATTCTtcaTGCTTCCTCGGTTGT CGTATTCCGGGGATCCGTCGACC
VM214	*motA* downstream with P2 for gene deletion		CTGACGACTGAACATCCTGTCAT GGTCAACAGTGGAAGGATGATGTC gtgTGTAGGCTGGAGCTGCTTCG
VM215	*cheZ* upstream with P1 for gene deletion		CGTGGTCACGCCACATCAGGCAA TACAAAtcaAAATCCAAGACTATCC AAATTCCGGGGATCCGTCGACC
VM216	*cheZ* downstream with P2 for gene deletion		AAAACTCAACAAAATCTTTGAGA AACTGGGCATGTGAGGATGCGACT atgTGTAGGCTGGAGCTGCTTCG
VM239	upstream for *wzxc* promoter	XhoI	GAGAGActcgagAGTTTATCAATGT GCTGACC
VM240	downstream for *wzxc* promoter	BamHI	GAGAGAggatccACCAGCCCGAGG CCGATGATG
VM241	upstream for *pga* promoter	XhoI	GAGAGActcgagTAGTCTTTTTCCA TAAAGCTACAC
VM242	downstream for *pga* promoter	BamHI	GAGAGAggatccCAATTTGGTTA TTGCTGAGTGCTG
VM245	upstream for *csgD* promoter	XhoI	GAGAGActcgagGCGTTACGATGG AAAGTATGTC
VM246	downstream for *csgD* promoter	BamHI	GAGAGAggatccGATACGCAG CTTATTCAGGATC
VM250	upstream for amplification of synthetically synthesized RBS-*sfgfp*	BamHI	gagagaGGATCCACAACTTAAGGAG GTATTCATGTC [1]
VM251	*sfgfp* downstream	SbfI	GAGAGAcctgcaggTTAAGAACCTT TGTACAGTTCG
VM259	*yjdA* upstream with ATG as start for BACTH (pKNT25 and pUT18)	PstI	GAGAGActgcagcGTGTACACACA GACCCTGTATG
VM260	*yjdA* downstream without STOP, with 5xGlx linker for BACTH (pKNT25 and pUT18)	BamHI	GAGAGAggatccccATATCGTTCTGCCG TGAAAAGT
VM261	*yjdA* upstream with linker and GTG as start for BACTH (pKT25 and pKT25)	PstI	GAGAGActgcagGAGGAGGAGGAGGA gTGTACACACAGACCCTGTATG
VM262	*yjdA* upstream with linker and GTG as start for BACTH (pUT18C)	PstI	GAGAGActgcagGGGAGGAGGAGG AGGAgTGTACACACAGACCCTGTATG
VM263	*yjdA* downstream with stop for BACTH (pUT18C)	BamHI	gagagaGGATCCtcaATATCGTTCTGCCGT GAAAAGT
VM264	*yegE* upstream with GTG as start for BACTH (pKTN25)	PstI	GAGAGActgcagcGTGAGCAAACAATCA CAGCATG
VM265	*yegE* downstream, no Stop, for BACTH (pKTN25)	KpnI	GAGAGAggtaccctGTTAATCGCGAAAT AACTAC
VM266	*yegE* upstream with 5x Gly linker for BACTH (pKT25)	PstI	GAGAGActgcagGAGGAGGAGG AGGAgTGAGCAAACAATCACAGCATG
VM267	*yegE* downstream with STOP for BACTH (pKT25)	KpnI	GAGAGAggtaccTCAGTTAATCGC GAAATAACTAC
VM268	*hflK* upstream with 5x Gly linker for BACTH (pUT18C)	PstI	GAGAGActgcagGGGAGGAGGAGGAGGA gtgGCGTGGAATCAGCCCGGTAATAAC

Continued on next page

[1] ACAACTTAAGGAGGTATTC is strong RBS [195]

continued from previous page

Name	Description	Restriction site	Sequence
VM269	*hflC* downstream with STOP for BACTH (pUT18C)	BamHI	gagagaGGATCCttaACGCGTTGCGGA AGTCGGCGTCAAGTCGGCGTC
VM272	*hflK* upstream to check KO		gagagaGGTGGCGCAGCATACATTGCGTC
VM273	*hflK* downstream to check KO		gagagaAATCGCTGATGCGCCATTTGATG
VM274	*hflC* upstream to check KO		gagagaTACTCGCGAGCGTCTGTATATCG
VM275	*hflC* downstream to check KO		gagagaCAATCGTTTTCCTCAACATGTAG
VM276	*aer* upstream to check KO		gagagaGCTATCTGTTAACATTTGTTG
VM277	*aer* downstream to check KO		gagagaGGATTTACGCGTCAACCAGAGC
VMseq1	*yegE* sense sequencing primer, binds at pos. 2051		ATGATGCACTGACGCATC
VMseq2	*yegE* antisense sequencing primer, binds at pos. 2141		TGTCGCTGATGTGTACTG
VMseq3	*yegE* antisense sequencing primer, binds at pos. 1420		CCTGCCAGTTCGGTTTGAT
VMseq4	*yegE* sense sequencing primer		CCTGCACATTACGCTTGA
VMseq8	pUA66 antisense sequencing primer		CAAACTAGCAACACCAGAAC
VMseq9	*yegE* sense sequencing primer binds at pos. 1701		CGTGGTCTGTATTGATATG
VMseq10	*yjdA* sense sequencing primer, binds at pos. 1338		CGCTTGTGAACAATTGCG
VMseq11	*yjdA* sense sequencing primer, binds at pos. 985		CAGATATTTCCGGTGTCGTCG
VMseq12	*yjdA* sense sequencing primer, binds at pos. 406		CAACAGCGCCTGCGTGATTGC
hflKC	*hflKC* sequencing primer, binds approx. at pos 580		GGTAAATACACCATGGACCG
pUT18 fw	pUT18 and pKNT25 sequencing primer		CAGCTGGCACGACAGGTTTC
pUT18 rev	pUT18 sequencing primer		GTCGCCGTCGTAGCGGAACTG
pUT18C fw	pUT18C sequencing primer		CTACGAGAACCGTGCATACG
pUT18C rev	pUT18C sequencing primer		ACAGCTTGTCTGTAAGCGGATG
pKT fw	pKT25 sequencing primer		GCAATGCCGCCGGTATTCCAC
pKT rev	pKT25 sequencing primer		GATCGGTGCGGGCCTCTTCG
pKNT rev	pKNT25 sequencing primer		GTGGAATGGGGGTTGACCAG
OB14_2	*gfp* upstream from O. Besharova	KpnI	TGAGGTACCACAACTTAAGGAGGTATTC ATGGTGAGCAAGGGCGAGGAG [1]
MF30d	*gfp* downstream from M. Fischer	HindIII	GAGAAAGCTTTTACTTGTACAGCTCGT
Linda10a	*motA* upstream from L. Lovdok to check KO		CGCGCGTCTAGACCTGACGACTGAACATCCT
DK5a	*tar* upstream from D. Kentner to check KO		ATGCCATGGGTATGATTAACCGTATCCGCG
DK6a	*tsr* upstream from D. Kentner to check KO		ATGCCATGGGTATGTTAAAACGTAT CAAAATTG
Eri121	K1 primer from E. Sommer[2]		CAGTCATAGCCGAATAGCCT
Eri122	K2 primer from E. Sommer[2]		CGGTGCCCTGAATGAACTGC
yegE-RBS-pDK66-f	*yegE* upstream from H. Li	SpeI	ACTAGTGAAGGAGTGTGCCAT GAGCAAACAATCACAGCATG
yegE-pDK66-r	*yegE* downstream from H. Li	SacI	aagcacGAGCTCGTTAATC GCGAAATAACTACTATTC
Vic21[3]	*yfp/cfp* fw primer with 5x Gly linker		GGAGGCGGAGGCG GAGTGGTGAGCAAGGGCGAGGAG
Vic66	*cfp/yfp* antisense sequencing primer		GGTCAGCTTGCCGTAGGTGGC

Continued on next page

[2] sequence from [183]
[3] all Vic-primer are from V. Sourjik

continued from previous page

Name	Description	Restriction site	Sequence
Vic121	sense for pBAD sequencing		TTTATCGCAACTCTCTACTG
Vic122	sense for pBAD sequencing		CTGATTTAATCTGTATCAGG
Vic131a	sense for pTrc sequencing		CGCACTCCCGTTCTGGATAA
Vic131	sense for pTrc sequencing		ATGTGTGGAATTGTGAGCGG
Vic132	antisense for pTrc sequencing		CTGATTTAATCTGTATCAGG

B.3 Plasmids

All plasmids used in this work are listed in table B.3. If not otherwise stated, reference of plasmids is this work.

Tab. B.3. Plasmids

Name	Res.	Vector	Insert	Comment
pVM13	Amp	pTrc99a-RBS	*yegE-yfp*	PCR *yegE* with SacI and SpeI sites, cloning into pDK66; primer yegE-RBS-pDK66-f and yegE-pDK66-r
pVM14	Amp	pTrc99a	*cfp-yjcZ*	PCR *yjcZ* with BglII/XbaI into pDK2, PCR with primer VM17/VM18
pVM15	Kan	pBAD-DK-Kan	*cfp-yjcZ*	Subloned *cfp-yjcZ* from pVM14 into pDK6 with NcoI/XbaI
pVM17	Amp	pTrc99a-RBS	*yjcZ-cfp*	PCR *yjcZ* with NcoI/BglII sites, cloning into pDK113; primer VM15/VM16
pVM18	Kan	pBAD-DK-Kan	*yjcZ-cfp*	Subcloned *yjcZ-cfp* from pVM17 into pDK6 with NcoI/XbaI
pVM38	Amp	pTrc99a-RBS	*yjdA T103D-yfp*	PCR 1 with VM19 and VM92, PCR 2 with VM91 and VM20, then fusion PCR of 1 and 2 with VM19, 20; cloning into pDK112 with NcoI/BamHI
pVM39	Amp	pTrc99a-RBS	*yjdA K82A-yfp*	PCR 1 with VM19 and VM130, PCR 2 with VM129 and VM20, then fusion PCR of 1 and 2 with VM19, 20; cloning into pDK112 with NcoI/BamHI
pVM41	Cam	pBAD33	*yegE-cfp*	PCR of *yegE* with RBS-pDK66-yegE-f and VM165, PCR of CFP with Vic121, VM166; then fusion PCR of *yegE* and *cfp* with RBS-pDK66-yegE-f and VM166, cloned into pBAD33 with SpeI (XbaI) and HindIII
pVM42	Amp	pTrc99a	RBS2-*gfp*	PCR with primer OB14 and MF30;new cloning vector with strong RBS [4], has GFPA206K
pVM47	Kan	pUA66	Promotor *wzxc*	PCR with VM239, VM240, digest with XhoI and BamHI
pVM48	Kan	pUA66	Promotor *pgaA*	PCR with VM241, VM242, digest with XhoI and BamHI
pVM49	Kan	pUA66	Promotor *csgD*	PCR with VM245, VM246, digest with XhoI and BamHI
pVM53	Kan	pUA66	Promotor *pgaA*	cut out RBS and GFPmut2 from pVM48 and inserted RBS2-sfGFP with *E.coli* codon usage with BamHI/SbfI
pVM55	Kan	pUA66	Promoter *wzxc*	cut out promoter from pVM47 with BamHI/ XhoI and cloned into pVM54
pVM65	Kan	pKNT25	*yjdA-T25*	PCR with VM259 and VM260, digest with PstI, BamHI
pVM66	Kan	pKT25	*T25-yjdA*	PCR with VM261 and VM20, digest with PstI, BamHI
pVM67	Amp	pUT18	*yjdA-T18*	PCR with VM259 and VM260, digest with PstI and BamHI
pVM68	Amp	pUT18C	*T18-yjdA*	PCR with VM262, VM263, digest with PstI and BamHI
pVM69	Kan	pKNT25	*yegE-T25*	PCR with VM264, VM265, digest with

Continued on next page

[4] ACAACTTAAGGAGGTATTC, RBS from [195]

continued from previous page

Name	Res.	Vector	Insert	Comment
				PstI, KpnI
pVM70	Kan	pKT25	*T25-yegE*	PCR with VM266, VM267,digest with PstI, KpnI
pVM71	Amp	pUT18C	*T18-hflK-hflC*	PCR with VM268, VM269, digest with PstI, BamHI
pVM76	Kan	pKNT25	*yjdA T103D-T25*	PCR with VM259 and VM260 (template pVM38), digest with PstI, BamHI
pVM77	Kan	pUT18C	*T18-yjdA T103D*	PCR with VM262 and VM263 (template pVM38), digest with PstI, BamHI
pKT25-zip	Kan	pKT25	leucine zipper	received from E. Lacanna, MPI Marburg; REF: EUROMEDEX EUP-25Z
pUT18C-zip	Amp	pUT18C	leucine zipper	received from E. Lacanna, MPI Marburg; REF: EUROMEDEX EUP-18Z
pKNT25	Kan	pKNT25		received from E. Lacanna, MPI Marburg; REF: EUROMEDEX EUP-25N
pKT25	Kan	pKT25		received from E. Lacanna, MPI Marburg; REF: EUROMEDEX EUP-25C
pUT18	Amp	pUT18		received from E. Lacanna, MPI Marburg; REF: EUROMEDEX EUP-18N
pUT18C	Amp	pUT18C		received from E. Lacanna, MPI Marburg; REF: EUROMEDEX EUP-18C
pKD13-YjdA-YFP	Kan	pKD13 derivative		received from H. Li; for recombination of *yjdA-yfp*
pKD13-YegE-YFP	Kan	pKD13 derivative		received from H. Li; for recombination of *yegE-yfp*
pVS910	Kan, Amp	pKD13 derivative		received from J. Winkler, ZMBH Heidelberg
pVS942	Cam	pKD46		λ Red genes; [183]
pVS456	Cam	pACBSR		λ Red genes, I-SceI; [185]
pVS473	Amp	pCP20		FLP recombinase; [184]
pVS197	Cam	pBAD33		[196]
pVS198	Amp	pTrc99a		[197]
166-mCh-hflKC	Amp	pTrc99a	mCherry-*hflk-hflC*	received from A. Pollard
pVS130	Amp	pTrc99a	*ecfp*A206K	received from V. Sourjik
pVS147	Amp	pTrc99a	*eyfp*A206K	received from V. Sourjik
pUA66	Kan	pUA66	*gfpmut2*	[198]
pOB2	Amp	pTrc99a	*mCherry*	strong RBS [3]
				received from O. Besharova
pHL14	Kan	pBAD-DK-Kan	*motA-cfp*	received from H. Li, [146]
pHL55	Amp	pDK4 [191]	*yfp-ycgR*	received from H. Li, [146]
pHL18	Amp	pDK66	*fliF-yfp*	received from H. Li
pDK2	Amp	pTrc99a	*ecfp*A206K	eCFP-backlinker; [191]
pDK6	Kan	pBD-DK-Kan	*ecfp*A206K	eCFP-backlinker; received from D. Kentner
pDK66	Amp	pTrc99a-RBS	*eyfp*A206K	pTrc-RBS-linker-YFP; received from D. Kentner; [191]
pDK112	Amp	pTrc99a-RBS	*cheB*(1-134)-GTG-*yfp*	received from D. Kentner
pDK113	Amp	pTrc99a-RBS	*cheB*(1-134)-GTG-*cfp*	received from D. Kentner
pVS18	Amp	pTrc99a	*cheY-eyfp*	received from V. Sourjik
YFP-YjdA-pDK4	Amp	pDK4	*yfp-yjdA*	received from H. Li
YjdA-YFP-pDK66	Amp	pDK66	*yjdA-yfp*	received from H. Li
YjcZ-YFP-pDK66	Amp	pDK66	*yjcZ-yfp*	received from H. Li

B.4 Strains

Tab. B.4. Strains

Name	Background	Relevant genotype	Comment	Reference
W3110		*wild type*, *rpoS396(Am)*		from G. Kramer, ZMBH Heidelberg; [138]
W3110^{RH}		*wild type*		from R. Hengge, HU Berlin; [138]
AR3110		*bcsQ*(TTG)	cellulose producing	from R. Hengge, HU Berlin; [27]
HCB33	RP437	*wild type*		from V. Sourjik; [199]
BTH101		F$^-$, *cya-99*, Strp^R	strain for EUROMEDEX BACTH assay	from E. Lacanna MPI Marburg
DH5α		F$^-$		Invitrogen, Karlsruhe; [200]
VM5	W3110	Δ*yjda*::Kan	P1 from Keio	this work
VM6	W3110	Δ*yegE*::Kan	P1 from Keio	this work
VM8	W3110	Δ*yhjH*::Kan	P1 from Keio	this work
VM21	W3110	Δ*cheY*::Kan	P1 from Keio	this work
VM22	W3110	Δ*yjcZ*::Kan	P1 from Keio	this work
VM24	W3110	Δ*fliC*::Kan	P1 from Keio	this work
VM28	W3110	Δ*yegE*::Frt	VM6 Kan^S	this work
VM35	W3110	Δ*fliC*::Frt	VM24 Kan^S	this work
VM37	W3110	Δ*yjcZ*::Frt	VM22 Kan^S	this work
VM38	W3110	Δ*yhjH*::Frt	VM8 Kan^S	this work
VM39	W3110	Δ*yjdA*::Frt	VM5 Kan^S	this work
VM76	W3110	Δ*trg*::Kan	P1 from Keio	this work
VM89	W3110	Δ*cheA*::Kan	P1 from Keio	this work
VM94	W3110	Δ*yjcZ*::Kan	P1 from Keio	this work
VM100	W3110	Δ*cheB*::Kan	P1 from Keio	this work
VM101	W3110	Δ*cheR*::Kan	P1 from Keio	this work
VM102	W3110	Δ*cheW*::Kan	P1 from Keio	this work
VM103	W3110	Δ*cheZ*::Kan	P1 from Keio	this work
VM108	W3110	Δ*cheY*::Frt	VM21 Kan^S	this work
VM109	W3110	Δ*trg*::Frt	VM76 Kan^S	this work
VM110	W3110	Δ*cheA*::Frt	VM89 Kan^S	this work
VM111	W3110	Δ*cheB*::Frt	VM100 Kan^S	this work
VM112	W3110	Δ*cheR*::Frt	VM101 Kan^S	this work
VM113	W3110	Δ*cheW::Frt*	VM102 Kan^S	this work
VM114	W3110	Δ*cheZ*::Frt	VM103 Kan^S	this work
VM124	W3110	Δ*csgA*::Kan	P1 from Keio	this work
VM125	W3110	Δ*csgA*::Frt	VM124 Kan^S	this work
VM153	W3110	Δ*aer*::Kan	P1 from Keio	this work
VM154	W3110	Δ*tar*::Kan	P1 from Keio	this work
VM155	W3110	Δ*tsr*::Kan	P1 from Keio	this work
VM174	W3110	Δ*aer*::Frt	VM153 Kan^S	this work
VM175	W3110	Δ*tar*::Frt	VM154 Kan^S	this work
VM176	W3110	Δ*tsr*::Frt	VM155 Kan^S	this work
VM194	W3110	Δ*ycgR*::Kan	P1 from Keio	this work
VM195	W3110	Δ*yjdA*::Frt Δ*ycgR*::Kan	P1 from Keio in VM39	this work
VM196	W3110	Δ*yegE*::Frt Δ*ycgR*::Kan	P1 from Keio in VM28	this work
VM197	W3110	Δ*yjcZ*::Frt Δ*ycgR*::Kan	P1 from Keio in VM37	this work
VM198	W3110	Δ*yhjH*::Frt Δ*ycgR*::Kan	P1 from Keio in VM38	this work
VM262	W3110	Δ*cheA*::Kan	KO made with PCR product clone 1	this work
VM263	W3110	Δ*cheA*::Kan	KO made with PCR product clone 2	this work

Continued on next page

continued from previous page

Name	Background	Relevant genotype	Comment	Reference
VM265	W3110	Δ*motA*::Kan	P1 from Keio	this work
VM270	W3110	Δ*cheA*::Frt	VM262 Kan^S	this work
VM271	W3110	Δ*cheA*::Frt	VM263 Kan^S	this work
VM321	W3110	Δ*motA*::Frt	VM265 Kan^S	this work
VM322	W3110^{RH}	Δ*yjdA*::Kan	KO made with PCR product	this work
VM323	W3110^{RH}	Δ*yegE*::Kan	KO made with PCR product	this work
VM325	W3110^{RH}	Δ*yjcZ*::Kan	KO made with PCR product	this work
VM326	W3110^{RH}	Δ*ycgR*::Kan	KO made with PCR product	this work
VM327	W3110^{RH}	Δ*fliC*::Kan	KO made with PCR product	this work
VM328	W3110^{RH}	Δ*cheZ*::Kan	KO made with PCR product	this work
VM329	W3110^{RH}	Δ*motA*::Kan	KO made with PCR product	this work
VM330	AR3110	Δ*yjdA*::Kan	KO made with PCR product	this work
VM331	AR3110	Δ*yegE*::Kan	KO made with PCR product	this work
VM332	AR3110	Δ*yhjH*::Kan	KO made with PCR product	this work
VM333	AR3110	Δ*yjcZ*::Kan	KO made with PCR product	this work
VM335	AR3110	Δ*fliC*::Kan	KO made with PCR product	this work
VM336	AR3110	Δ*cheZ*::Kan	KO made with PCR product	this work
VM337	AR3110	Δ*motA*::Kan	KO made with PCR product	this work
VM348	W3110^{RH}	Δ*yjdA*::Frt	VM322 Kan^S	this work
VM349	W3110^{RH}	Δ*yegE*::Frt	VM323 Kan^S	this work
VM351	W3110^{RH}	Δ*yjcZ*::Frt	VM325 Kan^S	this work
VM352	W3110^{RH}	Δ*ycgR*::Frt	VM326 Kan^S	this work
VM354	W3110^{RH}	Δ*cheZ*::Frt	VM328 Kan^S	this work
VM355	W3110^{RH}	Δ*fliC*::Kan	P1 from VM24	this work
VM360	W3110^{RH}	Δ*yhjH*::Kan	P1 from VM8	this work
VM376	W3110^{RH}	Δ*cheY*::Kan	P1 VM21	this work
VM383	W3110^{RH}	Δ*cheY*::Frt	VM376 Kan^S	this work
VM384	W3110^{RH}	Δ*pgaC*::Kan	P1 from Keio	this work
VM387	W3110^{RH}	Δ*motA*::Frt	VM329 Kan^S	this work
VM388	W3110^{RH}	Δ*fliC*::Frt	VM355 Kan^S	this work
VM389	W3110^{RH}	Δ*yhjH*::Frt	VM360 Kan^S	this work
VM390	W3110	Δ*pgaC*::Kan	P1 from Keio	this work
VM391	W3110^{RH}	Δ*pgaC*::Frt	VM384 Kan^S	this work
VM392	W3110^{RH}	Δ*csgA*::Kan	P1 from Keio	this work
VM425	W3110	Δ*wcaF*::Kan	KO made with PCR product	this work
VM482	W3110^{RH}	Δ*wcaF*::Kan	P1 from VM425	this work
VM536	W3110^{RH}	*yegE-yfp*-Kan	*yegE-yfp* genomic fusion clone 1 made by recombination	this work
VM537	W3110^{RH}	*yegE-yfp*-Kan	*yegE-yfp* genomic fusion clone 2 made by recombination	this work
VM538	W3110^{RH}	Δ*yjdA*::Frt *yegE-yfp*-Kan	*yegE-yfp* genomic fusion clone 1 made by recombination	this work
VM539	W3110^{RH}	Δ*yjdA*::Frt *yegE-yfp*-Kan	*yegE-yfp* genomic fusion clone 2 made by recombination	this work
VM540	W3110^{RH}	Δ*yjcZ*::Frt *yegE-yfp*-Kan	*yegE-yfp* genomic fusion clone 1 made by recombination	this work
VM541	W3110^{RH}	Δ*yjcZ*::Frt *yegE-yfp*-Kan	*yegE-yfp* genomic fusion clone 2 made by recombination	this work
VM563	W3110^{RH}	Δ*yegE*::FrtΔ*yjdA*::Kan	P1 from VM323 in VM348	this work
VM564	W3110^{RH}	Δ*yegE*::FrtΔ*yjcZ*::Kan	P1 from VM323 in VM351	this work
VM565	W3110^{RH}	Δ*yegE*::FrtΔ*yhjH*::Kan	P1 from VM323 in VM389	this work
VM566	W3110^{RH}	Δ*yegE*::FrtΔ*yjdA*::Frt	VM563 Kan^S	this work
VM567	W3110^{RH}	Δ*yegE*::FrtΔ*yjcZ*::Frt	VM564 Kan^S	this work
VM568	W3110^{RH}	Δ*yegE*::FrtΔ*yhjH*::Frt	VM565 Kan^S	this work
VM569	W3110^{RH}	Δ*yhjH*::FrtΔ*yegE*::FrtΔ*yjdA*::Kan	P1 from VM360 in VM566	this work
VM570	W3110^{RH}	Δ*yhjH*::FrtΔ*yegE*::FrtΔ*yjcZ* ::Kan	P1 from VM360 in VM567	this work

Continued on next page

continued from previous page

Name	Background	Relevant genotype	Comment	Reference
VM599	W3110^{RH}	Δ*yhjH*::FrtΔ*yegE*::FrtΔ*yjdA*::Frt	VM569 Kan^{S}	this work
VM600	W3110^{RH}	Δ*yhjH*::FrtΔ*yegE*::FrtΔ*yjcZ* ::Frt	VM570 Kan^{S}	this work
VM606	W3110^{RH}	Δ*yjdA*::FrtΔ*yhjH*::Kan	P1 from VM360 in VM348	this work
VM607	W3110^{RH}	Δ*yjcZ*::FrtΔ*yhjH*::Kan	P1 from VM360 in VM351	this work
VM608	W3110^{RH}	Δ*yjdA*::FrtΔ*yhjH*::Frt	VM606 Kan^{S}	this work
VM609	W3110^{RH}	Δ*yjcZ*::FrtΔ*yhjH*::Frt	VM607 Kan^{S}	this work
VM616	W3110^{RH}	*yegE-yfp*-Frt	*yegE-yfp* genomic fusion (VM536 Kan^{S})	this work
VM617	W3110^{RH}	Δ*yjdA*::Frt *yegE-yfp*-Frt	*yegE-yfp* genomic fusion (VM538 Kan^{S})	this work
VM618	W3110^{RH}	Δ*yjcZ*::Frt *yegE-yfp*-Frt	*yegE-yfp* genomic fusion (VM540 Kan^{S})	this work
VM620	W3110^{RH}	Δ*yhjH*::Kan *yegE-yfp*-Frt	*yegE-yfp* genomic fusion; P1 from VM360 in VM616	this work
VM623	W3110^{RH}	Δ*yhjH*::FrtΔ*yddV*::Kan	P1 from VM295 into VM389	this work
VM625	W3110^{RH}	Δ*yjdA*::FrtΔ*yhjH*::FrtΔ*yddV*::Kan	P1 from VM295 into VM608	this work
VM626	W3110^{RH}	Δ*yjcZ*::FrtΔ*yhjH*::FrtΔ*yddV*::Kan	P1 from VM295 into VM609	this work
VM627	W3110^{RH}	Δ*yhjH*::FrtΔ*yfiN*::Kan	P1 from VM301 into VM389	this work
VM629	W3110^{RH}	Δ*yjdA*::FrtΔ*yhjH*::FrtΔ*yfiN*::Kan	P1 from VM301 into VM608)	this work
VM630	W3110^{RH}	Δ*yjcZ*::FrtΔ*yhjH*::FrtΔ*yfiN*::Kan	P1 from VM301 into VM609	this work
VM631	W3110^{RH}	Δ*yhjH*::FrtΔ*yedQ*::Kan	P1 from VM276 into VM389	this work
VM633	W3110^{RH}	Δ*yjdA*::FrtΔ*yhjH*::FrtΔ*yedQ*::Kan	P1 from VM276 into VM608	this work
VM634	W3110^{RH}	Δ*yjcZ*::FrtΔ*yhjH*::FrtΔ*yedQ*::Kan	P1 from VM276 into VM609	this work
VM687	W3110^{RH}	Δ*ycgR*::FrtΔ*fliC* ::Kan	P1 from VM355 into VM352	this work
VM695	W3110^{RH}	Δ*hflC*::Kan	P1 from Keio	this work
VM697	W3110^{RH}	Δ*hflK*::Kan	P1 from Keio	this work
VM701	W3110^{RH}	Δ*hflC*::Frt	VM695 Kan^{S}	this work
VM703	W3110^{RH}	Δ*hflK*::Frt	VM697 Kan^{S}	this work
VM709	W3110^{RH}	Δ*fliC*::Frt	VM327 Kan^{S}	this work
VM716	W3110^{RH}	Δ*fliC*::Kan *csgBA-STOP-sfgfp dest*	P1 from VM355 in OB37	this work
VM717	W3110^{RH}	Δ*motA*::Kan *csgBA-STOP-sfgfp dest*	P1 from VM329 in OB37	this work
VM719	W3110^{RH}	Δ*fliC* ::Frt *csgBA-STOP-sfgfp dest*	VM716 Kan^{S}	this work
VM720	W3110^{RH}	Δ*motA*::Frt *csgBA-STOP-sfgfp dest*	VM717 Kan^{S}	this work
VM735	W3110^{RH}	Δ*hflK*::Kan	P1 from Keio in *yegE-yfp* (VM616) genomic fusion	this work
VM736	W3110^{RH}	Δ*hflC*::Kan	P1 from Keio in *yegE-yfp* (VM616) genomic fusion	this work
VM737	W3110^{RH}	Δ*hflC*::Frt	VM736 Kan^{S}	this work
OB37	W3110^{RH}	*csgBA-STOP-sfgfp dest*::Kan		from O. Besharova
LL108	W3110^{RH}	Δ*fimA*::Kan		from L. Lagonenko
OB147	W3110^{RH}	Δ*sfmA*::Kan		from O. Besharova
OB153	W3110^{RH}	Δ*ybgP*::Kan		from O. Besharova
OB154	W3110^{RH}	Δ*yraH*::Kan		from O. Besharova
OB155	W3110^{RH}	Δ*yehB*::Kan		from O. Besharova
OB167	W3110^{RH}	Δ*yfaL*::Kan		from O. Besharova
OB168	W3110^{RH}	Δ*ycgV*::Kan		from O. Besharova
flu Kan^{R}	W3110^{RH}	Δ*flu*::Kan		from L. Lagonenko
flu Kan^{S}	W3110^{RH}	Δ*flu*::Frt	flu Kan^{S}	from L. Lagonenko

Bibliography

[1] C. Beloin, A. Roux, and J. M. Ghigo. *Escherichia coli* biofilms. *Current Topics in Microbiology and Immunology*, 322:249–289, 2008.

[2] J W Costerton, P S Stewart, and E P Greenberg. Bacterial biofilms: a common cause of persistent infections. *Science*, 284(5418):1318–1322, 1999.

[3] J W Costerton, Z Lewandowski, D E Caldwell, D R Korber, and H M Lappin-Scott. Microbial biofilms. *Annual Reviews in Microbiology*, 49:711–745, 1995.

[4] M E Davey and G A O'Toole. Microbial biofilms: from ecology to molecular genetics. *Microbiology and molecular biology reviews : MMBR*, 64(4):847–67, dec 2000.

[5] Morten Rybtke, Louise Dahl Hultqvist, Michael Givskov, and Tim Tolker-Nielsen. *Pseudomonas aeruginosa* Biofilm Infections: Community Structure, Antimicrobial Tolerance and Immune Response. *Journal of Molecular Biology*, 427(23):3628–3645, 2015.

[6] James B. Kaper, James P. Nataro, and Harry L. T. Mobley. Pathogenic *Escherichia coli*. *Nature Reviews Microbiology*, 2(2):123–140, 2004.

[7] Luanne Hall-Stoodley, J William Costerton, and Paul Stoodley. Bacterial biofilms: from the natural environment to infectious diseases. *Nature reviews. Microbiology*, 2(2):95–108, feb 2004.

[8] David Davies. Understanding biofilm resistance to antibacterial agents. *Nature reviews. Drug discovery*, 2(2):114–22, feb 2003.

[9] Russell D. Monds and George A. O'Toole. The developmental model of microbial biofilms: ten years of a paradigm up for review. *Trends in Microbiology*, 17(January):73–87, feb 2009.

[10] Urs Jenal and Jacob Malone. Mechanisms of cyclic-di-GMP signaling in bacteria. *Annual review of genetics*, 40:385–407, jan 2006.

[11] Regine Hengge. Principles of c-di-GMP signalling in bacteria. *Nature reviews. Microbiology*, 7(4):263–73, apr 2009.

[12] Ute Römling, Michael Y Galperin, and Mark Gomelsky. Cyclic di-GMP: the first 25 years of a universal bacterial second messenger. *Microbiology and molecular biology reviews : MMBR*, 77(1):1–52, mar 2013.

[13] Ken F Jarrell and Mark J McBride. The surprisingly diverse ways that prokaryotes move. *Nature reviews. Microbiology*, 6(6):466–476, 2008.

[14] Daniel B Kearns. A field guide to bacterial swarming motility. *Nature reviews. Microbiology*, 8(9):634–44, sep 2010.

[15] Salim T. Islam and Tâm Mignot. The mysterious nature of bacterial surface (gliding) motility: A focal adhesion-based mechanism in Myxococcus xanthus. *Seminars in Cell and Developmental Biology*, 46:143–154, 2015.

[16] Berenike Maier and Gerard C L Wong. How Bacteria Use Type IV Pili Machinery on Surfaces. *Trends in Microbiology*, 23(12):775–788, 2015.

[17] George H Wadhams and Judith P Armitage. Making sense of it all: bacterial chemotaxis. *Nature reviews. Molecular cell biology*, 5(12):1024–37, dec 2004.

[18] L A Pratt and R Kolter. Genetic analysis of *Escherichia coli* biofilm formation: roles of flagella, motility, chemotaxis and type I pili. *Molecular microbiology*, 30(2):285–93, oct 1998.

[19] P Genevaux, S Muller, and P Bauda. A rapid screening procedure to identify mini-Tn10 insertion mutants of *Escherichia coli* K-12 with altered adhesion properties. *FEMS microbiology letters*, 142(1):27–30, aug 1996.

[20] George a O'Toole and Roberto Kolter. Flagellar and twitching motility are necessary for *Pseudomonas aeruginosa* biofilm development. *Mol Microbiol*, 30(2):295–304, 1998.

[21] L A Pratt and R Kolter. Genetic analyses of bacterial biofilm formation. *Current opinion in microbiology*, 2(6):598–603, dec 1999.

[22] Mikkel Klausen, Arne Heydorn, Paula Ragas, Lotte Lambertsen, Anders Aaes-Jørgensen, Søren Molin, and Tim Tolker-Nielsen. Biofilm formation by *Pseudomonas aeruginosa* wild type, flagella and type IV pili mutants. *Molecular Microbiology*, 48(6):1511–1524, may 2003.

[23] Mikkel Klausen, Anders Aaes-Jørgensen, Søren Molin, and Tim Tolker-Nielsen. Involvement of bacterial migration in the development of complex multicellular structures in *Pseudomonas aeruginosa* biofilms. *Molecular Microbiology*, 50(1):61–68, aug 2003.

[24] Thomas K Wood, Andrés F González Barrios, Moshe Herzberg, and Jintae Lee. Motility influences biofilm architecture in *Escherichia coli*. *Applied microbiology and biotechnology*, 72(2):361–7, sep 2006.

[25] Emma Tabe Eko Niba, Yoshiaki Naka, Megumi Nagase, Hirotada Mori, and Madoka Kitakawa. A genome-wide approach to identify the genes involved in biofilm formation in *E. coli*. *DNA research : an international journal for rapid publication of reports on genes and genomes*, 14(6):237–46, dec 2007.

[26] Juliane Schmidt, Mathias Müsken, Tanja Becker, Zofia Magnowska, Daniela Bertinetti, Stefan Möller, Bastian Zimmermann, Friedrich W Herberg, Lothar Jänsch, and Susanne Häussler. The *Pseudomonas aeruginosa* chemotaxis methyltransferase CheR1 impacts on bacterial surface sampling. *PloS one*, 6(3):e18184, jan 2011.

[27] D. O. Serra, A. M. Richter, and R. Hengge. Cellulose as an Architectural Element in Spatially Structured *Escherichia coli* Biofilms. *Journal of Bacteriology*, 195(24):5540–5554, 2013.

[28] Melinda D Baker, Peter M Wolanin, and Jeffry B Stock. Signal transduction in bacterial chemotaxis. *BioEssays : news and reviews in molecular, cellular and developmental biology*, 28(1):9–22, jan 2006.

[29] Victor Sourjik and Ned S Wingreen. Responding to chemical gradients: bacterial chemotaxis. *Current opinion in cell biology*, 24(2):262–8, apr 2012.

[30] Ann M. Stock, Victoria L. Robinson, and Paul N. Goudreau. Two-Component Signal Transduction. *Annual Review of Biochemistry*, 69(1):183–215, 2000.

[31] Peter M Wolanin, Peter A Thomason, and Jeffry B Stock. Histidine protein kinases: key signal transducers outside the animal kingdom. *Genome biology*, 3(10):REVIEWS3013, 2002.

[32] J. J. Falke, R. B. Bass, S. L. Butler, S. A. Chervitz, and M. A. Danielson. CHEMOTAXIS : A Molecular View of Signal Transduction by. pages 1–55, 2010.

[33] Linda Turner, WS Ryu, and HC Berg. Real-Time Imaging of Fluorescent Flagellar Filaments. *Journal of Bacteriology*, 182(10):2793–2801, 2000.

[34] Howard C Berg. The Rotary Motor of Bacterial Flagella. *Annual Review of Biochemistry*, 72(1):19–54, 2003.

[35] M Welch, K Oosawa, S Aizawa, and M Eisenbach. Phosphorylation-dependent binding of a signal molecule to the flagellar switch of bacteria. *Proceedings of the National Academy of Sciences of the United States of America*, 90(October):8787–8791, 1993.

[36] A S Toker and R M Macnab. Distinct regions of bacterial flagellar switch protein FliM interact with FliG, FliN and CheY. *Journal of molecular biology*, 273(3):623–634, 1997.

[37] Richard C. Stewart. Kinetic characterization of phosphotransfer between CheA and CheY in the bacterial chemotaxis signal transduction pathway. *Biochemistry*, 36(8):2030–2040, 1997.

[38] Victor Sourjik and Howard C Berg. Binding of the *Escherichia coli* response regulator CheY to its target measured in vivo by fluorescence resonance energy transfer. *Proc Natl Acad Sci USA*, 99(20):12669–12674, 2002.

[39] Victor Sourjik. Receptor clustering and signal processing in *E. coli* chemotaxis. *Trends in microbiology*, 12(12):569–76, dec 2004.

[40] Y Blat and M Eisenbach. Phosphorylation-dependent binding of the chemotaxis signal molecule CheY to its phosphatase, CheZ. *Biochemistry*, 33(4):902–6, feb 1994.

[41] R Zhao, E J Collins, R B Bourret, and R E Silversmith. Structure and catalytic mechanism of the *E. coli* chemotaxis phosphatase CheZ. *Nat Struct Biol*, 9(8):570–575, 2002.

[42] Ganesh S. Anand and Ann M. Stock. Kinetic basis for the stimulatory effect of phosphorylation on the methylesterase activity of CheB. *Biochemistry*, 41(21):6752–6760, 2002.

[43] Mikhail N. Levit and Jeffry B. Stock. Receptor methylation controls the magnitude of stimulus-response coupling in bacterial chemotaxis. *Journal of Biological Chemistry*, 277(39):36760–36765, 2002.

[44] Peter M Merritt, Thomas Danhorn, and Clay Fuqua. Motility and chemotaxis in *Agrobacterium tumefaciens* surface attachment and biofilm formation. *Journal of bacteriology*, 189(22):8005–14, nov 2007.

[45] Kim B Barken, Sünje J Pamp, Liang Yang, Morten Gjermansen, Jacob J Bertrand, Mikkel Klausen, Michael Givskov, Cynthia B Whitchurch, Joanne N Engel, and Tim Tolker-Nielsen. Roles of type IV pili, flagellum-mediated motility and extracellular DNA in the formation of mature multicellular structures in *Pseudomonas aeruginosa* biofilms. *Environmental microbiology*, 10(9):2331–43, sep 2008.

[46] Joshua Armitano, Vincent Méjean, and Cécile Jourlin-Castelli. Aerotaxis governs floating biofilm formation in *Shewanella oneidensis*. *Environmental Microbiology*, 15(11):3108–3118, 2013.

[47] M Ko and C Park. Two novel flagellar components and H-NS are involved in the motor function of *Escherichia coli*. *Journal of molecular biology*, 303(3):371–382, 2000.

[48] Jonathan Frye, Joyce E Karlinsey, Heather R Felise, Bruz Marzolf, Naeem Dowidar, Michael Mcclelland, Kelly T Hughes, T Kelly, Bruz Marzolf, and Kelly T Hughes. Identification of New Flagellar Genes of *Salmonella enterica Serovar* Typhimurium. *Society*, 188(6):2233–2243, 2006.

[49] Ivan Rychlik, Gerald Martin, Ulrich Methner, Margaret Lovell, Lenka Cardova, Alena Sebkova, Mojmor Sevcik, Jiri Damborsky, and Paul A. Barrow. Identification of *Salmonella enterica serovar* Typhimurium genes associated with growth suppression in stationary-phase nutrient broth cultures and in the chicken intestine. *Archives of Microbiology*, 178(6):411–420, 2002.

[50] Hany S Girgis, Yirchung Liu, William S Ryu, and Saeed Tavazoie. A comprehensive genetic characterization of bacterial motility. *PLoS genetics*, 3(9):1644–60, sep 2007.

[51] Dorit Amikam and Michael Y Galperin. PilZ domain is part of the bacterial c-di-GMP binding protein. *Bioinformatics (Oxford, England)*, 22(1):3–6, jan 2006.

[52] Dmitri a Ryjenkov, Roger Simm, Ute Römling, and Mark Gomelsky. The PilZ domain is a receptor for the second messenger c-di-GMP: the PilZ domain protein YcgR controls motility in enterobacteria. *The Journal of biological chemistry*, 281(41):30310–4, oct 2006.

[53] Ute Römling and Dorit Amikam. Cyclic di-GMP as a second messenger. *Current Opinion in Microbiology*, 9(2):218–228, apr 2006.

[54] A. J. Wolfe and K. L. Visick. Get the Message Out: Cyclic-Di-GMP Regulates Multiple Levels of Flagellum-Based Motility. *Journal of Bacteriology*, 190(2):463–475, jan 2008.

[55] Christina Pesavento, Gisela Becker, Nicole Sommerfeldt, Alexandra Possling, Natalia Tschowri, Anika Mehlis, and Regine Hengge. Inverse regulatory coordination of motility and curli-mediated adhesion in *Escherichia coli*. *Genes & development*, 22(17):2434–46, sep 2008.

[56] Alex Boehm, Matthias Kaiser, Hui Li, Christian Spangler, Christoph Alexander Kasper, Martin Ackermann, Volkhard Kaever, Victor Sourjik, Volker Roth, and Urs Jenal. Second messenger-mediated adjustment of bacterial swimming velocity. *Cell*, 141(1):107–16, apr 2010.

[57] Xin Fang and Mark Gomelsky. A post-translational, c-di-GMP-dependent mechanism regulating flagellar motility. *Molecular microbiology*, 76(5):1295–305, jun 2010.

[58] Koushik Paul, Vincent Nieto, William C Carlquist, David F Blair, and Rasika M Harshey. The c-di-GMP binding protein YcgR controls flagellar motor direction and speed to affect chemotaxis by a " backstop brake" mechanism. *Molecular cell*, 38(1):128–39, apr 2010.

[59] Sarah B Guttenplan and Daniel B Kearns. Regulation of flagellar motility during biofilm formation. *FEMS microbiology reviews*, 37(6):849–71, nov 2013.

[60] Nadim Majdalani and Susan Gottesman. The Rcs phosphorelay: a complex signal transduction system. *Annual review of microbiology*, 59:379–405, jan 2005.

[61] Christina Pesavento and Regine Hengge. The global repressor FliZ antagonizes gene expression by Sigma S-containing RNA polymerase due to overlapping DNA binding specificity. *Nucleic Acids Research*, 40(11):4783–4793, 2012.

[62] H. Ogasawara, K. Yamamoto, and A. Ishihama. Role of the Biofilm Master Regulator CsgD in Cross-Regulation between Biofilm Formation and Flagellar Synthesis. *Journal of Bacteriology*, 193(10):2587–2597, may 2011.

[63] Debra W Jackson, Kazushi Suzuki, Lawrence Oakford, Jerry W Simecka, Mark E Hart, and Tony Romeo. Biofilm formation and dispersal under the influence of the global regulator CsrA of *Escherichia coli*. *Journal of bacteriology*, 184(1):290–301, jan 2002.

[64] Johan Timmermans and Laurence Van Melderen. Post-transcriptional global regulation by CsrA in bacteria. *Cellular and Molecular Life Sciences*, 67(17):2897–2908, 2010.

[65] B L Wei, A M Brun-Zinkernagel, J W Simecka, B M Prüss, P Babitzke, and T Romeo. Positive regulation of motility and flhDC expression by the RNA-binding protein CsrA of *Escherichia coli*. *Molecular microbiology*, 40(1):245–56, apr 2001.

[66] Kristina Jonas, Adrianne N Edwards, Roger Simm, Tony Romeo, Ute Römling, and Ojar Melefors. The RNA binding protein CsrA controls cyclic di-GMP metabolism by directly regulating the expression of GGDEF proteins. *Molecular microbiology*, 70(1):236–57, oct 2008.

[67] Xin Wang, Ashok K Dubey, Kazushi Suzuki, Carol S Baker, Paul Babitzke, and Tony Romeo. CsrA post-transcriptionally represses *pgaABCD*, responsible for synthesis of a biofilm polysaccharide adhesin of *Escherichia coli*. *Molecular microbiology*, 56(6):1648–63, jun 2005.

[68] Franziska Mika and Regine Hengge. Small Regulatory RNAs in the Control of Motility and Biofilm Formation in *E. coli* and *Salmonella*. *International journal of molecular sciences*, 14(3):4560–79, jan 2013.

[69] P Ross, H Weinhouse, Y Aloni, D Michaeli, P Weinberger-Ohana, R Mayer, S Braun, E de Vroom, G A van der Marel, J H van Boom, and M Benziman. Regulation of cellulose synthesis in *Acetobacter xylinum* by cyclic diguanylic acid. *Nature*, 325:279–281, 1987.

[70] Ute Römling, Mark Gomelsky, and Michael Y Galperin. C-di-GMP: the dawning of a novel bacterial signalling system. *Molecular microbiology*, 57(3):629–39, aug 2005.

[71] Tilman Schirmer and Urs Jenal. Structural and mechanistic determinants of c-di-GMP signalling. *Nature reviews. Microbiology*, 7(10):724–35, oct 2009.

[72] Ute Römling and Roger Simm. Prevailing concepts of c-di-GMP signaling. *Contributions to microbiology*, 16:161–81, jan 2009.

[73] Erez Mills, Ingrid S Pultz, Hemantha D Kulasekara, and Samuel I Miller. The bacterial second messenger c-di-GMP: mechanisms of signalling. *Cellular microbiology*, 13(8):1122–9, aug 2011.

[74] Chelsea D Boyd and George a O'Toole. Second messenger regulation of biofilm formation: breakthroughs in understanding c-di-GMP effector systems. *Annual review of cell and developmental biology*, 28:439–62, jan 2012.

[75] Ralf Paul, Stefan Weiser, Nicholas C Amiot, Carmen Chan, Tilman Schirmer, Bernd Giese, and Urs Jenal. Cell cycle-dependent dynamic localization of a bacterial response regulator with a novel di-guanylate cyclase output domain. *Genes & development*, 18(6):715–27, mar 2004.

[76] Matthias Christen, Beat Christen, Marc Folcher, Alexandra Schauerte, and Urs Jenal. Identification and characterization of a cyclic di-GMP-specific phosphodiesterase and its allosteric control by GTP. *The Journal of biological chemistry*, 280(35):30829–37, sep 2005.

[77] Anna D Tischler and Andrew Camilli. Cyclic diguanylate (c-di-GMP) regulates *Vibrio cholerae* biofilm formation. *Molecular microbiology*, 53(3):857–69, aug 2004.

[78] Robert P Ryan, Yvonne Fouhy, Jean F Lucey, Lisa C Crossman, Stephen Spiro, Ya-Wen He, Lian-Hui Zhang, Stephan Heeb, Miguel Cámara, Paul Williams, and J Maxwell Dow. Cell-cell signaling in *Xanthomonas campestris*
involves an HD-GYP domain protein that functions in cyclic di-GMP turnover. *Proceedings of the National Academy of Sciences of the United States of America*, 103(17):6712–7, apr 2006.

[79] Robert P Ryan, Tim Tolker-Nielsen, and J Maxwell Dow. When the PilZ don't work: effectors for cyclic di-GMP action in bacteria. *Trends in microbiology*, 20(5):235–42, may 2012.

[80] P. D. Newell, R. D. Monds, and G. A. O'Toole. LapD is a bis-(3',5')-cyclic dimeric GMP-binding protein that regulates surface attachment by *Pseudomonas fluorescens* Pf0-1. *Proceedings of the National Academy of Sciences*, 106(9):3461–3466, mar 2009.

[81] Peter D Newell, Chelsea D Boyd, Holger Sondermann, and George A O'Toole. A c-di-GMP effector system controls cell adhesion by inside-out signaling and surface protein cleavage. *PLoS biology*, 9(2):e1000587, 2011.

[82] Richard A Alm, Amanda J Bodero, Patricia D Free, and John S Mattick. Identification of a novel gene, *pilZ*, essential for type 4 fimbrial biogenesis in *Pseudomonas aeruginosa*. *Journal of Bacteriology*, 178(1):46–53, 1996.

[83] Dmitri a Ryjenkov, Roger Simm, Ute Römling, and Mark Gomelsky. The PilZ domain is a receptor for the second messenger c-di-GMP: the PilZ domain protein YcgR controls motility in enterobacteria. *The Journal of biological chemistry*, 281(41):30310–4, oct 2006.

[84] Anna Duerig, Sören Abel, Marc Folcher, Micael Nicollier, Torsten Schwede, Nicolas Amiot, Bernd Giese, and Urs Jenal. Second messenger-mediated spatiotemporal control of protein degradation regulates bacterial cell cycle progression. *Genes and Development*, 23(1):93–104, 2009.

[85] N Sudarsan, E R Lee, Z Weinberg, R H Moy, J N Kim, K H Link, and R R Breaker. Riboswitches in eubacteria sense the second messenger cyclic di-GMP. *Science (New York, N.Y.)*, 321(5887):411–413, 2008.

[86] Diego O Serra, Anja M Richter, and Regine Hengge. Cellulose as an architectural element in spatially structured *Escherichia coli* biofilms. *Journal of bacteriology*, 195(24):5540–54, dec 2013.

[87] Sünje Johanna Pamp, Morten Gjermansen, and Tim Tolker-Nielsen. *The Biofilm Matrix: A Sticky Framework*. 2007.

[88] Xin Wang, James F Preston Iii, and Tony Romeo. The *pgaABCD* Locus of *Escherichia coli* Promotes the Synthesis of a Polysaccharide Adhesin Required for Biofilm Formation. 186(9):2724–2734, 2004.

[89] Letizia Tagliabue, Davide Antoniani, Anna Maciag, Paola Bocci, Nadia Raffaelli, and Paolo Landini. The diguanylate cyclase YddV controls production of the exopolysaccharide poly-N-acetylglucosamine (PNAG) through regulation of the PNAG biosynthetic *pgaABCD* operon. *Microbiology (Reading, England)*, 156(Pt 10):2901–11, oct 2010.

[90] Alex Boehm, Samuel Steiner, Franziska Zaehringer, Alain Casanova, Fabienne Hamburger, Daniel Ritz, Wolfgang Keck, Martin Ackermann, Tilman Schirmer, and Urs Jenal. Second messenger signalling governs *Escherichia coli* biofilm induction upon ribosomal stress. *Molecular microbiology*, 72(6):1500–16, jun 2009.

[91] Samuel Steiner, Christian Lori, Alex Boehm, and Urs Jenal. Allosteric activation of exopolysaccharide synthesis through cyclic di-GMP-stimulated protein-protein interaction. *The EMBO journal*, 32(3):354–68, feb 2013.

[92] Michelle M Barnhart and Matthew R Chapman. Curli Biogenesis and Function. pages 131–147, 2010.

[93] Luz P Blanco, Margery L Evans, Daniel R Smith, Matthew P Badtke, and Matthew R Chapman. Diversity, biogenesis and function of microbial amyloids. *Trends in microbiology*, 20(2):66–73, feb 2012.

[94] Nani Van Gerven, Roger D. Klein, Scott J. Hultgren, and Han Remaut. Bacterial Amyloid Formation: Structural Insights into Curli Biogensis. *Trends in Microbiology*, 23(11):693–706, 2015.

[95] M Hammar, Anna Arnqvist, Zhao Bian, Arne Olsdn, and Staffan Normark. Expression of two *csg* operons is required for production of fibronectin- and Congo red-binding curli polymers in *Escherichia coli* K-12. *Molecular Microbiology*, 18(4):661–670, 1995.

[96] Matthew R Chapman, Lloyd S Robinson, Jerome S Pinkner, Robyn Roth, Mårten Hammar, Staffan Normark, and Scott J Hultgren. Role of *Escherichia coli* Curli Operons in Directing Amyloid Fiber Formation. 295(5556):851–855, 2010.

[97] Harald Weber, Christina Pesavento, Alexandra Possling, Gilbert Tischendorf, and Regine Hengge. Cyclic-di-GMP-mediated signalling within the sigma network of *Escherichia coli*. *Molecular microbiology*, 62(4):1014–34, nov 2006.

[98] Sandra Lindenberg, Gisela Klauck, Christina Pesavento, Eberhard Klauck, and Regine Hengge. The EAL domain protein YciR acts as a trigger enzyme in a c-di-GMP signalling cascade in *E. coli* biofilm control. *The EMBO journal*, pages 1–14, may 2013.

[99] Nicole Sommerfeldt, Alexandra Possling, Gisela Becker, Christina Pesavento, Natalia Tschowri, and Regine Hengge. Gene expression patterns and differential input into curli fimbriae regulation of all GGDEF/EAL domain proteins in *Escherichia coli*. *Microbiology (Reading, England)*, 155(Pt 4):1318–31, apr 2009.

[100] Letizia Tagliabue, Anna Maciag, Davide Antoniani, and Paolo Landini. The *yddV-dos* operon controls biofilm formation through the regulation of genes encoding curli fibers' subunits in aerobically growing *Escherichia coli*. *FEMS immunology and medical microbiology*, 59(3):477–84, aug 2010.

[101] M H Deinema and L P Zevenhuizen. Formation of cellulose fibrils by gram-negative bacteria and their role in bacterial flocculation. *Archiv für Mikrobiologie*, 78(1):42–51, 1971.

[102] P Ross, R Mayer, and M Benziman. Cellulose biosynthesis and function in bacteria. *Microbiological reviews*, 55(1):35–58, mar 1991.

[103] X Zogaj, M Nimtz, M Rohde, W Bokranz, and U Römling. The multicellular morphotypes of *Salmonella typhimurium* and *Escherichia coli* produce cellulose as the second component of the extracellular matrix. *Molecular microbiology*, 39(6):1452–63, mar 2001.

[104] Andrew J Spiers, John Bohannon, Stefanie M Gehrig, and Paul B Rainey. Biofilm formation at the air-liquid interface by the *Pseudomonas fluorescens* SBW25 wrinkly spreader requires an acetylated form of cellulose. *Molecular microbiology*, 50(1):15–27, oct 2003.

[105] Cristina Solano, Begoña García, Jaione Valle, Carmen Berasain, Jean-Marc Ghigo, Carlos Gamazo, and Iñigo Lasa. Genetic analysis of *Salmonella enteritidis* biofilm formation: critical role of cellulose. *Molecular microbiology*, 43(3):793–808, feb 2002.

[106] Chapel Hill. Bacterial cellulose biosynthesis: diversity of operons, subunits, products and functions. 73(4):389–400, 2015.

[107] Eva Brombacher, Andrea Baratto, Corinne Dorel, and Paolo Landini. Gene expression regulation by the Curli activator CsgD protein: modulation of cellulose

biosynthesis and control of negative determinants for microbial adhesion. *Journal of bacteriology*, 188(6):2027–37, mar 2006.

[108] Alexander M. Van Der Bliek. Functional diversity in the dynamin family. *Trends in Cell Biology*, 9(3):96–102, 1999.

[109] Shogo Ozaki, Yusaku Matsuda, Kenji Keyamura, Hironori Kawakami, Yasunori Noguchi, Kazutoshi Kasho, Komomo Nagata, Tamami Masuda, Yukari Sakiyama, and Tsutomu Katayama. A replicase clamp-binding dynamin-like protein promotes colocalization of nascent DNA strands and equipartitioning of chromosomes in *E.coli*. *Cell Reports*, 4(5):985–995, 2013.

[110] Lewis Y Geer, Michael Domrachev, David J Lipman, and Stephen H Bryant. CDART: protein homology by domain architecture. *Genome research*, 12(10):1619–23, oct 2002.

[111] T A Grigliatti, L Hall, R Rosenbluth, and D T Suzuki. Temperature-sensitive mutations in *Drosophila melanogaster*. XIV. A selection of immobile adults. *Molecular & general genetics : MGG*, 120(2):107–14, jan 1973.

[112] H S Shpetner and R B Vallee. Identification of dynamin, a novel mechanochemical enzyme that mediates interactions between microtubules. *Cell*, 59(3):421–32, nov 1989.

[113] R A Obar, C A Collins, J A Hammarback, H S Shpetner, and R B Vallee. Molecular cloning of the microtubule-associated mechanochemical enzyme dynamin reveals homology with a new family of GTP-binding proteins. *Nature*, 347(6290):256–61, sep 1990.

[114] A M van der Bliek and E M Meyerowitz. Dynamin-like protein encoded by the *Drosophila shibire* gene associated with vesicular traffic. *Nature*, 351(6325):411–4, may 1991.

[115] M S Chen, R A Obar, C C Schroeder, T W Austin, C A Poodry, S C Wadsworth, and R B Vallee. Multiple forms of dynamin are encoded by *shibire*, a *Drosophila* gene involved in endocytosis. *Nature*, 351(6327):583–6, jun 1991.

[116] Gerrit J K Praefcke and Harvey T McMahon. The dynamin superfamily: universal membrane tubulation and fission molecules? *Nature reviews. Molecular cell biology*, 5(2):133–47, 2004.

[117] Shawn M Ferguson and Pietro De Camilli. Dynamin, a membrane-remodelling GTPase. *Nature reviews. Molecular cell biology*, 13(2):75–88, feb 2012.

[118] P L Tuma and C A Collins. Activation of dynamin GTPase is a result of positive cooperativity. *The Journal of biological chemistry*, 269(49):30842–7, dec 1994.

[119] D E Warnock, J E Hinshaw, and S L Schmid. Dynamin self-assembly stimulates its GTPase activity. *The Journal of biological chemistry*, 271(37):22310–4, sep 1996.

[120] M H Stowell, B Marks, P Wigge, and H T McMahon. Nucleotide-dependent conformational changes in dynamin: evidence for a mechanochemical molecular spring. *Nature cell biology*, 1(1):27–32, may 1999.

[121] H Damke, T Baba, D E Warnock, and S L Schmid. Induction of mutant dynamin specifically blocks endocytic coated vesicle formation. *The Journal of cell biology*, 127(4):915–34, nov 1994.

[122] Byeong Doo Song, Marilyn Leonard, and Sandra L Schmid. Dynamin GTPase domain mutants that differentially affect GTP binding, GTP hydrolysis, and clathrin-mediated endocytosis. *The Journal of biological chemistry*, 279(39):40431–6, sep 2004.

[123] K Salim, M J Bottomley, E Querfurth, M J Zvelebil, I Gout, R Scaife, R L Margolis, R Gigg, C I Smith, P C Driscoll, M D Waterfield, and G Panayotou. Distinct specificity in the recognition of phosphoinositides by the pleckstrin homology domains of dynamin and Bruton's tyrosine kinase. *The EMBO journal*, 15(22):6241–50, nov 1996.

[124] Harry H Low and Jan Löwe. A bacterial dynamin-like protein. *Nature*, 444(7120):766–9, dec 2006.

[125] Harry H Low, Carsten Sachse, Linda a Amos, and Jan Löwe. Structure of a bacterial dynamin-like protein lipid tube provides a mechanism for assembly and membrane curving. *Cell*, 139(7):1342–52, dec 2009.

[126] Harry H. Low and Jan Löwe. Dynamin architecture-from monomer to polymer. *Current Opinion in Structural Biology*, 20(6):791–798, 2010.

[127] Johanna Haiko and Benita Westerlund-Wikström. The role of the bacterial flagellum in adhesion and virulence. *Biology*, 2(4):1242–67, jan 2013.

[128] Ronn S Friedlander, Hera Vlamakis, Philseok Kim, Mughees Khan, Roberto Kolter, and Joanna Aizenberg. Bacterial flagella explore microscale hummocks and hollows to increase adhesion. *Proceedings of the National Academy of Sciences of the United States of America*, 110(14):5624–9, apr 2013.

[129] Ronn S. Friedlander, Nicolas Vogel, and Joanna Aizenberg. Role of Flagella in Adhesion of *Escherichia coli* to Abiotic Surfaces. *Langmuir*, 31(22):6137–6144, 2015.

[130] Lynne S Cairns, Victoria L Marlow, Emma Bissett, Adam Ostrowski, and Nicola R Stanley-Wall. A mechanical signal transmitted by the flagellum controls signalling in *Bacillus subtilis*. *Molecular microbiology*, 90(1):6–21, oct 2013.

[131] Jia Mun Chan, Sarah B Guttenplan, and Daniel B Kearns. Defects in the flagellar motor increase synthesis of poly-γ-glutamate in *Bacillus subtilis*. *Journal of bacteriology*, 196(4):740–53, feb 2014.

[132] Robert Belas. When the swimming gets tough, the tough form a biofilm. *Molecular microbiology*, 90(1):1–5, oct 2013.

[133] Robert Belas. Biofilms, flagella, and mechanosensing of surfaces by bacteria. *Trends in microbiology*, pages 1–11, may 2014.

[134] G. D. Christensen, W. a. Simpson, J. J. Younger, L. M. Baddour, F. F. Barrett, D. M. Melton, and E. H. Beachey. Adherence of coagulase-negative *staphylococci* to plastic tissue culture plates: A quantitative model for the adherence of *staphylococci* to medical devices. *Journal of Clinical Microbiology*, 22(6):996–1006, 1985.

[135] D. Mack, N. Siemssen, and R. Laufs. Parallel induction by glucose of adherence and a polysaccharide antigen specific for plastic-adherent *Staphylococcus epidermidis*: Evidence for functional relation to intercellular adhesion. *Infection and Immunity*, 60(5):2048–2057, 1992.

[136] Judith H. Merritt, Daniel E. Kadouri, and George A. O'Toole. Growing and analyzing static biofilms. *Current Protocols in Microbiology*, (August):1–17, 2011.

[137] George A. O'Toole. Microtiter Dish Biofilm Formation Assay. *Journal of Visualized Experiments*, (47):10–11, 2011.

[138] Koji Hayashi, Naoki Morooka, Yoshihiro Yamamoto, Katsutoshi Fujita, Katsumi Isono, Sunju Choi, Eiichi Ohtsubo, Tomoya Baba, Barry L Wanner, Hirotada Mori, and Takashi Horiuchi. Highly accurate genome sequences of *Escherichia coli* K-12 strains MG1655 and W3110. *Molecular Systems Biology*, 2, 2006.

[139] M Jishage and a Ishihama. Variation in RNA polymerase sigma subunit composition within different stocks of *Escherichia coli* W3110. *Journal of bacteriology*, 179(3):959–63, 1997.

[140] A J Wolfe and H C Berg. Migration of bacteria in semisolid agar. *Proceedings of the National Academy of Sciences of the United States of America*, 86(18):6973–6977, sep 1989.

[141] Julius Adler. Chemotaxis in Bacteria. *Advancement Of Science*, 153(3737):708–716, 1966.

[142] Tomoya Baba, Takeshi Ara, Miki Hasegawa, Yuki Takai, Yoshiko Okumura, Miki Baba, Kirill a Datsenko, Masaru Tomita, Barry L Wanner, and Hirotada Mori. Construction of *Escherichia coli K-12* in-frame, single-gene knockout mutants: the Keio collection. *Molecular systems biology*, 2:2006.0008, jan 2006.

[143] P D Frymier, R M Ford, H C Berg, and P T Cummings. Three-dimensional tracking of motile bacteria near a solid planar surface. *Proceedings of the National Academy of Sciences of the United States of America*, 92(13):6195–6199, jun 1995.

[144] J Frye, J E Karlinsey, H R Felise, B Marzolf, N Dowidar, M McClelland, and K T Hughes. Identification of new flagellar genes of *Salmonella enterica serovar* Typhimurium. *J Bacteriol*, 188(6):2233–2243, 2006.

[145] Hany S Girgis, Yirchung Liu, William S Ryu, and Saeed Tavazoie. A comprehensive genetic characterization of bacterial motility. *PLoS genetics*, 3(9):1644–60, sep 2007.

[146] Alex Boehm, Matthias Kaiser, Hui Li, Christian Spangler, Christoph Alexander Kasper, Martin Ackermann, Volkhard Kaever, Victor Sourjik, Volker Roth, and Urs Jenal. Second messenger-mediated adjustment of bacterial swimming velocity. *Cell*, 141(1):107–16, apr 2010.

[147] Xin Fang and Mark Gomelsky. A post-translational, c-di-GMP-dependent mechanism regulating flagellar motility. *Molecular microbiology*, 76(5):1295–305, jun 2010.

[148] Harald Weber, Tino Polen, Johanna Heuveling, Volker F Wendisch, and Regine Hengge. Genome-Wide Analysis of the General Stress Response Network in *Escherichia coli* : σ S -Dependent Genes, Promoters, and Sigma Factor Selectivity. *J. Bacteriol.*, 187(5):1591–1603, 2005.

[149] Letizia Tagliabue, Anna Maciag, Davide Antoniani, and Paolo Landini. The *yddV-dos* operon controls biofilm formation through the regulation of genes encoding curli fibers' subunits in aerobically growing *Escherichia coli*. *FEMS immunology and medical microbiology*, 59(3):477–84, aug 2010.

[150] U. Römling. Characterization of the rdar morphotype, a multicellular behaviour in *Enterobacteriaceae*. *Cellular and Molecular Life Sciences*, 62(11):1234–1246, 2005.

[151] G. M. Wolfaardt, J. R. Lawrence, R. D. Robarts, S. J. Caldwell, and D. E. Caldwell. Multicellular organization in a degradative biofilm community. *Applied and Environmental Microbiology*, 60(2):434–446, 1994.

[152] Claus Sternberg and Tim Tolker-Nielsen. Growing and Analyzing Biofilms in Flow Cells. *Current Protocols in Microbiology*, 2006.

[153] Shanika a. Crusz, Roman Popat, Morten Theil Rybtke, Miguel Cámara, Michael Givskov, Tim Tolker-Nielsen, Stephen P. Diggle, and Paul Williams. Bursting the bubble on bacterial biofilms: a flow cell methodology. *Biofouling*, 28(8):835–842, 2012.

[154] Steven S Branda, Åshild Vik, Lisa Friedman, and Roberto Kolter. Biofilms: The matrix revisited. *Trends in Microbiology*, 13(1):20–26, 2005.

[155] Charalampia-Georgia Korea, Réana Badouraly, Marie-Christine Prevost, Jean-Marc Ghigo, and Christophe Beloin. *Escherichia coli K-12* possesses multiple cryptic but functional chaperone-usher fimbriae with distinct surface specificities. *Environmental microbiology*, 12(7):1957–77, 2010.

[156] Paul N. Danese, Leslie A. Pratt, Simon L. Dove, and Roberto Kolter. The outer membrane protein, Antigen 43, mediates cell-to-cell interactions within *Escherichia coli* biofilms. *Molecular Microbiology*, 37(2):424–432, 2000.

[157] K. Kjaergaard, M. a. Schembri, C. Ramos, S. Molin, and P. Klemm. Antigen 43 facilitates formation of multispecies biofilms. *Environmental Microbiology*, 2(6):695–702, 2000.

[158] Maria Das Graças de Luna, Anthony Scott-Tucker, Mickael Desvaux, Paul Ferguson, Nicholas P Morin, Edward G Dudley, Sue Turner, James P Nataro, Peter Owen, and Ian R Henderson. The *Escherichia coli* biofilm-promoting protein Antigen 43 does not contribute to intestinal colonization. *FEMS microbiology letters*, 284(2):237–46, 2008.

[159] Agnes Roux, Christophe Beloin, and Jean-marc Ghigo. Combined Inactivation and Expression Strategy To Study Gene Function under Physiological Conditions : Application to Identification of New *Escherichia coli* Adhesins. *Journal of Bacteriology*, 187(3):1001–1013, 2005.

[160] B. Diderichsen. *flu*, A metastable gene controlling surface properties of *Escherichia coli*. *Journal of Bacteriology*, 141(2):858–867, 1980.

[161] Ian R. Henderson, Fernando Navarro-Garcia, and James P. Nataro. The great escape: Structure and function of the autotransporter proteins. *Trends in Microbiology*, 6(9):370–378, 1998.

[162] a Kihara, Y Akiyama, and K Ito. A protease complex in the *Escherichia coli* plasma membrane: HflKC (HflA) forms a complex with FtsH (HflB), regulating its proteolytic activity against SecY. *The EMBO journal*, 15(22):6122–6131, 1996.

[163] Duncan T. Browman, Maja B. Hoegg, and Stephen M. Robbins. The SPFH domain-containing proteins: more than lipid raft markers. *Trends in Cell Biology*, 17(8):394–402, 2007.

[164] Daniel Lopez. Molecular composition of functional microdomains in bacterial membranes. *Chemistry and Physics of Lipids*, 192:3–11, 2015.

[165] G Karimova, J Pidoux, a Ullmann, and D Ladant. A bacterial two-hybrid system based on a reconstituted signal transduction pathway. *Proceedings of the National Academy of Sciences of the United States of America*, 95(10):5752–5756, 1998.

[166] Daniel Ladant and Agnes Ullmann. Bordetella pertussis adenylate cyclase: A toxin with multiple talents. *Trends in Microbiology*, 7(4):172–176, 1999.

[167] Robert W Crawford, Kristin E Reeve, and John S Gunn. Flagellated but not hyperfimbriated *Salmonella enterica serovar* Typhimurium attaches to and forms biofilms on cholesterol-coated surfaces. *Journal of bacteriology*, 192(12):2981–90, jun 2010.

[168] MAS Vigeant and RM Ford. Reversible and irreversible adhesion of motile *Escherichia coli* cells analyzed by total internal reflection aqueous fluorescence microscopy. *Applied and environmental microbiology*, 68(6):2794–2801, 2002.

[169] Knut Drescher and Jörn Dunkel. Fluid dynamics and noise in bacterial cell-cell and cell-surface scattering. *PNAS*, 108(27):10940–10945, 2011.

[170] Benjamin Misselwitz, Naomi Barrett, Saskia Kreibich, Pascale Vonaesch, Daniel Andritschke, Samuel Rout, Kerstin Weidner, Milos Sormaz, Pascal Songhet, Peter Horvath, Mamta Chabria, Viola Vogel, Doris M Spori, Patrick Jenny, and Wolf-Dietrich Hardt. Near surface swimming of *Salmonella Typhimurium* explains target-site selection and cooperative invasion. *PLoS pathogens*, 8(7):e1002810, jan 2012.

[171] Viviana Sanchez-Torres, Hongbo Hu, and Thomas K. Wood. GGDEF Proteins YeaI, YedQ, and YfiN Reduce Early Biofilm Formation and Swimming Motility in Escherichia coli. *Appl Microbiol Biotechnol*, 90(2):651–658, 2011.

[172] Olga E. Petrova and Karin Sauer. Sticky situations: Key components that control bacterial surface attachment. *Journal of Bacteriology*, 194(10):2413–2425, 2012.

[173] Dae-Gon Ha and George A O'Toole. c-di-GMP and its effects on biofilm formation and dispersion: a *Pseudomonas aeruginosa* review. *Microbiol Spectr.*, 3(2), 2015.

[174] Claudine Baraquet, Keiji Murakami, Matthew R Parsek, and Caroline S Harwood. The FleQ protein from *Pseudomonas aeruginosa* functions as both a repressor and an activator to control gene expression from the *pel* operon promoter in response to c-di-GMP. *Nucleic acids research*, 40(15):7207–18, aug 2012.

[175] Claudine Baraquet and Caroline S Harwood. Cyclic diguanosine monophosphate represses bacterial flagella synthesis by interacting with the Walker A motif of the enhancer-binding protein FleQ. *Proceedings of the National Academy of Sciences of the United States of America*, 110(46):18478–83, nov 2013.

[176] Claudine Baraquet and Caroline S. Harwood. FleQ DNA Binding Consensus Sequence Revealed by Studies of FleQ-Dependent Regulation of Biofilm Gene Expression in *Pseudomonas aeruginosa*. *Journal of Bacteriology*, 198(1):178–186, jan 2016.

[177] Jason W Hickman and Caroline S Harwood. Identification of FleQ from *Pseudomonas aeruginosa* as a c-di-GMP-responsive transcription factor. *Molecular microbiology*, 69(2):376–89, jul 2008.

[178] Laura Hobley, Catriona Harkins, Cait E. MacPhee, and Nicola R. Stanley-Wall. Giving structure to the biofilm matrix: An overview of individual strategies and emerging common themes. *FEMS Microbiology Reviews*, 39(5):649–669, 2015.

[179] Felix Dempwolff and Peter L. Graumann. Genetic links between bacterial dynamin and flotillin proteins. *Communicative and Integrative Biology*, 7(5):2–4, 2014.

[180] Giovanni Candiano, Maurizio Bruschi, Luca Musante, Laura Santucci, Gian Marco Ghiggeri, Barbara Carnemolla, Paola Orecchia, Luciano Zardi, and Pier Giorgio Righetti. Blue silver: A very sensitive colloidal Coomassie G-250 staining for proteome analysis. *Electrophoresis*, 25(9):1327–1333, 2004.

[181] C T Chung, S L Niemela, and R H Miller. One-step preparation of competent *Escherichia coli*: transformation and storage of bacterial cells in the same solution. *Proceedings of the National Academy of Sciences of the United States of America*, 86(7):2172–2175, 1989.

[182] U K Laemmli. Cleavage of structural proteins during the assembly of the head of bacteriophage T4. *Nature*, 227(5259):680–685, 1970.

[183] K a Datsenko and B L Wanner. One-step inactivation of chromosomal genes in *Escherichia coli K-12* using PCR products. *Proceedings of the National Academy of Sciences of the United States of America*, 97(12):6640–6645, 2000.

[184] P P Cherepanov and W Wackernagel. Gene disruption in *Escherichia coli*: TcR and KmR cassettes with the option of Flp-catalyzed excision of the antibiotic-resistance determinant. *Gene*, 158(1):9–14, may 1995.

[185] Christopher D Herring, Jeremy D Glasner, and Frederick R Blattner. Gene replacement without selection: regulated suppression of amber mutations in *Escherichia coli*. *Gene*, 311:153–163, 2003.

[186] E Burton, N Yakandawala, K LoVetri, and M S Madhyastha. A microplate spectrofluorometric assay for bacterial biofilms. *Journal of industrial microbiology & biotechnology*, 34(1):1–4, jan 2007.

[187] Malena Elise Skogman, Pia Maarit Vuorela, and Adyary Fallarero. Combining biofilm matrix measurements with biomass and viability assays in susceptibility assessments of antimicrobials against *Staphylococcus aureus* biofilms. *The Journal of antibiotics*, 65(9):453–9, sep 2012.

[188] Nobuyuki Otsu. A threshold selection method from gray-level histograms. *IEEE Transactions on systems, man, and cybernetics*, 20(9):62–66, 1979.

[189] J M Prewitt and M L Mendelsohn. The analysis of cell images. *Annals of the New York Academy of Sciences*, 128(3):1035–1053, 1966.

[190] I. F. Sbalzarini and P. Koumoutsakos. Feature point tracking and trajectory analysis for video imaging in cell biology. *Journal of Structural Biology*, 151(2):182–195, 2005.

[191] David Kentner, Sebastian Thiem, Markus Hildenbeutel, and Victor Sourjik. Determinants of chemoreceptor cluster formation in *Escherichia coli*. *Molecular microbiology*, 61(2):407–17, jul 2006.

[192] David Kentner and Victor Sourjik. Dynamic map of protein interactions in the *Escherichia coli* chemotaxis pathway. *Molecular systems biology*, 5(238):238, jan 2009.

[193] Silke Neumann, Karin Grosse, and Victor Sourjik. Chemotactic signaling via carbohydrate phosphotransferase systems in *Escherichia coli*. *Proceedings of the National Academy of Sciences of the United States of America*, 109(30), jul 2012.

[194] Victor Sourjik, Ady Vaknin, Thomas S. Shimizu, and Howard C. Berg. In Vivo Measurement by FRET of Pathway Activity in Bacterial Chemotaxis, 2007.

[195] H M Salis, E A Mirsky, and C A Voigt. Automated Design of Synthetic Ribosome Binding Sites to Precisely Control Protein Expression. *Nat Biotechnol*, 27(10):946–950, 2010.

[196] L. M. Guzman, D. Belin, M. J. Carson, and J. Beckwith. Tight regulation, modulation, and high-level expression by vectors containing the arabinose P(BAD) promoter. *Journal of Bacteriology*, 177(14):4121–4130, 1995.

[197] Egon Amann, Birgit Ochs, and Karl-Josef Abel. Tightly regulated *tac* promoter vectors useful for the expression of unfused and fused proteins in *Escherichia coli*. *Gene*, 69(2):301–315, 1988.

[198] Alon Zaslaver, Anat Bren, Michal Ronen, Shalev Itzkovitz, Ilya Kikoin, Seagull Shavit, Wolfram Liebermeister, Michael G Surette, and Uri Alon. A comprehensive library of fluorescent transcriptional reporters for *Escherichia coli*. *Nature Methods*, 3(8):623–628, 2006.

[199] J S Parkinson and S E Houts. Isolation and behavior of *Escherichia coli* deletion mutants lacking chemotaxis functions. *Journal of Bacteriology*, 151(1):106–113, 1982.

[200] D Hanahan. Studies on transformation of *Escherichia coli* with plasmids. *J Mol Biol*, 166(4):557–580, jun 1983.

LIST OF FIGURES

LIST OF TABLES